Monotonic and Cyclic Behaviour of Innovative High Capacity Hybrid Beam-Columns

Fatemeh Javidan

M.Sc. in Structural Engineering

A thesis submitted for the degree of Doctor of Philosophy at Monash University in 2017

Department of Civil Engineering

Copyright notice

Abstract

With the ever-increasing application of high strength steel material in industries due to their unique characteristics such as strength, energy absorption, weight and cost saving, there is a high potentiality for taking advantage of the exceptional capacities of this material in construction practice. Steel materials with yield strengths higher than 700MPa are quite rarely used as the main construction material in civil structures and are lacking from available design standards. The present thesis investigates an innovative application for high and ultra-high strength steel tubes in hybrid fabricated members taking advantage of the combined material properties of the constituting elements under monotonic and cyclic loading states in terms of strength, local buckling behaviour and ductility.
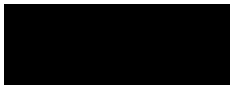
Component-scale pure axial compression, pure flexural bending and combined axial force-bending moment interaction tests are performed on members consisting of mild steel, high strength steel and ultra-high strength steel tubes and the behaviour of individual members are compared against each other and also against conventional fabricated sections. The effect of welding on the mechanical properties of high and ultra-high strength steel tubes in hybrid members is investigated in both micro and macro scales. A finite element model has been developed incorporating nonlinear material and geometry, plastic material models, heat effects due to welding, damage models, section and member imperfections, etc. leading to a robust simulation tool for various section geometries and loading scenarios. Experimental and numerical results have been compared against available design recommendations.

For implementation of structures consisting of high and ultra-high strength steel elements in earthquake prone areas, the seismic performance of these members in both material scale and large scale needs to be investigated. The main purpose of conducting material scale tension-compression analysis is to obtain a combined plastic model for cyclically

strained high and ultra-high strength steel materials subjected to various strain or stress histories for a wide range of simulation purposes. In the next stage, large scale multi-directional cyclic tests are conducted on the proposed hybrid fabricated components evaluating strength, stiffness and plastic deformations under realistic cyclic loading paths. Seismic experimental results can be incorporated in the development of reliable nonlinear analysis models of frames consisting of these components for damage and collapse simulation of structures.

Declaration

This thesis contains no material which has been accepted for the award of any other degree or diploma at any university or equivalent institution and that, to the best of my knowledge and belief, this thesis contains no material previously published or written by another person, except where due reference is made in the text of the thesis.

Fatemeh Javidan

January 2017

Publications during Enrolment

Peer reviewed published journal papers:

1. Performance of innovative fabricated long hollow columns under axial compression

F. Javidan, A. Heidarpour, X.-L. Zhao, J. Minkkinen,
Journal of Constructional Steel Research, Volume 106, March 2015, Pages 99-109.

2. Effect of weld on the mechanical properties of high strength and ultra-high strength steel tubes in fabricated hybrid sections

F. Javidan, A. Heidarpour, X.-L. Zhao, C.R. Hutchinson, J. Minkkinen,
Engineering Structures, Volume 118, July 2016, Pages 16-27.

3. Application of high strength and ultra-high strength steel tubes in long hybrid compressive members: Experimental and numerical investigation

F. Javidan, A. Heidarpour, X.-L. Zhao, J. Minkkinen,
Thin-Walled Structures, Volume 102, May 2016, Pages 273-285.

4. Fundamental behaviour of high strength and ultra-high strength steel subjected to low cycle structural damage

F. Javidan, A. Heidarpour, X.-L. Zhao, Hossein Fallahi,
Engineering Structures, Volume 143, April 2017, Pages 427-440.

Submitted papers:

5. Bending moment and axial compression interaction of high capacity hybrid fabricated members

F. Javidan, A. Heidarpour, X.-L. Zhao, R. Al-Mahaidi, *Submitted to Thin-walled Structures.*

6. Multiaxial seismic performance of high capacity hybrid fabricated beam-columns

F. Javidan, A. Heidarpour, X.-L. Zhao, R. Al-Mahaidi, *Submitted to Journal of Structural Engineering (ASCE)*

Peer reviewed conference papers:

7. The compressive behaviour of innovative hollow long columns consisting of mild steel plates and tubes

F. Javidan, A. Heidarpour, X.-L. Zhao, J. Minkkinen,

7th European conference on steel and composite structures (EUROSTEEL 2014), Pages 973-974

8. Compressive behaviour of innovative hollow long fabricated columns with high strength and ultra-high strength tubes

F. Javidan, A. Heidarpour, X.-L. Zhao, J. Minkkinen,

15th International Symposium on Tubular Structures, 2015, Pages 319-325

9. Seismic performance of high capacity hybrid beam-columns

F. Javidan, A. Heidarpour, X.-L. Zhao, R. Al-Mahaidi,

8th European conference on steel and composite structures (EUROSTEEL 2017), 2017.

Thesis including published works declaration

I hereby declare that this thesis contains no material which has been accepted for the award of any other degree or diploma at any university or equivalent institution and that, to the best of my knowledge and belief, this thesis contains no material previously published or written by another person, except where due reference is made in the text of the thesis.

This thesis includes 4 original papers published in peer reviewed journals and 2 submitted publications. The core theme of the thesis is Structural Engineering. The ideas, development and writing up of all the papers in the thesis were the principal responsibility of myself, the student, working within the department of Civil Engineering under the supervision of Dr. Amin Heidarpour.

(The inclusion of co-authors reflects the fact that the work came from active collaboration between researchers and acknowledges input into team-based research.)

In the case of chapters 2-7 my contribution to the work involved the following:

Ch.	Publication Title	Status	Nature and % of student contribution	Co-author names(s) Nature and % of Co-author's contribution	Co-author Monash student
2	Performance of innovative fabricated long hollow columns under axial compression	Published	Developing ideas, Establishing methodologies, Experimental work, Data analysis, Write-up and revision, 70%	1) Dr. Amin Heidarpour: Developing ideas, input into manuscript, revision, financial support, 18% 2) Prof. Xiao-Ling Zhao: Revision, financial support, 10% 3) Mr. Jussi Minkkinen: Providing tube specimens, revision, 2%	No
3	Effect of weld on the mechanical properties of high strength and ultra-high strength steel tubes in fabricated hybrid sections	Published	Developing ideas, Establishing methodologies, Experimental work, Data analysis, Write-up and revision, 70%	1) Dr. Amin Heidarpour: Developing ideas, input into manuscript, revision, financial support, 10% 2) Prof. Xiao-Ling Zhao: Revision, financial support, 8% 3) Prof. Christopher R. Hutchinson: Input into manuscript, revision, 10% 4) Mr. Jussi Minkkinen: Providing tube specimens, revision, 2%	No

4	Application of high strength and ultra-high strength steel tubes in long hybrid compressive members: Experimental and numerical investigation	Published	Developing ideas, Establishing methodologies, Experimental work, Data analysis, Write-up and revision, 70%	1) Dr. Amin Heidarpour: Developing ideas, input into manuscript, revision, financial support, 18% 2) Prof. Xiao-Ling Zhao: Revision, financial support, 10% 3) Mr. Jussi Minkkinen: Providing tube specimens, revision, 2%	No
5	Bending moment and axial compression interaction of high capacity hybrid fabricated members	Submitted	Developing ideas, Establishing methodologies, Experimental work, Data analysis, Write-up and revision, 70%	1) Dr. Amin Heidarpour: Developing ideas, input into manuscript, revision, financial support, 15% 2) Prof. Xiao-Ling Zhao: Revision, financial support, 7% 3) Prof. Riadh Al-Mahaidi: revision, Financial support through access to Swinburne testing facilities, 8%	No
6	Fundamental behaviour of high strength and ultra-high strength steel subjected to low cycle structural damage	Published	Developing ideas, Establishing methodologies, Experimental work, Data analysis, Write-up and revision, 70%	1) Dr. Amin Heidarpour: Developing ideas, input into manuscript, revision, financial support, 18% 2) Prof. Xiao-Ling Zhao: Revision, financial support, 7% 3) Mr. Hossein Fallahi: Input to manuscript, Microscopic imaging, 5%	Yes
7	Multiaxial seismic performance of high capacity hybrid fabricated beam-columns	Submitted	Developing ideas, Establishing methodologies, Experimental work, Data analysis, Write-up and revision, 70%	1) Dr. Amin Heidarpour: Developing ideas, input into manuscript, revision, financial support, 15% 2) Prof. Xiao-Ling Zhao: Revision, financial support, 7% 3) Prof. Riadh Al-Mahaidi: revision, Financial support through access to Swinburne testing facilities, 8%	No

I have renumbered sections of submitted or published papers in order to generate a consistent presentation within the thesis.
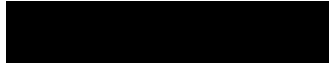
Student signature: ██████████   Date: 30/01/2017

The undersigned hereby certify that the above declaration correctly reflects the nature and extent of the student's and co-authors' contributions to this work. In instances where I am not the responsible author I have consulted with the responsible author to agree on the respective contributions of the authors.

Main Supervisor signature: ██████████████   Date: 30/01/2017

Acknowledgements

List of Contents

List of Figures

List of Tables

Introduction

1.1. Motivation

Due to their unique characteristics such as strength, energy absorption, weight and cost saving, thermo-mechanically processed ultra-high tensile steel is widely used in industrial productions. One of the most wide spread applications of high strength steel is in automobile manufacturing, for instance its utilisation in propeller shafts, suspension parts and doors under impact and crush conditions [1-3]. However, civil construction has fallen behind other industries in terms of taking advantage of the superior characteristics of these steel materials. Accordingly, the unique specifications of this material can be proposed as an exceptional alternative for conventional mild steel. This is due to the fact that high strength steel and mild steel possess similar weights per equal volume. Applications of high strength steel materials can be found in literature and construction practice such as roof structures, stadiums, bridges, airports etc. [4, 5] (Figure 1.1). Although the utilisation of these steel materials in the past couple of decades has been a noticeable improvements in construction practice, the grade of all these high strength steel materials was limited to 690MPa. This limitation may arise from regulation of yield strength of steel recommended in standards. Most popular standards on design of steel structures, such as Eurocode3 (EN-1993-1-12:2007) [6], AISC-360-10[7], and AS-4100 [8] allow for the use of steel with yield strength not more than 690MPa and ultimate strength as far as 760MPa. These limitations are due to the distinct material properties of higher grades of steel mainly with regards to ductility.
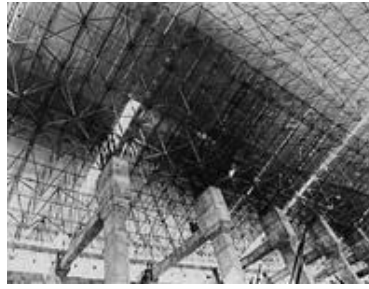
| Salt Lake Stadium roof, Calcutta, India [4] | Fiumicino Airport Railway terminal, Italy [5] |

Figure 1.1. Applications of high strength steel tubes in structures

One of the main intentions of utilising high tensile steel material in structures is their sustainability compared to conventional construction materials. The use of high tensile steel leads to longer life span of structure. For instance, the high strength steel material utilised in this study exhibits an increase of 2.5 times of life span than that of mild tubes [9]. From another point of view, the cost effectiveness of high strength material is a main ambition for replacing this material with conventional construction steel and concrete materials. The use of high tensile steel can lead to a great deal of reduction in the consumed mass, transportation and labour costs while increasing the overall load bearing capacity; which makes the structure more safe and sustainable. In terms of cost, a comparison among high strength steel tubes and normal steel tubes in realistic possibilities of building columns, considering the strength, stability and stiffness conditions, clearly indicated that using high strength steel in structures is more economic [10].

In compressive loading conditions, high strength and ultra-high strength tubes experience failure modes due to the brittle behaviour of the material as well as global buckling, depending on the geometry and slenderness. In fact, the lower ductility of sections consisting only of high strength steel material compared to mild steel sections has an undermining effect on the global performance of the whole structure. Therefore, an innovative hybrid section consisting of high strength tubes welded to the corners of mild

steel plates has been proposed [11] which significantly enhances the compressive capabilities of steel material in terms of both strength and ductility. There has been recommendations on ductility requirements for steel sections in the literature. The innovative steel sections fabricated from both mild steel plates and high strength or ultra-high strength steel tubes perform in an interactive way that the overall ductility of section meets the structural requirements. The closed geometry of the proposed section consisting of circular tubes, on the other hand, exhibits exceptional performance in terms of local buckling under various loading conditions.

1.2.   State of the art

Full-scale testing of structural elements is of special importance in terms of the necessity to develop realistic nonlinear models for analytical and simulation purposes. No previous work in literature is available on large-scale structural performance of fabricated members consisting of ultra-high strength steel under various loading scenarios. Limited work is found in small scales of members in which only compression and fire loadings have been taken into consideration. For instance, employment of high strength circular steel tubes as stub columns [12-15] have been investigated. In this thesis, large-scale experimental tests on hybrid members with two and three meters length are undertaken on innovative sections under static compression and bending in addition to cyclic loading.

For the purpose of design and analysis of structures incorporating high and ultra-high strength steel, the material scale behaviour has thoroughly been focused on in this thesis. The effects of heat induced by welding on the performance of high tensile steel as well as damage modellings are inevitable aspects influencing the large scale results as well as

numerical models which have been widely covered in this thesis. Moreover, material scale cyclic tests conducted on high strength and ultra-high strength tubes are a new step for characterising and modelling the constitutive equations of cyclically strained steel (grades 800 and 1200) which has not previously been taken into consideration from a structural point of view.

Component cyclic tests performed throughout this thesis provide demanding data required to develop and calibrate analytical models and seismic design recommendations of high strength structural systems in earthquake prone areas. In large scale testing on hybrid fabricated beam-columns, all relevant experimental aspects such as the designed test specimens, boundary conditions, the applied loading states and direction of loadings are implemented in accordance with the unique requirements of the proposed sections to obtain as much reliability and practicality from the results as possible.

The novel experimental test programs designed and developed in this thesis are applicable for analysing and predicting the failure and fracture of structures and structural elements consisting of a welded combination of two types of steel elements. Numerical finite element models developed at all stages for all materials considered in this research employed realistic plastic models, nonlinear material and geometry, heat affects due to welding, initial section imperfections, etc. leading to a robust simulation tool for any future case study.

1.3.   Thesis objectives

1.3.1.   Material scale phase

Monotonic:

Analysis and design of innovative structural elements are not possible unless of having a comprehensive understanding of the behaviour of the constituting materials. An important part of experimental efforts undertaken in the present thesis was dedicated to the design and performance of material scale testing and modelling. The first and foremost step of material scale testing is standard tensile tests on four types of materials included in this research work: mild steel (MS) plates, mild steel (MS) tubes, high strength steel (HSS) tubes and ultra-high strength steel (UHSS) tubes. Tension material tests are conducted on each steel type following the guidelines of ASTM-E8M-04 [16] and AS1391[17]. Flow curves obtained from these tests yield basic information from the mechanical properties of the above mentioned steel such as elastic modulus, yield and ultimate tensile strength (UTS), strain hardening rates, strains corresponding to yield and ultimate stresses, deformation and ductility (Figure 1.2). A summary of the main material properties of different steel types are presented in Table 1.1. Due to the different failure modes of ultra-high strength material compared to mild steel and with the aim of an accurate prediction of the onset of damage, the results of tensile tests on this material are also used to derive a damage initiation model followed by damage evolution extracted from the standard tensile tests conducted.

- Mild steel tube (UTS:350 MPa)
- High strength steel tube (UTS: 850 MPa)
- Ultra-high strength tube (UTS:1400 MPa)

External welds
Mild steel plate
Tubes
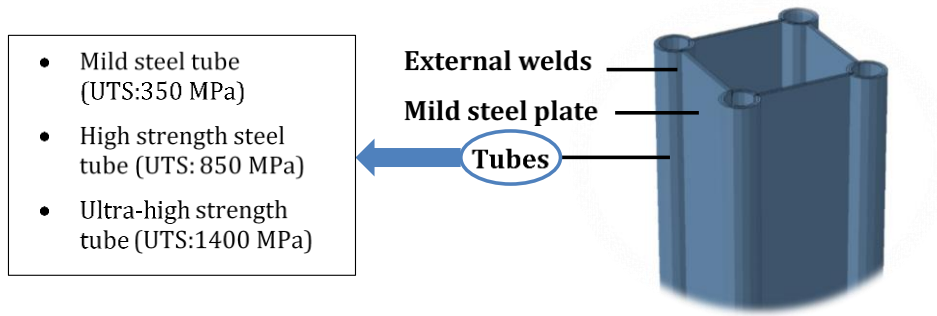
Figure 1.2. Innovative fabricated hybrid section and steel materials included

Table 1.1. Introduction to the material properties of steel elements included in this thesis

Material	Elastic modulus (GPa)	Yield strength (MPa)	Ultimate strength (MPa)	Strain at UTS %
MS plate	207	265	376	23%
MS tube	198	305	342	11%
HSS tube	205	772	847	2.5%
UHSS tube	209	1247	1385	2.1%

As opposed to hot-rolled and cold-formed structural sections, when it comes to hybrid fabricated ones, welding has a significant effect on the material properties and behaviour in the vicinity of weld, known as the heat affected zone (HAZ). These heat effects are accounted for in the numerical simulations using two different methods. Since a wide range of research is available for heat affected mild steel, these effects are considered in Chapter 2 by introducing the pre-stresses generated in mild steel tubes and plates based on Dwight's model [18]. In this method values of pre-stress are calculated and assigned to the relevant segments of each section and analysed accordingly. The alternative method is conducting tensile tests to directly obtain the heat-affected material properties for different types of steel material. A number of research works are available investigating the effect of heat and high temperatures, specifically welding on high strength and ultra-high strength tube

materials [19-21]. For the sake of obtaining a comprehensive set of material properties at locations with various distances from weld in fabricated sections consisting of high strength and ultra-high strength steel tubes, tensile coupons are extracted and material properties are obtained with respect to the tube manufacturing process, type of welding and post-welding conditions (Figure 1.3). Particular attention is placed on the ultimate tensile strength and the strain corresponding to that with regards to the effects of yield strength and strain hardening rate. The microstructural behaviour of all steel materials at the vicinity of weld is obtained in Chapter 3 and is used as material inputs for component-scale finite element simulations of sections in Chapters 4 and 5.
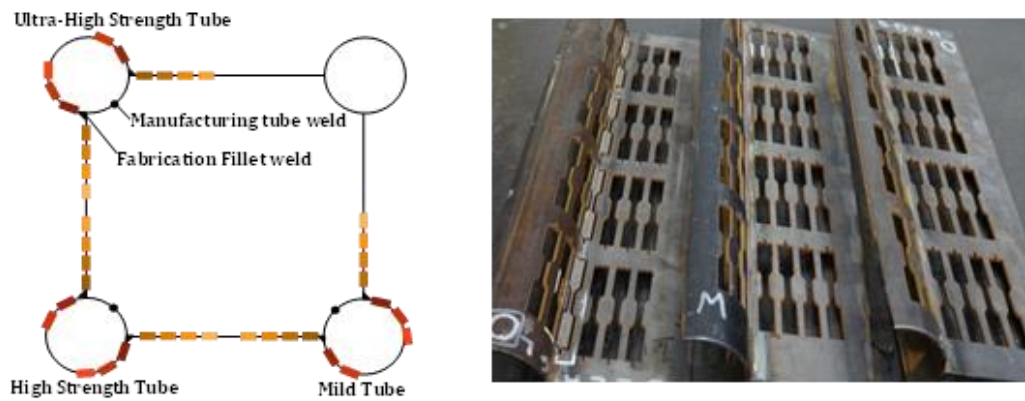
Figure 1.3. Specimen extraction for HAZ analysis

Cyclic:

Plastic behaviour of high strength and ultra-high strength steel material under periodic tension-compression is proven to be completely different from that of mild steel. As opposed to conventional structural mild steel both grades of steels considered in this study exhibit cyclic softening with plastic straining having a more prominent strength reduction in higher strengths of steel. Cyclical damage applied on high tensile steel evidently influences the preserved mechanical properties of microstructure at fracture. Therefore, an important part of the material-scale part of this thesis aims to analytically and theoretically

study the cyclic behaviour of high strength steel tubes, with individual applications or incorporated in fabricated structural elements. The experimental strain and stress controlled cyclic tests conducted on HSS and UHSS material specimens presented in Chapter 6, not only facilitate the analytical understanding of the cyclic softening and preserved material properties of steel, but also lead to obtaining a robust material model. Accordingly, the final part of material investigations on HSS and UHSS tubes in Chapter 6 is devoted to calibration and validation of a combined plastic model including essential isotropic and kinematic parameters.

1.3.2. Large scale phase

In general, three types of innovative hybrid sections are considered in this thesis: Fabricated sections consisting MS tubes welded to corners of mild steel plates, sections consisting of HSS tubes welded to corners of mild steel plates and UHSS tubes welded to corners of mild steel plates. The behaviour of these innovative hybrid members is compared to similar welded box members consisting of mild steel plates at different stages of experimental testing, analytical investigations and numerical modellings. All above mentioned specimens are tested under the application of various loading scenarios followed by analytical evaluations or relevant numerical modelling of each case. These large scale experimental tests can be categorised to four phases described below.

Pure compression phase:

Quasi-static axial compression tests are applied on hybrid sections, welded box sections and also single tube specimens. It is important for this part of the work to have a comprehensive comparison among the compressive behaviour of individually tested members in addition to a comparison of the superposition of individual elements. Under compression loading the main concern is global or local buckling in both tube and plate elements in sections with

various lengths. The experimental part of thesis at this stage comprises of two phases; one set of experiments are conducted on innovative fabricated members consisting of MS tubes only, in which the overall performance, buckling and failure of one, two and three meters specimens are taken into consideration with special focus on the section design and geometry (Chapter 2). In the second phase, experimental tests are conducted on members including higher strengths of tubes of one and two meters length where results can be compared to that of the previous phase (Chapter 4). Numerical finite element models developed at this phase of thesis for various section geometries and materials consider many critical data inputs such as realistic plastic models, nonlinear material and geometry, heat affects due to welding and initial section imperfections.

A cost-analysis study is also essential to be conducted at the early stages of experimental testing to evaluate the estimated production cost of the innovative sections and compare that with equivalent welded box sections in a structural and economic point of view.

Pure bending phase:

Pure bending experimental tests play an important role in understanding the moment-bearing capacity of these innovative fabricated sections and consequently the axial-lateral interaction behaviour. Due to the thin-walled geometry of these sections, several challenges are faced to design a realistic setup to measure the pure bending capacity. In conducting four point bending tests on specimens, point loads should be transferred through special uniform bearing links to the side of sections. In order to avoid local failure in either plates or tubes, these element are required to be strengthened under local point loads. At the end of the experimental stage, bending capacity obtained from tests and validated finite element models are compared against relevant design recommendations for regular steel sections and the applicability of the guidelines are discussed (Chapter 5).

Axial load-bending moment interaction:

The basic design procedure for a beam-column element is mainly executed based on the combined actions of axial load and bending moments. Taking advantage of the wide range of experimental tests conducted on the innovative hybrid sections, namely, pure axial compression and pure bending moment in previous chapters, Chapter 5 comes together to investigate the overall beam-column capacity of these sections. The verified finite element model developed during the previous steps of this thesis is incorporated to run a wide range of numerical simulations with various combinations of axial force and lateral displacement-controlled pushover tests until complete failure. Due to the fact that the hybrid fabricated sections consist of thin-walled elements, an important application for the numerical model is to practically derive the optimum cross-sectional geometry in a way that the ultimate interaction performance of section is obtained.

Multiaxial cyclic phase:

The main objectives of conducting multiaxial cyclic tests on hybrid fabricated sections is to derive all relevant seismic characteristics of these sections under common and realistic loading patterns which is the main focus of Chapter 7. The first stage of tests are designed following common unidirectional lateral cyclic loading pattern which helps identify and quantify the main seismic parameters such as force and deformation characteristics, plastic deformations and failure types. All required instrumentations for relevant property measurements will be taken into action at all stages of experiments. Gravity loads are an essential part of test design in which they have been considered relative to the axial capacity of each section. Bidirectional lateral cyclic tests have also been conducted with the aim of finding the effect of a more realistic loading state on the extent of damage of sections. The bidirectional lateral deformation-controlled loadings are applied along with a cyclically varying axial load with the aim of introducing the effects of resulting frame moments and

uplifting due to overall earthquake induced displacements on frame stories affecting the axial load applied on one single column. All test requirements for different degrees of freedoms of each test specimen are applied using the multi-axis substructure testing (MAST) system. Finally, further seismic analysis and parameter extractions can be conducted on hysteresis curves for the development of reliable nonlinear analysis models resulting in damage and collapse simulation of structures.

1.4. Thesis outline

An overall outline of each chapter and the structure of thesis chapters along with chapter titles are presented in Figure 1.4. The overall structure of thesis is divided into two main parts based on the loading phase.
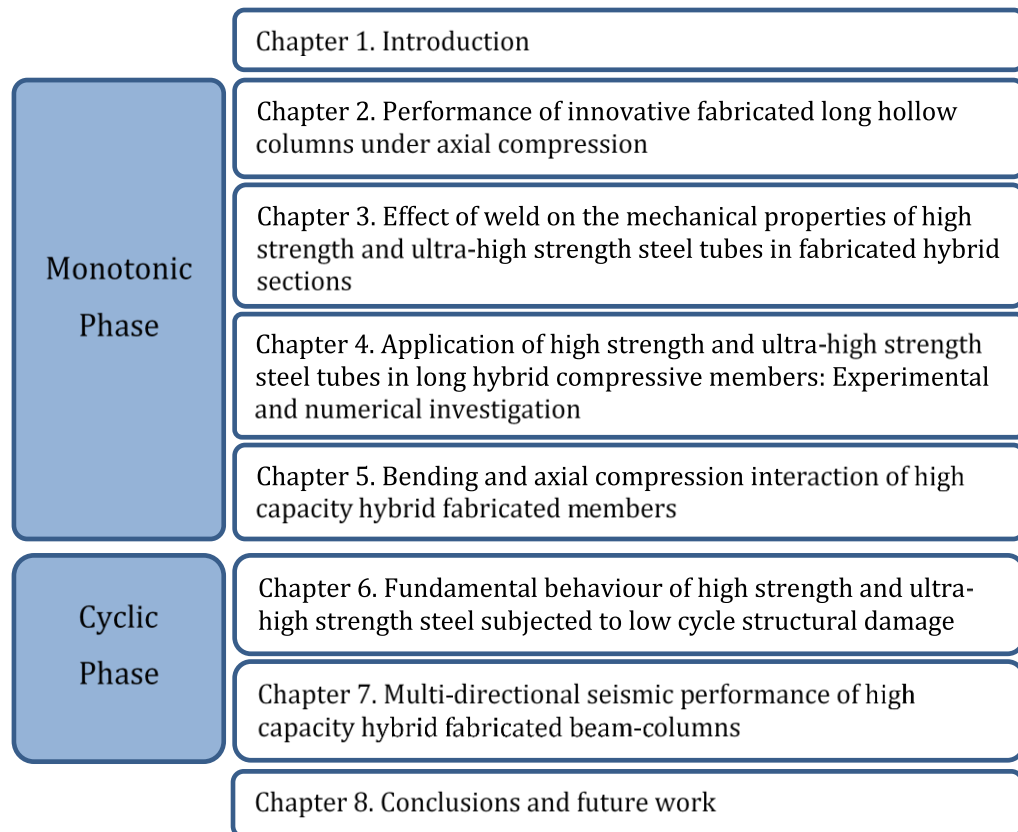
Figure 1.4. Thesis outline and structure

Each of the above mentioned chapters are organised in a way that the main aims of investigating the monotonic and cyclic behaviour of innovative high capacity hybrid members is fulfilled. The main arrangement of chapters is based on the loading type (monotonic or cyclic), while each main phase itself includes both material scale and large scale examinations. The material scale parts are used as a pre-requisite section for the

component scale studies. A schematic representation of the individual studies included in this thesis and their contribution towards the main focus of thesis is illustrated in Figure 1.5.
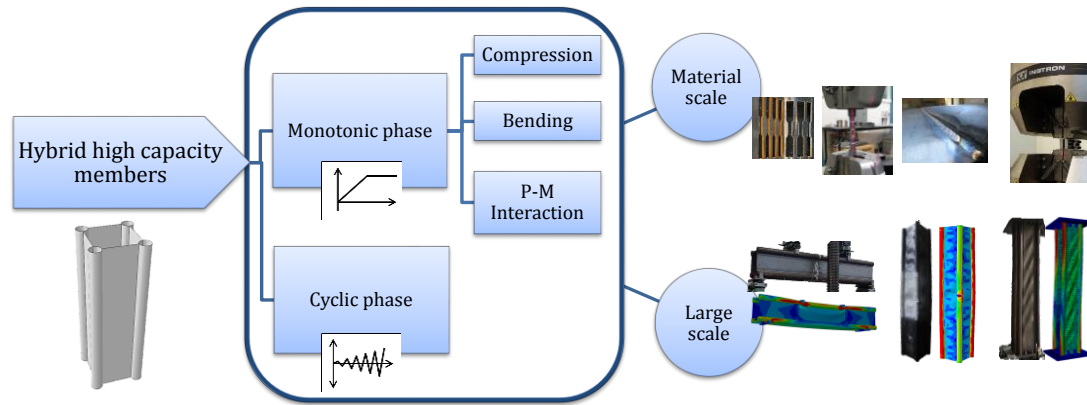
Figure 1.5. Innovative fabricated hybrid section

Chapter 1: Introduction

This chapter is an introduction to the overall structure of thesis. This includes the main objectives of thesis, explanations on the originality of thesis topic and how the research addresses knowledge gaps in the field. Thesis subject can be divided into two main sections, first being monotonic part and second cyclic section. First part consists of four chapters covering the basic compression studies on conventional and hybrid fabricated sections, bending investigations and the interaction of axial and flexural behaviour of sections. Second part of thesis focuses on the cyclic behaviour of hybrid members. Both main parts comprise of comprehensive experiments, detailed material tests and robust numerical modelling relevant to the loading conditions.

Chapter 2: Performance of innovative fabricated long hollow columns under axial compression

This chapter investigates the performance of full-scale innovative fabricated columns consisting of mild steel tubes in order to obtain a comprehensive view of the practical global and local bucking behaviour of the columns. Unlike all previous research conducted on innovative fabricated stub columns, this study is the first to look into the behaviour of long columns. Experimental compression tests are conducted on fabricated sections with one meter, two meters and three meters in addition to three similar-height control columns and three similar-length single tubes for comparison purposes. Besides the experimental work, a robust finite element model is developed. Initial conditions such as material and geometric nonlinearities, geometric imperfections and the residual stresses due to welding are also considered. Local and global buckling behaviour of each column, mechanical interactions, geometrical effects, and cost benefit analysis are also studied.

Chapter 3: Effect of weld on the mechanical properties of high strength and ultra-high strength steel tubes in fabricated hybrid sections

Following the previous works on ultra-high strength steel tubes, this chapter examines the behaviour of the heat affected material extracted directly from a fabricated hybrid section and presents analysis on the effect of weld on the properties of high and ultra-high strength tube. In this study, the axial material properties in the direction parallel to weld are examined, comparisons are performed and conclusions are presented based on the observations from three types of steels: Mild Steel (MS), High Strength Steel (HSS) and Ultra-High Strength Steel (UHSS) tubes welded to Mild steel plate material. Particular attention is placed on the ultimate tensile strength (UTS) and the strain corresponding to the UTS with regards to the effects of yield strength and strain hardening rate. Micro-scale observations are made on various locations of the affected steel and based on the microstructure and material type, welding procedures and post-welding conditions, the

mechanical properties are rationalised. Microhardness profiles are also obtained to justify the microstructure at various distances from weld.

Chapter 4: Application of high strength and ultra-high strength steel tubes in long hybrid compressive members: Experimental and numerical investigation

This chapter, as opposed to previous literature on fabricated hybrid sections which is only available on stub columns, experimentally investigates the behaviour of long innovative specimens fabricated from high strength (HSS) or ultra-high strength (UHSS) steel tubes and mild steel plates under static compression. The load-bearing performance of sections with HSS and UHSS is investigated and compared to ones consisting of mild steel tubes. The effect of welding on each individual constitutive element is taken into consideration to understand the detailed structural characteristics of the proposed high strength section. A basic simplified damage initiation model, followed by damage evolution extracted from the uniaxial tensile tests is introduced in simulations. These precise modelling factors have led to achieving a robust and precise numerical finite element model.

Chapter 5: Bending and axial compression interaction of high capacity hybrid fabricated sections

Due to the limited knowledge available, only on centrally loaded hybrid high capacity sections, this chapter extends the work to bending and combined interaction loading conditions, focusing on section geometry and steel material. Pure flexural performance of this innovative type of hollow fabricated section is investigated as a special case of the interactive condition where no axial compression loads are applied. Due to the unique geometry of the hybrid sections, an exclusive experimental setup was designed. Taking the event of local mechanisms into consideration the bending capacity of these thin-walled elements are predicted. Interaction curves are extracted for three types of fabricated hybrid beam-columns comprising of mild steel plates and mild steel (MS), high strength steel (HSS)

or ultra-high strength steel (UHSS) corner tubes. Analytical results obtained from plastic section investigations are compared against relevant practical design recommendations. In full-scale members, influence of generated shear stresses on beam-column member performance is particularly taken into considerations. Axial-lateral force interaction curves are parametrically studies for various geometries and steel materials.

Chapter 6: Fundamental behaviour of high strength and ultra-high strength steel subjected to low cycle structural damage

This chapter, examines the hysteretic response of high strength (grade 800) and ultra-high strength (grade 2100) steel material to contribute to the limited data currently available on these grades of steels in structural applications. All test specimens are extracted from high and ultra-high strength circular steel tubes and tested under strain and stress controlled amplitudes. Strain controlled tests are conducted in two types of constant and incremental amplitudes. Number of cycles and strain amplitude percentage are the two parameters considered in the constant strain controlled tests. Incremental strain amplitude tests are also conducted with varying strain steps. The obtained results show the occurrence of cyclic softening in both high and ultra-high strength steel materials. Based on the hysteretic response, relevant kinematic/isotropic plasticity parameters are proposed for high strength and ultra-high strength steel tubes which are applicable for modelling various scales of structures and structural components.

Chapter 7: Multiaxial seismic performance of high capacity hybrid fabricated beam-columns

Following previous series of experimental tests conducted on proposed fabricated hybrid sections, this paper focuses on the behaviour of these sections under multiaxial cyclic loads. For the aim of quantifying hysteretic performance of fabricated hybrid sections uniaxial, cyclic tests are conducted under unilateral displacement controlled conditions with

constant axial forces. Furthermore, multiaxial cyclic tests are performed investigating the coupled influence of varying axial forces and bilateral cyclic deformations. Strength and stiffness degradations are compared considering the effect of steel tube material. Plastic hinge development along hybrid members is also studied in the case of unilateral and bilateral reversed amplitudes. Influence of tube material, loading directions and varying compression force on failure modes and axial shortening of sections are also described. Results obtained from complete set of experimental cyclic tests lead to an overview of seismic performance of thin-walled high strength fabricated hybrid sections and can be incorporated in nonlinear structural models to accurately assess structures consisting of these types of high capacity components from onset of damage through to collapse.

1.5. References

[1] Shunsuke T, Koji S, Akio S. High strength steel tubes for automotive suspension parts - High strength steel tubes with excellent formability and forming technology for light weight automobiles. JFE Technical Report. 2004:32-7.

[2] Tanabe H, Anai I, Miyasaka A, Tanioka S. HAZ softening-resistant high-strength steel tubes for automobile propeller shafts. Nippon Steel Technical Report1995. p. 62-8.

[3] Vankuren RC, Scott JE. Energy absorption of high-strength steel tubes under impact crush conditions. SAE Technical Papers. 1977.

[4] Gangopadhyay KK, Guha D, Reddy PVN. Salt Lake Stadium roof, Calcutta, with high strength steel tubes. Structural engineer London. 1990;68:397-404.

[5] http://www.tenaris.com/en/default.aspx. In: tenaris.com, editor.

[6] EN/BS. 1-12. Eurocode 3: Design of steel structures: Part 1–12: Additional rules for the extension of EN 1993 up to steel grades S700. London: BSI2007.

[7] ANSI/AISC. Specification for structural steel buildings. AISC 360-10: American institute of steel construction; 2010.

[8] AS 4100-1998, Steel structures. Sydney: Standards Australia; 1998.

[9] RAEX® R. Demand more from wear-resistant steels. RUUKKI RAEX® REFERENCES.

[10] Long HV, Jean-François D, Lam LDP, Barbara R. Field of application of high strength steel circular tubes for steel and composite columns from an economic point of view. Journal of Constructional Steel Research. 2011;67:1001-21.

[11] Zhao XL, Van Binh D, Al-Mahaidi R, Tao Z. Stub column tests of fabricated square and triangular sections utilizing very high strength steel tubes. Journal of Constructional Steel Research. 2004;60:1637-61.

[12] Rhodes J, Zhao XL, Van Binh D, Al-Mahaidi R. Rational design analysis of stub columns fabricated using very high strength circular steel tubes. Thin-Walled Structures. 2005;43:445-60.

[13] Van Binh D, Al-Mahaidi R, Zhao XL. Finite element analysis (FEA) of fabricated square and triangular section stub columns utilizing very high strength steel tubes. Advances in Structural Engineering. 2004;7:447-57.

[14] Heidarpour A, Cevro S, Song QY, Zhao XL. Behaviour of innovative stub columns utilising mild-steel plates and stainless steel tubes at ambient and elevated temperatures. Engineering Structures. 2013;57:416-27.

[15] Heidarpour A, Cevro S, Song QY, Zhao XL. Behaviour of stub columns utilising mild-steel plates and VHS tubes under fire. Journal of Constructional Steel Research. 2014;95:220-9.

[16] E606-04 Standard Practice for Strain-Controlled Fatigue Testing. ASTM International; 2004.

[17] AS 1391-2007 Metallic Materials-Tensile testing at ambient temperature. Sydney: Standards Australia; 2007.

[18] Dwight JB. Welded Steel Plates in compression. The structural engineer. 1969;47:49-66.

[19] Mazzina R, Gomez G, Solano M, Perez T, Lopez E. Study on weldability of high strength steel for structural applications. ASM Proceedings of the International Conference: Trends in Welding Research2013. p. 208-16.

[20] Jiao H, Zhao X-L. Tension Capacity of Very High Strength (VHS) Circular Steel Tubes after Welding. Advances in Structural Engineering. 2004;7:285-96.

[21] Shi G, Jiang X, Zhou W, Chan T-M, Zhang Y. Experimental investigation and modeling on residual stress of welded steel circular tubes. Int J Steel Struct. 2013;13:495-508.

CHAPTER 2

Performance of innovative fabricated long hollow columns under axial compression

Monash University

Declaration for Thesis Chapter 2

Declaration by candidate

In the case of chapter 2 my contribution to the work involved the following:

Nature of contribution	Extent of contribution (%)
Developing ideas, Establishing methodologies, Experimental work, Data analysis, Write-up and revision	70%

The following authors contributed to the work:

Name	Nature of contribution	Extent of contribution (%)
Dr. Amin Heidarpour	Developing ideas, Input into manuscript, Revision, Financial support	18%
Prof. Xiao-Ling Zhao	Revision, Financial support	10%
Mr. Jussi Minkkinen	Providing tube specimens, Revision	2%

The undersigned hereby certify that the above declaration correctly reflects the nature and extent of the student's and co-authors' contributions to this work.

Student signature ███████ Date: 30/01/2017

Main Supervisor's signature ████████ Date: 30/01/2017

2.1.   Abstract

Fabricated sections are a convenient option for structures or structural elements in demand of very high strength capacities in which conventional hot-rolled and cold-formed elements with limited sizes have inadequate capacities. When it comes to the design of compressive members, buckling is a critical design provision. In this paper the compressive and buckling behaviour of an innovative long column is described. The innovative fabricated columns are consisting of mild steel plates which are welded to mild steel tubes at corners. Experimental tests are conducted on one, two and three-meter columns whilst a robust finite element model is also developed which is validated against the results obtained from the experiments. Detailed focus is brought to the effect of fabrication imperfections, type of welding and residual stresses on the behaviour of the proposed long hollow columns in test result analysis and the finite element modelling. The examined innovative column specimens are shown to exhibit superior compressive behaviour since the interaction between section's plates and tubes leads to a significant increase in both strength and ductility. In addition to the structural benefit, the production cost of these columns is estimated which also justifies its advantage compared to the equivalent welded box sections in an economic point of view.

Keywords: Innovative hollow column, mild-steel plate, tube, compressive strength, buckling.

2.2.   Introduction

In addition to usual design factors such as strength and ductility, the buckling behaviour turns into a main concern when it comes to the design of a compressive member. Basically, apart from global buckling and yield of structural elements under compression, local buckling is particularly an effective factor when the column section consists of thin plate elements. Most hot rolled members having thick plate elements are unlikely to experience such local buckling behaviour, whereas in fabricated (built-up), cold formed and light-gauge steel sections this is considered a main concern in the design procedure. However, the later types of sections mentioned above can be designed in various geometries and are more convenient in structures that are in demand to withstand a considerable amount of load. Thus, in the case where conventional hot-rolled sections have inadequate capacities, it can be highly beneficial to design fabricated columns with innovative cross-sectional shapes with convenient local or overall buckling behaviour and a very high load-bearing capacity at the same time. Furthermore, the available cold-formed sections namely, circular and square hollow sections, have limitations in the available dimensions and increasing the width or diameter will require a much higher production cost. In the analysis procedure of fabricated sections, imperfections and the heat effects due to the welding or shaping procedures are factors which need attention [1-3].

A number of different experimental and analytical studies can be found on the introduction of new unaccustomed section shapes considering the effect of geometry on the local and interactional buckling behaviour [4-7]. These innovative column members are produced by cold-forming in which section are open unless in situations where the ends of shaped plates are welded together. This welding procedure requires an extra effort in terms of industrial production in addition to the forming procedure. Based on studies conducted by Vales [8], besides the normal stresses produced in compressive sections, torsion, warping and bi-

moment lead to additional stresses. These circumstances result in a reduction in the load carrying capacity of open sections compared to closed ones. Unlike previous types of conventional and new sections, the innovative section chosen in this study, namely innovative fabricated column (IFC), is unique in terms of having an overall closed square core consisting of four plates in addition to four closed tube elements. This results in a relatively high bending and torsional stiffness in the column. Another geometric advantage of this innovative cross-sectional shape is its practicality in construction, especially in terms of connecting to other structural members.

The spoken innovative fabricated section has lately been introduced and a number of researchers have worked on various aspects of its behaviour. Steel sections fabricated from the combination of plates and tubes were introduced by Aoki and Ji [9]. Stub columns with triangular shaped plate sections consisting of pipes at each apex were experimentally investigated under uniform compression and eccentric loading. The initiating local buckling load was investigated by obtaining the load-displacement curves of the stub columns and the load-strain curves of the plates. Zhao et al. [10] further improved the compressive behaviour of square-tube and tri-tube fabricated sections by substituting conventional tubes with very high strength steel at each corner. Experimental tests were conducted on different section geometries and two design models were proposed for these sections. Finite element analysis was also done by Van Binh et al. [11] with results compared to experimental outcomes and two analytical procedures were also proposed. The analysis procedure of fabricated sections up to the yield of VHS tubes, and the failure mechanism after that were studied by Rhodes et al. [12]. Experimental and numerical results were also matched. In the plastic mechanism analysis carried out by Ye et al. [13] three different stages were considered and a simplified theoretical formula was proposed. In two recent research works in this area, Heidarpour et al. [14, 15] utilised both very high strength steel tubes and stainless steel tubes in the corners of plates and tested a variety of geometries.

The behaviours were examined in elevated temperatures in addition to ambient temperatures and observations were reported. Furthermore, numerical models were developed and compared to experimental data. The behaviour of concrete filled innovative sections, under axial loading in addition to some design formulations has been presented by Mashiri et al [16].

In this paper the performance of real scale innovative fabricated columns are investigated in order to obtain a comprehensive view of the practical global and local bucking behaviour of the columns. Unlike all previous research conducted on innovative fabricated stub columns, this study is the first to look into the behaviour of long columns. Experimental compression tests are conducted on the specimens with one meter, two meters and three meter fabricated columns in addition to three similar-height control columns and three similar-length single tubes for comparison purposes. Besides the experimental work, a robust finite element model is developed. Initial conditions such as material and geometric nonlinearities, geometric imperfections and the residual stresses due to welding are also considered. Local and global buckling behaviour of each column, mechanical interactions, geometrical effects, and cost benefit analysis are also studied.
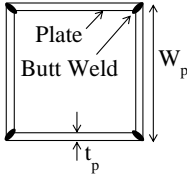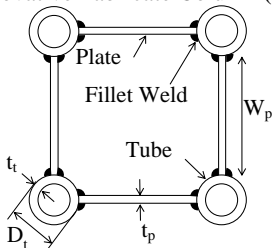
2.3. Experimental Phase

2.3.1. Section Specifications

Three different fabricated specimens with lengths equal to one, two and three meters have undergone compressive tests. The geometric configuration and specification of fabricated square sections and single tubes are shown in Table 2.1. **S**ingle **t**ubes are denoted as **ST** which is followed by the tube length. **C**onventional welded box **c**olumns and **i**nnovative

fabricated columns are denoted as **CC** and **IFC,** respectively, which are followed by the column length. The nominal diameter (D_t) and wall thickness (t_t) of tubes are 76.1mm and 3.2mm, respectively, while the flat steel plates have a width of 210mm and a thickness of 3mm. Material utilised for both the plate and tube elements of each column is Grade 250 mild steel. Long fabricated columns utilising high strength and ultra-high strength steel tubes are currently being studied at Monash University.

Table 2.1. Geometric properties

Title and Geometry	Specimen Label	Length L (mm)	Maximum Imperfection (mm)	
			Transverse direction	Longitudinal direction
Single Tube (ST)	ST1	1000	-	less than 0.4
	ST2	2000	-	
	ST3	3000	-	
Conventional Column (CC)	CC1	1000	0.5	0.9
	CC2	2000	1.8	1.5
	CC3	3000	1.0	1.3
Innovative Fabricate Column (IFC)	IFC1	1000	1.0	2.4
	IFC2	2000	1.2	3.0
	IFC3	3000	1.1	2.1

2.3.2.   Material Properties

In order to have a realistic modelling of the columns for further numerical analysis, tension testing on the specimens taken from both mild steel plate and tube are conducted following the guidelines of ASTM [17] and at the same time meeting the recommendations of Australian Standard AS1391 [18]. Three tensile specimens are extracted from the two different steel members of the section, plates and tubes, as shown in Figure 2.1(a) and (b). The final material results are based on averaged values. Knowing standard guidelines, care is taken in tube coupon extraction to have an acceptable distance from the welded area and accurate dimensional measurement of coupon specimens is done prior to testing. For accurate data collection throughout the test, one strain-gauge is used at each side of the specimen centre in addition to a non-contact laser extensometer. Strain gauges help to have precise initial data reading for obtaining the modulus of elasticity and the pre-yield strain, while the laser extensometer is more useful to capture a wider range of strain data until reaching the failure load. Nominal averaged mechanical properties of mild steel plate and tube are shown in Table 2.2. Proof stress for the specimens taken from mild steel plate and tube is determined using the offset method with a lay-off equal to 0.2%.

Table 2.2. Nominal mechanical properties of steel material

	Module of Elasticity (MPa)	Proof stress (MPa)	Tensile Strength (MPa)	Strain corresponding to tensile strength (εu)
Plate Mild Steel	207609	265	376	23%
Tube Mild Steel	198809	305	342	11%
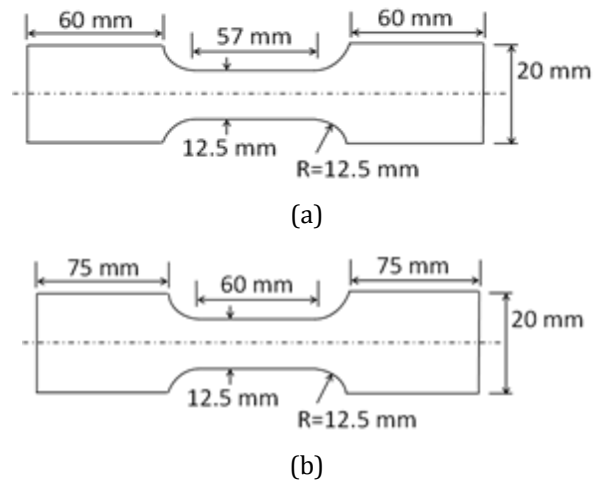
Figure 2.1 Dimensions of tension test specimens: (a) Extracted from mild steel plate; (b) Extracted from mild steel tube (not to scale)

2.3.3. Fabrication Process, Welding and Imperfections

Fabrication procedure and type of welding has an important effect on the behaviour, ease of production and economic feasibility of columns. The type of welding used for the fabricated columns proposed in this paper is fillet weld and that for conventional fabricated box sections is a two pass butt weld from the outer area penetrating to the inside. In terms of fabrication, both inner and outer parts of the connections between plates and tubes of an innovative fabricated column can be welded. In order to assess the weld effect on the behaviour of columns, different weld patterns are selected for each specimen. Two-sided fillet welds are used in the one meter column, complete outer side and half inner side welding pattern is accomplished in the two meters column, and finally the three meters column is only welded externally (Figure 2.2). The effect of this variation is investigated and efficient recommendations are presented based on observations. Different welding specifications are applied in three meters columns compared to the shorter ones. In one and two meters columns, the weld wire is 0.9mm of classification AS 2717.1 (AWS: ER 70S-6). Type of welding is MIG–with a yield stress and tensile strength equal to 450MPa and 550MPa, respectively. In the three meters column, the welding wire is 2.4mm of the

category AWS A5.9 ER2209. Type of welding is gas tungsten arc welding (G.T.A.W) with a 0.2% proof stress and tensile strength equal to 560 – 620MPa and 800 – 835 MPa, respectively. The rate of welding for all fabrications is in a range of 75-95 mm/min and the gas used is 99.9% argon gas. All welding methods used are in compliance with AS/NZS1554.7:2006 [19].
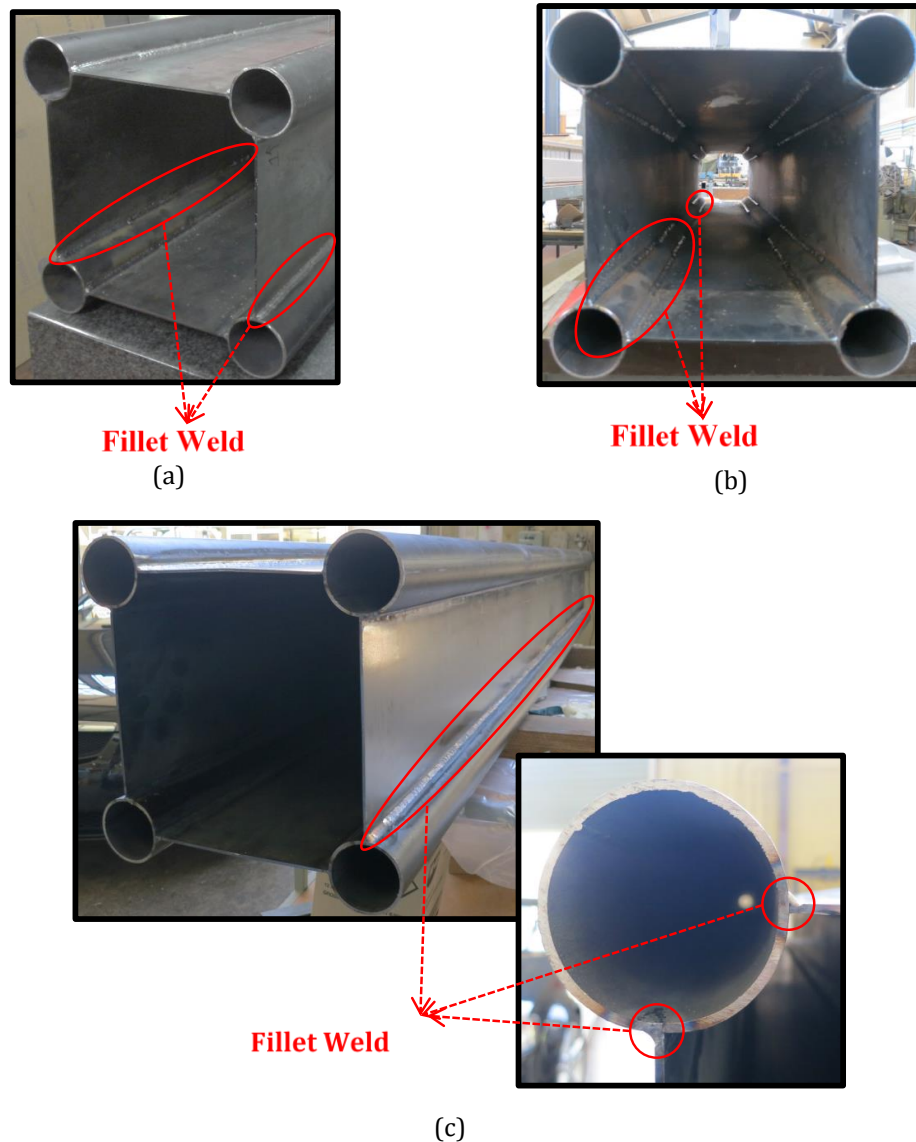
Figure 2.2 (a) 1m column complete inside and outside welding; (b) 2m column complete outside and half inside welding; (c) 3m column complete outside welding only.

In welded sections, dislocations and imperfections are an inevitable aftereffect of fabrication. These initial conditions impinge upon the peak load, local buckling of each

element and also the overall behaviour of structure. In this study, the effect of imperfections is taken into consideration for analysing the buckling behaviour of different specimens. Imperfection measurements are operated in two directions in all fabricated columns considering a unique reference point using the setup shown in Figure 2.3(a). The measurement device consists of a digital indicator mounted on a vertical stand ruler both located on a precise horizontal table. Along the width of each plate, out-of-square (δ) and out-of-flatness (Δ) are measured (Figure 2.3(b)) and compared to the maximum values allowed for web elements of fabricated sections in Australian Standard 4100 [20]. Furthermore, deviations along the overall length of column plates and tubes are measured and compared with the maximum straightness permitted. All maximum imperfections satisfy the standard provisions and are presented in Table 2.3.

(a) (b)
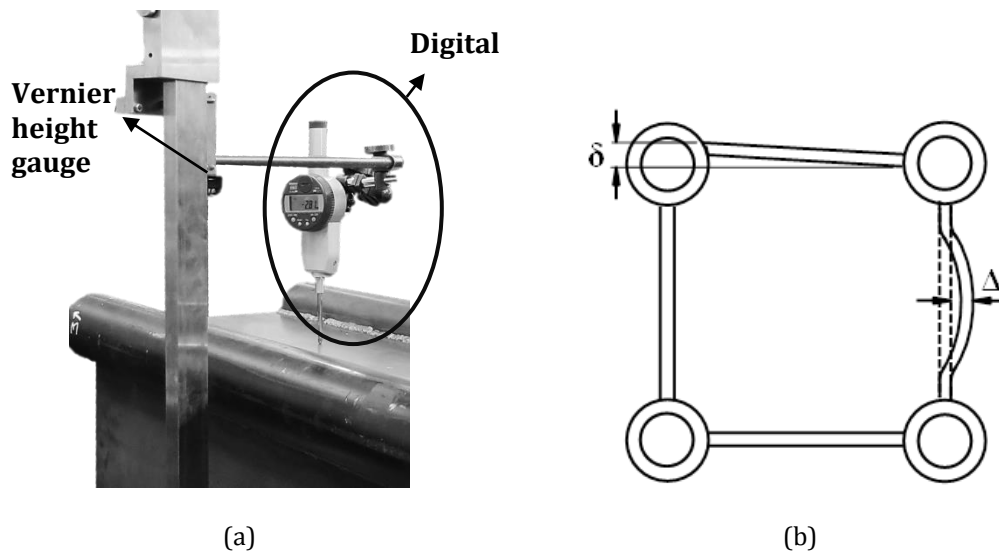
Figure 2.3. (a) Imperfection measurement setup; (b) Out-of-square and Out-of-flatness of section.

2.3.4. Test Setup

All specimens in this study are tested using a 5000kN capacity Amsler Testing Machine. Fixing heavy blocks are used on the top and bottom plates of the machine to reach maximum possible clamped condition in both sides of each column. For accurate monitoring the geometric changes in the specimens, two Linear Variable Differential Transformers (LVDTs) are used on two opposite corners of the loading plate in addition to a number of strain gauges mounted on all column specimens. In the innovative fabricated columns, three strain gauges are used in quarters of the length of one plate and one tube and all the remaining plates and tubes have one strain gauge on their mid-length. The same pattern of three strain gauges on quarter-lengths on one side and one strain gauge on the mid-length of the remaining sides are used for the conventional welded box columns and single tube specimens. To minimise the inertial effects for simulating a static compressive test, loading with a rate equal to 0.5mm/min is applied. During each test the loads, displacements and strains are recorded corresponding to each second of the test using a data-taker. In order to avoid intensive local buckling of tube in the vicinity of loading plates, two steel supports with a thickness equal to 25mm are used for fully fixing each end of the single steel tube.

2.4. Numerical simulations

Instability can become one of the major issues of nonlinear analysis of structures due to a variety of reasons such as local and global buckling which are dominant phenomena in the present study. Methods such as performing a displacement controlled analyse, stabilising the structure during a static test with the aid of (artificial) damping or dashpots and using the modified Riks method are approaches by which these types of unstable situations can be dealt with. Finite element software such as ABAQUS [21], perform several increments

each having a number of iterations in which the system of equations is finally solved and an equilibrium state is found for the whole structure. Imperfections are also applied on the perfect geometry in order to achieve response in the buckling mode before reaching the critical load.

2.4.1.   Initial Modelling

The numerical modelling is made in the commercial finite element software, ABAQUS. Validation of a numerical model with the experimental results helps to have a robust model for further studies on the behaviour of various types of the proposed fabricated columns with different geometries. Due to the small thickness of plates and tubes compared to other column dimensions, sections are modelled as shell. Welds are also modelled as solid elements connecting a specific area of each plate to the adjacent tube. S4R (four node shell element) and C3D6 (six node wedge element) with a size of 5mm mesh are used for meshing shell and solid parts, respectively. Nonlinear material properties are accurately processed and used as input material data in ABAQUS. The elastic modulus and yield strength of mild steel is extracted directly from the nominal data obtained through material tests. Isotropic hardening behaviour of steel is calculated from true material data since the initially measured dimensions are no longer valid at this stage. Based on the fact that in the plastic phase material flows with negligible change in volume, true stresses and logarithmic strains are calculated from

$$\sigma_t = \sigma_e(1+\varepsilon_e) \quad , \quad \varepsilon_t = \ln(1+\varepsilon_e) \tag{2.1}$$

where σ_e and ε_e are the engineering stresses and strains, respectively, and σ_t and ε_t are the true stresses and strains, respectively. The plastic hardening strain input for ABAQUS is calculated from the true properties and given to the software as tabular input data.

2.4.2.   Imperfections and Analysis Procedure

Two subsequent methods are used to conduct the compressive loading and post-buckling analysis of columns. The first step is a linear perturbation buckling analysis on the column. Fixed boundary conditions in all end nodes are set except in axial directions of one end which unit displacement is applied. Critical buckling displacement and final nodal displacements of the model in each buckling mode are obtained. The next step is a nonlinear Riks analysis. An important input for the nonlinear analysis is the initial imperfection data. With the lack of initial imperfection input, the nonlinear post-buckling analysis returns a discontinuous response at the point of buckling, namely the bifurcation point. Imperfection inputs turn the post-buckling analysis into a continuous response. In this case, a response is achieved in the buckling mode and after that the structure reaches a maximum load which is called a limit or snapping point. In the present numerical study, initial imperfections explained in Section 2.3.3 are given as a factor of the first mode of the linear perturbation buckling analysis. The factor is obtained based on the maximum imperfection measurements of individual column elements.

2.4.3.   Residual stresses due to welding

During the welding procedure on each section, very high amounts of temperature (over 2000^0C) is applied to the steel plate material which has direct effects on the final strength of the columns and is necessary to be considered in numerical analysis and design calculations. Welding procedure produces shrinkage forces leading to generation of residual stresses in the welded area. Throughout the cooling stage, thermal unloading generates tension in the welded area and, due to equilibrium in the overall length of plate, the remaining parts undergo a certain amount of compression. Obtaining the exact amount of these stresses requires additional experimental measurements or specific thermal analysis. In order to peruse a simple simulation of the stresses induced in plates, a model

proposed by Dwight [22] is adopted. In this model a specific width in the vicinity of weld undergoes a tensile stress equal to the yield strength of steel and in the remaining parts of the plate compressive stress is generated satisfying the longitudinal equilibrium. The width of tension block is calculated from Eq (2.2) for plates with different thicknesses in which

$$\eta_n t_n = \frac{C\,A}{\sigma_y \sum t} \tag{2.2}$$

where C is the design bending moment, A is the cross-section area of the added metal, t is the coefficient with dimension of stress and σ_y is the yield stress. The above formula is also applicable for two or more plates being welded at one intersection and for welds occurring at the middle of plates. Residual stress distribution in tube elements are also modelled based on previous studies specifically undertaken on circular tubes [23]. The residual stress distribution of the section part specified in Figure 2.4(a) is presented in Figure 2.4(b) while the rest of the residual stresses are obtained based on symmetry. Coloured zone in the small section shows the tension block and shaded colour shows the parts under compressive stress. Corresponding weld residual stresses of different material elements are introduced to ABAQUS as initial conditions according to their local axis directions.

(a)   (b)
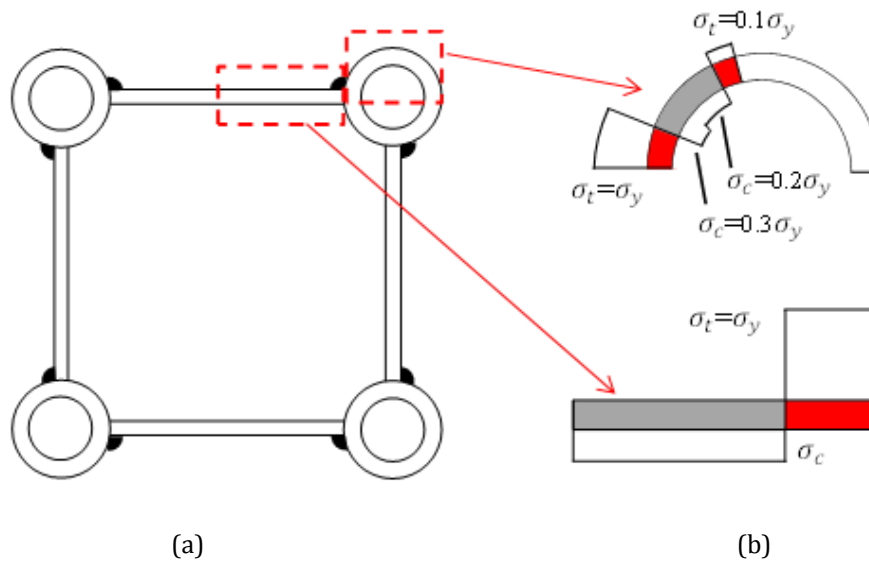
Figure 2.4. (a) A view of typical column cross-section; (b) Weld residual stresses

2.5.   Results and discussions

2.5.1.   Strength and ductility

The load bearing capacity of each specimen obtained from experimental compressive test is presented in the first three columns of Table 2.3. It is obvious to observe a decline in the peak load undertaken by the two meters IFC member compared to the one meter one, due to the increase in length and more geometrical imperfections generated during the fabrication process. As mentioned in Section 2.3.3, the manufacturing procedure applied in the three meters IFC member was changed compared to the method used in the one and two meters columns. The alternative method results in much less imperfections in the plates which directly affects the compressive results and justifies the irregularity. In addition to the reduction in imperfection values in the three meters column, the welding wire strength and thickness increased compared to the weld in the two shorter columns which also justifies the irregularity in the compressive strength trend with length increase. This leads to a conclusion regarding the fabrication which is omitting the inner weld in IFC members does not have a significant effect on the overall behaviour. In addition to the compressive strengths, two other key factors are extracted and compared in Table 2.3. The first is the ratio of peak load of IFC members to that of the CC members without corner tubes. It can be seen from Table 2.3 that in all three column lengths this proportion is approximately equal to four. Since the configuration of plates is similar in both IFCs and CCs, other behavioural aspects of these two elements are later compared in detail. In the interest of having a comparison among two sections with same cross sectional areas, the second comparison is drawn. Accordingly, four times of the capacity of a single tube tested under static compression is added to the capacity of a CC member with the same length in which the summation of cross-sectional areas is the same as that for the corresponding IFC member. The last column of Table 2.3 draws an analogy between the two aforementioned

values. On the basis of these ratios, it is clearly evident that IFC members exhibit around 20-30% higher strength compared to the summation of similar elements acting individually. The significant increase in the strength of IFC sections shows that a more efficient buckling performance observed in these sections leads to taking highest advantage of the material and section capacity. The mechanical theory that leads to the high performance of columns is further argued in next sections. Beside the ratio comparison, the complete load versus displacement curves for the one meter and three meters length single tubes, CC and IFC members as well as superposition case described above are also shown in Figure 2.5.

Table 2.3. Experimental compressive load bearing capacities (kN) and important ratios

Length	IFC capacity	CC capacity	ST capacity	Superposition: $4 \times ST + CC$	IFC to CC ratio	IFC to Superposition ratio
1m	1523	379	222	1266	4.0	1.2
2m	1411	361	204	1179	3.9	1.2
3m	1465	398	176	1102	3.7	1.3

Two apparent differences are noticeable in the behaviour of IFC and CC members: strength and ductility. With a view to obtain a measurement for the ductile compressive behaviour of the innovative fabricated columns, the displacement ductility factor is introduced as [24]

$$\mu = D_u / D_y \tag{2.3}$$

in which D_u is the displacement corresponding to the ultimate compressive load, and D_y is the displacement where the first yield point occurs in the system. In order to obtain μ, corresponding displacements are extracted from Figure 2.5. Dividing the two values of

displacements for 1m and 3m CC members gives displacement ductility factor respectively equal to 3.0 and 3.9. For 1m and 3m IFC members displacement ductility factors are equal to 9.42 and 5.4, respectively. From Figure 2.5 it can be seen that the IFC3 member shows a very ductile behaviour under its ultimate capacity such that under a displacement equal to 35mm, the column can carry around 98.4% of the ultimate load. If this displacement is considered to calculate the μ factor, the ductility of long IFC3 member is advanced to around two times of the corresponding conventional column. It is perceived that the main cause of high ductility of the IFC member is due to the different behaviour and mechanisms in plates and the load bearing effect of tubes which is further explained in the next section. High ductility of the innovative fabricated columns is an advantage for its use in the design of structures undergoing seismic loadings. The seismic behaviour of these columns is currently studied at Monash University.
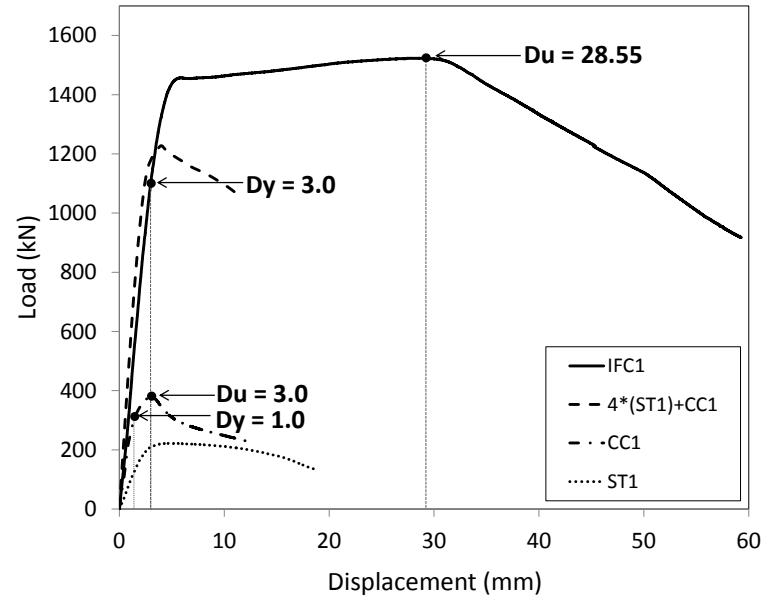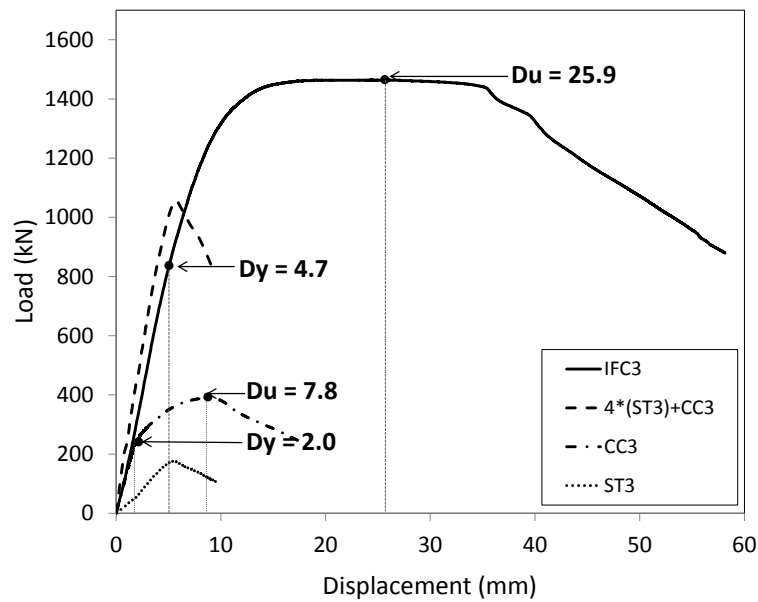
Figure 2.5. Load-displacement curves for (a) 1m and (b) 3m specimens

In addition to the aforementioned performance comparison of IFC with conventional fabricated box columns, it is also worth to compare the compressive behaviour of the proposed sections with cold-formed steel sections due to their wide application in steel construction. However, since in the current civil engineering market there is no cold-formed section whose weight, coverage area and steel grade are similar to those of IFC members

used in this paper, in order to have a fair comparison a virtual square cold-formed hollow section is chosen in a way such that it has similar weight, coverage area and steel grade to those of IFC members and its ultimate compressive strength is calculated based on the following design formulations given by AS4100 [20]:

$$N_s = A_n f_y k_f, \qquad \lambda_n = \left(\frac{l_e}{r}\right)\sqrt{\frac{k_f f_y}{250}}, \qquad N_c = \alpha_c N_s \qquad (2.4)$$

in which, N_s, k_f, λ_n, α_c, N_c respectively are the nominal section capacity, form factor, nominal slenderness ratio, dimensionless nominal axial force capacity factor and nominal member capacity. The typical cold-formed section made of Grade 250 steel with dimensions of 360×360×4 mm weighing equal to 44.9kg which is somewhat higher than the IFC section weight of 42.5kg. Using Equation (2.4) the compressive strength of the 1m cold-formed column is equal to 670kN which compared to the compressive strength of IFC1 (Table 2.3), 227% increase in the load bearing capacity is achieved by incorporating the innovative section.

2.5.2.   Failure mechanism

Failure mechanism of long innovative fabricated columns is affected by the interactive behaviour of the individual elements. During the loading process, plates show significant deformations while tubes undergo a high amount of stress. Detailed understanding of plate and tube performance can be traced from the load and strain-gauge data recorded during the test. Variation curves of the absolute value of the strain-gauge undergoing the highest deformation on each column versus load are presented in Figure 2.6(a)-(e). The magnitude of stress in the peak load of each tube or column is extracted from the corresponding material curves. The value of strain and its corresponding stress is shown on each curve for comparison purposes. As for the magnitude of strains and stresses experienced in single tubes against the tubes incorporated in innovative fabricated sections Figure 2.6(a)-(c), a

significant difference is observed. With the increase in length, the peak resisted stress in the corner tubes of IFC members drops, however, even in the 3m IFC member the peak generated stress is just slightly (3%) less than the ultimate strength, whereas, in the 3m single tube the stress even fails to reach the yield strength. Same argument can be made for all other column lengths. This behaviour brings out an important fact about the high strength characteristic of long IFC members and that is, unlike single steel tubes, the special design of the innovative sections gives the tube elements a chance to withstand stresses as high as their ultimate strength.

Similarly, the Figure 2.6(d) and e curves are drawn out for the strain-gauges attached on the mild steel plates undergoing the highest deformation in conventional box sections and mild steel plates in the innovated fabricated sections. It is interesting to point out that in the mild steel plates used in IFC members the maximum strain level grows in the 3 meters column compared to the 1 meter one. However as mentioned before, since the plates do not undergo a significant amount of stress, the highest value observed in all plates is around the yield strength. Attention to failure mechanism of these columns helps justify this fact. Figure 2.7 shows failure mechanism of single tubes, innovative and conventional columns with three different lengths. Regardless of length, global buckling in single tubes, flip-disk mechanism in conventional box columns and roof-shaped mechanism in innovative fabricated columns are observed. The formation of plastic hinges in plates with roof-shaped deformations results in a high ductile behaviour. In the conventional box sections only one flip-disk mechanism is observed on the plates which that leads to the failure of column. However, in the IFC members, roof-shaped mechanism is occurred in several locations through the length, mostly close to the centre, and the number of this occurrence increases along with the height of columns. This is the reason of the high ductility and lets the column more efficiently take advantage of the plate capacity.

(a)

(b)

(c)

(d)

(e)
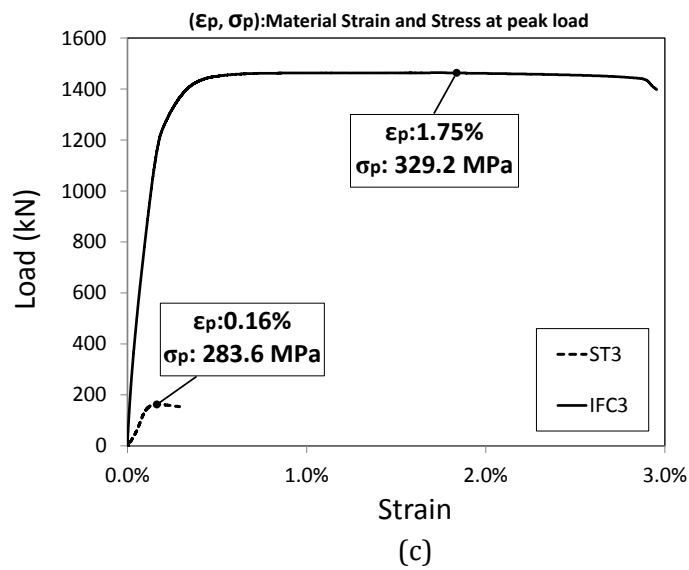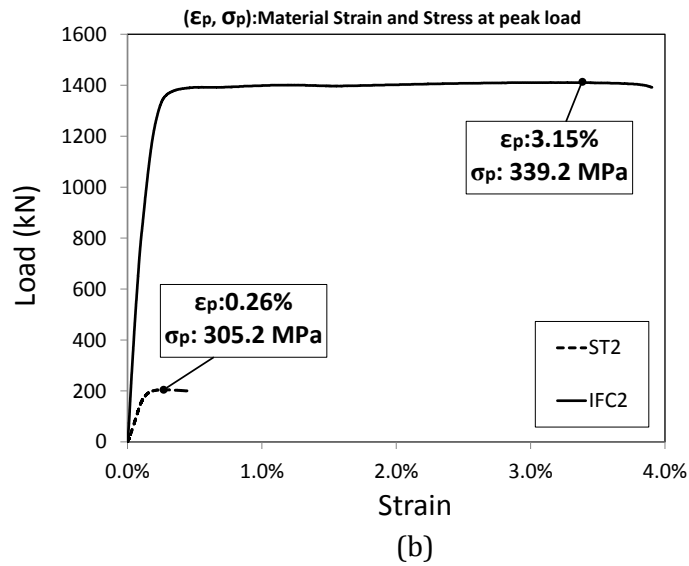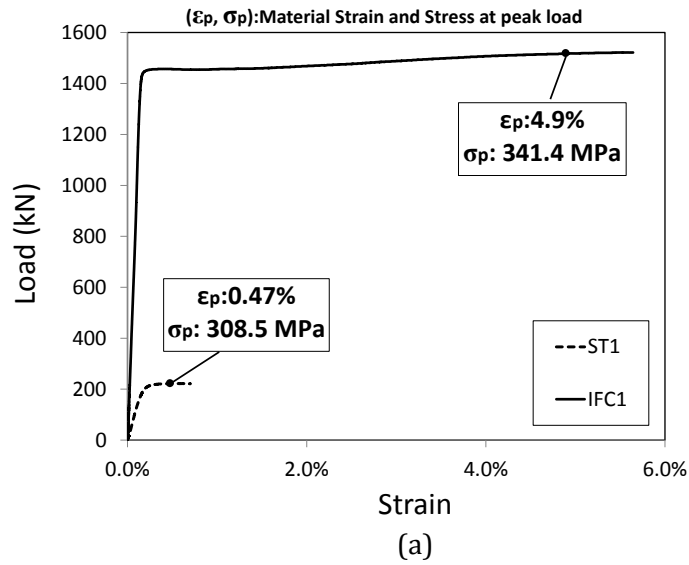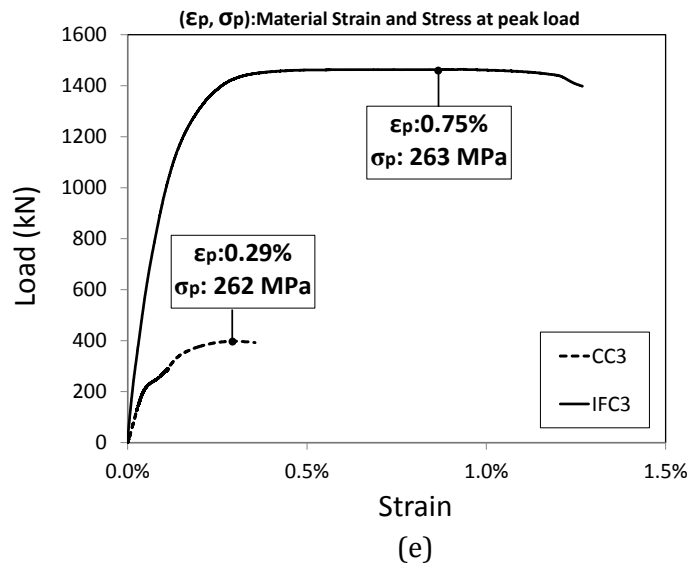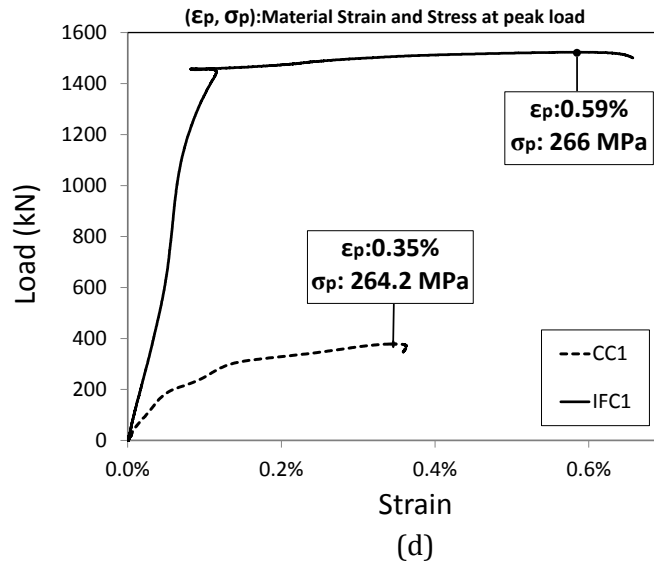
Figure 2.6. Load versus strain in single tubes and tubes of innovative fabricated columns (a) 1m, (b) 2m, (c) 3m; Load versus strain in plates of conventional column and innovative fabricated column (d) 1m, (e) 3m
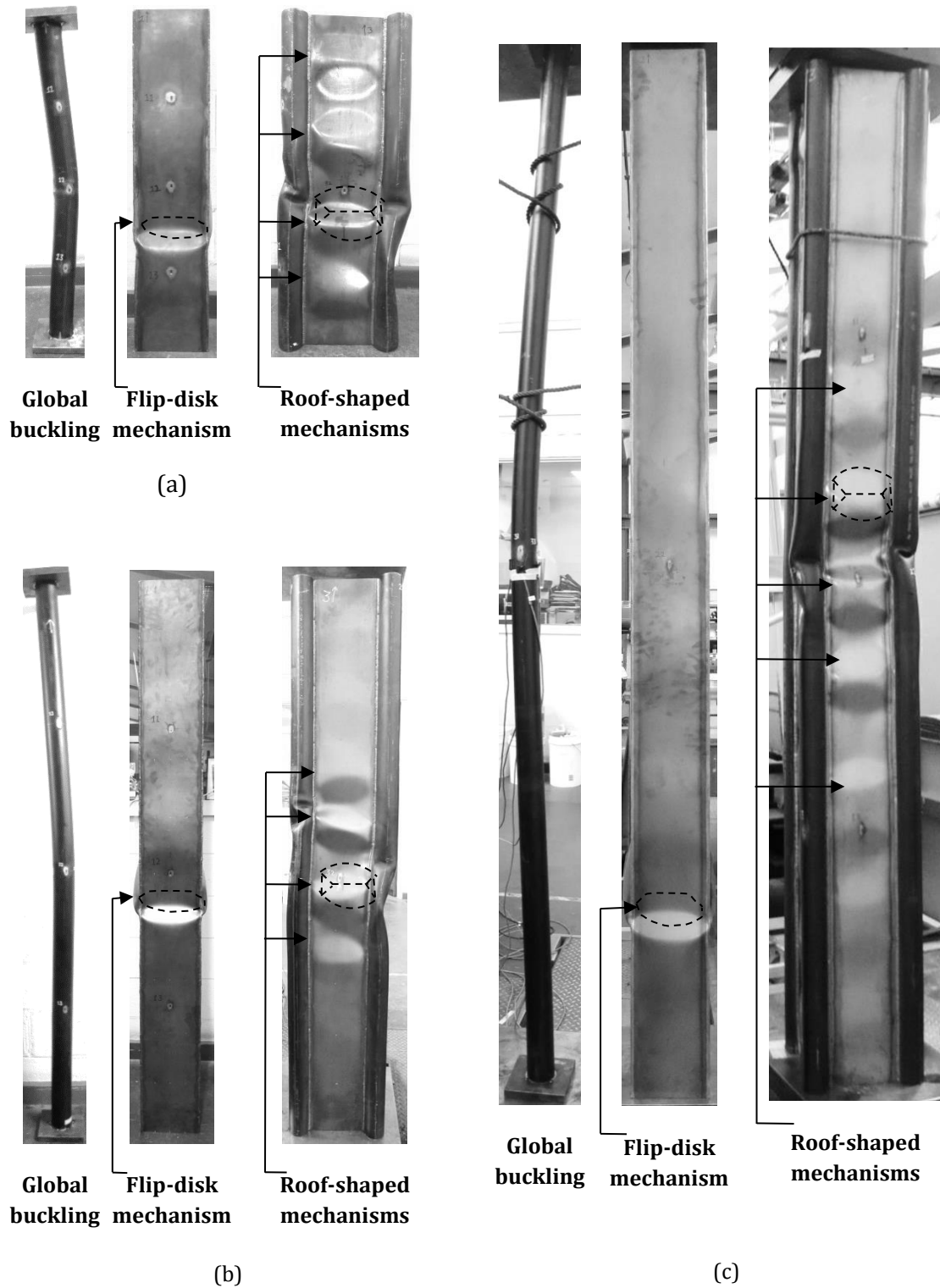
Figure 2.7. Failure mode comparison of innovative fabricated column, conventional box column and single tube (a) 1m, (b) 2m, (c) 3m.

Due to the fact that stresses in plates in a box section, are mostly carried by the edges [25], existence of tubes at corners becomes an extra advantage in innovative sections. Subsequently once plates reach the yield stress, tubes continue undertaking more stresses and further increasing the overall capacity of the section until the ultimate load and plates continue to have more deformations and experience higher strain quantities.

2.5.3. Model validation

Results of one meter and three meters IFC members' strength from numerical simulations and experimental tests are compared in Figure 2.8. The curve in Figure 2.8 shows the load versus strain in each specimen type. Strain data in the horizontal axis of each curve is obtained from the average strain-gauge readings on columns before the local buckling in members and from the total displacement of column measured by LVDTs after that point. Failure modes are also compared in the numerical and experimental specimens showing a reasonable agreement. It can be seen from Figure 2.8 that the individual local buckling and overall behaviour of the model in one meter and three meters columns represent similar performance in comparison to the experiments. As a matter of fact, the column strength which is the main concern for structural design purposes is also captured with a deviation less than 1%.
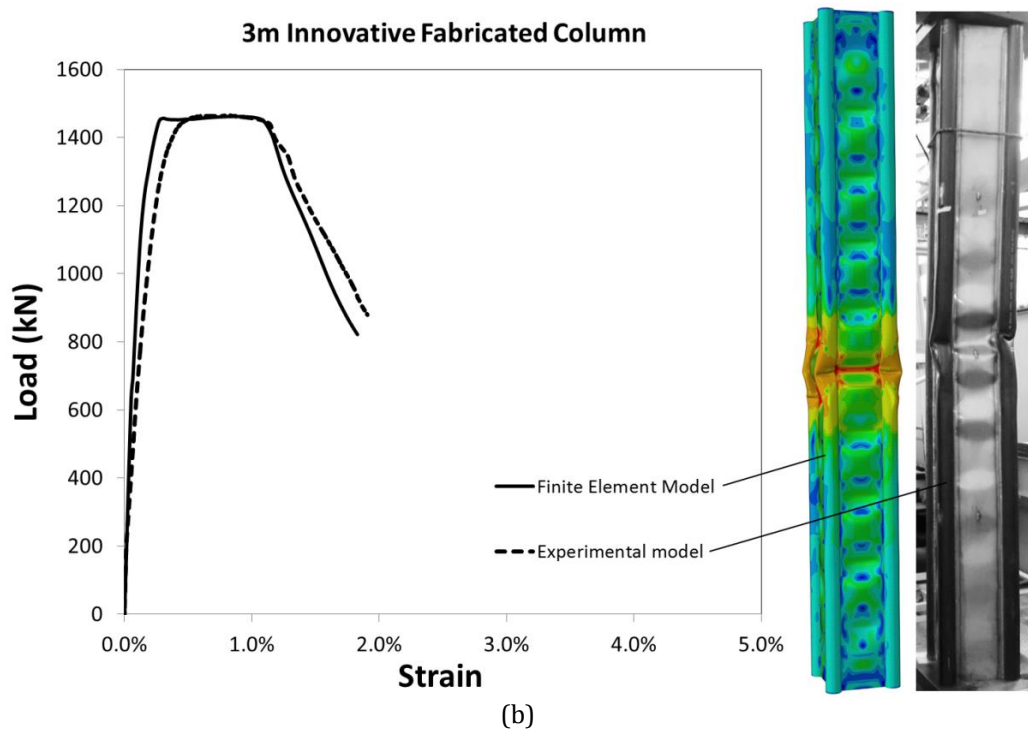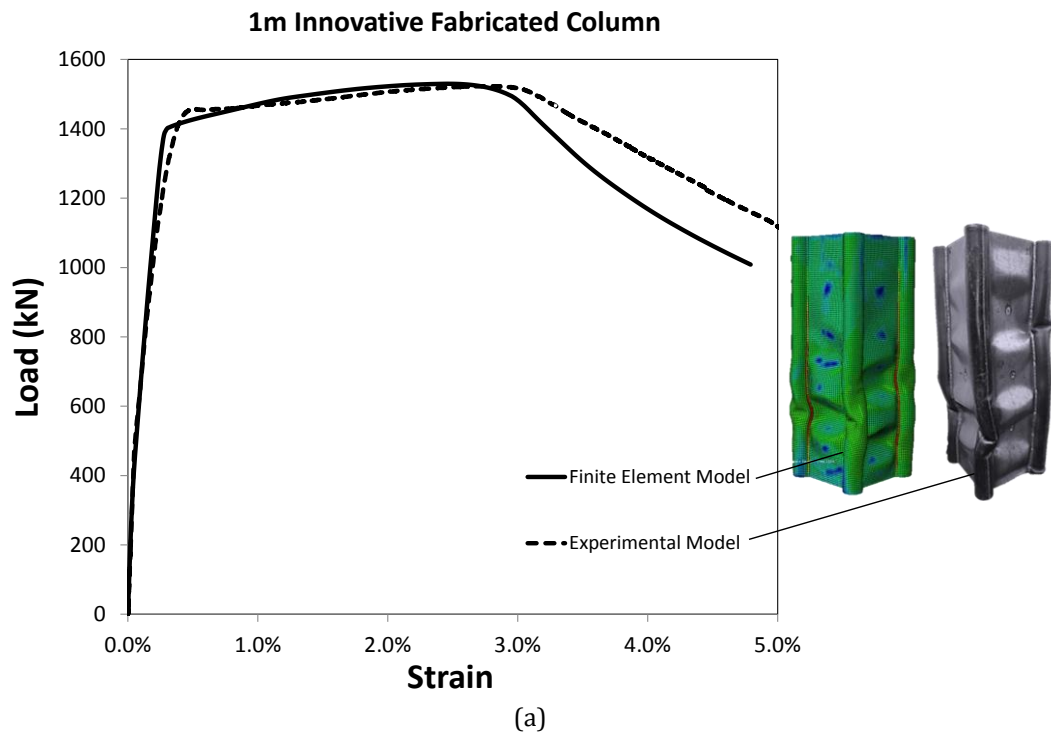
Figure 2.8. Numerical model validation (a) One meter, (b) Three meter innovative fabricated column.

2.6.   Cost analysis

An innovative product is less likely to immediately be accepted for use in construction projects, unless proven to be beneficial in an economic point of view compared to the wide range of alternative options available in the market. It is difficult to come up with an exact cost estimation for the whole fabrication process of any new product, due to the variety of factors to be considered; some of which are unknown at the initial design phase. However, early-stage cost estimations conducted in this section helps to propose an overall idea of the costs and advantages of this innovative section compared to conventional ones. Major factors such as material and fabrication costs are taken into account. The aim of this section is to estimate the cost of different lengths of innovative fabricated columns and comparing it with an equivalent conventional welded box column with the same length. Equivalence, in this context, refers to sections having the same coverage width (equal to 362.2mm) as well as the same strength.

Main differences in the production cost of these two structural elements refer to their material cost, type (butt or fillet) and amount of welding, whereas, filler metal, welding process (GTAW), overhead and finishing costs are similar and are not the focus of this comparison. Using the formulations suggested by Jung [26] manufacturing cost is obtained from the following equation:

$$Manufacturing\ cost = (R_0 + R_m) \times (time) + material\ cost \tag{2.5}$$

All money units presented in this section are extracted from current 2014 supplier's costs in Australian Dollars (AUD) units. In Equation (2.5), R_0 is the operator's rate which refers to the welding labour's charge approximately equal to AUD 25-35 per hour. R_m is the machine rate which highly depends on the size of welding shop and here it is roughly assumed to be 50% of the labour cost per hour. The total time considered in this procedure

consists of the summation of operational and non-operational hours. The operational time of welding can be obtained according to the welding speed which for both columns fabricated in this study is equal to 85 mm/min. Welding of the conventional box section is a two pass butt welds at each of the four corners which gives a total of 1.6 hours of welding operation for a 1 meter CC member. For the innovative section at each corner, two plates are individually welded to a tube which also gives a total of 1.6 hours of welding operation. Non-operational time is obtained based on the operating factor for each welding type. This factor is a percentage of a welder's working day that is actually spent on welding [27]. Assuming the operation factor for GTAW welding process equal to 20-30%, the non-operational time is equal to 4.8 hours [28]. This gives a total of 6.4 hours of welding time per meter for each column type. The ultimate cost of fabrication for one meter of columns is equal to $288. This cost needs to be added to the material cost per meter of each item. Details of this cost analysis are presented in Table 2.4.

Table 2.4. Fabricated versus conventional cost estimation (AUD)

Item (Per meter column)	IFC member		CC members
Material Supply	Plates	Tubes	Plates: AUD23.3*4
	AUD13.5*4	AUD17.7*4	
	Total: AUD124.8		Total: AUD93.2
Fabrication cost	AUD288		AUD288
Total:	AUD443.4		AUD381.2

In order to obtain the material cost it is necessary to find out the weight of each type of column. As mentioned before, it is assumed that the overall section widths as well as strengths of both sections are the same, so the only unknown geometrical parameter in the conventional section is its thickness. The corresponding thickness is derived based on the

equality of strengths in the innovative and conventional columns with similar lengths. The strength of innovative fabricated columns is known from the test results explained in Section 2.5.1. The design formulations of the Australian Standard 4100 [20] (Equation 2.4) are used to calculate the unknown corresponding plate thickness of the equivalent conventional column.

With the aim of reaching the known section capacity, an initial thickness is assumed for the box section and with a few iterations the final corresponding thickness is derived. Knowing N_s and α_c which are derived from Equation (2.4) and relevant design curves of the reference standard, the column strength is found. The justification of this procedure is initially found by comparing the nominal capacity of the one meter CC member consisting of mild steel plates of 210 mm width with that from the experimental results. Based on the AS4100 [20] formulations, the ultimate load capacity of the aforementioned section is equal to 370.6 kN which is fairly close to the experimental strength of one meter CC member mentioned in Table 2.3.

Based on the procedure described above and the equivalent experimental section capacity for each column length, the corresponding thickness is presented in Table 2.5. Due to the lack of experimental result for the 4m IFC member, the compressive strength is derived based on the validated numerical model using ABAQUS. Curves comparing the weight and total cost of the IFC and CC members are presented in Figure 2.9. Both of these graphs confirm the advantage of the innovative fabricated columns compared to the conventional ones in terms of total weight of the structure and economic point of view. The ratios of weight and the total cost of the IFC member to the CC member are approximately equal to 0.6 and 0.92 respectively for all four column lengths considered. It is a key factor in structural design, to keep the strength and production cost of an element within an expected demand level and at the same time reduces its overall weight. Beside the direct effect of the low mass on the ease of construction and lower costs of the structure, this is also a

significant benefit for its seismic behaviour. Since the earthquake generates inertial forces on a structure, the mass reduction of these sections leads to lower design forces. The slope of both curves shown in Figure 2.9 for the innovative section is less than that for the conventional type. This clearly reflects the benefit enhancement of innovative sections with increase in the column length.

Table 2.5. Properties related to the equivalent welded box column

	1m column	2m column	3m column	4m column
CC strength equivalent to IFC strength (kN)	1523	1411	1465	1451
Corresponding CC member thickness (mm)	6.08	5.85	5.96	5.93
Column Weight (kg)	68.7	132.3	202.2	268.5

(a)

(b)
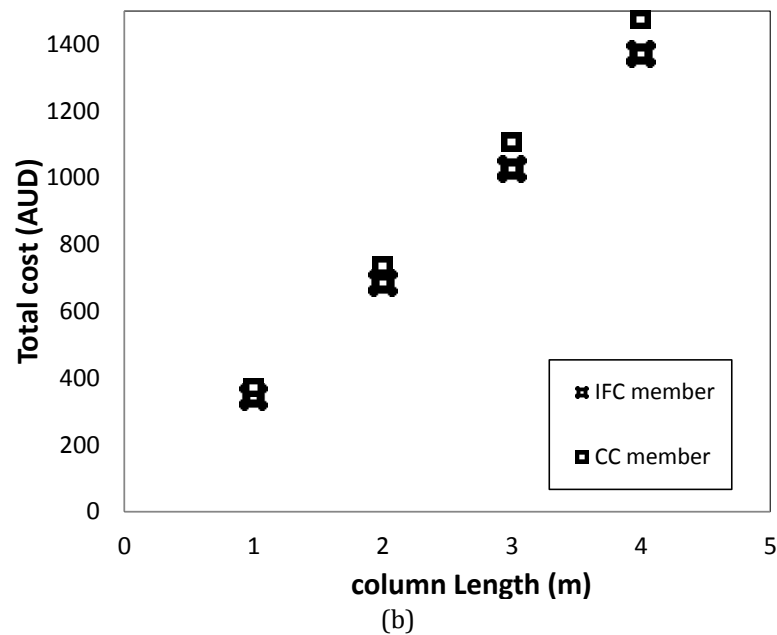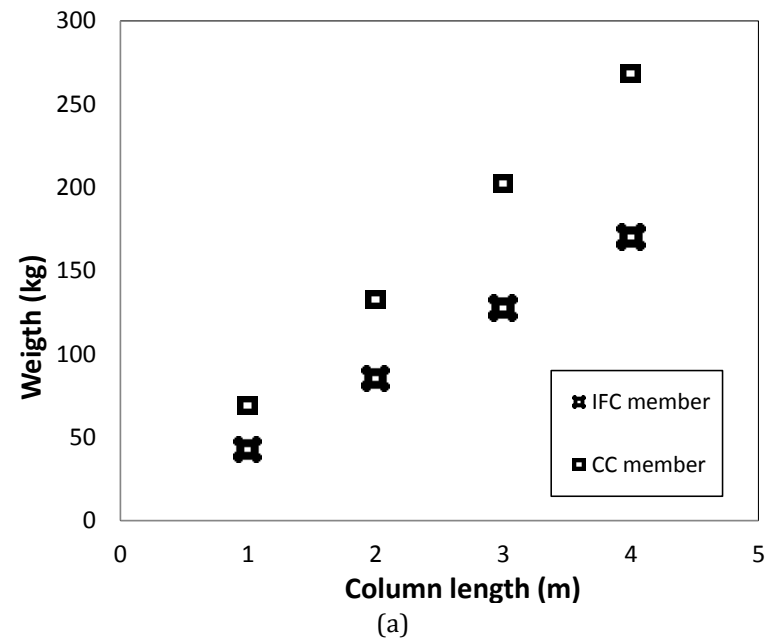
Figure 2.9. Comparison between IFC and equivalent CC members of (a) weight; (b) total cost

2.7.   Conclusions

The behaviour of long innovative fabricated columns (IFC) is studied in this paper and the following conclusion are made

- These members show a strength increase of approximately four times the conventional welded box columns consisting of similar plate elements. Comparison of IFC strength with the strength superposition of individual welded box sections and four single tube elements showed an increase of about 20-30% in strength. Section ductility increases around 200% compared to welded box section.

- The IFC compressive strength is also found to be 227% higher than a typical cold-formed square-hollow-section with almost similar weight, coverage area and steel grade.

- Based on the welding differences between the three different IFC specimens and the results obtained from the tests, it is recommended that only outer welding of plate and tube connections will result in a sufficient performance while significantly reducing fabrication cost and time.

- The comparison of failure mechanisms and strain behaviour of innovative sections with the control specimens showed an effective interaction between tubes and plates of IFC member justifying the high strength and ductility performance.

- Detailed finite element results conducted in this research work showed an acceptable match with the experimental behaviour of the proposed sections in different heights which was used for modelling the results of 4m column strength for the cost analysis.

- In an economical point of view, a primary cost estimation analysis is conducted which justifies the absolute benefit of IFCs in terms of overall weight and production compared to that for a conventional column with similar width, length and compressive strength. These sections are found to have beneficial application in structures in demand of very high strength compressive members such as bridges and high rise buildings with significant ductility and desirably low weight and also acceptable architectural appearance.

2.8.   Acknowledgments

2.9.   References

[1] Rasmussen KJR, Hancock GJ. Geometric imperfections in plated structures subject to interaction between buckling modes. Thin-Walled Structures. 1988;6:433-52.

[2] Degée H, Detzel A, Kuhlmann U. Interaction of global and local buckling in welded RHS compression members. Journal of Constructional Steel Research. 2008;64:755-65.

[3] Schillinger D, Papadopoulos V, Bischoff M, Papadrakakis M. Buckling analysis of imperfect I-section beam-columns with stochastic shell finite elements. Computational Mechanics. 2010;46:495-510.

[4] Chen J, Jin W-l. Experimental investigation of thin-walled complex section concrete-filled steel stub columns. Thin-Walled Structures. 2010;48:718-24.

[5] Gilbert BP, Savoyat TJM, Teh LH. Self-shape optimisation application: Optimisation of cold-formed steel columns. Thin-Walled Structures. 2012;60:173-84.

[6] Migita Y, Aoki T, Fukumoto Y. Local and interaction buckling of polygonal section steel columns. Journal of structural engineering New York, NY. 1992;118:2659-76.

[7] Narayanan S, Mahendran M. Ultimate capacity of innovative cold-formed steel columns. Journal of Constructional Steel Research. 2003;59:489-508.

[8] Valeš J. Effect of random axial curvature on the performance of open and closed section steel columns. AIP Conference Proceedings. 2013;1558:2512-5.

[9] Aoki T, Ji B. Experimental study on buckling strength of tri-tube steel members. The 3th international Conference on Coupled Instabilities in Metal Structures. Lisbon, Portugal2000. p. 283-90.

[10] Zhao XL, Van Binh D, Al-Mahaidi R, Tao Z. Stub column tests of fabricated square and triangular sections utilizing very high strength steel tubes. Journal of Constructional Steel Research. 2004;60:1637-61.

[11] Van Binh D, Al-Mahaidi R, Zhao XL. Finite element analysis (FEA) of fabricated square and triangular section stub columns utilizing very high strength steel tubes. Advances in Structural Engineering. 2004;7:447-57.

[12] Rhodes J, Zhao XL, Van Binh D, Al-Mahaidi R. Rational design analysis of stub columns fabricated using very high strength circular steel tubes. Thin-Walled Structures. 2005;43:445-60.

[13] Ye JH, Zhao XL, Van Binh D, Al-Mahaidi R. Plastic mechanism analysis of fabricated square and triangular sections under axial compression. Thin-Walled Structures. 2007;45:135-48.

[14] Heidarpour A, Cevro S, Song QY, Zhao XL. Behaviour of innovative stub columns utilising mild-steel plates and stainless steel tubes at ambient and elevated temperatures. Engineering Structures. 2013;57:416-27.

[15] Heidarpour A, Cevro S, Song Q-Y, Zhao X-L. Behaviour of stub columns utilising mild-steel plates and VHS tubes under fire. Journal of Constructional Steel Research. 2014;95:220-9.

[16] Mashiri FR, Uy B, Tao Z, Wang Z-B. Concrete-filled VHS-to-steel fabricated section stub columns subjected to axial compression. Journal of Constructional Steel Research. 2014;95:141-61.

[17] E606-04 Standard Practice for Strain-Controlled Fatigue Testing. ASTM International; 2004.

[18] AS 1391-2007 Metallic Materials-Tensile testing at ambient temperature. Sydney: Standards Australia; 2007.

[19] AS/NZS1554.7 Structural steel welding-Welding of sheet steel structures. Part7. Sydney: Standards Australia; 2006.

[20] AS 4100 Steel Structures-Supp1. Sydney: Standards Australia; 1999.

[21] Dassault Systèmes Simulia Corp. P, RI, USA. ABAQUS/CAE 6.14-1. 2014.

[22] Dwight JB. Welded Steel Plates in compression. The structural engineer. 1969;47:49-66.

[23] Gao S, Usami T, Ge H. Ductility of steel short cylinders in compression and bending. Journal of Engineering Mechanics. 1998;124:176-83.

[24] Park R. Evaluation of ductility of structures and structural assemblages from laboratory testing. Bulletin of the New Zealand National Society for Earthquake Engineering. 1989;22:155-66.

[25] Mahendran M. Local plastic mechanisms in thin steel plates under in-plane compression. Thin-Walled Structures. 1997;27:245-61.

[26] Jung JY. Manufacturing cost estimation for machined parts based on manufacturing features. Journal of Intelligent Manufacturing. 2002;13:227-38.

[27] Jeffus LF. Welding principles and applications. Clifton Park, N.Y.: Clifton Park, N.Y. : Delmar Publishers; 2012.

[28] Muhammad AR. Welding Techniques and Inspections Final. 17 April 2014 ed. www.scribd.com2014.

CHAPTER 3

Effect of weld on the mechanical properties of high strength and ultra-high strength steel tubes in fabricated hybrid sections

Monash University

Declaration for Thesis Chapter 3

Declaration by candidate

In the case of chapter 3 my contribution to the work involved the following:

Nature of contribution	Extent of contribution (%)
Developing ideas, Establishing methodologies, Experimental work, Data analysis, Write-up and revision	70%

The following authors contributed to the work:

Name	Nature of contribution	Extent of contribution (%)
Dr. Amin Heidarpour	Developing ideas, Input into manuscript, Revision, Financial support	10%
Prof. Xiao-Ling Zhao	Revision, Financial support	8%
Prof. Christopher R. Hutchinson	Input into manuscript, Revision	10%
Mr. Jussi Minkkinen	Providing tube specimens, Revision	2%

The undersigned hereby certify that the above declaration correctly reflects the nature and extent of the student's and co-authors' contributions to this work.

Student signature ███████████ Date: 30/01/2017

Main Supervisor's signature █████████████ Date: 30/01/2017

3.1.   Abstract

The effect of welding on the mechanical properties of high and ultra-high strength tubes in hybrid sections is a critical factor which influences the global performance of fabricated members and should be considered in the design and incorporation of these materials. To investigate and quantify these effects on the material of welded steel, a specific type of hybrid section composed of plates and tubes is considered in which two scales of experimental analysis are conducted at different positions from weld. In the macro scale, standard tensile tests are performed at various distances from weld to obtain the mechanical properties of heat affected steel in the axial direction parallel to the weld. Comparisons are made among three different welded materials: mild steel, high strength steel and ultra-high strength steel. The original and after-weld alteration in the ultimate tensile strength (UTS) and the strain corresponding to the UTS are investigated giving particular attention to the effect of yield strength and strain hardening rate. At the micro level, the microstructure of three above-mentioned materials in addition to microhardness profiles have been examined providing extensive data of the material behaviour after welding. It is shown that the welding and post welding process, such as heat input and cooling rate affect the local material properties at different distances from weld leading to an overall heterogeneity in the material influencing the mechanical behaviour.

Keywords: Ultra-high strength tube, fabricated hybrid section, heat affected zone, mechanical properties, strain hardening rate, microstructure

3.2. Introduction

High strength steel (HSS) and ultra-high strength steel (UHSS) materials are widely used in industry (e.g. automotive, pressure vessels, etc.) [1-3] due to their unique characteristics such as strength, energy absorption, weight saving, etc. In structural engineering, taking advantage of the strength capacity of these materials can be beneficial especially in structures with high load-bearing demands. High strength steel tubes are utilised in structures for their superior load bearing capacities and therefore their performance has been studied under various loading conditions [4-6]. Innovative sections fabricated from high and ultra-high strength steel tubes have recently been proposed due to their convenient structural application providing high performance and sustainable construction [7-11].

During the design and incorporation of these high strength materials in fabricated sections, the defects and material modifications due to welding need to be considered. Depending on the applied loads such as axial [12] or bending [13], the behaviour of high strength material is enhanced by welding and the heat induced by that. Welding results in the formation of material softening at the Heat Affected Zone (HAZ) which is of decisive influence on the response of the structure. Various analytical and experimental analyses have been conducted on high strength steel plates to find the governing phenomenon in the behaviour of high strength material affected by welding from a metallurgical point of view [14-19]. The HAZ microstructure depends on the steel material, type of weld, heat input during welding, and the post welding conditions.

Steel production procedures such as quenching and tempering, thermomechanical rolling and techniques like direct quenching affect the properties of the heat affected zone (HAZ) after welding. This is because High strength steels made through different methods differ in

chemical composition and carbon equivalences and therefore exhibit various weldabilities. Indeed it has been shown that a quenched and tempered high strength steel compared to a thermomechanically processed high strength steel with same strengths and under similar arc welding conditions, possess different HAZ widths and microstructures [17]. Depending on the steel chemical composition, heat input in welding should be limited to a specific amount so the presence of carbides in the heat affected zone (HAZ) can be removed which increases the impact toughness of microstructure in this region [18]. In case of low heat input welding of quenched and tempered high strength steels, a very high tensile material will develop within the HAZ area whereas, in high heat input welding, the yield and tensile strength of base material may be reduced [20]. The amount of heat input varies in different welding types. In types such as laser welding (LW) [21] and Electron Beam Welding (EBW) [22] heat input is quite low which results in a smaller HAZ width in these types of welding. However, these are not currently popular types of welding for mass fabrications.

Post-welding cooling conditions also strongly influence the HAZ properties. Welding can lead to excessive hardening for short cooling times in ultra-high strength quenched and tempered steel, which can increase the risk of cold cracking in the HAZ [23]. The cold cracking in ultra-high strength steels, which are known as steels with ultimate stresses of more than 900 MPa [24], can be prevented by preheating [25]. Several studies are available specifically on the performance of HAZ areas of high strength steel in the form of tubes. Steel strengths of less than 500MPa have been experimentally and numerically studied for different tube geometries, in which effect of welds results in various residual stress distributions produced in circular tubes [26]. On ultra-high strength steel, studies have been conducted on cold formed circular tubes in the axial direction of tube [12] and obtaining the ductility of each material and making comparisons with standards [27].

Following the previous works on ultra-high strength steel tubes, the present study examines the behaviour of the heat affected material extracted directly from a fabricated

hybrid section and presents analysis on the effect of weld on the properties of high and ultra-high strength tube. In this study, the axial material properties in the direction parallel to weld are examined, comparisons are performed and conclusions are presented based on the observations from three types of steels: Mild Steel (MS), High Strength Steel (HSS) and Ultra-High Strength Steel (UHSS) tubes welded to Mild steel plate material. Particular attention is placed on the ultimate tensile strength (UTS) and the strain corresponding to the UTS with regards to the effects of yield strength and strain hardening rate. Micro-scale observations are made on various locations of the affected steel and based on the microstructure and material type, welding procedures and post-welding conditions, the mechanical properties are rationalised. Microhardness profiles have also been obtained to justify the microstructure at various distances from weld.

3.3. Test Specimens

3.3.1. Fabrication and welding

A fabricated hybrid sample section is prepared consisting of different tube materials welded to plates (Figure 3.1). Such section configuration has previously been proposed for high load bearing capacity structural performance [7-9]. The proposed fabricated section consists of square-shaped Mild steel plates strengthened by steel tubes at corners. From a practical point of view, depending on the expected load bearing capacity and ductility of the section, different strengths of tube materials can be adopted. The structural role of Mild steel plates is to increase the overall ductility and postpone the displacement corresponding to peak load, while the high strength tubes bear the applied load until failure. For the purposes of the current study, a 500mm-long hybrid sample section is fabricated consisting of different tube materials at each corner. The configurations and dimensions are shown in Figure 3.1.

To connect the tubes and plates, fillet weld is used on the outer surface [28]. Gas tungsten arc welding (G.T.A.W) is used which helps to maintain a consistent weld thickness throughout the length of section. The welding wire is 2.4mm of the category AWS A5.9 ER2209 with a 0.2% proof stress and tensile strength equal to 560 – 620MPa and 800 – 835 MPa, respectively. Weld metal elongation is around 30%. The speed of welding for all fabrications is in a range of 75–95 mm/min and the gas used is 99.9% argon gas. Using a welding amperage of 80A and voltage of 10V the heat input of welding is calculated and equal to 0.6kJ/mm [29] which is considered to be a relatively low range of heat input. Throughout the welding process, argon gas was purged through welded tubes. All welding methods used are in compliance with AS/NZS1554.7:2006 [30].
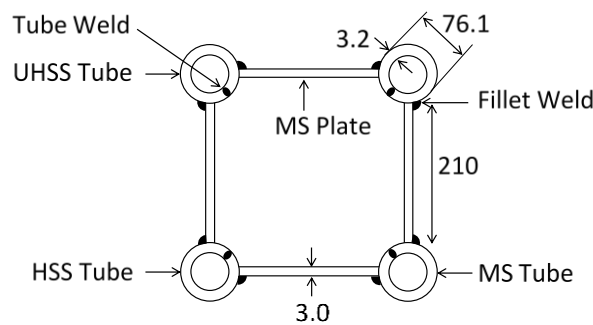
Figure 3.1. Configuration of the 500mm hybrid fabricated
section (nominal dimensions in mm).

3.3.2. Original tensile specimens

Three types of materials are chosen for tube specimens welded to one type of plate specimen. The tube materials consist of Mild steel, high strength steel (HSS) and ultra-high strength steel (UHSS) welded to a Mild steel plate. HSS material is manufactured through thermomechanical rolling (TM). The strength and toughness of the steel in this procedure is improved by combined hot rolling and accelerated cooling. This leads to a very fine grain structure which results in the toughening effect. The UHSS, however, is produced by direct

quenching. In this process, the steel is quenched directly after controlled rolling and subsequently reaches ambient temperature. This results in a fine sub-structure of bainite which helps improve the strength of steel [31].

Conventional tension tests are conducted for each steel type following the guidelines of ASTM-E8M-04 [32] and AS1391[33]. Water jet technique was chosen to cut coupons with the aim of having minimal effect on the mechanical properties of specimens throughout the cutting procedure. The coupon geometries sectioned from the plates and tubes are shown in Figure 3.2(a). The longitudinal specimens are extracted from tube samples with 90 degrees angle from the tube weld as outlined in above standards. All quasi-static tests were performed in a Shimadzu tensile test machine with a load capacity of 300kN applying a constant grip displacement rate of 0.3mm/min. Data acquisition is followed using both strain-gauges and non-contact MTS laser extensometer (model LX500). Due to the occasional early failure in strain gauges, the laser extensometer provides the material results until failure. Average stress versus strain curves read from the laser extensometer data for the Mild steel plate and three different steel tubes are shown in Figure 3.2(b). Along with the strength increase in HSS and UHSS materials, the ductility exhibits a significant decrease. The average mechanical properties of three repeat tests for each kind of Mild steel plate, Mild steel tube, high strength steel tube and ultra-high strength steel tube are summarised in Table 3.1 along with the error values which is the percentage of the difference of each test with respect to the average. Yield strength for HSS and UHSS is determined using the proof strength with a lay-off equal to 0.2% and the ultimate strain is defined as the equivalent strain at ultimate stress. The tension to yield ratio is specified in the last column of Table 3.1 which is bigger than 1.08 in all four materials [34]. The chemical compositions of the steels used are summarised in Table 3.2.

(a)

(b)
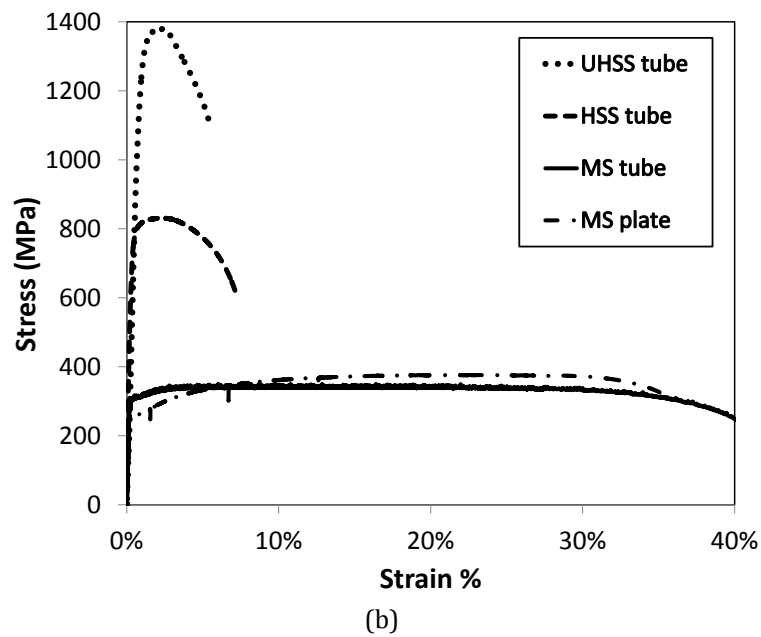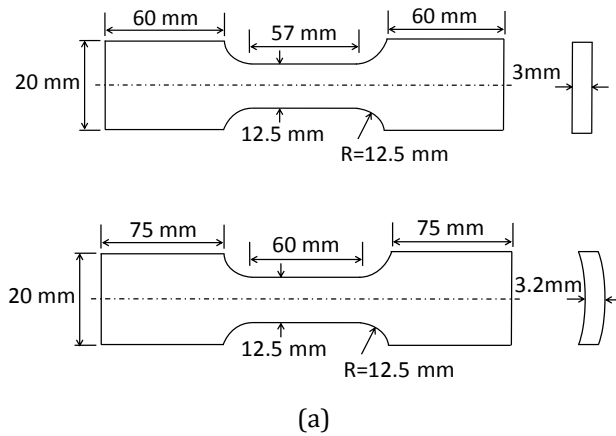
Figure 3.2. (a) Tensile test specimen configuration and dimensions for plate and tube; (b) Engineering stress vs. engineering strain curve for each material type.

Table 3.1. Measured mechanical properties of material (±error%)

Material	Elastic modulus (GPa)	Yield strength (MPa)	Ultimate strength (MPa)	Strain at UTS %	Tension to Yield ratio
MS plate	207 (±0.1%)	265 (±0.4%)	376 (±4%)	23%	1.42
MS tube	198 (±0.1%)	305 (±0.3%)	342 (±0.1%)	11%	1.12
HSS tube	205 (±1%)	772 (±2%)	847 (±2%)	2.5%	1.10
UHSS tube	209 (±0.5%)	1247 (±4%)	1385 (±2%)	2.1%	1.11

Table 3.2. Chemical composition of test specimens (content %)

Material	C	Si	Mn	P	S	Al	Cr	Ni	Mo	Ti	Cu
Mild steel	0.22	0.55	1.7	0.04	0.03	0.10	0.3	0.5	0.1	0.04	0.4
High strength steel*	0.10	0.5	2.1	0.02	0.01	0.015	-	-	-	-	-
Ultra-high strength steel	0.23	0.80	1.7	0.025	0.015	-	1.5	1.0	0.5	0.005	-

* In addition, niobium (Nb), vanadium (V), molybdenum (Mo) and titanium (Ti), or combinations of these, are used as microalloying.

3.3.3. Weld affected tensile specimens

With the purpose of identifying the material properties of weld affected areas in the hybrid fabricated sample section (Figure 3.3(a)), standard tensile coupons were extracted from the section at various locations using water jet technique and tested. The specimen size was chosen following test piece recommended in AS1391[33] with the smallest possible gauge width (Figure 3.3(b)) in order to test and obtain the material properties of steel at the closest distance to weld. The specimen locations begin in the vicinity of the weld joining the tubes and plates and continues all the way to the furthest region with a separation of 6mm between each specimen. To have a consistent understanding of the behaviour of the steel material at all distances from the weld, coupons are also extracted from the location between two specimens on the other side of the same tube to plate connection (Figure 3.3(a)). Figure 3.3(c) summarises the tensile specimen numbering system based on the order of their distance from weld. The numbers in specimen labels are followed by letters representing the element type, where P stands for plate and T for tube. These labels are applicable for all specimens on each side of the section. Figure 3.4 shows how close the gauge length of the first coupon is located to the weld line. Quasi-static tensile tests on the above series of specimens was performed using an Instron-4204 tensile test machine with a load capacity of 50kN applying constant grip displacement rate of 0.3mm/min.
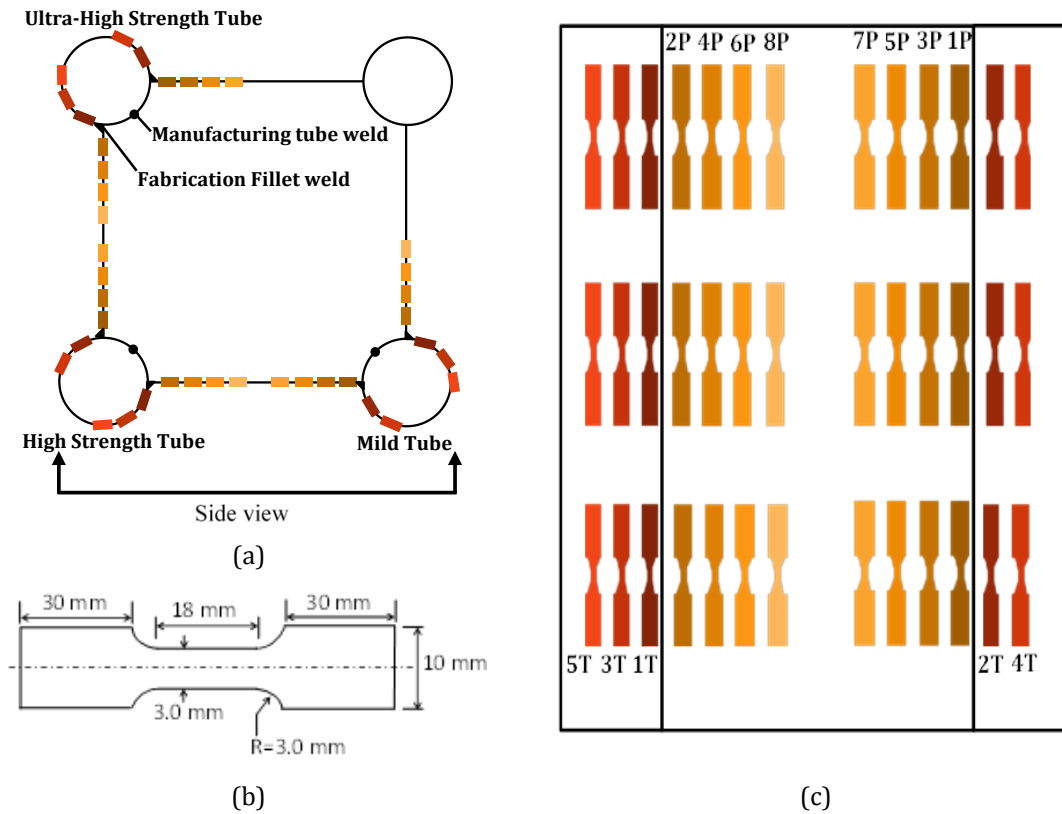
Figure 3.3. Tensile specimen configurations for weld affected material analysis (a) cross sectional view showing extracted specimens; (b) tensile test dimensions for plate and tube; (c) side view showing extracted specimens labelled according to position.

Figure 3.4. Tensile specimens extracted from the sample section.

3.4.   Weld affected material properties

3.4.1.   General results

Due to the high amount of heat induced during manufacturing of HSS and UHSS tubes and fabrication of welded sections, the material properties of constitutive elements exhibit a significant change in areas close to the welds. This may affect the overall behaviour of sections. Results of the tensile tests show the significant effect of welding on the behaviour of the steel. However, the behaviour is highly dependent on the material type, cooling procedure and distance to the weld. From the outputs of all tensile tests conducted, the ultimate tensile strength (UTS), yield stress and the strain corresponding to UTS are summarised in Figure 3.5 to Figure 3.10. The presented results are averaged from three repeat tests on each material position which gives a total of 63 tensile tests. In more than 90% of the specimens, the error of the repeated tests compared to the average of the three is less than 1.5%. However, in a few tests this reaches values up to 5%, especially in the uniform elongation results, which is still within the acceptable range. The mechanical properties are compared to those of a so-called "comparison line" which is the material with no heat-effect from welding. In the current study, the coupons are extracted from a distance starting from more than 29mm from the manufacturing weld of tubes. It is shown in Section 3.6 that this distance is not located within the region affected by the tube manufacturing seam and the main source of this heat, affecting the material properties, is due to the fabrication weld. The effect of dimensions in sub-size specimens compared to the standard size of specimens mentioned in Section 3.3.2 can be understood when comparing the results of both specimen sizes at areas furthest from weld. It was understood from the strength and the corresponding strain values that the quantities of tensile strength converge to the standard values (Table 3.1) with increase in their distance and angle from weld. This

convergence shows the negligible effect of specimen size for the two above mentioned parameters.

3.4.2.   Results of tube properties

Figure 3.5 shows the normalised strength of Mild, HSS and UHSS tubes at various locations from the weld. The normalised strength values were obtained as the ratio between each position value to the value of strength at the position furthest to weld with no heat effects. The closer the ratio is to one means there is less heat effects in that area. Each position value represents the average mechanical properties of three tested specimens having the same distance from weld. Position 1T is in the immediate vicinity of weld whereas position 5T is the furthest away not being affected from weld. The heat produced from welding leads to a decrease in the tensile strength of the HSS and UHSS tube material at position 1T (Figure 3.5). This reduction is ~8% for the HSS and reaches 30% for the UHSS tube. This is due to the HAZ softening as a result of exposure to high temperature. In contrast, for Mild steel the welding increases the tensile strength to ~13% above its original value. The reason behind these behaviours will be discussed in Section 3.5.
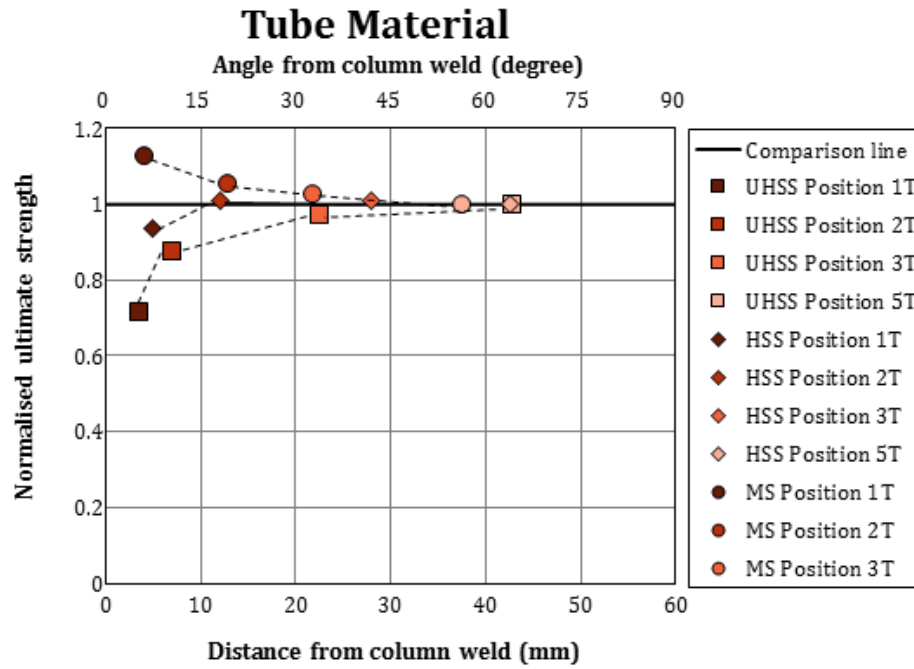
Figure 3.5. Effect of heat induced by fabrication weld on the tensile strength of tubes incorporated in proposed hybrid section (Ultimate strength values normalised to ~350 for MS, ~850 for HSS and ~1380 MPa for UHSS).

Figure 3.6 shows the results of average yield strength of the three tube materials with respect to their distance from the fabrication weld. Consistent with Figure 3.5, the yield strength values are again normalised with respect to the material at a location furthest from weld. Yield strength is not affected by the heat induced from welding in the Mild steel tube but is slightly increased in HSS tube material (less than 10% with maximum error of 3%). However, the yield strength of the UHSS tube material is reduced by ~30% (with a maximum error of 4%) after the welding and cooling procedure. A different trend is observed in the effect of heat on the strain corresponding to ultimate strength (i.e. uniform elongation) in the tubes after fabrication (Figure 3.7).
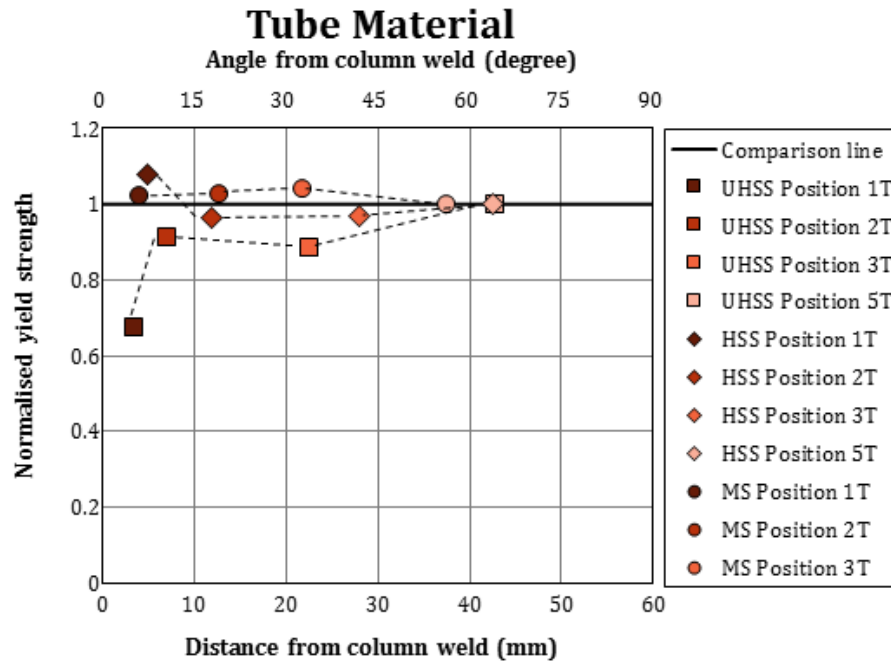
Figure 3.6. Effect of heat induced by fabrication weld on the yield strength of tubes incorporated in proposed hybrid section (Yield strength values normalised to ~300 for MS, ~700 for HSS and ~1100 MPa for UHSS).

The ductile behaviour of all three materials (Mild Steel, HSS and UHSS) shows an increasing trend when getting closer to the weld. Highest possible precaution has been taken to obtain the strain corresponding to the tensile strength in all specimens using the measurements of a non-contact laser extensometer. The amount of deviation observed in the measurement of strain is larger than that for stress especially when getting close to the heat affected area. Nevertheless, the conclusion is based on average test results in all tested specimens and which follows a logical trend in behaviour. Welding heat increases the ultimate strain of MS, HSS and UHSS tube material by factors of 2.5, 2.1 and 3.5 compared to the original ultimate strain, respectively. All uniform elongations are normalised with respect to that at a position furthest from weld.
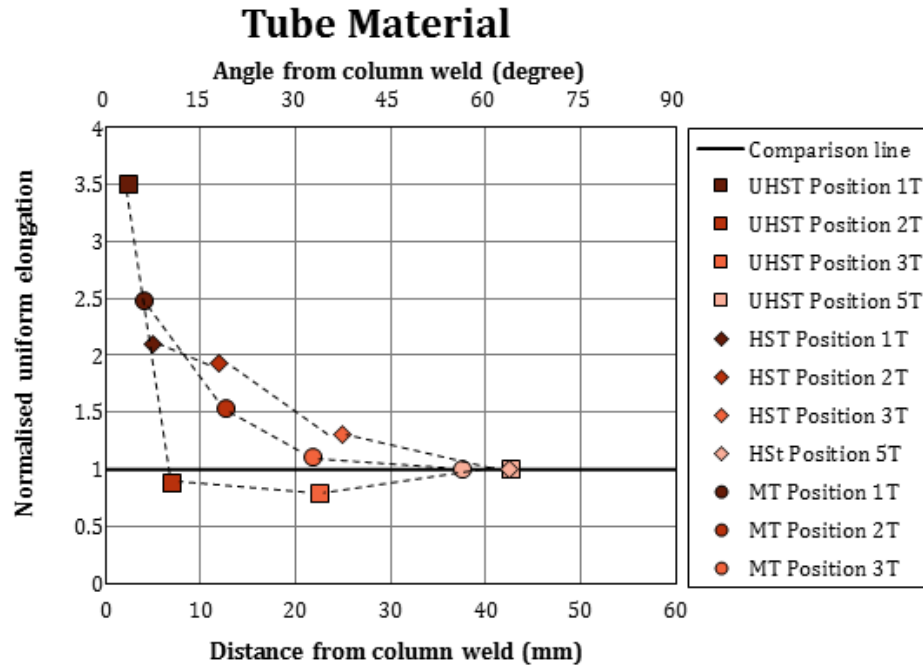
Figure 3.7. Effect of heat induced by fabrication weld on the strain corresponding to tensile strength of tube material incorporated in proposed hybrid section (Uniform elongation values normalised to ~8% for MS, ~2.5% for HSS and ~2% for UHSS).

3.4.3.   Results of plate properties

Mild steel material is widely used in structural elements thus it is vital to understand the behaviour of this material when it comes to welding for section fabrication, welded connections or other external high temperature sources [35-40]. The mechanical properties and microstructure of Mild steel plates and sections at elevated temperatures [41-43] have been extensively studied in the past. Similar to the strength observations of heat affected Mild steel tube, Mild steel plates experience an increase in the ultimate strength with values of 9%, 10% and 7%, when welded to Mild, HSS and UHSS tube material, respectively (Figure 3.8). However, as opposed to welded Mild steel tube (Figure 3.6) , Mild steel plate shows an increase of ~20% in the yield strength (Figure 3.9) and a reduction of ~20% in the uniform elongation (Figure 3.10). The reason of these observations will be discussed in Section 3.5.
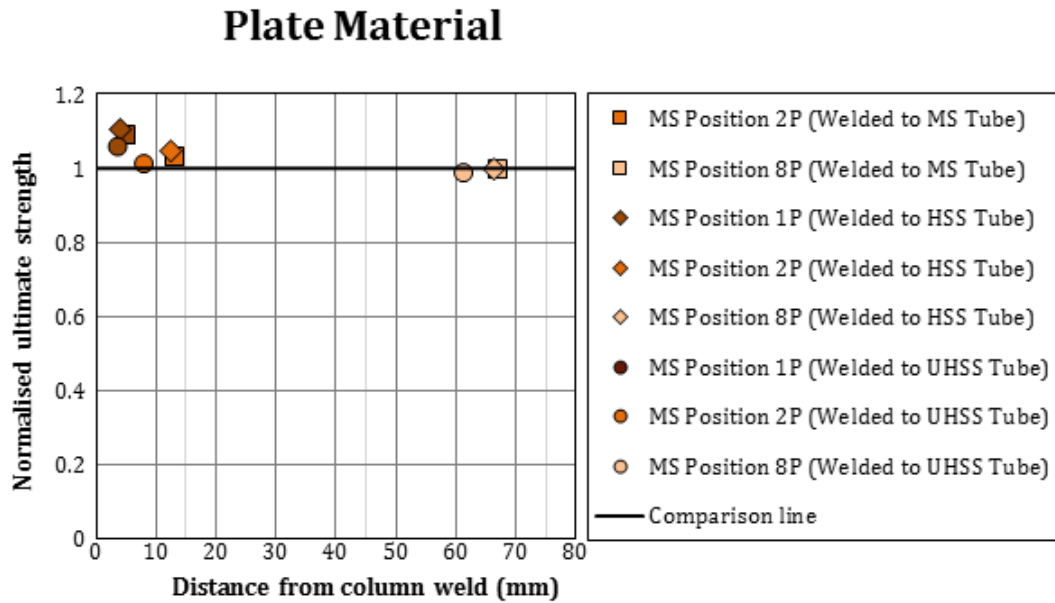
Figure 3.8. Effect of heat induced by fabrication weld on the tensile strength of Mild steel plates welded to various tube materials (Ultimate strength values normalised to ~376 MPa).

The conclusion made regarding the strength reduction of different steel materials here is obtained in the case of welding specifications and the testing configurations outlined in Section 3.3.1 and may vary depending on the type of welding and also the test setup and procedure. Jiao et al [12] have reported a reduction factor of around 0.5 for UHSS tube fillet welded T joints to a steel plate. In that case, welding specifications were quite similar to what was used in the current study. However, the tensile testing sample geometry was quite different. In the case of Jiao et al., the welding of tube to plate was in the transversal direction and perpendicular to the load with the welded part also subjected to tension force. In the configuration used in the present study, tensile specimens were longitudinal coupons extracted from the vicinity of welded area and gauge lengths do not include any of the weld itself. As a result we should expect a smaller strength reduction than what was observed by Jiao et al. which is consistent with the maximum of 30% reduction in the vicinity of weld shown in Figure 3.6 and decreasing with further distance from the heat affected area.

Plate Material
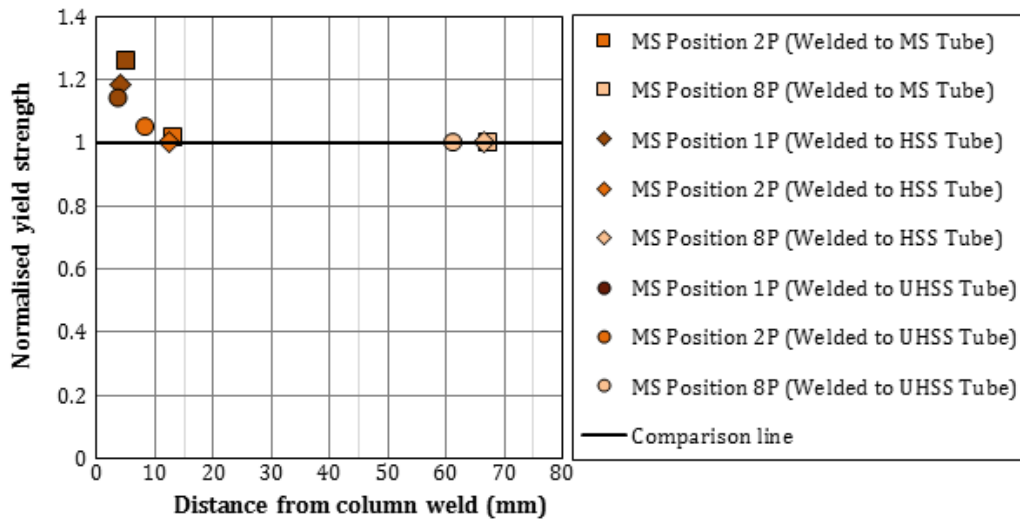
Figure 3.9. Effect of heat induced by fabrication weld on yield strength of Mild steel plates welded to various tube materials (Yield strength values normalised to ~250 MPa).

Plate Material
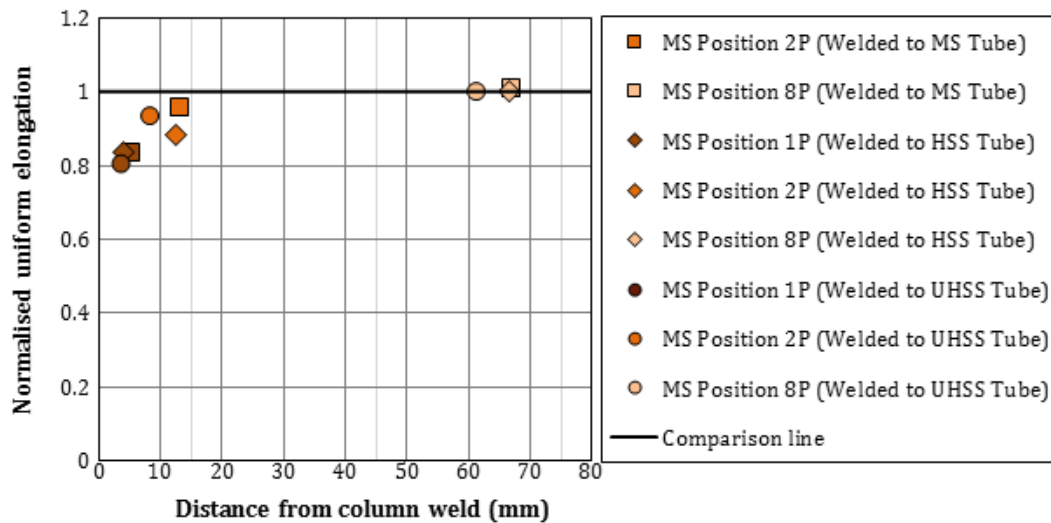
Figure 3.10. Effect of heat induced by fabrication weld on the strain corresponding to tensile strength of Mild steel plates welded to various tube materials (Uniform elongation values normalised to ~23%).

3.4.4.   Ultimate strength and uniform elongation

The two important factors governing the ultimate strength and its corresponding strain (uniform elongation) are the yield strength and strain hardening rate. In order to interpret

the ultimate strength and corresponding strain observations of steel material under weld effects, both of these properties must be considered.

At a condition where the maximum force occurs, the force-strain curve can be written as below

$$\frac{dF \ (= \sigma_t \times A)}{d\varepsilon_t} = 0 \tag{3.1}$$

where σ_t and ε_t are the true stresses and strains, respectively calculated from the engineering stresses (σ_e) and strains (ε_e) according to (3.2).

$$\sigma_t = \sigma_e(1 + \varepsilon_e), \quad \varepsilon_t = ln(1 + \varepsilon_e) = ln(\frac{A_0}{A}) \tag{3.2}$$

Where A is the cross-sectional area of specimen. Since volume remains constant during plastic deformation, one can obtain:

$$\frac{dA}{A} = -d\varepsilon_t \tag{3.3}$$

Substituting (3.3) into (3.1) leads to the well-known Considère's criterion, shown in (3.4) [44], which indicates the onset of plastic instability and is the signal for necking. This onset of necking is a point where the rate of hardening falls below the true stress curve.

$$\frac{d\sigma_t}{d\varepsilon_t} = \sigma_t \tag{3.4}$$

The true stress versus true strain curves and the strain hardening rates were obtained for all four materials in two different locations of immediate vicinity of fabrication weld and further away with no weld effects as shown in Figure 3.11. The intersection of the true stress

and strain hardening rate curves represents the point of ultimate stress and corresponding strain for a material failing in a ductile manner. For Mild plate material, at the position close to fabrication weld yield strength increases around 20% compared to material far from the weld, whereas the strain hardening rate remains relatively unchanged. Therefore, the increase observed in material ultimate strength is mainly caused by the increase in yield stress. This claim is justified in Figure 3.11(a). Consequently, the uniform elongation slightly decreases in the heat affected area. However, quite different behaviour is observed in Mild steel tube material subjected to the effect of heat induced by the weld. The yield strength of Mild tube material doesn't change significantly as a result of the weld compared to that of a non-heat affected area. Therefore, the significant increase in ultimate strength is due to the rise in the strain hardening rate shown in Figure 3.11(b). This rise in strain hardening rate also leads to a significant increase in the uniform elongation of the heat affected Mild steel tube material.

(a)
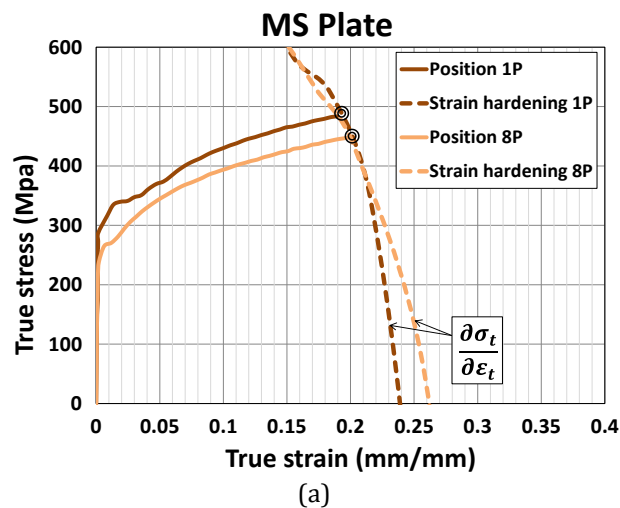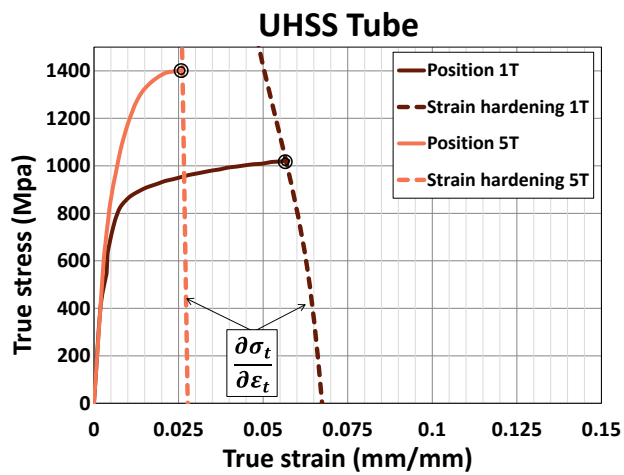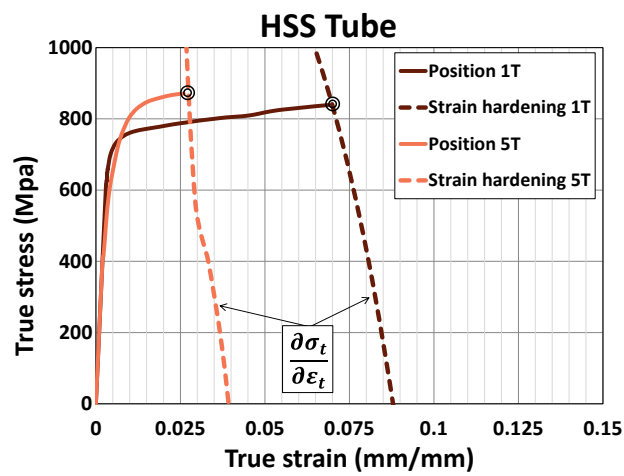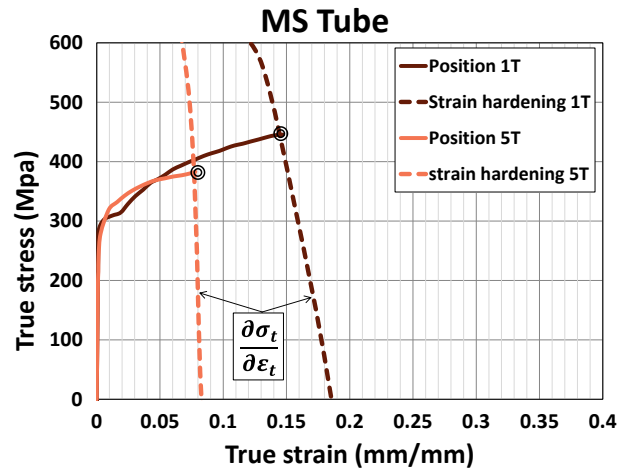
Figure 3.11. True stress-strain curve and strain hardening curve intersection of two locations from fabrication weld for: (a) MS plate, (b) MS Tube, (c) HSS tube and (d) UHSS tube material.

In the HSS tube material (Figure 3.11(c)), similar to the Mild steel tube, the uniform elongation of the heat affected material is enhanced because of a significant increase in the strain hardening rate. The ultimate tensile strength, however, decreases and this mechanical property does not clearly follow the yield strength or the strain hardening. Finally, for UHSS tube material (Figure 3.11(d)), reduction in 0.2% yield strength is also the main reason for the decrease in ultimate strength which is more significant compared to that of HSS tube. Uniform elongation shifts to a higher value as a result of higher rate of strain hardening at the position affected by weld.

3.5.   Microstructure analysis of heat affected material

3.5.1.   Mild steel plate and Mild steel tube

In order to obtain a better understanding of the behaviour of four types of steel materials, under the effect of fabrication welding, the microstructures have also been examined. Optical micrographs have been obtained from bulk material of Mild steel plate and Mild steel tube both close to the weld and at a position far from the weld as shown in Figure 3.12. The lighter regions surrounded by black boundaries are ferrite grains and some small black volumes which can also be observed in the microstructure represent pearlite (consisting of a composite of ferrite and cementite). These are typical Mild steel microstructures. In Mild steels such as those observed here, the yield strength is governed by the ferrite grain size. Therefore, the obvious decrease in ferrite grain size of Mild steel plate (Figure 3.12(a) and (b)) in the vicinity of weld is the reason for the 10% increase in its yield strength (Figure 3.8 and Figure 3.9). When considering the effect of the welding treatment on the microstructure of a steel it is useful to separate the expected effect of microstructure into two classes depending on whether the local temperature went above the so-called A1 or A3

temperatures or not [45-47]. If the temperature remained below the A1, then the expected changes on the Mild steel microstructure would consist only of a small amount of growth of the ferrite grains corresponding to a slight decrease in the strength. If the local temperature was raised above the A1, the ferrite grains will begin to be replaced by the high temperature phase of steels, known as austenite. If the temperature is raised above the A3, all of the ferrite will be replaced by austenite and the final microstructure obtained will depend especially on the cooling rate from high temperature since this determines which room temperature microstructure will form from austenite during cooling.

(a) Mild steel plate position 8P   (b) Mild steel plate position 1P

(c) Mild steel tube position 5T   (d) Mild steel tube position 1T
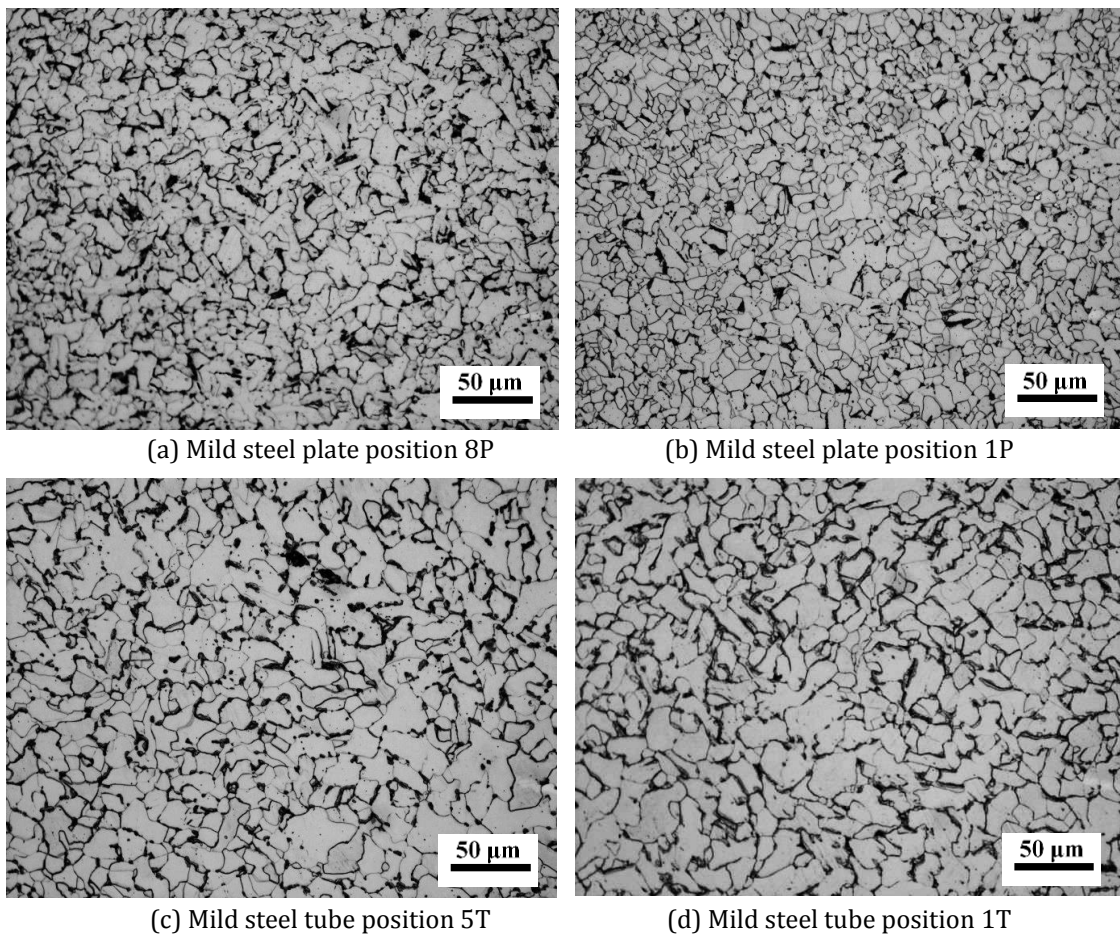
Figure 3.12. Optical micrographs of Mild steel plate and tube material.

The refinement of the ferrite grain size at the region in the vicinity of the weld of the Mild steel plate (Figure 3.12(a) and (b)) and the fact that the microstructure is uniformly fine is an indication that the local temperature in this part of the material was sufficient to go above

the A3 and transform the original ferrite grain structure to austenite and then a ferrite/pearlite structure was reformed during cooling. Furthermore, it can be concluded that the cooling rate from high temperature during the weld was faster than the cooling rate used in the production of the original Mild steel plate. In the case of the Mild steel tube in the two mentioned positions (Figure 3.12(c) and (d)), the ferrite grainsizes are very similar. This indicates that the cooling rate at position 1T after welding was very similar to the cooling rate used in the original fabrication of the Mild steel tube. This is the reason why there is negligible change in yield strength for this material (Figure 3.6).

3.5.2. High strength steel tube

The microstructure of HSS material was investigated at different distances from the weld to help explain the mechanical properties reported in previous sections. At a distance far enough from the from weld that is not heat affected (position 5T), the optical micrograph shows a very fine ferrite grain size exhibiting a more elongated grain shape compared to Mild steel (Figure 3.13(a)). This is a typical bainitic grain structure. As we move closer to the weld, the microstructure shows greater variability and heterogeneity. A low magnification optical micrograph showing the cross section of a sample taken from position 1T, very close to the weld, is shown in Figure 3.13(b). Position 1T has undergone significant heat induced by welding and even within this one sample, the microstructure varies significantly. During welding cooling has been performed by passing argon gas inside the tube elements and the rate is expected to be similar for all locations. The differences in microstructure are likely due to different upper temperatures reached during the welding process. Closer locations to the weld are exposed to higher temperatures. Accordingly, points I and II of position 1T (Figure 3.13(b)) are both affected by the high temperature of weld, the latter being close to weld and being exposed to higher temperatures. The final grain distribution at point II (Figure 3.13(b)) shows that the HSS material now exhibits a

fine equiaxed ferrite grain structure unlike point I which exhibits a slightly coarsened version of the original bainitic microstructure. It is likely that position II was raised to a temperature above the A3 and position I reached an upper temperature that did not exceed the A1. The transition region between the two locations is indicated by the dotted line on the specimen cross section (Figure 3.13(a)) which in this case is located ~2mm from the edge of weld. These observations help explain the strength decrease of HSS tube in the vicinity of weld. From microstructure observations in previous studies [48] on welded high strength tubes, a similar, but wider, was observed in the vicinity of Butt welds which resulted in a larger strength reduction in the material.
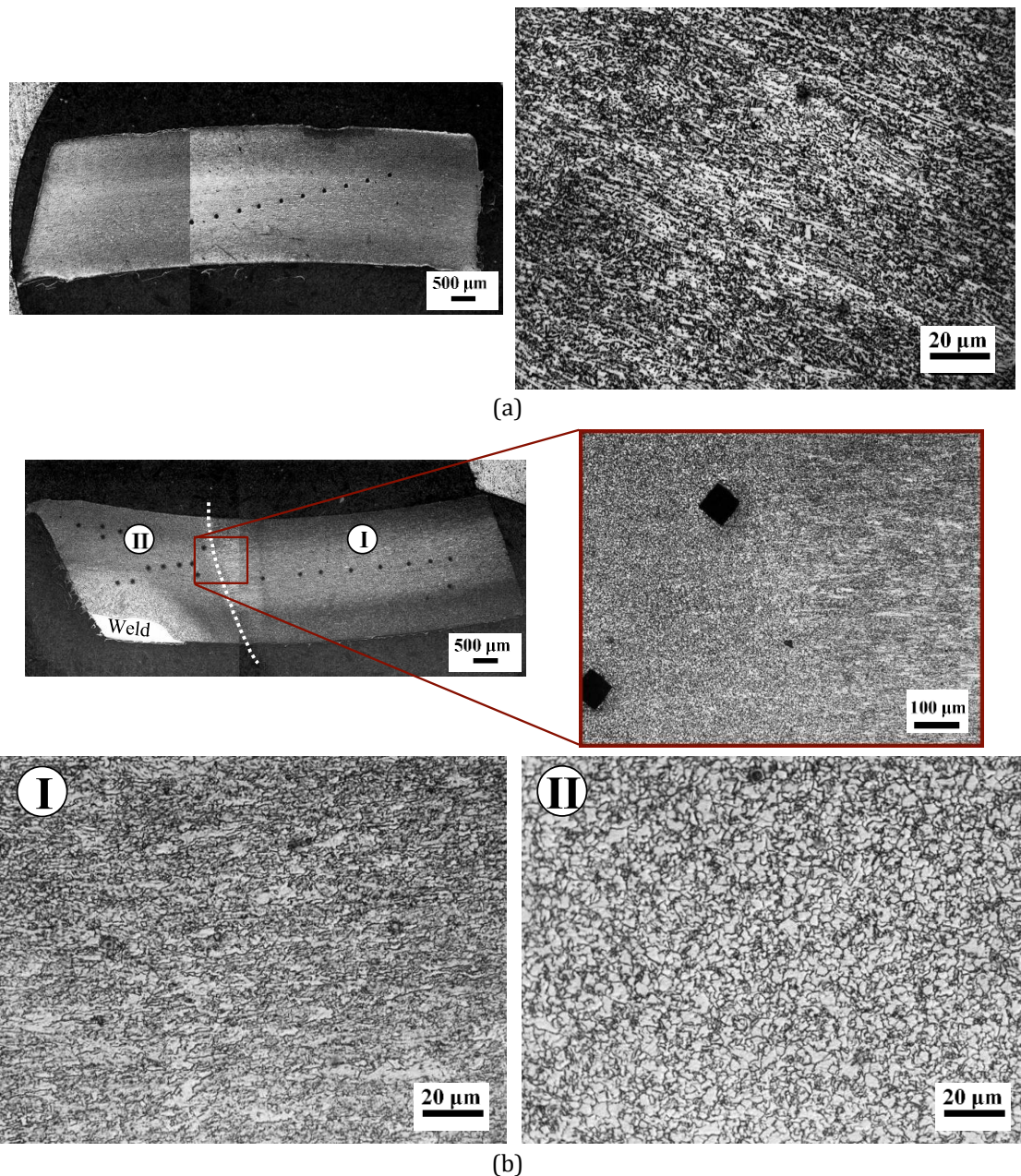
Figure 3.13. Optical metallography images from HSS tube material: (a) at position 5T furthest from weld, (b) at position 1T closest to weld.

3.5.3.   Ultra-high strength steel tube

The UHSS material has a completely different microstructure to that of the Mild steel or HSS. The UHSS steel consists of a very strong phase known as martensite. The grains are lath shaped and very fine as shown in Figure 3.14(a) (taken from position 5T far from the weld), compared with the equaixed grains observed in Mild steel (Figure 3.12). Martensite is a non-

equilibrium phase which is related to the ferrite in Mild and HSS but has much higher strength and less ductility. If we examine the microstructure of the sample taken from position 1T (closest to the weld), we can observe substantial heterogeneity in the microstructure across the specimen width (Figure 3.14(b)). This was the same as that observed at location 1T for the HSS (Figure 3.13(b)).

Overall, the heat affected area of sample 1T in the vicinity of weld can be divided into different regions based on microstructure variations (Figure 3.14(b)). Region I, at the furthest distance from weld in sample 1T, shows a similar martensitic microstructure to the original ultra-high strength steel. However, the Vickers hardness is only 400VHN which is a little softer than the hardness of the material very far from the weld (e.g. position 5T) (~450VHN) (Figure 3.16(c)). This indicates that the material in this region has been heat-affected but the upper temperature did not exceed the A1. Instead the martensite has been 'tempered' by the welding process and this is the reason for the slight decrease in the hardness. Region IV also shows a similar martensitic structure. However, this region is very close to the weld and has been exposed to very high amounts of heat, well above the A3 temperature. During welding this region will have transformed to the high temperature phase of steel, austenite, however due to its vicinity to the Mild steel plate which will act as a heat sink, in addition to the cooling argon gas, rapid cooling has resulted in the re-forming of the martensite microstructure. The hardness of this region is only ~360VHN due to tempering of the martensite during cooling (ie. autotempering [49, 50]).

(a)

(b)
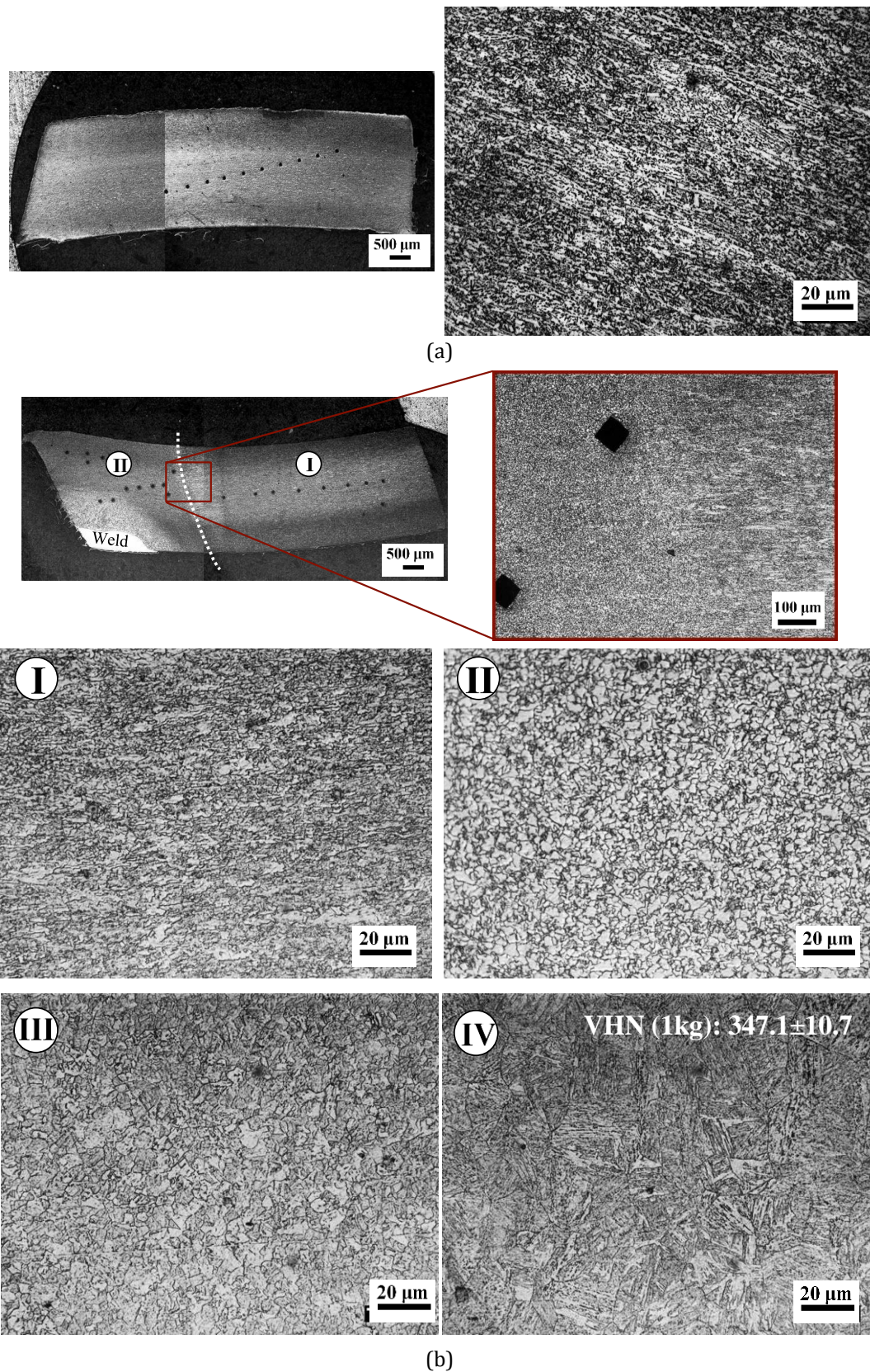
Figure 3.14. Optical metallography images from UHSS tube material (a) at position 5T furthest from weld, (b) at position 1T closest to weld

Between regions I and IV there is a great change in the microstructures observed. Regions II and III both exhibit a mix of what appears to be ferrite and bainite, indicating that the upper temperature reached was raised above the A1 but that cooling was not very fast (consistent with this position being a little further away from the Mild steel plate acting as a heat sink). Such a conclusion would be consistent with the position in sample 1T and the behaviour observed at position I in sample 1T (Figure 3.14(b)). An SEM image taken from region II to further investigate the microstructure of the softened region is shown in Figure 3.15. This is a mixed microstructure containing ferrite and bainite. Region II has the softest material which is the transition zone between the two surrounding martensitic regions. This transition area starts at ~4mm distance (a value close to the thickness of specimen) from the end of weld substance and for a width of ~3mm (again close to the thickness of specimen) while getting closer to weld. The tensile tests conducted from this position, showed a decrease in the strength of steel which has been due to the fact that the gauge length was extracted from the transition area.
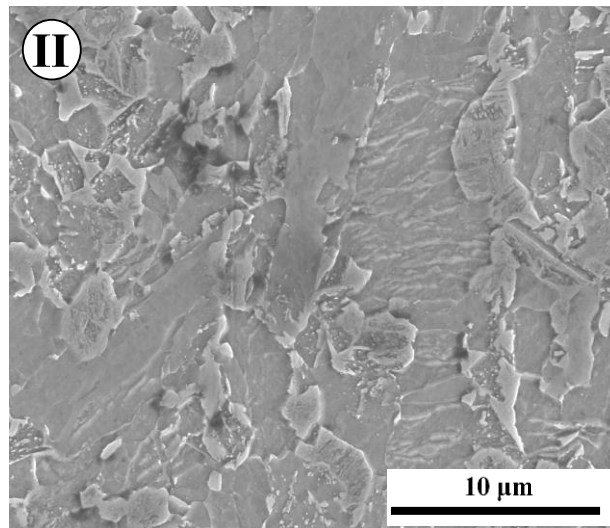
Figure 3.15. SEM 5000x magnification of region II

3.6.   Microhardness

Microhardness profiles were measured using a Vickers microhardness tester along the welded intersection of Mild steel plate and UHSS tube. These profiles are shown in Figure 3.16. The cross-section of the tube-plate hybrid section showing the directions where the hardness profiles were measured in shown in Figure 3.16(a). These hardness results correlate well with the microstructural properties of steel discussed in the previous section. Hardness values were taken starting from point O along the centre line of Mild steel plate (direction OA, Figure 3.16(b)) and the centreline of UHSS tube (directions OB (Figure 3.16(c)) and OC (Figure 3.16(d)). In each of the microhardness graphs, the location where tensile coupons where sectioned is also shown. For Mild steel plate, in the heat affected area, hardness increases to an average of 145VHN which is 14% increase compared to the base metal hardness of 127VHN. UHSS Tube material also shows a consistent trend with the observations made in the tensile tests and microstructural analysis Sections. The average hardness at the vicinity of weld which was referred to as region IV in Figure 3.14, shows a hardness average of 362VHN which is higher that the softened region of HAZ having an average of 357VHN. This justifies that at the immediate vicinity of the weld, the microstructure has recovered its martensitic lath shaped structure. The average hardness of base UHSS tube material is equal to 449VHN in regions far from the heat affected area. Direction OC (Figure 3.16(d)) illustrates the hardness values of welded UHSS tube as we approach the tube manufacturing seam weld. It was found that the HAZ area close to the fabrication weld has an average hardness of 354VHN while a value of 374VHN is obtained for the HAZ area close to the tube manufacturing weld. It is interesting to note that the effect of tube weld on the properties of UHSS affects a distance only around 3mm from the manufacturing tube seam.
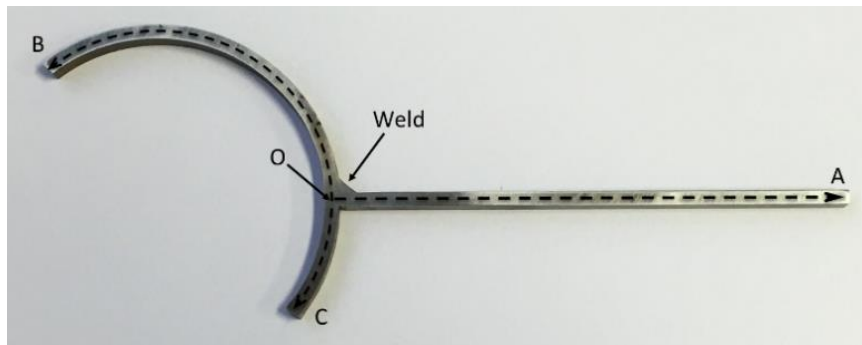
(a)
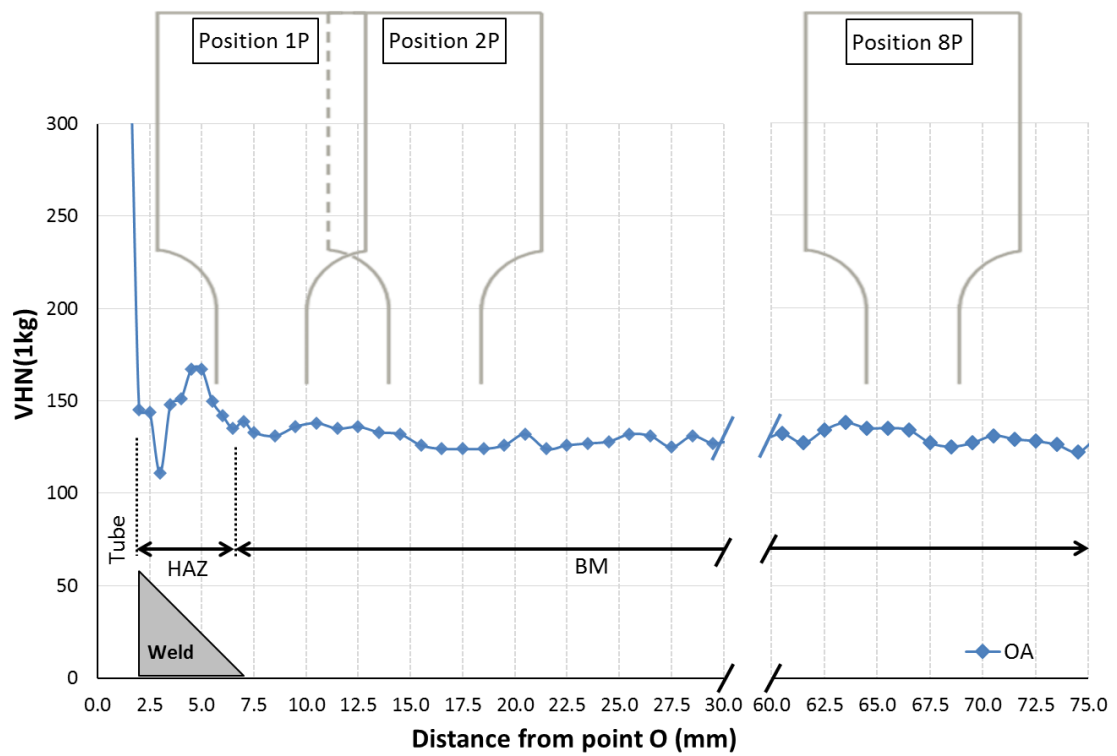
(b)
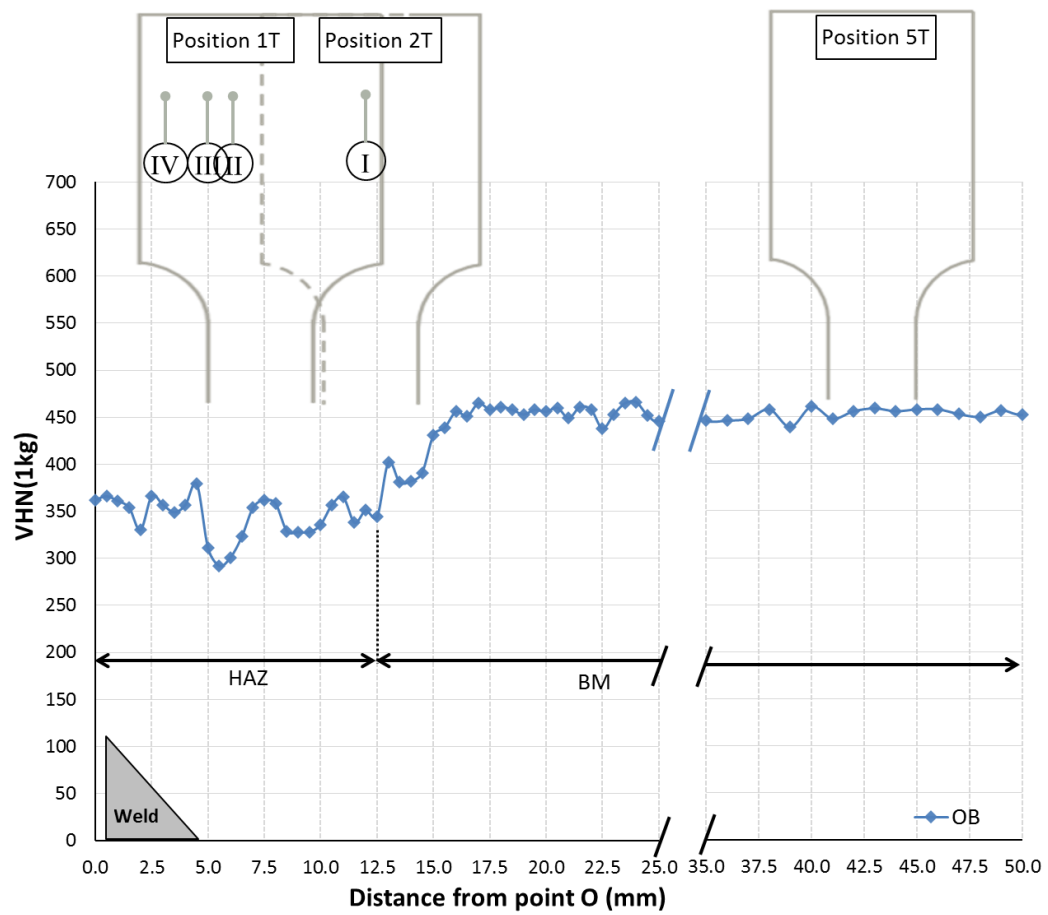
(c)
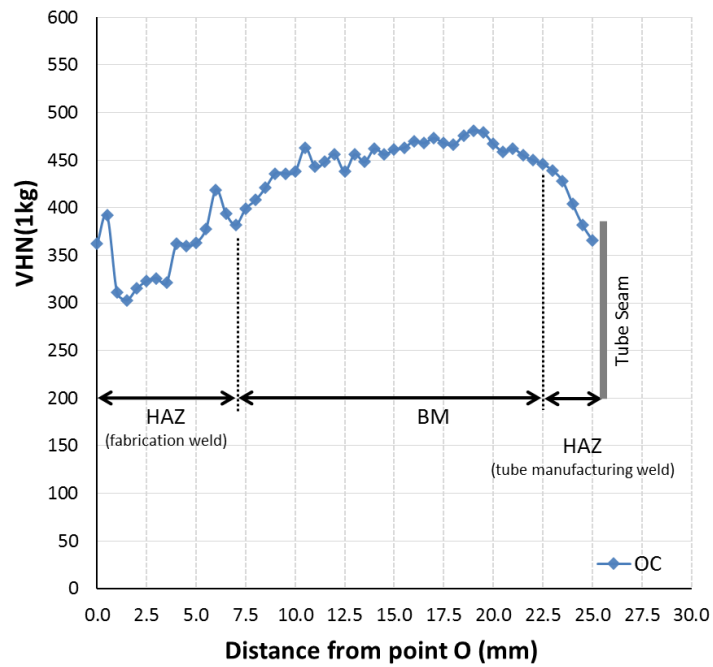
(d)

Figure 3.16. (a) Lines where Micro-hardness profiles where taken; (b) Micro-hardness profile OA; (c) Micro-hardness profile OB; (d) Micro-hardness profile OC.

3.7.   Conclusions

The effect of heat induced by welding on the mechanical properties of Mild steel plate and three different tube materials of Mild steel (MS), high strength steel (HSS) and ultra-high strength (UHSS) steel has been investigated.

Effect of weld induced heat on the mechanical properties of steel tubes in the vicinity of weld (up to ~4mm from weld) results in an overall reduction around 8% in HSS and 30% in UHSS tubes. In contrast, welding enhances the tensile strength of Mild steel to around 13% above its original value. Welding heat also increases the ultimate strain of MS, HSS and UHSS tube material to 2.5, 2.1 and 3.5 times of the original ultimate strain, respectively.

The individual effect of strain hardening rate and yield strength on the mechanical properties was studied for each steel type in both the heat affected position and furthest areas from weld. Optical micrographs were obtained from different locations from weld in each of the steel materials and analyses have helped rationalise the HAZ properties. The effects of original steel manufacturing process, heat input due to welding and the cooling after welding were analysed by observing the microstructure and also microhardness profiles taken along the welded connection of MS plate and UHSS tubes. It can be concluded that at the immediate vicinity of UHSS to weld, due to the presence of Mild steel plate which will act as a heat sink, in addition to the cooling argon gas, rapid cooling has resulted in the re-forming of the martensite microstructure. Moving further from the vicinity of weld, the material softening occurs within the transition zone which starts at 4mm from weld substance having a width around ~3mm which are values close to the dimension of material thickness.

3.8. Acknowledgements

3.9. References

[1] Kuziak R, Kawalla R, Waengler S. Advanced high strength steels for automotive industry. Archives of Civil and Mechanical Engineering. 2008;8:103-17.

[2] Link TM, Grimm JS. Axial crash testing of advanced high strength steel tubes. SAE Technical Papers. 2005.

[3] Vankuren RC, Scott JE. Energy absorption of high-strength steel tubes under impact crush conditions. SAE Technical Papers. 1977.

[4] Ling TW, Zhao XL, Al-Mahaidi R, Packer JA. Investigation of block shear tear-out failure in gusset-plate welded connections in structural steel hollow sections and very high strength tubes. Engineering Structures. 2007;29:469-82.

[5] Qian X, Dodds Jr RH, Choo YS. Elastic–plastic crack driving force for tubular X-joints with mismatched welds. Engineering Structures. 2005;27:1419-34.

[6] Wang Y-B, Li G-Q, Chen S-W, Sun F-F. Experimental and numerical study on the behavior of axially compressed high strength steel box-columns. Engineering Structures. 2014;58:79-91.

[7] Heidarpour A, Cevro S, Song Q-Y, Zhao X-L. Behaviour of stub columns utilising mild-steel plates and VHS tubes under fire. Journal of Constructional Steel Research. 2014;95:220-9.

[8] Rhodes J, Zhao XL, Van Binh D, Al-Mahaidi R. Rational design analysis of stub columns fabricated using very high strength circular steel tubes. Thin-Walled Structures. 2005;43:445-60.

[9] Van Binh D, Al-Mahaidi R, Zhao XL. Finite element analysis (FEA) of fabricated square and triangular section stub columns utilizing very high strength steel tubes. Advances in Structural Engineering. 2004;7:447-57.

[10] Zhao XL, Van Binh D, Al-Mahaidi R, Tao Z. Stub column tests of fabricated square and triangular sections utilizing very high strength steel tubes. Journal of Constructional Steel Research. 2004;60:1637-61.

[11] Heidarpour A, Cevro S, Song QY, Zhao XL. Behaviour of innovative stub columns utilising mild-steel plates and stainless steel tubes at ambient and elevated temperatures. Engineering Structures. 2013;57:416-27.

[12] Jiao H, Zhao X-L. Tension Capacity of Very High Strength (VHS) Circular Steel Tubes after Welding. Advances in Structural Engineering. 2004;7:285-96.

[13] Xu F, Sun G, Li G, Li Q. Experimental investigation on high strength steel (HSS) tailor-welded blanks (TWBs). Journal of Materials Processing Technology. 2014;214:925-35.

[14] Ito R, Shiga C, Kawaguchi Y, Nakamura T, Hiraoka K, Hayashi T et al. Controlling of the softened region in weld heat affected zone of ultra fine grained steels. ISIJ International. 2000;40:S29-S33.

[15] Jia J, Yang SL, Ni WY, Bai JY. Microstructure and mechanical properties of fiber laser welded joints of ultrahigh-strength steel 22MnB5 and dual-phase steels. Journal of Materials Research. 2014;29:2565-75.

[16] Modenesi PJ, Fajardo RF, Santos DB. Microstructure and mechanical property development in the heat affected zone of ultrafine grained HSLA steel. Materials Science Forum2010. p. 3704-9.

[17] Pirinen M, Martikainen Y, Ivanov SY, Karkhin VA. Comparative analysis of the microstructure of the heat-affected zone metal in welding of high-strength steels. Welding International. 2015;29:301-5.

[18] Wang J, Li Y, Liu P. Effect of weld heat input on toughness and structure of HAZ of a new super-high strength steel. Bulletin of Materials Science. 2003;26:301-5.

[19] Frydman S, Konat Ł, PĘKalski G. Structure and hardness changes in welded joints of Hardox steels. Archives of Civil and Mechanical Engineering. 2008;8:15-27.

[20] Akselsen OM, Rorvik G, Onsoien MI, Grong O. Assessment and predictions of HAZ tensile properties of high-strength steels. Welding Journal (Miami, Fla). 1989;68:356s-62s.

[21] Němeček S, Mužík T, Míšek M. Differences between Laser and Arc Welding of HSS Steels. Physics Procedia. 2012;39:67-74.

[22] Ferro P, Tiziani A. Metallurgical and mechanical characterization of electron beam welded DP600 steel joints. Journal of Materials Science. 2012;47:199-207.

[23] Zeman M. Assessment of weldability of WELDOX 1100 high-strength quenched and tempered steel. Welding International. 2009;23:73-82.

[24] Hall AM. Introduction to Today's Ultrahigh-strength Structural Steels: Issued Under the Auspices of American Society for Testing and Materials and the Defense Metals Information Center: ASTM International; 1971.

[25] St. Węglowski M, Zeman M. Prevention of cold cracking in ultra-high strength steel Weldox 1300. Archives of Civil and Mechanical Engineering. 2014;14:417-24.

[26] Shi G, Jiang X, Zhou W, Chan T-M, Zhang Y. Experimental investigation and modeling on residual stress of welded steel circular tubes. Int J Steel Struct. 2013;13:495-508.

[27] Jia-Lin Ma, Tak-Ming Chan, Young B. Material characterization of cold-formed high strength steel hollow sections through tensile coupon tests. 7th European conference on steel and composite structures (EUROSTEEL 2014). Naples, Italy2014.

[28] Javidan F, Heidarpour A, Zhao XL, Minkkinen J. Performance of innovative fabricated long hollow columns under axial compression. Journal of Constructional Steel Research. 2015;106:99-109.

[29] Klas W. Welding processes handbook2003.

[30] AS/NZS1554.7 Structural steel welding-Welding of sheet steel structures. Part7. Sydney: Standards Australia; 2006.

[31] Shikanai N, Mitao S, Endo S. Recent Development in Microstructural Control Technologies through the Thermo-Mechanical Control Process (TMCP) with JFE Steel's High-Performance Plates. JFE technical report. 2008;11:1-6.

[32] E606-04 Standard Practice for Strain-Controlled Fatigue Testing. ASTM International; 2004.

[33] AS 1391-2007 Metallic Materials-Tensile testing at ambient temperature. Sydney: Standards Australia; 2007.

[34] AS/NZS 4600:2005 Cold-formed steel structures. Australian/New Zealand Standard; 2005.

[35] Song QY, Heidarpour A, Zhao XL, Han LH. Performance of Unstiffened Welded Steel I-Beam to Hollow Tubular Column Connections Under Seismic Loading. International Journal of Structural Stability and Dynamics. 2014;15:Article number: 1450033.

[36] Nassirnia M, Heidarpour A, Zhao X-L, Minkkinen J. Innovative Hollow Corrugated Columns: A Fundamental Study. Engineering structures 2015;94:43-53.

[37] Heidarpour A, Bradford MA. Behaviour of a T-stub assembly in steel beam-to-column connections at elevated temperatures. Engineering Structures. 2008;30:2893-9.

[38] Farahi M, Heidarpour A, Zhao XL, Al-Mahaidi R. Compressive behaviour of concrete-filled double-skin sections consisting of corrugated plates. Engineering Structures. 2016;111:467-77.

[39] Kang L, Ge H, Kato T. Experimental and ductile fracture model study of single-groove welded joints under monotonic loading. Engineering Structures. 2015;85:36-51.

[40] Lee C-H, Chang K-H, Do VNV. Finite element modeling of residual stress relaxation in steel butt welds under cyclic loading. Engineering Structures. 2015;103:63-71.

[41] Mirmomeni M, Heidarpour A, Zhao X-L, Hutchinson CR, Packer JA, Wu C. Mechanical properties of partially damaged structural steel induced by high strain rate loading at elevated temperatures – An experimental investigation. International Journal of Impact Engineering. 2015;76:178-88.

[42] Hosseini S, Heidarpour A, Collins F, Hutchinson CR. Effect of strain ageing on the mechanical properties of partially damaged structural mild steel. Construction and Building Materials. 2015;77:83-93.

[43] Sinaie S, Heidarpour A, Zhao XL. Stress-strain-temperature relation for cyclically-damaged structural mild steel. Engineering Structures. 2014;77:84-94.

[44] Considere A. Memoire sur lemploi du fer et de lacier dans les constructions. Ann Ponts Chaussees 1885;9:574-775.

[45] Azhari F, Heidarpour A, Zhao X-L, Hutchinson CR. Mechanical properties of ultra-high strength (Grade 1200) steel tubes under cooling phase of a fire: An experimental investigation. Construction & Building Materials. 2015;in press.

[46] Callister WD, Rethwisch DG. Materials Science and Engineering: An Introduction (9th Edition). 2014.

[47] Chipman J. Thermodynamics and phase diagram of the Fe-C system. MT. 1972;3:55-64.

[48] Ling TW. The tensile behaviour of gusset-plate welded connections in very high strength (vhs) tubes. Australia: Monash University; 2005.

[49] Bhadeshia HKDH, Honeycombe SR. 9 - The Tempering of Martensite. In: Honeycombe HKDHBR, editor. Steels (Third Edition). Oxford: Butterworth-Heinemann; 2006. p. 183-208.

[50] Matsuda H, Mizuno R, Funakawa Y, Seto K, Matsuoka S, Tanaka Y. Effects of auto-tempering behaviour of martensite on mechanical properties of ultra high strength steel sheets. Journal of Alloys and Compounds. 2013;577, Supplement 1:S661-S7.

Application of high strength and ultra-high strength steel tubes in long hybrid compressive members: experimental and numerical investigation

Monash University

Declaration for Thesis Chapter 4

Declaration by candidate

In the case of chapter 4 my contribution to the work involved the following:

Nature of contribution	Extent of contribution (%)
Developing ideas, Establishing methodologies, Experimental work, Data analysis, Write-up and revision	70%

The following authors contributed to the work:

Name	Nature of contribution	Extent of contribution (%)
Dr. Amin Heidarpour	Developing ideas, Input into manuscript, Revision, Financial support	18%
Prof. Xiao-Ling Zhao	Revision, Financial support	10%
Mr. Jussi Minkkinen	Providing tube specimens, Revision	2%

The undersigned hereby certify that the above declaration correctly reflects the nature and extent of the student's and co-authors' contributions to this work.

Student signature ████████ Date: 30/01/2017

Main Supervisor's signature ████████████ Date: 30/01/2017

4.1. Abstract

With the increasing application of high strength steel material in industries, there is a high potentiality for taking advantage of the exceptional load-bearing capacities of this material in construction practice. In the present study, an innovative application for high and ultra-high strength steel material is proposed which enhances the overall behaviour of structural elements. The high strength and ultra-high strength steel with nominal tensile strength of 750 MPa and 1250 MPa, respectively, are proposed to be utilised as tube elements welded to corners of mild steel plates shaping an innovative hybrid section. This section takes advantage of the combined material properties of the two constituting elements in terms of strength, local buckling behaviour and ductility. Large-scale tests and numerical analysis have been conducted to compare the behaviour of the proposed sections against conventional welded sections. The effect of heat on the material properties of the hybrid section has also been considered. These effects are included in the finite element modelling of innovative columns where numerical outputs have been verified accordingly.

Keywords: High strength steel tubes, ultra-high strength steel tube, hybrid fabricated section, compressive behaviour, finite element modelling

4.2.   Introduction

Due to their unique characteristics such as strength, energy absorption, weight saving etc. high strength (HS) and ultra-high strength (UHS) steel materials are widely used in industrial productions. One of the most wide spread applications of high strength steel has been in automobile manufacturing, for instance its utilisation in propeller shafts, suspension parts and doors under impact and crush conditions [1-3]. Accordingly, the unique specifications of high strength steel can be proposed as an exceptional alternative for conventional structural material. The use of this material can lead to a great deal of reduction in the consumed mass and increase the overall load bearing capacity. This is due to the fact that high strength steel and mild steel possess similar weights per equal volume. Published researches can be found on the employment of high strength circular steel tubes in structures and structural elements. Namely, roof structures [4], stub columns consisting of high strength steel tubes under compression and members under bending and tension [5-7], tube joints and welded connections in hollow steel sections [8-10] and CFRP strengthened butt-welded ultra-high strength steel tubes [11]. In terms of material properties, fracture-mechanical characterisation of high-strength steel tubes adopting numerical and experimental data was done with respect to the specimen geometry and also thermo-mechanical conditioning during the production of tubes [12]. The use of high strength material also leads to longer life span of structure. Specifically, UHS steel material utilised in this study exhibits an increase of 2.5 times of life span than that of mild tubes [13]. The cost effectiveness of high strength material has also thoroughly been studied in previous literature [14, 15]. In terms of cost, a comparison among high strength steel tubes and normal steel tubes in realistic possibilities of building columns, considering the strength, stability and stiffness conditions, clearly indicated that using high strength steel in structures is more economic [16].

In compressive loading conditions, HS and UHS tubes experience failure modes due to the brittle behaviour of material as well as global buckling, depending on the geometry and slenderness. In fact the lower ductility of sections consisting only of HS and UHS steel compared to mild steel sections has an undermining effect on the global performance of the whole structure. Therefore, an innovative hybrid section consisting of HS or UHS tubes welded to mild steel plates has been proposed [17] which significantly enhances the compressive capabilities of high strength steel material in terms of both strength and ductility. In this section type, high strength steel tubes are welded to the corners of mild steel plates. The closed geometry of the proposed section consisting of circular tubes exhibits exceptional performance under compression in terms of local buckling [15]. The behaviour of short lengths of these innovative sections was investigated under various conditions such as fire [18-20]. This study looks into the behaviour of higher lengths of columns and the effect of section configuration on the overall ductility of hybrid columns.

As opposed to cold-formed material elements [21], when it comes to hybrid sections, welding has a significant effect on the material properties and behaviour in the vicinity of weld, known as the heat affected zone (HAZ). Several research works are available investigating the effect of heat and high temperatures on steel [22-27] and specifically welding on high strength and ultra-high strength tube materials [28-30]. Properties of the material located at various distances from weld in fabricated sections consisting of high strength and ultra-high strength steel tubes have been derived with respect to the tube manufacturing process, type of welding and post-welding conditions [31].

The present research work, as opposed to previous literature available on this specific section focusing only on stub columns, experimentally investigates the behaviour of long innovative specimens fabricated from HS or UHS steel tubes and mild steel plates under static compression. The load-bearing performance of high strength and ultra-high strength steel tube in the compressive behaviour is investigated and compared to mild steel tubes.

The effect of welding on each of the column constitutive elements have been taken into consideration to understand the detailed structural characteristics of the proposed high strength section. This has also led to achieving a robust and precise numerical finite element model.

4.3. Specimen specifications

4.3.1. Geometric specifications

The hybrid fabricated column section welded from steel plates and tubes is shown in Figure 4.1. The plate elements used for innovative fabricated columns are Grade 250 mild steel with nominal width of 210mm and thickness of 3mm. Tubes with nominal outer diameter of 76.1mm and thickness of 3.2mm are used having three different material properties. In total, 14 specimens are tested in different lengths of one and two meters including individual tubes, conventional welded box columns and the hybrid fabricated columns. Individual tubes have similar sections used in the hybrid column in terms of geometry. Likewise, the width and thickness of the plates incorporated in the conventional box section are equal to those of plates used in the innovative hybrid section. Geometric specifications of all test specimens are shown in Table 4.1. As for specimen labelling, **S** represents **s**ingle tube, **WB** represents conventional **w**elded **b**ox and **IFC** shows the initials of **i**nnovative **f**abricated **c**olumn. The letters that come after the dash indicated the material type of the tube where **m**ild steel **t**ube, **h**igh **s**trength **t**ube and **u**ltra-**h**igh **s**trength **t**ube are represented by **MT**, **HST** and **UHST**, respectively. The number at the end of each specimen label refers to the length of column. Effective design slenderness ratios are also calculated for each column by dividing the ratio of design effective length to radius of gyration. Considering the
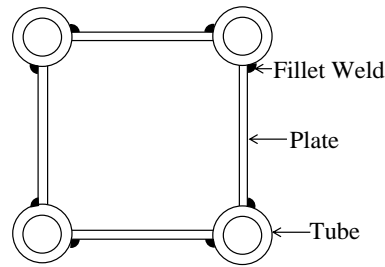
Figure 4.1. IFC section geometry.

Table 4.1. Geometric specifications of test specimens.

Specimen cross-section	Specimen label	Length (mm)	Design Slenderness ratio
◎	S-MT1	1000	27.1
◎	S-HST1	1000	27.1
◎	S-UHST1	1000	27.1
▢	WB-1	1000	8.2
⊞	IFC-MT1	1000	6.3
⊞	IFC-HST1	1000	6.3
⊞	IFC-UHST1	1000	6.3
◎	S-MT2	2000	54.2
◎	S-HST2	2000	54.2
◎	S-UHST2	2000	54.2
▢	WB-2	1000	16.3
⊞	IFC-MT2	2000	12.6
⊞	IFC-HST2	2000	12.6
⊞	IFC-UHST2	2000	12.6

4.3.2. Fabrication, welding and imperfections

In the proposed fabricated section, fillet weld is used to connect the plates and tubes to each other. This welding configuration is more convenient in terms of cost and performing only on the outside of column [15]. The welding wire is 2.4mm of the category AWS A5.9 ER2209. Type of welding is gas tungsten arc welding (G.T.A.W) with a 0.2% proof stress and tensile strength equal to 560 – 620MPa and 800 – 835 MPa, respectively. This type of arc welding leads to consistence weld thickness throughout the length of column as opposed to other welding types such as metal inert gas (MIG) welding which helps to have a more consistent behaviour in the column. The rate of welding for all fabrications is in a range of 75–95 mm/min and the gas used is 99.9% argon gas. All welding methods used are in compliance with AS/NZS1554.7:2006 [32].

The existence of imperfections has a direct effect on the compressive behaviour of members and provisions are made in design standards regarding the maximum value allowed for imperfections of different elements in welded members. Therefore, the out-of-flatness and out-of-square of the column section and the length deviations of each fabricated section is obtained using a precise measuring system. The centre of each plate and tube in one end of the column is considered as a reference point for that member and measurements are done accordingly throughout the length. Besides, the distance of the reference points of plates and tubes are also measured relative to each other. These values meet the standard requirements and are also considered in the numerical modelling. According to the Australian standard provisions for fabricated sections [33], local plate imperfections for a section with the geometries used in this study should not be more than 3mm for one flange and 6mm for two parallel flanges. Here, the local imperfections of points at two opposite plate elements are measured relative to each other. These maximum imperfections of plate elements in the transverse direction are in the range of 0.7-3mm for different sections. For

the longitudinal direction, the straightness of plates and tubes satisfied the standard regulation which is the greatest of 3mm or L/1000 where L is the length of column.

4.3.3. Material properties

Tension material tests are conducted for each steel type following the guidelines of ASTM-E8M-04 [34] and AS1391[35]. The coupon geometry taken from the plates and tubes are shown in Figure 4.2(a). The longitudinal specimens are extracted from tube samples with 90 degrees angle from the tube weld as outlined in above standards. All quasi-static tests are done in a Shimadzu tensile test machine with a load capacity of 300kN applying constant grip displacement rate of 0.5mm/min. Data acquisition is followed using both strain-gauges and non-contact MTS laser extensometer (model LX500) data to have sufficient understanding of yield and post-yield behaviour. Due to the occasion of early failure in strain gauges, the laser extensometer provides the material results until failure. Stress versus strain curves read from the laser extensometer data of the average test specimen for the mild steel plate and three different steel tubes are shown in Figure 4.2(b). Along with the strength increase in HS and UHS materials, the ductility experiences a significant decrease. The stress values are obtained from precise measurement of each individual test coupon. The average mechanical properties of three repetitions for each kind of mild steel plate, mild steel tube, high strength steel tube and ultra-high strength steel tube are presented in Table 4.2. Yield strength is determined based on proof strength using the offset method with a lay-off equal to 0.2% and the ultimate strain is defined as the equivalent strain at ultimate stress. The ratio of ultimate strength to yield strength is specified in the last column of Table 4.2 which is bigger than 1.08 in all four materials [36].

Table 4.2. Average measured mechanical properties of material (±error%)

Material	Elastic modulus (GPa)	Yield strength (MPa)	Ultimate strength (MPa)	Strain at UTS	Ultimate to Yield ratio
MS plate	207 (±0.1%)	265 (±0.4%)	376 (±4%)	23%	1.42
MS tube	198 (±0.1%)	305 (±0.3%)	342 (±0.1%)	11%	1.12
HSS tube	205 (±1%)	772 (±2%)	847 (±2%)	2.5%	1.10
UHSS tube	209 (±0.5%)	1247 (±4%)	1385 (±2%)	2.1%	1.11

(a)   (b)
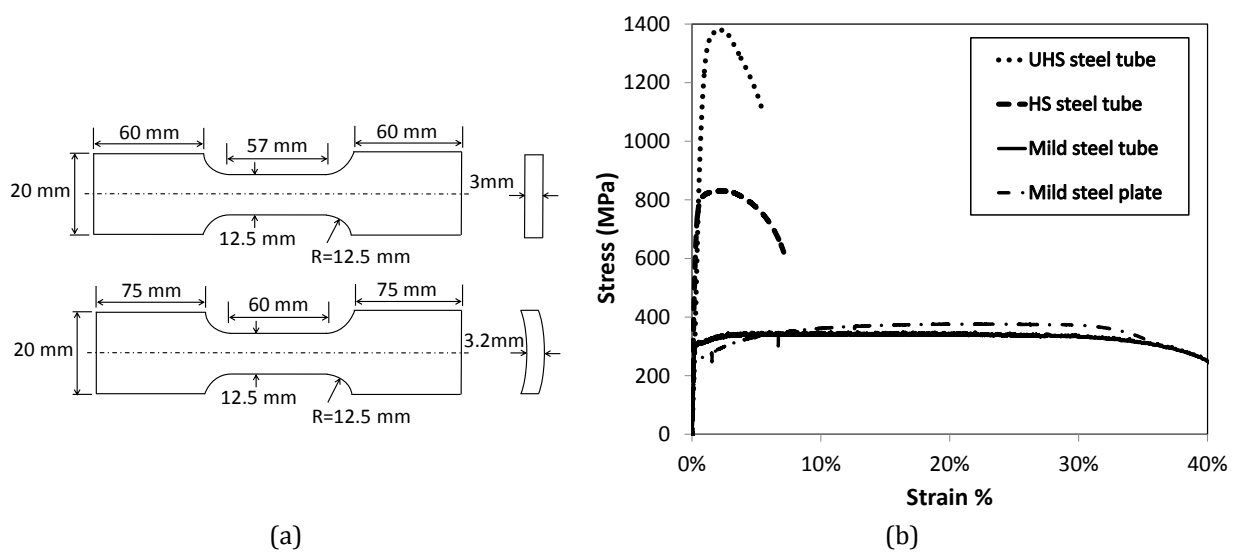
Figure 4.2. (a) Tensile specimen dimensions of plate and tube materials; (b) Stress vs. strain curve for each material type.

4.4. Experimental compressive tests

The machine used in all the large scale column compression tests is a 5000kN capacity Amsler machine with fixed ends and clamped conditions. Strain gauges are installed on column surfaces to record the longitudinal strain magnitude in different locations of column. Linear Variable Differential Transformers (LVDTs) are also used for reporting the displacements of the loading plate. Static loading is applied with a rate equal to 1mm/min.

4.4.1. Single tubes

For having a comparable overview of the behaviour of the tubes incorporated in the fabricated columns in terms of strength and ductility, all single tubes with different material properties and lengths are individually tested subjected to static compression. To avoid the local failure taking place in the vicinity of loading plates, steel rings with the thickness of 25mm were placed on both ends which provide fixed conditions at both ends. Figure 4.3(a) and (b) compare the load versus displacement curves of the three types of single tubes with one and two-meter lengths, respectively. The peak load undergone by MT, HST and UHST with one meter and two-meter lengths is shown in Table 4.3.

(a)	(b)
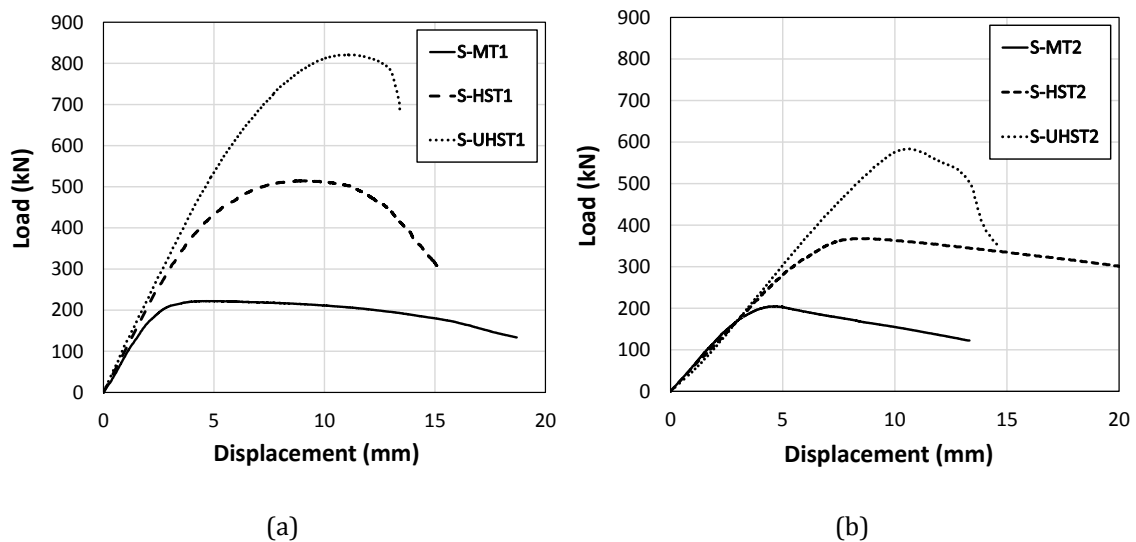
Figure 4.3. Load vs. displacement curves of single MT, HST and UHST specimens: (a) 1m, (b) 2m.

The failure modes of the three specimens with one and two-meter lengths are also shown in Figure 4.4. The dominant failure mechanism of mild steel single tube is global buckling. However, with changing the material of steel from mild to higher strength steel, the global buckling at failure experiences a noticeable difference. It is obvious from Figure 4.4 for one and two-meter specimens that the bending deformation reduces in HST and UHST compared to MT. The ratio of maximum stress generated in single tubes to the ultimate

material strength of each specimen is calculated (see Table 4.3). The maximum stress is obtained from the load bearing capacity of each tube divided by the original cross-sectional area. These values for single tubes with similar lengths indicate that tube material affects the compressive behaviour by reducing its capacity compared to the actual material capacity. It can also be understood that with the increase in length of single tubes, this strength reduction is more obvious which reaches to about half the actual strength of the material. In such circumstances, it is highly beneficial to utilise the high strength of structural material in a way that the brittle failure and buckling effects are reduced compared to the actual material capacity. To quantify deformation capacity, ductility factor (Equation 4.1) is also calculated which is the ratio of ultimate displacement (D_u - displacement corresponding to the ultimate load) to the first yield displacement (D_y - displacement where yielding first occurs in the system). This factor is a non-dimensional term adopted here from available literature [37] to assess the displacement capacity of columns in their nonlinear region.

$$\mu = \frac{D_u}{D_y} \qquad\qquad (4.1)$$

The ductility factor also reduces with the increase in material strength and length. This performance of single tubes can be compared to those incorporated in the proposed hybrid sections and discussions are made in future sections.

Figure 4.4. Failure mechanism comparison of one and two-meter single MT, HST and UHST specimens

Table 4.3. Compressive behaviour of single tubes

Specimen label	Peak load (kN)	Peak stress (Mpa)	Ultimate strength (Mpa)	Ratio of peak stress to ultimate strength	Ductility factor
S-MT1	222	283	342	0.83	3.6
S-HST1	514	672	841	0.80	2.9
S-UHST1	822	1070	1397	0.77	2.5
S-MT2	204	261	342	0.76	2.3
S-HST2	368	477	841	0.57	1.9
S-UHST2	584	760	1397	0.54	1.4

4.4.2.   Fabricated one and two- meter columns

Four one-meter steel tubes are welded to corners of four mild steel plates shaping the innovative fabricated section as introduced in Section 4.4.2. These columns are fabricated

in one and two meters lengths. Behavioural variations resulted from material alteration of steel tubes from mild steel to HS and UHS steel tubes in one and two-meter specimen column groups are shown in Figure 4.5 and Figure 4.7, respectively, in which the load versus displacement curves of each column is presented. Following the strength rise, softening behaviour exhibits a difference in both one and two-meter column types when varying the tube materials. It is observed from the load-displacement results that the softening part of column consisting of mild steel tube exhibits a very gradual drop after the peak load, while in the column consisting of HST the reduction is less gradual and that for UHST shows the most rapid post peak fall.
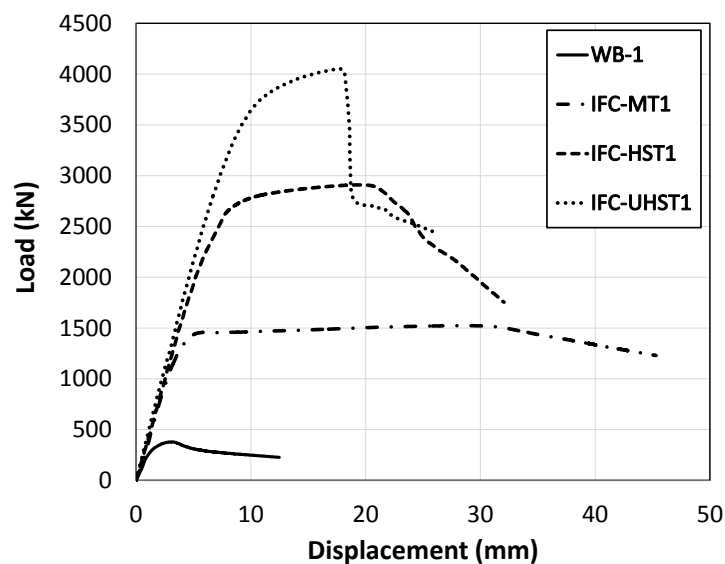
Figure 4.5. Load vs. displacement curves of one meter IFC column specimens

Further analysing the curves shown in Figure 4.5 and Figure 4.7, the displacement behaviour of columns with different tube material varies within one and two meter long columns. In one meter columns, the total displacement corresponding to the peak load decreases in columns with tube material from mild steel to HS and UHS while an opposite trend is observed in two-meter columns. The increase in peak-corresponding displacement in two meter columns with higher strength tubes compared to that of mild tubes leads to the understanding that with the increase in length, the column elements can undergo a

higher amount of displacement while reaching the load bearing capacity. Although, it can be seen that this higher displacement capacity also results in a more sudden softening curve. It is worth noting that the cross-sectional area and weight are kept constant among all three tested columns of same length. Therefore, the increase in the load bearing capacity of columns consisting of higher strength steel is significantly convenient in both design and economic point of view. Peak load undertaken by each of the test specimens is quantitatively discussed and comprehensively investigated in Section 4.5.
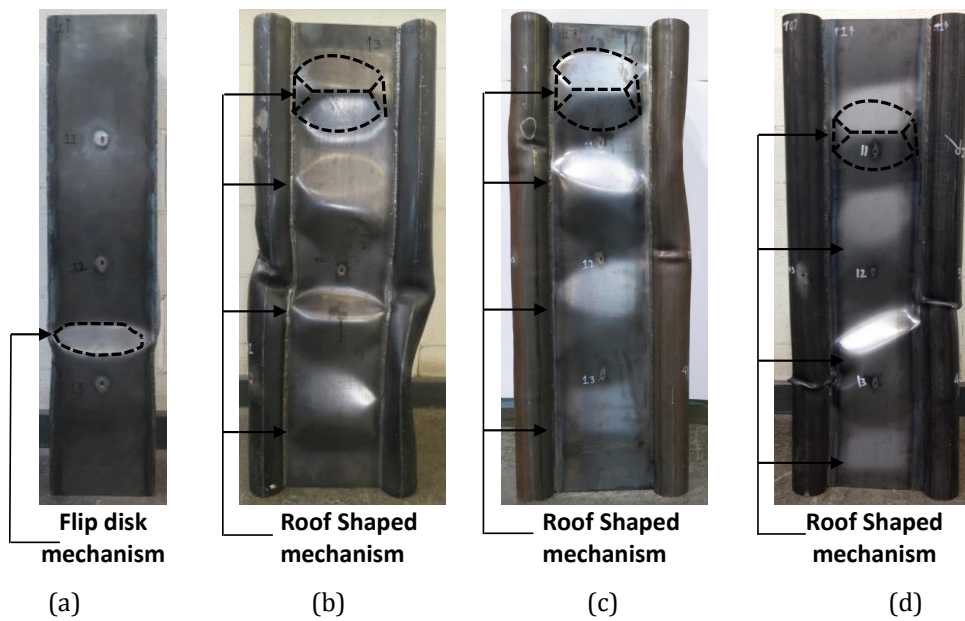
Figure 4.6. Failure mode of one meter IFC column specimens (a) WB-1, (b) IFC-MT1, (c) IFC-HST1 and (d) IFC-UHST1.
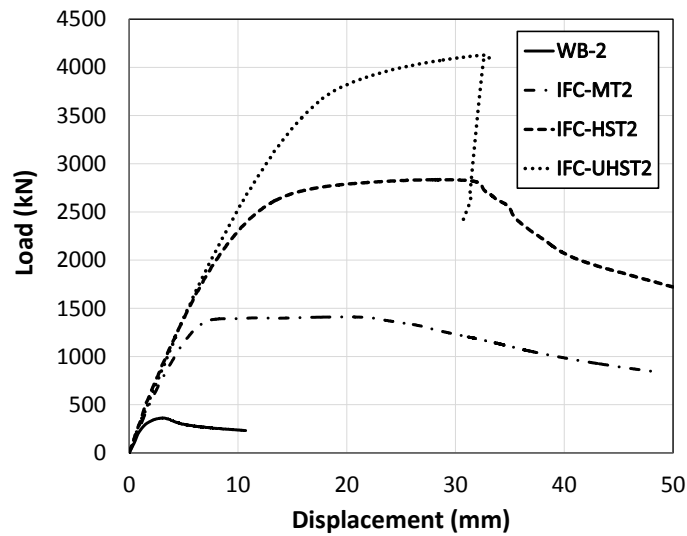
Figure 4.7. Load vs. displacement curves of two meters IFC column specimens

The failure mechanisms of three types of columns with one and two meters length are shown in Figure 4.6 and Figure 4.8, respectively. The dominant failure mode in the innovative hybrid section plates are roof shaped mechanism as opposed to the flip disk mechanism observed in the conventional box section. Both deformed shapes are shown with dashed line on each column figure. A step by step illustration of the failure sequence of innovative hybrid sections under compression is shown in Figure 4.9 where the relevant loading and displacement condition of each point is also shown. Up until the peak of the load-displacement curve, the plates undergo a relatively high amount of deformation, while the local deformation of tube has just initiated. Moving towards the end of the curve, the tubes also undergo severe deformations as well and following the tube material, column failure mechanism occurs.
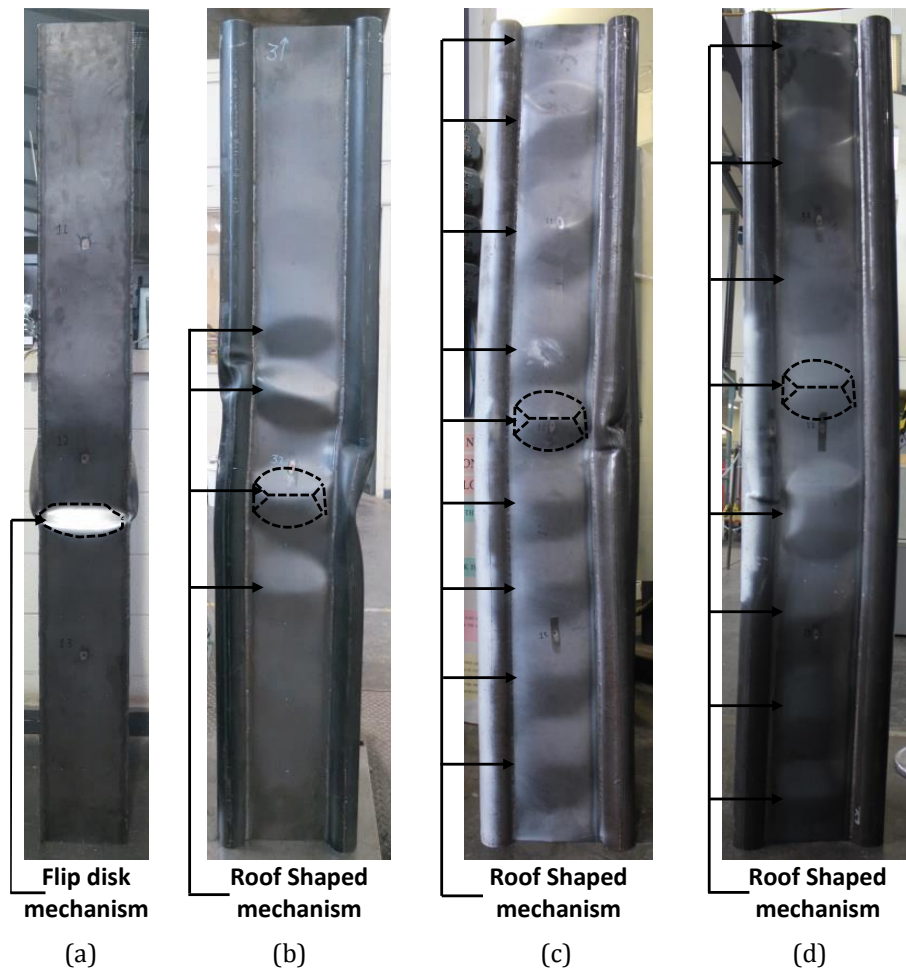
Figure 4.8. Failure mode of two meters IFC column specimens: (a) WB-2, (b) IFC-MT2, (c) IFC-HST2 and (d) IFC-UHST2
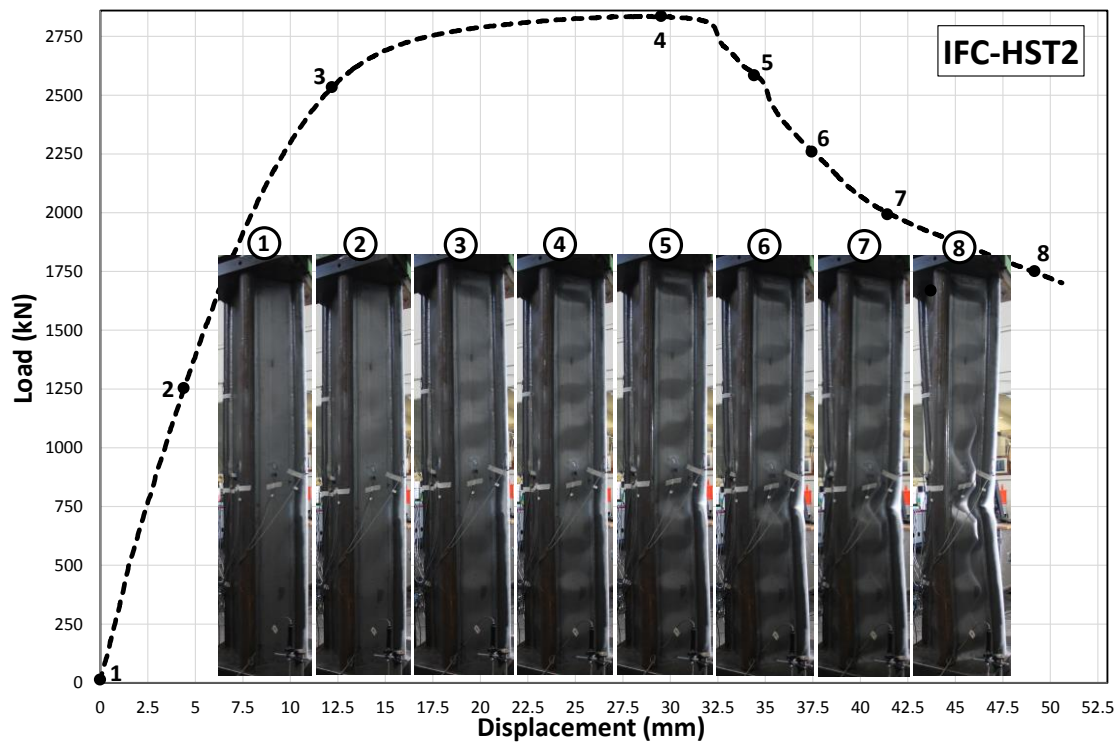
Figure 4.9. Failure mode sequence of IFC-HST2

4.5.   Experimental analysis

The load bearing capacity, displacements and ductility of innovative hybrid columns obtained from experimental compression tests are investigated in this section. With the aim of having a comparison among the behaviour of hybrid columns and a section with equal cross-sectional area, the capacity of four individual single tubes is added to that of a welded box column. The load summation of the four individual tubes and the box section is called superposition. As mentioned before, all individual plates and tubes incorporated in the superposition have geometries similar to those utilised in the innovative hybrid section. The results of compressive strength of single tubes, welded box sections, superposition and IFC elements of three different tube materials and two different lengths are presented in Table 4.4. It is obvious that increasing the length of a column may reduce its capacity. However, in case of one and two meter fabricated sections, imperfections also play an important role in

the behaviour of columns. In the case of IFC-UHS columns, the maximum longitudinal imperfection measured in the one meter fabricated column is 1.32 times more than that of the two-meter one which justifies the higher compressive strength in the later. The difference in imperfections is a result of the deformations during the manual fabrication process which are randomly induced in one and two meter columns. The IFC columns show a significantly higher strength compared to the welded conventional box sections. Calculating and interpreting the ratio of IFC compressive strength to the superposition of similar elements, shows extreme benefit when using the IFCs especially in higher lengths and consisting of higher strength steel tubes. This is due to the fact that the single HS and UHS tubes, as mentioned in section 4.4.1, experience a failure with a quite higher brittleness. Consequently, welding the tubes to corners of mild steel plates provides a superior interaction among the two elements, taking most advantage of the capacity of high strength material. As presented in the last column of Table 4.4, IFC -HST2 and IFC-UHST2 show more than 50% beneficial performance.

Table 4.4. Experimental compressive load bearing capacities and important ratios

| Single Tube | | Welded box strength (kN) | Superposition (kN) | IFC | | Ratio: IFC to Super-position |
Tube material	Strength (kN)			Tube material	Strength (kN)	
Cross section / Length (m)	◎	☐	4 × ◎ + ☐		⊚	
1	221	378	1266		1523	1.20
2	Mild 204	361	1179	Mild	1411	1.19
1	514	378	2436		2909	1.19
2	HST 367	361	1831	HST	2836	1.55
1	821	378	3665		4051	1.10
2	UHST 583	361	2695	UHST	4126	1.53

Table 4.5. The magnitudes of ductility factor for one and two-meter columns

Specimen	D_y	D_u	Ductility factor
WB-1	1	3.08	3.08
IFC-MT1	2.7	28.5	10.6
IFC-HST1	4.5	19.8	4.35
IFC-UHST1	5	17.8	3.5
WB-2	0.9	3.08	3.4
IFC-MT2	2.2	19.7	8.9
IFC-HST2	3.6	29.0	8.05
IFC-UHST2	5.1	32.6	6.4

Load versus displacement curve of the proposed hybrid column and that obtained from the superposition of individual elements for high strength and ultra-high strength steel tubes in addition to the compression test results of conventional welded box column with similar length are shown in Figure 4.10. The ductility of the IFC sections has also been examined with respect to the ductility of conventional welded box section. Table 4.5 shows the calculated ductility factors for all one and two-meter hybrid columns of three different tube materials under compression loading.

The recommended ductility factor for moderately ductile structures in standards is equal to 3 [38] that which all current compressive elements exceed. Comparing the ductile capacity of innovative hybrid section consisting of mild steel tube to the welded box section shows an increase of more than 3.4 times in ductility factor. This fraction reaches 1.35 and 1.14 in high and ultra-high strength columns due to the brittle nature of these materials. Longer columns, however, exhibit much higher ductility ratios compared to welded box sections in all tube materials which are 2.37 and 1.88 times in IFC-HST2 and IFC-UHST2 respectively.

(a)

(b)
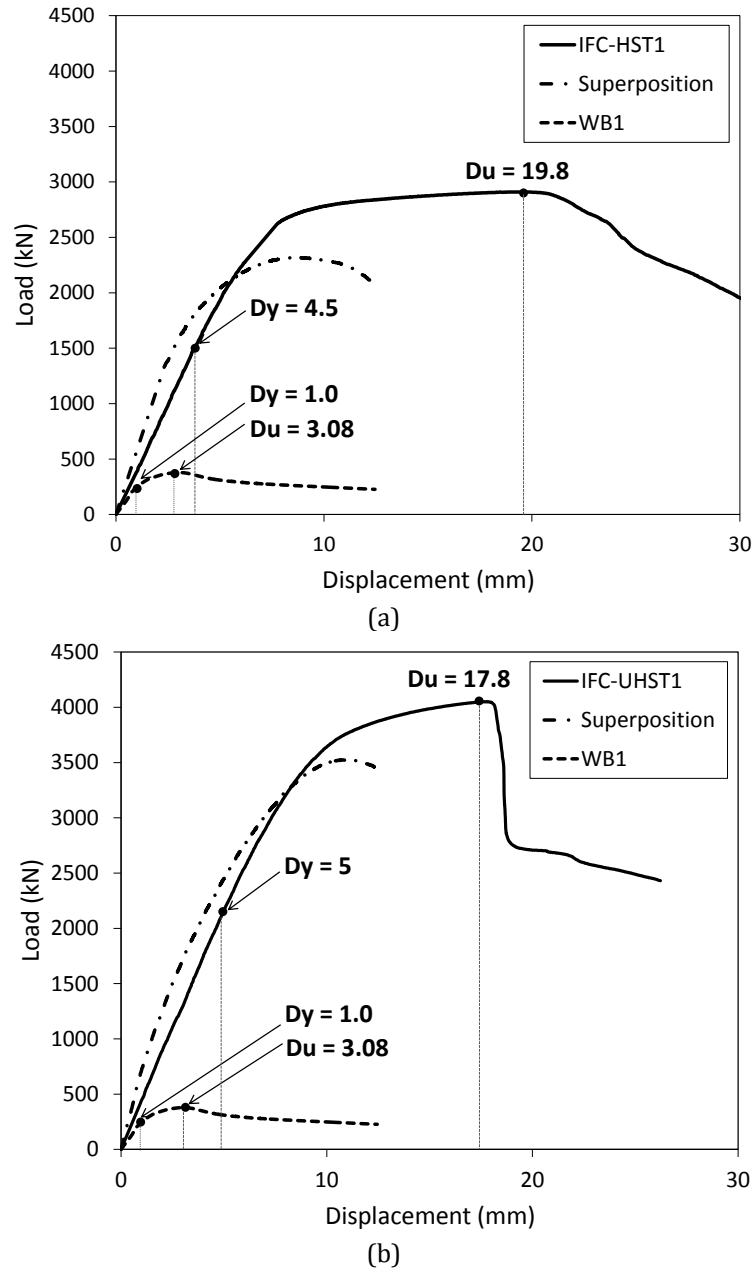
Figure 4.10. Load bearing capacity and ductility of: (a) one meter IFC-HST against one meter welded box and superposition of specimens; (b) Load bearing capacity and ductility of one meter IFC-UHST against one meter welded box and superposition of specimens.

From calculating the area underneath the load-displacement curve energy absorption characteristics of the innovative section with high strength and ultra-high strength are obtained which shows significant increase compared to the section consisting of mild tube with a percentage of 10 and 30, respectively. It should be noted that an analytical

comparison has also been conducted in section 4.8 on the proposed hybrid section and a conventional box section having similar slenderness and cross-sections. As opposed to single HS and UHS tubes that length increase resulted in lower ductility factors (see Table 4.3), the two-meter hybrid columns have higher ductility compared to one-meter ones.

4.6.   Numerical analysis

4.6.1.   Heat affected material properties

Based on previous research work on the effect of weld on steel material, the obtained mechanical properties of mild, high strength and ultra-high strength steel are incorporated in the numerical modelling of this study. Referring to previous studies [31], standard tensile tests have been conducted on tensile coupon specimens extracted from various locations from weld and mechanical properties reported. The heat induced by welding decreases the ultimate tensile strength but increases the corresponding strain of high and ultra-high strength steel tubes. However, in mild streel tube, test results showed an increase in both strength and ductility which the reason has thoroughly been explained in Ref. [31]. The normalised tensile strengths and the corresponding strains of steel tubes are summarised and shown in Table 4.6. For each material type, the ultimate strength values are normalised based on the furthest location (position 4) from weld which is proven not to be affected by weld.

Table 4.6. Normalised strength and ultimate strain of steel material at specific positions from weld

		Position 1	Position 2	Position 3	Position 4
Mild steel tube	Distance from weld (mm)	4	12.75	21.75	37.5
	Normalised tensile strength	1.13	1.05	1.03	1
	Ultimate strain	2.47	1.54	1.11	1
High strength steel tube	Label	Position 1	Position 2	Position 3	Position 4
	Distance from weld (mm)	5	12	28	42.5
	Normalised tensile strength	0.93	1.01	1.01	1
	Ultimate strain	2.28	1.93	1.3	1
Ultra-high strength steel tube	Label	Position 1	Position 2	Position 3	Position 4
	Distance from weld (mm)	3.5	7	22.5	42.75
	Normalised tensile strength	0.71	0.87	0.97	1
	Ultimate strain	2.39	0.88	0.79	1

4.6.2. Material model including fracture

Using the comprehensive material data discussed in the previous sections, a detailed numerical modelling of the proposed hybrid columns is obtained and verified with experiments. The numerical modelling is done in the commercial finite element software, ABAQUS [39]. Four-node shell elements (S4R) with the size of 10mm are used for meshing the tube and plate parts. The elastic modulus and yield strength of steel material is obtained from standard tensile material tests. Isotropic hardening behaviour of steel is calculated from true stress and logarithmic strain and given to the software as tabular input data based

on Equation (4.2) where σ_e and ε_e are the engineering stresses and strains, respectively, σ_t and ε_t are the true stresses and strains, respectively

$$\sigma_t = \sigma_e(1 + \varepsilon_e), \quad \varepsilon_t = \ln(1 + \varepsilon_e) \tag{4.2}$$

Two subsequent methods are used to conduct the compressive loading and post-buckling analysis of columns. The first step is a linear perturbation buckling analysis on the column. Degrees of freedoms are fixed in all end nodes except for the axial direction at one end where unit displacement is applied. Final nodal displacements of the model in each buckling mode are obtained and used as input for initial imperfection data in the next step which is a nonlinear Riks analysis. In the present numerical study, initial imperfections are given as a factor of the first mode of linear perturbation buckling analysis obtained from actual measurements.

As observed earlier from the experimental results, the ductility of UHS material is diminished compared to mild steel material. This distinctive behaviour of UHS tubes governs the failure modes of hybrid columns, leading to a less ductile trend in the load-displacement curve of the compression tests. To accurately reflect this behaviour in the numerical modelling of fabricated sections, following the hardening part of the material data, the softening behaviour is also necessary to be considered. For this aim, a basic simplified damage initiation model, followed by damage evolution extracted from the uniaxial tensile tests is introduced to ABAQUS. This ductile criterion is used for predicting the onset of damage which assumes that the equivalent plastic strain at the onset of damage is a function of stress triaxiality and strain rate [40]. The ductile fracture is obtained for quasi-static test speed so in this model fracture is not sensitive to steel strain rate. Based on the components of principal stress space, triaxiality factor is defined as

$$\eta = \frac{\sigma_m}{\sigma_{eq}} = \frac{(\sigma_1 + \sigma_2 + \sigma_3)/3}{\sqrt{\sigma_1^2 + \sigma_2^2 + \sigma_3^2 - \sigma_1\sigma_2 - \sigma_2\sigma_3 - \sigma_3\sigma_1}} \tag{4.3}$$

in which σ_m is the pressure stress and σ_{eq} is the Mises equivalent stress. The used damage model is compatible with the isotropic strain hardening behaviour of metal which is adopted for the behaviour of all material types in this study. Damage initiates in the material when the following integral criterion in ABAQUS is satisfied:

$$\omega_D = \int_0^{\varepsilon_{eq}^{**}} \frac{d\varepsilon_{eq}}{\varepsilon_{eq}^{**}(\eta)} = 1 \tag{4.4}$$

Here, ε_{eq}^{**} is the equivalent plastic strain at the onset of damage. In the above fracture criterion ω_D increases monotonically with plastic deformation and nonlinear strain paths are also accounted for [41].

The stress triaxiality which governs failure is considered to be characterised by plane strain state in UHS tubes in which the critical strain occurs. Due to the conditions of compression loading and failure modes in this study, the damage criterion is specified based on the results of uniaxial tensile test which gives a triaxiality factor equal to 1/3 and a fracture strain based on the obtained stress-strain curve for different materials. Following the damage initiation, its evolution is also introduced to ABAQUS based on a scalar damage approach shown in Equation (4.5). This considers both softening of yield stress and degradation of elasticity.

$$\sigma = (1 - D)\bar{\sigma} \tag{4.5}$$

In Equation (4.5) D is the overall damage variable and $\bar{\sigma}$ is the undamaged stresses that would have existed in the material in the absence of damage. Two limits of damage are equal to zero where the damage initiates and 1 where the material fractures completely (Figure 4.11(a)). Damage is obtained from the stress-displacement curve to avoid mesh

dependency in calculations. Results for four different material positions mentioned in section 4.6.1 tested from UHS tube is presented in Figure 4.11(b).
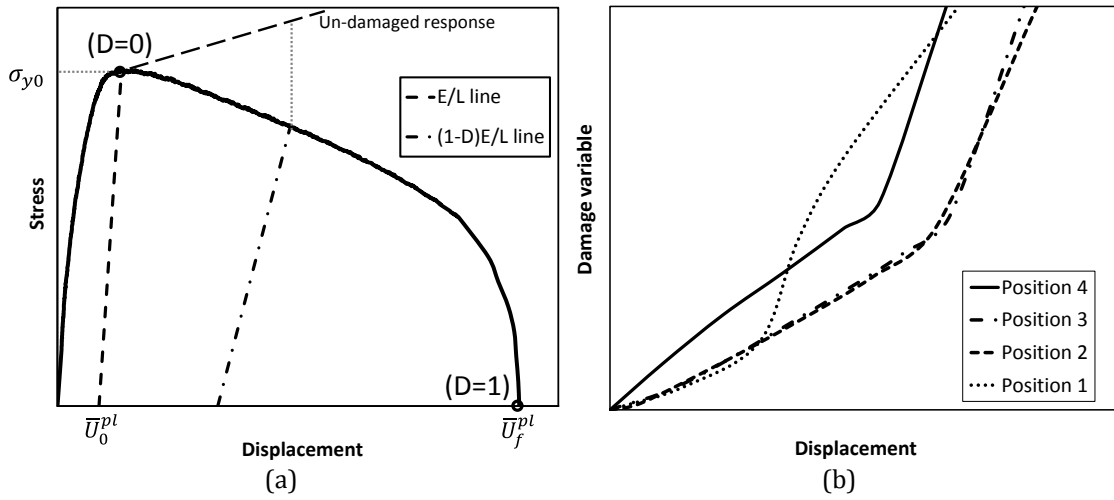
Figure 4.11. (a) Obtaining damage from the stress-displacement curve; (b) Damage variable derived for different UHS steel tube positions from weld.

4.6.3. Overall behaviour and weld effect analysis

Based on the material properties obtained from section 4.6.1, the load displacement curves for one and two meter columns consisting of HS and UHS tubes obtained from finite element model are validated against the experimental results and presented in Figure 4.12. The difference in the behaviour of the finite element model without considering weld heat effects differs in the peak load and ductility compared to that with considering the behaviour which this difference is more obvious in the IFC- UHS columns. When considering the heat effects, the strength of IFC-UHS1 and IFC-UHS2 columns decrease 11% and 7.1% respectively while that in IFC-HS1 and IFC-HS2 tubes reduces only around 1.2%. As opposed to strength, the ductility of IFC-UHS1 and IFC-UHS2 also reduces 21.7% and 23% respectively without considering the heat effects. Failure modes of the numerical finite element model are also depicted against the experimental outcomes in Figure 4.13. Failure modes in proposed hybrid columns are highly governed by the material properties of tubes and also column imperfections. Roof-shaped mechanism occurs in the plates of all column

types while HS tubes exhibit a more ductile failure compared to the UHS tubes which similar behaviour is predicted by the FE model.
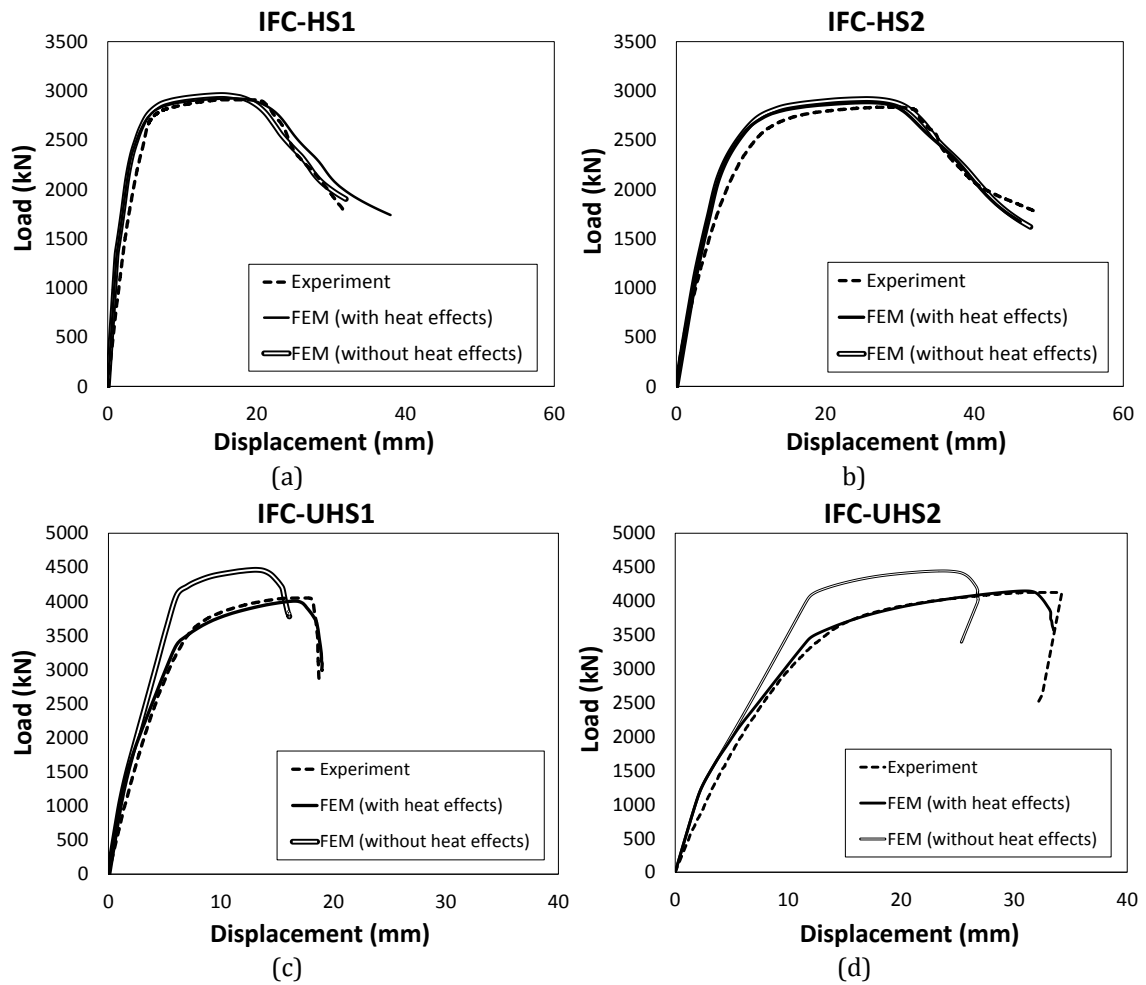
Figure 4.12. Load vs. displacement curves comparison of experimental results and numerical results of fabricated hybrid sections with and without heat effect modelling.

(a) IFC-HS1

(b) IFC-UHST1

(c) IFC-HST2

(d) IFC-UHST2
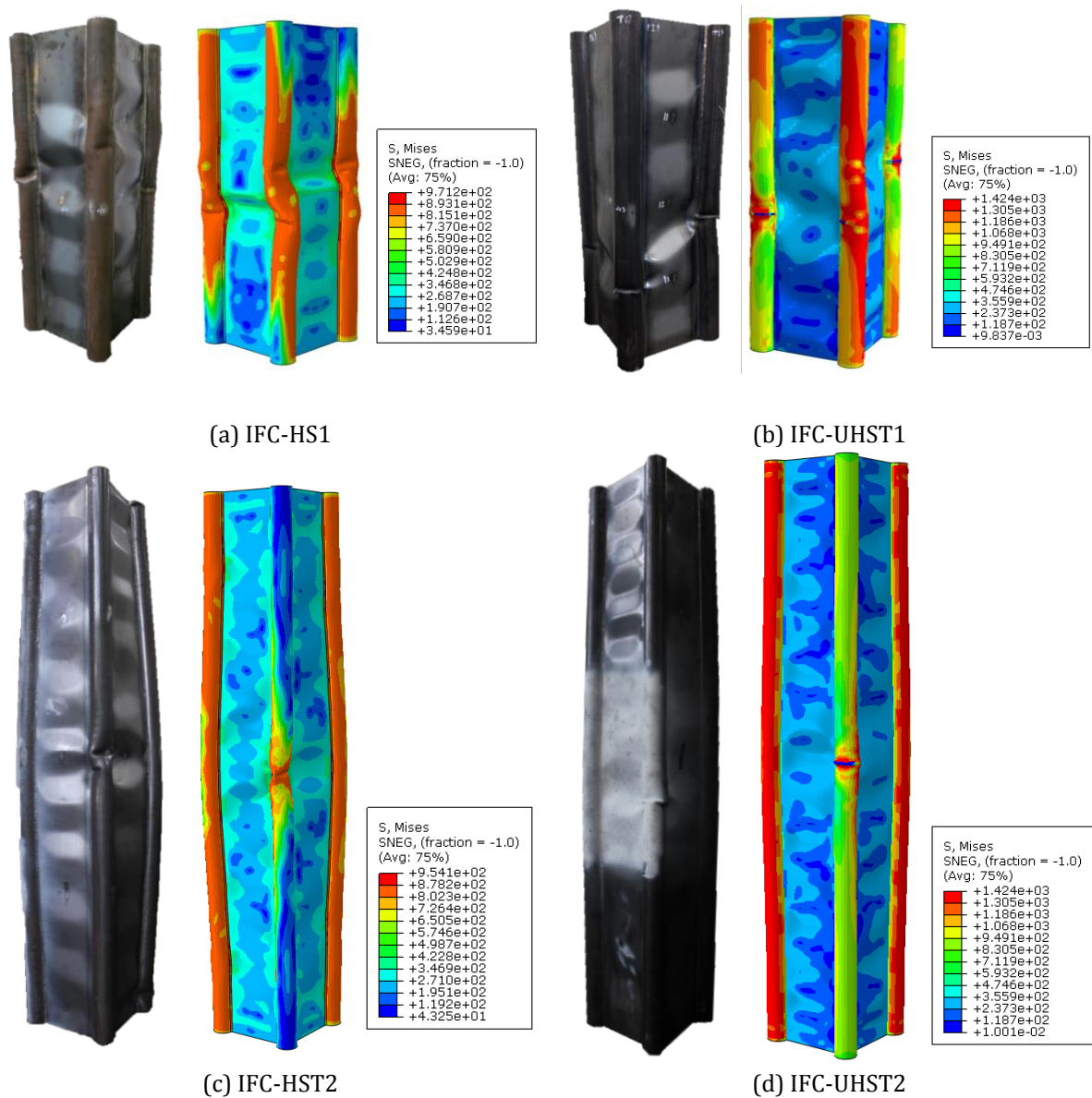
Figure 4.13. Failure mode comparison of experimental and numerical analysis along with stress couture (MPa).

4.7. Strain distribution

Using an optical measuring device called ARAMIS [42], the strain distribution on a specific part of the column mild plate in different stages of the test has been measured and analysed. This strain measurement is non-contact using cameras calibrated to read the strain from

the black and white pattern created on the desired part for measurement. The major (principle) strain distribution of a chosen stage after the peak load of test has been chosen and shown in Figure 4.14. This strain pattern is also compared to the output of major strain obtained from the FE model at the same location. It is noted that the strain values shown on the welds are not to be trusted due to their non-accurate calibration with respect to the ARAMIS. The values approximately higher than 7.5% correspond to the weld which is disregarded.
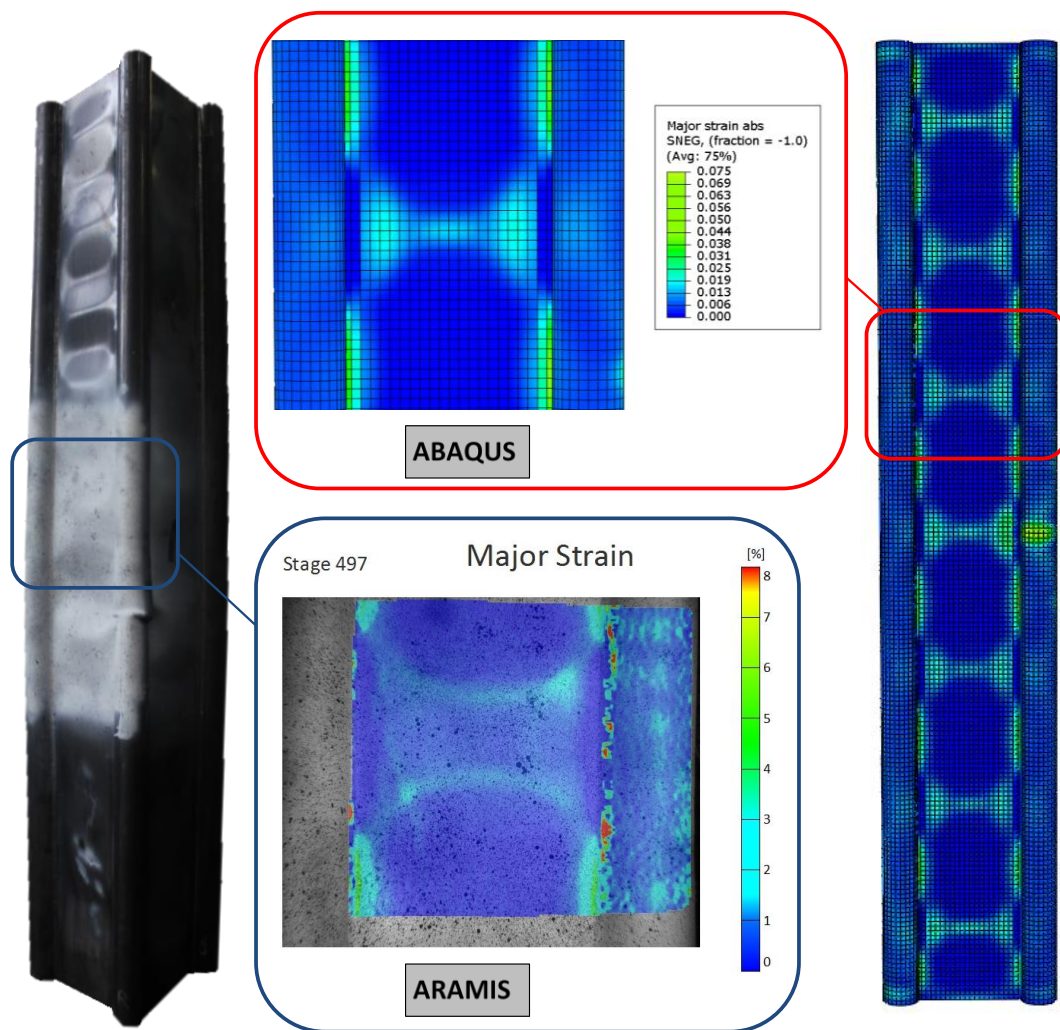
Figure 4.14. Mild steel strain distribution of a part of IFC-UHS2 compared to that of ABAQUS results.

Referring to studies conducted in this regard, plastic mechanism appearing in plates depends on the slenderness, yield strength and the point in which yield first occurs [43]. In the plates used in the proposed hybrid fabricated section this point occurs at the centre, where outward and inward deformations occur and roof shaped mechanism forms in the plates. Roof-shaped mechanism occurs at regular locations throughout the length of the column and plastic deformation continues while the welded tubes undergo high amounts of stress until final failure. Measured principle (major) strain at corners of plates welded to tubes reaches a value close to 7.5% (Figure 4.14).

4.8. Analytical slenderness comparison

In the experimental part of the current study, compressive behaviour of innovative sections was compared to individual welded box sections, single tubes and their superposition. In this section, the advantage of the proposed hybrid sections is investigated through conducting a comparison based on similar slenderness and cross-sectional areas. For this aim, a three meter welded box section labelled as WB-3 with plate width of 210mm and thickness of 6.5mm is chosen. The WB-3 column has similar cross section to the fabricated sections studied in this research work whilst due to section geometry differences, its slenderness is also the same as that of a four meter innovative column (Note that effective slenderness is the ratio of design effective length to radius of gyration). For the box section, compressive strength is derived from standard provisions given by Equation (4.6) [33] which also matches the analysis results of ABAQUS.

$$N_s = A_n f_y k_f, \qquad \lambda_n = \left(\frac{l_e}{r}\right)\sqrt{\frac{k_f f_y}{250}}, \qquad N_c = \alpha_c N_s \qquad (4.6)$$

in which, $N_s, k_f, \lambda_n, \alpha_c, N_c$ are the nominal section capacity, form factor, nominal slenderness ratio, dimensionless nominal axial force capacity factor and nominal member capacity, respectively. Looking at the compressive strength of the hybrid section compared to that of the welded box column with similar cross-section and slenderness, an advance of 63kN is obtained in terms of strength. The displacement corresponding to the load bearing capacity is also increased to 8 times which is due to the beneficial interaction between the tubes and plates. Four meter hybrid sections consisting of high and ultra-high strength steel tubes are also analysed and results presented in Table 4.7. Having similar slenderness, cross section and weight to the conventional section and also the section with mild steel tubes, the load bearing and deformation capacity of the proposed hybrid sections consisting of HST and UHST show a significant enhancement which is obvious from the results shown in Table 4.7.

Table 4.7. Analytical analysis of proposed hybrid sections with conventional box sections of similar slenderness.

Section type		Length (mm)	Cross sectional area (mm²)	Effective slenderness	Compressive strength (kN)	D_u (mm)
WB-3		3000	5460	24.5	1389	3.9
IFC-MT4		4000	5451	25.3	1452	32
IFC-HST4		4000	5451	25.3	2802	49
IFC-UHST4		4000	5451	25.3	4173	63.4

4.9.   Conclusions

The outcome of this research gives rise to the introduction of an innovative hybrid steel column taking advantage of the superior material properties of high strength and ultra-high

strength steel materials in construction. To avoid the undesirable brittleness of higher strength steel material, mild steel plates are welded to high strength tubes advancing the overall structural behaviour to a more ductile system. The following conclusions are made based on experimental data:

- Based on test results, sections fabricated from high strength steel tubes advance the load bearing limit of the column to around two times and the energy absorption to 10% of those for a similar section consisting of mild steel tubes. The strength improvement will reach a ratio of almost three times and energy absorption of 30% in the case where ultra-high strength steel tubes are utilised.

- Comparing the innovative column test outcomes to the quantitative superposition of four single tubes and a conventional box section with similar geometries and equal cross-sectional area shows a benefit of up to more than 50% in two meter columns of high and ultra-high steel tubes in terms of strength.

- Comparing ductility factors of the high strength innovative columns with conventional welded box columns made of similar plate dimensions shows a satisfactory increase which rises in two-meter columns compared to one-meter ones.

- Taking the effects of material characterisation and weld affected areas into consideration; a finite element model is validated against experimental results in terms of load-displacement curves, failure modes and strain distribution.

- Including HAZ properties in the numerical analysis of innovative hybrid sections reduces the load bearing capacity of sections consisting of UHT around 20%.

- Further analytical and numerical comparison among innovative and conventional columns with similar cross-section and slenderness ratios indicates that the

proposed section shows an increase in compressive load bearing capacity and the displacement corresponding to peak load especially in high strength tube material with respect to conventional welded box section.

4.10.   Acknowledgements

4.11.   References

[1] Shunsuke T, Koji S, Akio S. High strength steel tubes for automotive suspension parts - High strength steel tubes with excellent formability and forming technology for light weight automobiles. JFE Technical Report. 2004:32-7.

[2] Tanabe H, Anai I, Miyasaka A, Tanioka S. HAZ softening-resistant high-strength steel tubes for automobile propeller shafts. Nippon Steel Technical Report1995. p. 62-8.

[3] Vankuren RC, Scott JE. Energy absorption of high-strength steel tubes under impact crush conditions. SAE Technical Papers. 1977.

[4] Gangopadhyay KK, Guha D, Reddy PVN. Salt Lake Stadium roof, Calcutta, with high strength steel tubes. Structural engineer London. 1990;68:397-404.

[5] Jiao H, Zhao XL. Section slenderness limits of very high strength circular steel tubes in bending. Thin-Walled Structures. 2004;42:1257-71.

[6] Jiao H, Zhao X-L. Material ductility of very high strength (VHS) circular steel tubes in tension. Thin-Walled Structures. 2001;39:887-906.

[7] Zhao X-L. Section capacity of very high strength (VHS) circular tubes under compression. Thin-Walled Structures. 2000;37:223-40.

[8] Ling TW, Zhao XL, Al-Mahaidi R, Packer JA. Investigation of block shear tear-out failure in gusset-plate welded connections in structural steel hollow sections and very high strength tubes. Engineering Structures. 2007;29:469-82.

[9] Ling TW, Zhao XL, Al-Mahaidi R, Packer JA. Investigation of shear lag failure in gusset-plate welded structural steel hollow section connections. Journal of Constructional Steel Research. 2007;63:293-304.

[10] Jiao H, Mashiri F, Zhao X-L. Fatigue behavior of very high strength (VHS) circular steel tube to plate T-joints under in-plane bending. Thin-Walled Structures. 2013;68:106-12.

[11] Jiao H, Zhao XL. CFRP strengthened butt-welded very high strength (VHS) circular steel tubes. Thin-Walled Structures. 2004;42:963-78.

[12] Wiedemeier B, Sander M, Džugan J, Richard HA, Peters A. Fracure-mechanical characterization of high-strength steel tubes. 18th European Conference on Fracture: Fracture of Materials and Structures from Micro to Macro Scale2010.

[13] RAEX® R. Demand more from wear-resistant steels. RUUKKI RAEX® REFERENCES.

[14] Javidan F, Heidarpour A, Zhao X-L, Minkkinen J. Compressive Behavior of Innovative Hollow Long Fabricated Columns with High Strength and Ultra-High Strength tubes. 15th International Symposium on Tubular Structures. Rio de Janeiro, Brazil2015.

[15] Javidan F, Heidarpour A, Zhao XL, Minkkinen J. Performance of innovative fabricated long hollow columns under axial compression. Journal of Constructional Steel Research. 2015;106:99-109.

[16] Long HV, Jean-François D, Lam LDP, Barbara R. Field of application of high strength steel circular tubes for steel and composite columns from an economic point of view. Journal of Constructional Steel Research. 2011;67:1001-21.

[17] Zhao XL, Van Binh D, Al-Mahaidi R, Tao Z. Stub column tests of fabricated square and triangular sections utilizing very high strength steel tubes. Journal of Constructional Steel Research. 2004;60:1637-61.

[18] Heidarpour A, Cevro S, Song Q-Y, Zhao X-L. Behaviour of stub columns utilising mild-steel plates and VHS tubes under fire. Journal of Constructional Steel Research. 2014;95:220-9.

[19] Rhodes J, Zhao XL, Van Binh D, Al-Mahaidi R. Rational design analysis of stub columns fabricated using very high strength circular steel tubes. Thin-Walled Structures. 2005;43:445-60.

[20] Van Binh D, Al-Mahaidi R, Zhao XL. Finite element analysis (FEA) of fabricated square and triangular section stub columns utilizing very high strength steel tubes. Advances in Structural Engineering. 2004;7:447-57.

[21] Nassirnia M, Heidarpour A, Zhao X-L, Minkkinen J. Innovative Hollow Corrugated Columns: A Fundamental Study. Engineering structures 2015;94:43-53.

[22] Azhari F, Heidarpour A, Zhao X-L, Hutchinson CR. Mechanical properties of ultra-high strength (Grade 1200) steel tubes under cooling phase of a fire: An experimental investigation. Construction & Building Materials. 2015;in press.

[23] Mirmomeni M, Heidarpour A, Zhao X-L, Hutchinson CR, Packer JA, Wu C. Mechanical properties of partially damaged structural steel induced by high strain rate loading at elevated temperatures – An experimental investigation. International Journal of Impact Engineering. 2015;76:178-88.

[24] Hosseini S, Heidarpour A, Collins F, Hutchinson CR. Effect of strain ageing on the mechanical properties of partially damaged structural mild steel. Construction and Building Materials. 2015;77:83-93.

[25] Sinaie S, Heidarpour A, Zhao XL. Stress-strain-temperature relation for cyclically-damaged structural mild steel. Engineering Structures. 2014;77:84-94.

[26] Sinaie S, Heidarpour A, Zhao XL. A multi-objective optimization approach to the parameter determination of constitutive plasticity models for the simulation of multi-phase load histories. Computers & Structures. 2014;138:112-32.

[27] Sinaie S, Heidarpour A, Zhao XL. Mechanical properties of cyclically-damaged structural mild steel at elevated temperatures. Construction and Building Materials. 2014;52:465-72.

[28] Mazzina R, Gomez G, Solano M, Perez T, Lopez E. Study on weldability of high strength steel for structural applications. ASM Proceedings of the International Conference: Trends in Welding Research2013. p. 208-16.

[29] Jiao H, Zhao X-L. Tension Capacity of Very High Strength (VHS) Circular Steel Tubes after Welding. Advances in Structural Engineering. 2004;7:285-96.

[30] Shi G, Jiang X, Zhou W, Chan T-M, Zhang Y. Experimental investigation and modeling on residual stress of welded steel circular tubes. Int J Steel Struct. 2013;13:495-508.

[31] Javidan F, Heidarpour A, Zhao X-L, Hutchinson CR, Minkkinen J. Mechanical Properties of welded High strength and Ultra-high Strength Steel Tubes in Fabricated Sections. Engineering Structures. 2015.

[32] AS/NZS1554.7 Structural steel welding-Welding of sheet steel structures. Part7. Sydney: Standards Australia; 2006.

[33] AS 4100-1998, Steel structures. Sydney: Standards Australia; 1998.

[34] E606-04 Standard Practice for Strain-Controlled Fatigue Testing. ASTM International; 2004.

[35] AS 1391-2007 Metallic Materials-Tensile testing at ambient temperature. Sydney: Standards Australia; 2007.

[36] AS/NZS 4600:2005 Cold-formed steel structures. Australian/New Zealand Standard; 2005.

[37] Park R. Evaluation of ductility of structures and structural assemblages from laboratory testing. Bulletin of the New Zealand National Society for Earthquake Engineering. 1989;22:155-66.

[38] AS 1170.4-2007 Strcutural design actions Part4: Earthquake actions in Australia. Syndey: Standards Australia; 2007.

[39] Dassault Systèmes Simulia Corp. P, RI, USA. ABAQUS/CAE 6.14-1. 2014.

[40] Hooputra H, Gese H, Dell H, Werner H. A comprehensive failure model for crashworthiness simulation of aluminium extrusions. International Journal of Crashworthiness. 2004;9:449-64.

[41] Kessler L, Beier T, Werner H, Horstkott D, Dell H, Gese H. Material selection for an ultra high strength steel component based on the failure criteria of CrachFEM. AIP Conference Proceedings2005. p. 492-9.

[42] ARAMIS User Manual - Software V6.1. In: mbH G, editor. Mittelweg 7-8 D-38106 Braunschweig Germany2009.

[43] Mahendran M. Local plastic mechanisms in thin steel plates under in-plane compression. Thin-Walled Structures. 1997;27:245-61.

Bending moment and axial compression interaction of high capacity hybrid fabricated members

Monash University

Declaration for Thesis Chapter 5

Declaration by candidate

In the case of chapter 5 my contribution to the work involved the following:

Nature of contribution	Extent of contribution (%)
Developing ideas, Establishing methodologies, Experimental work, Data analysis, Write-up and revision	70%

The following authors contributed to the work:

Name	Nature of contribution	Extent of contribution (%)
Dr. Amin Heidarpour	Developing ideas, Input into manuscript, Revision, Financial support	15%
Prof. Xiao-Ling Zhao	Revision, Financial support	7%
Prof. Riadh Al-Mahaidi	Financial support through access to Swinburne testing facilities, Revision	8%

The undersigned hereby certify that the above declaration correctly reflects the nature and extent of the student's and co-authors' contributions to this work.

Student signature ████████ Date: 30/01/2017

Main Supervisor's signature ████████ Date: 30/01/2017

5.1. Abstract

Along with proposing any innovative structural element for design purposes it is necessary to understand its behaviour under combined structural actions. This paper includes experimental, numerical and analytical investigations on an innovative type of hybrid fabricated section under the effect of axial compression and bending moment interaction. As a special case of interactive condition, pure bending performance of the proposed fabricated member was individually examined with focus on the local failure mechanisms. Pure bending outcomes were also compared against moment resisting capacities obtained from a proposed analytical expression as well as plastic calculations. Furthermore, flexural strength of hybrid sections was investigated with the presence of an axial compression force. Compression-bending interaction curves were obtained from plastic analysis of hybrid hollow sections and compared to relevant standard formulations. This paper also includes beam-column tests accommodating combined effects of compression, shear and moment. Employing the developed and validated finite element model, a parametric study was conducted on the effect of section geometry and material on the axial-lateral interaction.

Keywords: Fabricated hollow sections, ultra-high strength steel tubes, pure bending, compression-bending interaction, local buckling

5.2.   Introduction

The main concern involved in the flexural behaviour of bending members, especially thin-walled fabricated sections is the local failures occurring before the section reaches its full capacity. Local buckling, yield or rupture can take place depending on the geometry and mechanical properties of the constituting elements of fabricated sections as well as the global restraining and support conditions of beams. These local mechanisms vary depending on the type of cross-section. Built-up members, for instance, are commonly used as structural elements such as bridge beams, plate-girders, etc. due to their high moment resisting capacities. Various buckling modes namely local, lateral-torsional and interactive buckling may also occur in I-sections depending on their geometry [1-4]. Sections with closed cross-sections such as box girders require additional design provisions such as distortion, buckling of wide flanges, force transfer to support bearings etc. [5]. New unaccustomed cross-sections have been proposed in previous research in order to optimise the flexural behaviour of beams [6, 7] in which I-shaped and H-shaped bridge girders with tubular flanges were examined and design criteria were proposed. These studies showed the benefits of having rigid hollow flanges and distributing section away from the neutral axis [8, 9]. Innovative hollow fabricated sections with high strength steel tubes at corners which have recently been proposed for structural purposes [10-12] and are the main focus of this study have hollow tube elements at far ends of sections which can act as torsionally rigid hollow flanges minimising the local buckling of plate elements. Furthermore, the location of tube elements at corners of section help distribute material away from the neutral axis which leads to an increase in the bending stiffness. In the current study, three different types of mild steel, high strength and ultra-high strength steel tubes are incorporated. Additionally, with the increase in strength of tubes fabricated in hybrid

sections from mild steel to grade 800 and grade 1200, stresses at far ends of sections increase resulting in a higher moment capacity.

Bending behaviour of structural components is a special case of beam-column performance where the applied axial forces are negligible. When axial forces are applied along with bending moments on fabricated sections, the interaction performance of these sections becomes a crucial aspect in the design and analysis of fabricated sections. In this study, the section is taken into consideration for beam-column interaction investigations. A method for plastic analysis of structures is considered when the full section reaches a plastic stress state under the applied loads. The interaction curves extracted from this type of plastic analysis is an upper bound estimation applicable to cases where the section does not fail under local mechanisms prior to the plastic failure of section. Plastic axial-flexural section interaction curves have previously been obtained for several symmetric cross sections such as bisymmetrical and mono-symmetrical I shaped sections and other types of un-accustomed cross sections [13-15]. Steel design standards also provide interaction formulas for the estimation of plastic section capacity under combined uniaxial or biaxial bending and axial compression [16, 17].

To date, hybrid fabricated sections consisting of mild steel plates and high strength tubes have been investigated under centrally loaded conditions where a significant portion of section undergoes compression. Accordingly, due to limited knowledge, this paper follows the comprehensive research previously conducted on the compressive performance of hybrid fabricated sections [18-20] and extends the work to bending and combined interaction loading conditions, focusing on section specifications such as geometry and steel material. Pure flexural performance of this innovative type of hollow fabricated section is investigated as a special case of the interactive condition where no axial compression loads are applied. Due to the unique geometry of the hybrid sections, an exclusive experimental setup was designed. Taking the event of local mechanisms into consideration the bending

capacity of these thin-walled elements are predicted. Interaction curves are extracted for three types of fabricated hybrid beam-columns comprising of mild steel plates and mild steel (MS), high strength steel (HSS) or ultra-high strength steel (UHSS) corner tubes. Analytical results obtained from plastic section investigations are compared against relevant practical design recommendations. In full-scale members, influence of generated shear stresses on beam-column member performance is particularly taken into considerations. Axial-Lateral force interaction curves are parametrically studies for various geometries and steel materials. This study has been conducted as part of a research work conducted on steel and fabricated hybrid elements under extreme loading scenarios [21-28].

5.3. Experimental program

5.3.1. Pure bending test

As a prerequisite stage for understanding the complete beam-column behaviour of the innovative hybrid fabricated sections, it is necessary to have an overview of their behaviour under pure bending. Therefore, with the aim of obtaining the moment capacity of the proposed innovative hybrid sections, four point bending tests were conducted on two meter fabricated beams. Geometry of the proposed section is shown in Figure 5.1(a). Mild steel (MS) tubes with yield and ultimate strengths of 305 and 340 MPa, high strength steel (HSS) tubes with yield and ultimate strengths of 770 and 850 MPa and ultra-high strength steel (UHSS) tubes with yield and ultimate strengths of 1250 and 1385 MPa were used. The plates used in all fabricated sections were grade 250 mild steel. A beam specimen with 2000mm length is fabricated for testing. This length is consistent and thus comparable with the previously tested compressive specimens [18-20]. In order to assure that all shear stresses

will dissipate while approaching the mid-span and that pure bending is recorded at the centre, the minimum allowable distance recommended in [29] is considered such that the length between loading point and the centre (L_2) is 900mm and L_1 is 500mm as shown in Figure 5.1(b).

$D_t=76.1$, $t_t=3.2$, $W_p=210$, $t_p=3$

(a)   (b)
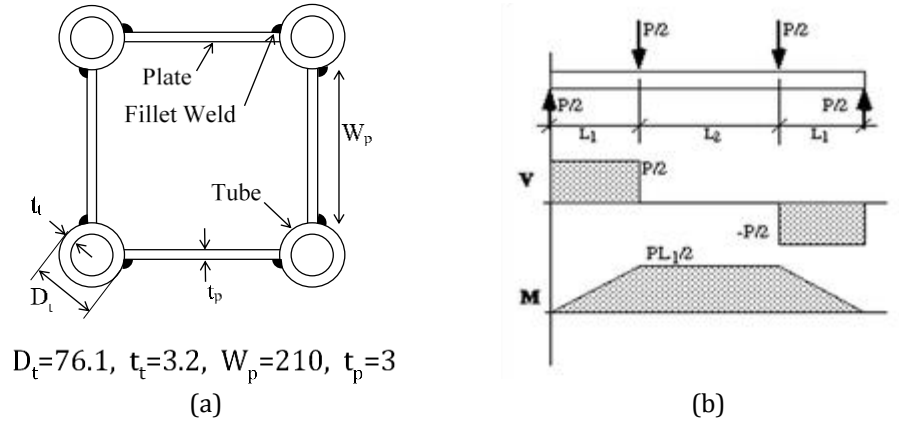
Figure 5.1. (a) Specimen geometry; (b) four point bending configuration.

Four point bending test was conducted on the hybrid beam specimen with mild steel tubes in a Amsler testing machine (Figure 5.2(a)) constant displacement was applied at a rate of 1.0mm/min to on two points along the top of member. The beam was simply supported with a pinned support on one end allowing rotations, and a roller on the other end allowing rotations and horizontal displacement. Three displacement transducers and a string pot were placed at the centreline of the tension face of the beam at four different points to record the vertical displacement of the beam. Strain-gauges were also attached at different location at the centre of beam at all plate and tube faces in both vertical and horizontal directions, recording the axial and shear strains of the beam. In order to evenly transform the load on plates and tubes of the beam element, a uniform bearing link was designed and placed under the point load supports Figure 5.4. This link consists of three steel segments connected to a main steel segment using bolts. Since the fabrication process can lead to imperfections along the surface of the beam section, fillers were used where required to align the top of the main steel segment with the loading rollers.
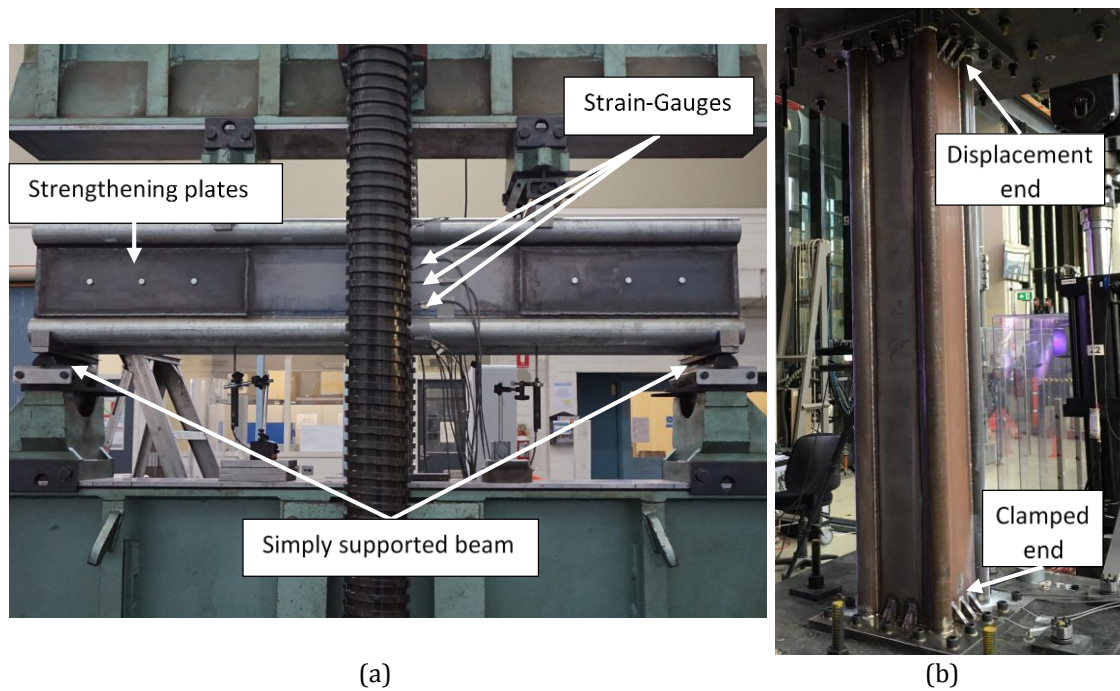
Figure 5.2. Experimental setup: (a) Four point bending test, (b) beam-column test (MAST system).

In bending performance of hybrid fabricated sections, there are two types of local failure mechanisms which are more likely to occur prior to reaching the full bending capacity: local shear failure of vertical plates and local tube deformations under load concentration. These local failure types can occur depending on the geometry of constituting elements of section. First type is probable in cases with thin vertical plates, in which plate thickness should be designed based on the total moment capacity demand of beam limiting the value of W_p/t_p. This procedure is defined in detail below. The second type is probable in cases where point loads are applied directly on the member in which local strengthening of tubes are necessary.

In order to avoid shear buckling failure in vertical plate elements and to reach the full bending capacity of member, these plates were strengthened by connecting mild steel plates on the shear spans at two ends of beam on both sides. The thickness of these plates were checked against the AS4100 standard recommendations [16]. For a uniform stress

distribution, depending on the maximum web panel depth to thickness ratio, the relevant

shear capacity needs to be satisfied so that

$$V_u = 0.6 f_y A_w \qquad \text{If} \quad \frac{d_p}{t_w} \leq \frac{82}{\sqrt{\frac{f_y}{250}}} \qquad\qquad (5.1)$$

$$V_u = V_b = \alpha_v V_w \qquad \text{If} \quad \frac{d_p}{t_w} > \frac{82}{\sqrt{\frac{f_y}{250}}} \qquad\qquad (5.2)$$

For the geometry of webs in the present hybrid sections, equation (5.1) governs. To prevent

the shear failure from buckling at regions under applied loads, the web under shear loads

are strengthened.
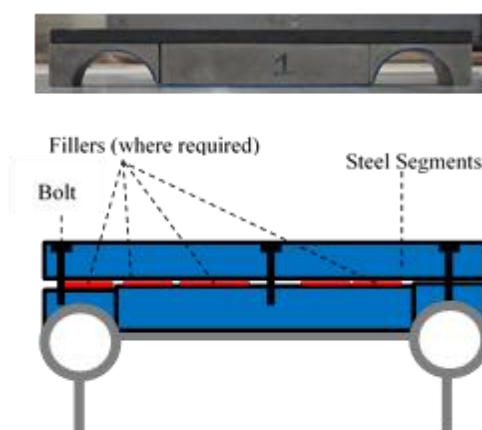
Figure 5.3. Configuration of uniform bearing link under point loads and supports in four point bending test

5.3.2.   Beam-column tests

Combined effect of compression and bending moment is a critical behavioural aspect of

sections which are considered to be used as beam-column elements in structures. In thin-

walled long structural members, effect of local buckling significantly influences the axial-

flexural interaction performance and in the case of hybrid fabricated sections the

interaction mechanism of welded elements also plays a vital role. For this aim, bending-compression tests were conducted on three types of fabricated sections. The tested members include welded box section, hybrid section with mild steel tubes and hybrid section with HSS steel tubes in which all elements have a nominal length of 2000mm. For a fair comparison of the behaviour of proposed fabricated sections with conventional sections, the dimensions of box beam-column are chosen in a way that this section possesses equivalent width and cross-sectional area with those of hybrid sections. A percentage (25%) of the axial load bearing capacity of each section is applied to each section in addition to a lateral displacement controlled pushover which continues until failure. Displacement controlled lateral tests were performed using a Multi-Axis Substructure Testing (MAST) system [30]. Using servo-hydraulic control system in all test cases, rotation degrees of freedom at both ends were controlled and kept zero throughout testing while end forces and moment reactions were continuously measured and recorded. To ensure adequate clamp conditions at both ends, outer specimen perimeters were welded to anchor plates and triangular stiffeners were also used at four sides. For ease of member instalment at each test, the end anchor plates were bolted to the concrete base plates connecting specimen to concrete pedestals and the MAST system. The beam-column test setup is shown in Figure 5.2(b).

Experimental results of the beam-column tests conducted on three fabricated sections are compared in in Figure 5.4 along with the applied axial force on each case. Effect of section geometry and material properties are understood from the 25% and 42% rise of lateral capacity of section with MS tubes and section with HSS tubes, respectively, compared to equivalent box section. Material properties of steel incorporated in fabricated sections also influences the failure mechanism of these sections under combined compression and bending as shown in Figure 5.5.
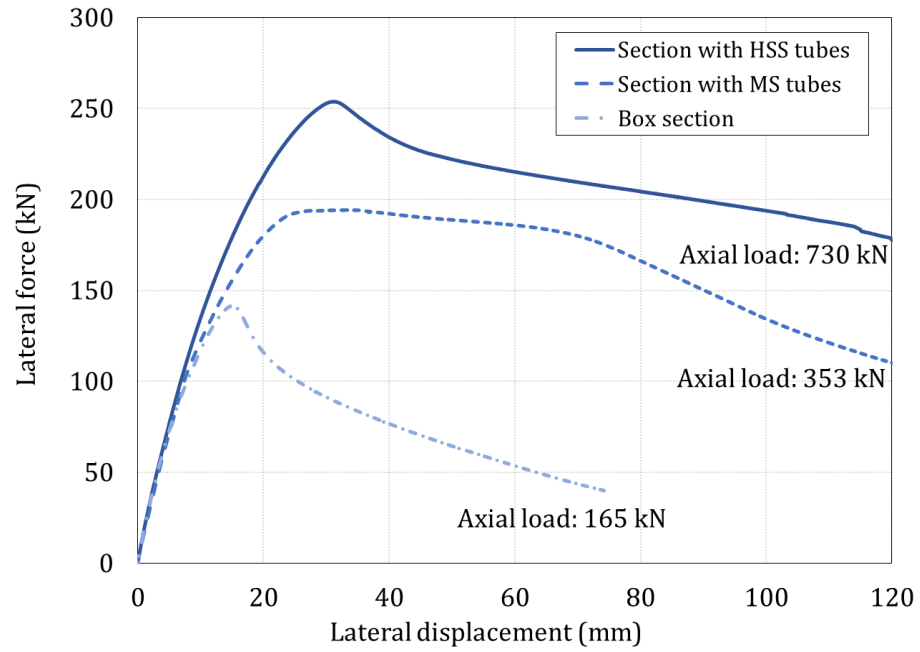
Figure 5.4. Experimental lateral load-displacement curves for fabricated sections.

| (a) | (b) | (c) |
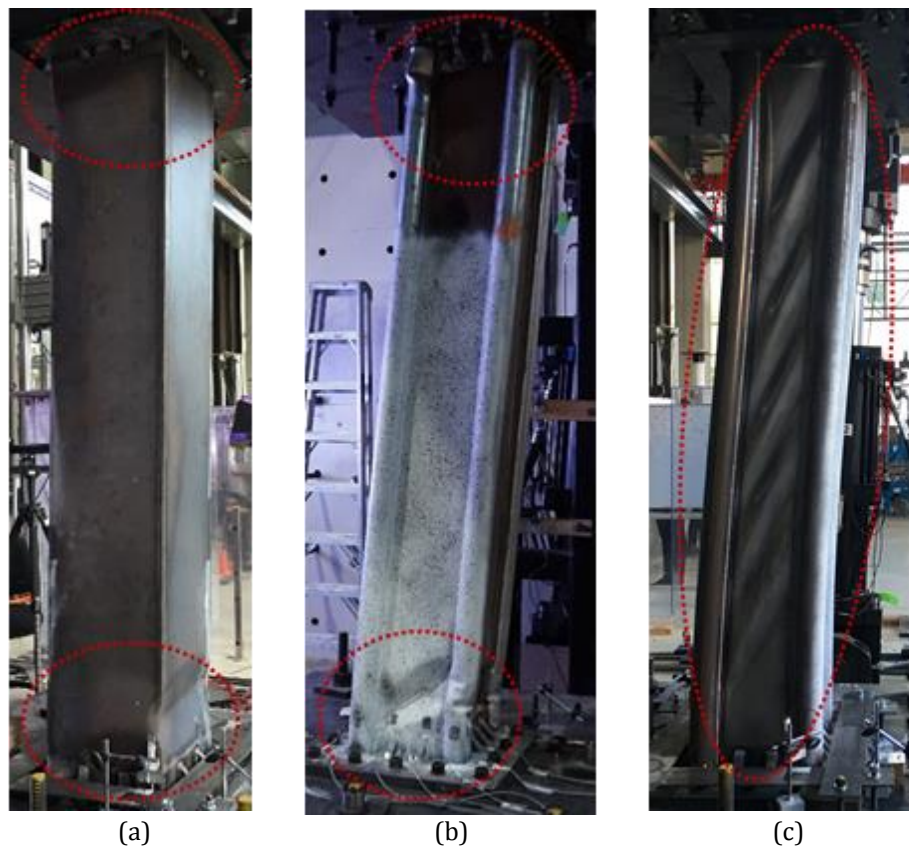
Figure 5.5. Failure mechanism of fabricated sections under monotonic lateral pushover: (a) fabricated box section; (b) Hybrid fabricated section with MS tubes; (c) Hybrid fabricated section with HSS tubes.

In the fabricated box section damage is mainly localised at the top and bottom regions close to fixed supports. Type of failure observed in this section is flip disk mechanism, the type of failure observed in similar fabricated box section under pure compression. Hybrid fabricated section with MS tubes exhibits damage in similar regions of box section, with different failure mechanism. Damage is observed in both plates and tubes at top and bottom. As opposed to the above sections, member comprising HSS tube elements fails with a completely different mechanism. Local shear buckling failure modes can be observed along the length of this section with less obvious local deformation in HSS tubes.

5.4.   Numerical finite element modelling and validation

A robust finite element model is developed for further investigations of the beam and beam-column performance of hybrid fabricated sections. Using finite element package ABAQUS/standard [31] both pure bending and axial force-bending moment interaction tests are simulated in detail with the aim of reproducing similar tests with a variety of cross-section specifications. In the four point bending simulations, as well as considering realistic nonlinear material models previously extracted for each element type [19, 20] all other aspects of test such as loadings, degrees of freedom, strengthening plates, uniform bearing links under point loads are accounted for in modelling. 4-node shell elements were considered in modelling the thin-walled elements and mesh sensitivity analysis were conducted for adopting an optimum mesh size.

The finite element results of the four point bending tests conducted on section with MS tubes are compared against experiments, illustrated in Figure 5.6. According to the deformed shapes in Figure 5.6(a), the tube elements have undergone local failure which affects the global behaviour of the beam. It is seen that the failure mechanisms in finite

element simulations correctly replicate the experiments. Figure 5.6(c) shows the load vs. displacement curve of the bending test. At the first stage, the curve levels off during the local deformation of tubes and after the local deformations, the load bearing capacity of member further increases. The peak load applied by the Amsler on the beam specimen during the experimental test was 400kN.

(a)

(b)

(c)
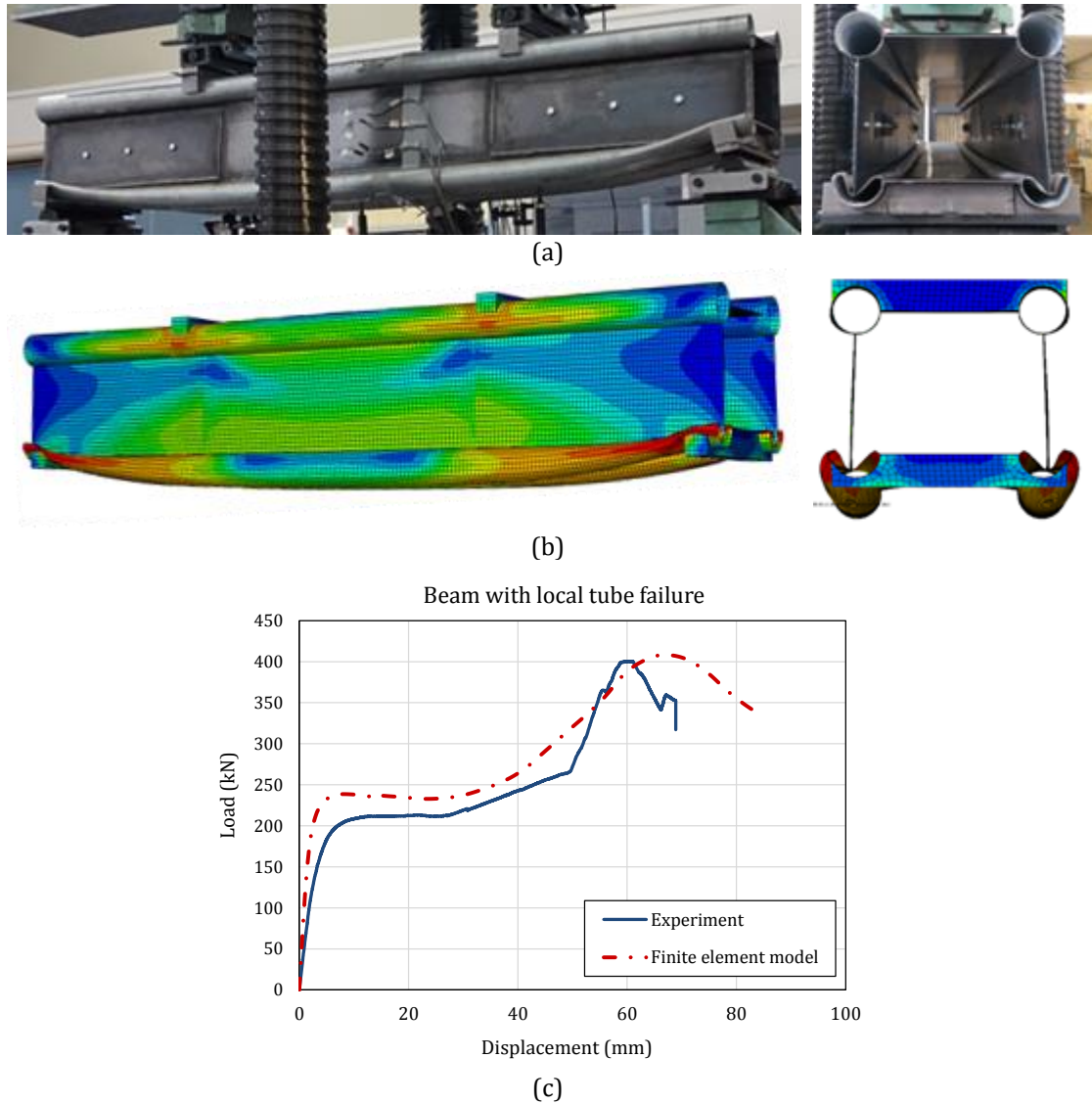
Figure 5.6. Local failure of hybrid beam consisting of mild steel tubes: (a) experimental test, (b) FE model.

The developed finite element model was also verified against the experimental tests of hybrid fabricated sections under combined axial-lateral performance. A detailed

comparison of results obtained for beam-column specimen with HSS tubes is presented in Figure 5.7. This includes lateral load versus displacement curve as well as the failure mechanism showing the overall deformed shape of specimen along with the local buckling of plate elements throughout the length which match the experimental results.

(a)   (b)
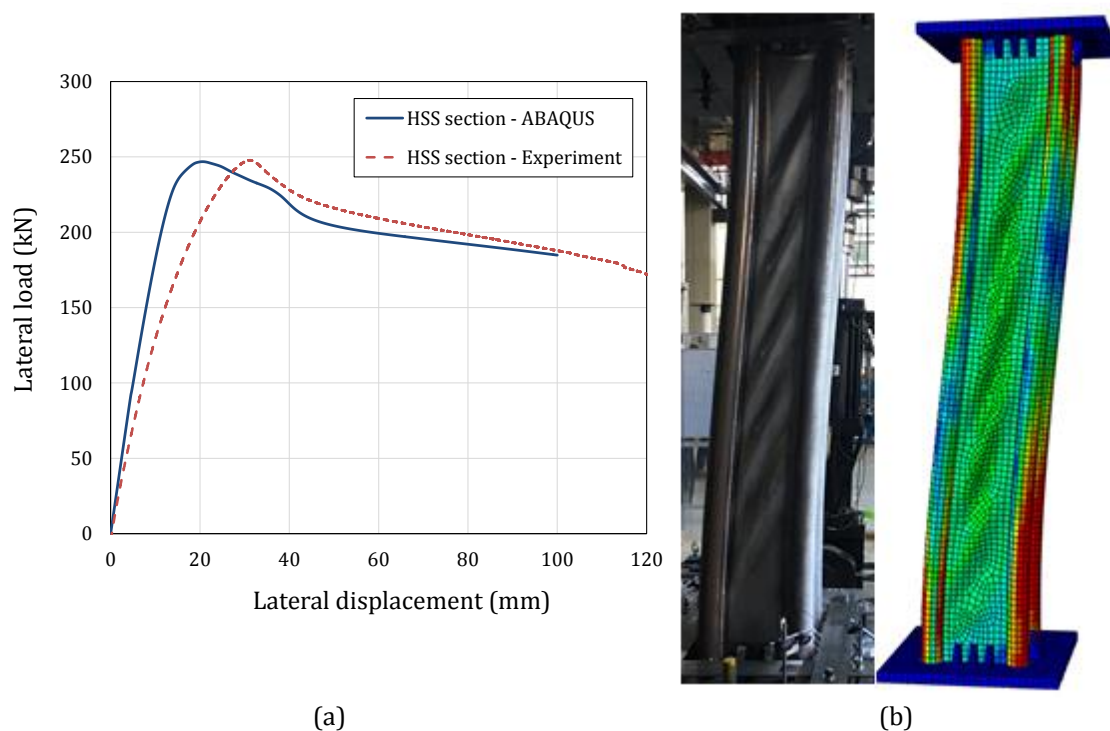
Figure 5.7. FE model verification against experimental results of specimen with HSS tubes: (a) lateral load-displacement curve, (b) failure mechanisms.

In addition to having a prediction of the expected performance of each tested specimen, the numerical modelling was used to further investigate the experimental setup. Several numerical analyses were conducted considering the effect of heat affected material on the axial-lateral behaviour of these sections. Due to the fact that weld induced heat affected zone (HAZ) affects the performance of hybrid sections one possible setup scenario for connections of hybrid fabricated sections could be welding only mild plates at the ends of fabricated sections to top and bottom anchor plates. An assumption is that this might increase the lateral load bearing capacity of sections by avoiding introducing any softening effect of weld in the system. Hence, a numerical model of section consisting of UHSS tubes,

which is the most vulnerable material to welding, was developed considering the altered heat affected material properties at various distances from weld line (see Figure 5.8) [19]. Results obtained from the above mentioned model and outputs of simulation where only plates were welded to the top and bottom anchor plates and tubes were not welded were compared to the case where plates and tubes are welded and no HAZ effects is introduced. An axial load equal to 25% of axial compression capacity of section is applied on each case. This comparison obtained from the described finite element models comparison showed that HAZ effects are negligible in the lateral performance of hybrid sections which result in 1.7% reduction in lateral strength compared the 4.7% reduction observed in section which tubes were not welded to anchor plates. This difference in lateral capacity shows the important role of tubes in transferring applied forces.
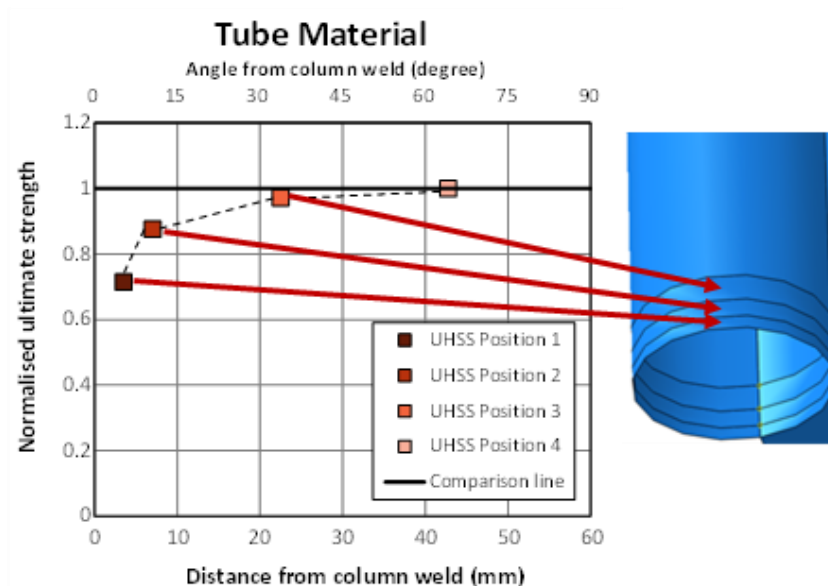
Figure 5.8. Tube HAZ modelling for axial-lateral test setup design

5.5. Results and discussions

5.5.1. Pure bending analysis

This part involves an analytical model to obtain moment capacity of hybrid fabricated sections about the principle axis using the formulations recommended in AS4100 [16] and comparing that with finite element outcomes. Depending on the type of elements incorporated in the beam cross-section, the geometric condition is recognised and the section modulus is calculated. Tubes or plates incorporated in hybrid sections might be one of compact sections, non-compact and slender type of element. According to AS4100 the effective section modulus for different elements can be obtained from equation below

$$Z_e = \min(1.5Z, S) \qquad \text{for compact elements}$$

$$Z_e = Z + \left[(\frac{\lambda_{sy}-\lambda_s}{\lambda_{sy}-\lambda_{sp}})(Z_c - Z)\right] \qquad \text{for non-compact elements} \qquad (5.3)$$

$$Z_e = Z(\frac{\lambda_{sy}}{\lambda_s}) \qquad \text{for slender elements}$$

In which yield slenderness (λ_{sy}) and the section plasticity limit (λ_{sp}) are taken into account if necessary. From the above equations, the total moment capacity (M_{bs}) of the hybrid section is estimated from the following formulation.

$$M_{bs} = f_{yt}Z_{et} + f_{yw}Z_{ew} + f_{yf}Z_{ef} \qquad (5.4)$$

Expression with the subscript of t, w and f respectively refer to tubes, vertical mild steel plates and horizontal mild steel plates. For hybrid sections with different tube materials, the analytical moment capacities are calculated and presented in Table 5.1.

Table 5.1. Comparison of predicted beam capacities obtained from standard formulations, plastic design and FE.

	From Equation 5.4			Plastic design	FE model
	Total Moment capacity (kN.m)	Support load: P/2 (kN)	Total load: P (kN)	Total load: P (kN)	Total load: P (kN)
Section with Mild tube	170	340	680	772	740
Section with high strength tube	365	730	1460	1552	1540
Section with ultra-high strength tube	566	1132	2265	2356	2398

Comparing the values of bending moment obtained from the experimental beam test on section with mild steel tubes shown in Figure 5.6(c) with the theoretical moment resisting capacity of the similar beam shown in Table 5.1 indicates that local tube failure prevents the beam from reaching its maximum capacity. It was concluded that achieving the full moment capacity of section requires preventing this local deformation in tubes. Therefore, the finite element model was developed by filling tubes with 100mm steel cylinders under load points. The new analyses are reported in Figure 5.9 and the last column of Table 5.1. Beams reach the maximum load bearing capacity until the onset of local bending failure in the shear free zone and the strength gradually reduces after that. As shown in Figure 5.9, the beam specimen consisting of mild steel tubes undergoes a maximum compression load of 740kN (with a bending moment capacity of 185 kN.m), the beam specimen with HSS tubes has a capacity of 1540kN (and a bending moment capacity of 385 kN.m) and finally the beam specimen with UHSS withstands a peak load of 2398kN (with a bending moment capacity of 600 kN.m). These values are quite close to the theoretical values predicted from the analytical formulations presented in Table 5.1; however, the analytical results are more conservative (by less than 10% in sections with basic cross-sectional geometries shown in

Figure 5.1(a). This is understood to be due to the dual interaction of tube and plate elements in the hybrid section which increases the moment bending capacity compared to the superposition of the summation of element capacities individually. Further analysis was conducted on section with increased plate thicknesses and the above comparison was drawn among the finite element and analytical results. It was observed that as the plate thickness increases, the difference between analytical and numerical model increases.
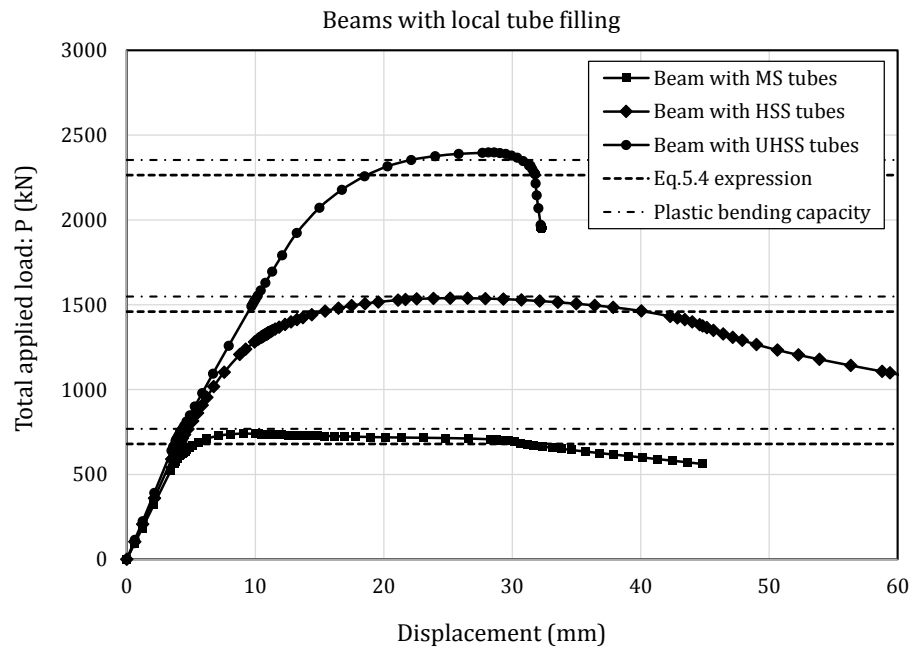
Figure 5.9. Finite element model results of pure bending with local tube filling in comparison with capacity prediction formulas.

The beam member with UHSS tubes experiences a sharper post failure degradation compared to the two other beam members. Based on the recommendations made in references [32, 33], the ductility of an element can be evaluated from the rotation capacity. Plastic rotation capacity (R) quantifies this difference by evaluating the ductility at a given level of load (M_p) which can be considered as a reference moment for calculations. The plastic rotation capacity (R) of hybrid beam consisting of UHSS tubes is calculated from the following equation and presented in Figure 5.10.

$$R = \frac{\theta_{max}}{\theta_p} - 1 \qquad (5.5)$$

The rotation capacity (R) is approximately equal to 2 and can increase depending on the considered value of plastic moment. This value is generally considered sufficient for building applications [33]. Similar procedure was repeated for beam specimens with HSS and MS tubes and rotation capacities found to be 5 and 7.3 respectively. It can be concluded here that the plastic rotation capacity and thus the bending ductility of hybrid fabricated sections reduces with the increase in strength of tube material.
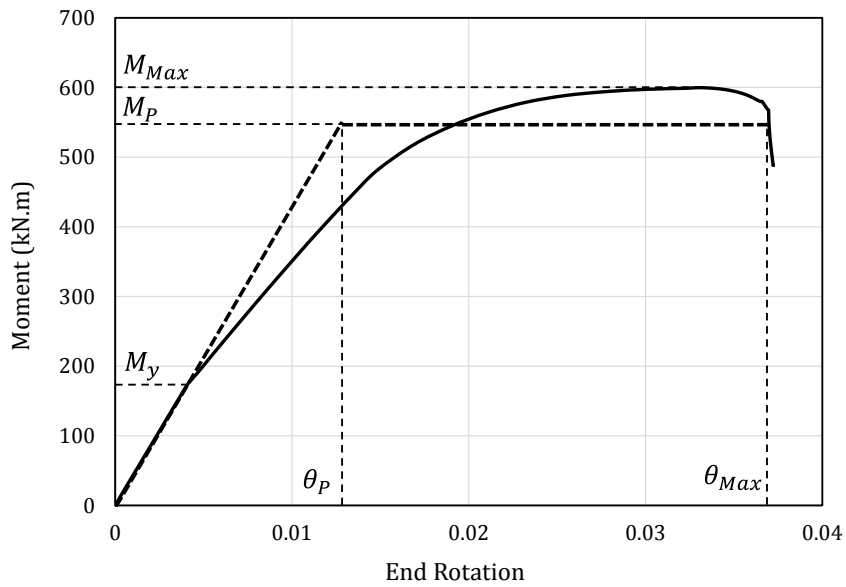
Figure 5.10. Rotation capacity of hybrid beam with UHSS tubes

Further to the above calculations, a plastic analysis is also driven to estimate the plastic bending capacity of sections (M_{pbs}) under pure bending where the neutral axis fall at the centre of section. Equation (5.6) proposes an expression for the summation of plate and tube capacities.

$$M_{pbs} = f_{yp}t_p\left[B(B - t_p) + \frac{1}{2}(B - 2t_p)^2 - D_t(2B - 2t_p - \frac{D_t}{2})\right] + f_{yt}t_t\left[2\pi(D_t - t_t)(B - t_p)\right] \qquad (5.6)$$

In the above equation f_{yp} and f_{yt} are yield stresses of plates and tubes respectively and B is the external distance of plates $W_p+D_t+t_p$. These dimensions are presented in Figure 5.1. Plastic moment capacity is obtained from the summation of plastic moment capacity of steel plates and corner tubes (Figure 5.11). The total plastic moment capacity for sections with MS, HSS and UHSS tubes are 193, 388 and 589 kN.m respectively. The values of total applied loads in a four point bending test on each of the considered cross sections are presented in Table 5.1 and shown as dashed lines in Figure 5.9. It is shown that plastic moment capacity calculations provide a close estimation to the peak load withstood by each section. This shows that with respect to the geometry of sections considered in this study, no reduction factor is required for the resistance of sections obtained from plastic analysis which is consistent with the obtained plastic rotation capacity values (i.e. R>3 for sections with MS and HSS and R>1 for section with UHSS).
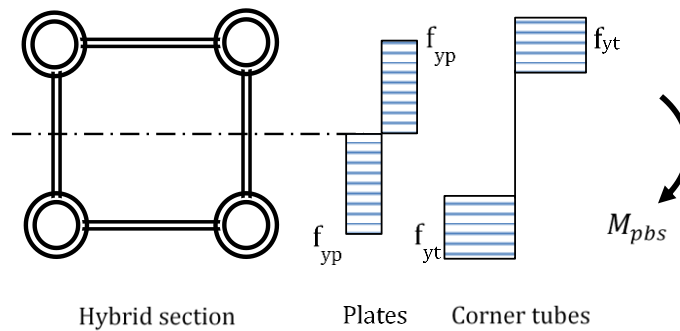
Figure 5.11. Plastic stress distribution of fabricated hybrid section under pure bending

5.5.2. Compression-bending interaction analysis

The rigid-plastic analysis of a beam-column is an upper bound estimation of the strength of structural element under combined bending moments and axial forces that causes the whole section to become fully plastic. This type of estimation is applicable for design of members that reach their full plastic capacity prior to undergoing any local buckling or failure or in very short beam-columns where bending governs the behaviour of beam-

column. In this part, the plastic interaction performance of the proposed hybrid fabricated sections under combined axial compression and bending about one axis is studied. It is worth noting that the effect of other types of forces such as shear, bi-moments and torsion are not considered in these calculations. For plastic analysis of fabricated hybrid sections, five different zones are considered for which the unstrained fibre axis crosses through and the total plastic axial force (N_{ps}) and moment (M_{ps}) are calculated from relevant areas and yield stress of plates (f_{yp}) and tubes (f_{yt}) (see Figure 5.12 and equation (5.7)).

$$N_{ps} = f_{yt}A_t + f_{yp}A_p \quad , \quad M_{ps} = f_{yt}A_t y + f_{yp}A_p y \qquad (5.7)$$
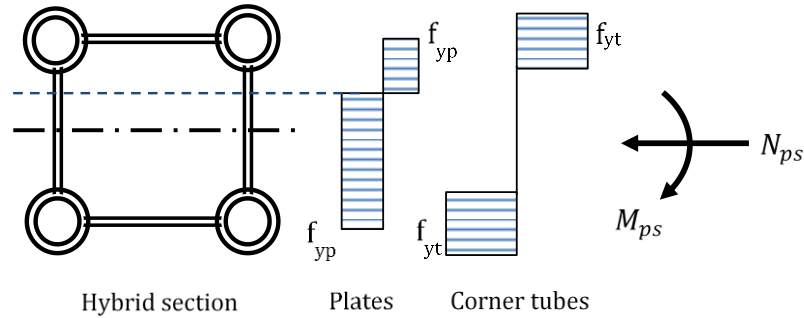
Figure 5.12. Plastic stress distribution of fabricated hybrid section under combined moment and compression

The interaction curve for hybrid fabricated sections consisting of MS plates and tubes are analysed and plotted in Figure 5.13(a). The curve plots the ratio of section's plastic moment in the presence of an axial force (M_{ps}) to the full plastic moment of section (M_p) against the ratio of axial force (N_{ps}) to the fully plastic cross-section strength under pure compression (N_p). This curve is shown in comparison with the standard provisions of interaction formulas recommended for sections. For uniaxial bending under the major principal axis, AS4100 proposes the nominal section moment capacity (M_{ps}) as a function of nominal section (M_p) capacity and axial forces such that

$$M_{ps} = M_p(1 - \frac{N_{ps}}{\phi N_p})$$

$$(5.8)$$

where ϕ is considered to be equal to one at the current plastic analysis. AISC proposes a bilinear formulation for interaction of non-dimensional axial and flexural strength ratios at the fully plastic status under applied axial load (N) with a reduction factor of unity:

$$\frac{N}{N_p} + \frac{8}{9}\frac{M_{ps}}{M_p} = 1 \qquad \text{for } \frac{N_{ps}}{N_p} \geq 0.2$$

$$\frac{N}{2N_p} + \frac{M_{ps}}{M_p} = 1 \qquad \text{for } \frac{N_{ps}}{N_p} < 0.2$$

$$(5.9)$$

According to Figure 5.13(a), AS4100 safely predicts the interaction behaviour of specific case of hybrid section with MS tubes, while the AISC bilinear formula makes a more satisfactory approximation at axial load ratios around 0.2 and a more conservative prediction at load and moment ratios close to 1. To have an estimation of the influence of section material and geometry on the interaction performance of hybrid fabricated sections, a wide range of section specifications are studied. Mild steel plate widths of 210 to 600mm, plate thicknesses of 3 to 10mm, plate strengths of 260 to 400MPa, tube strengths of 350 to 1250MPa and tube outer diameters of 46 to 76mm are considered. The results showed that the variation of compression-bending interaction highly depends on both material and geometric properties of hybrid sections. A non-dimensional section parameter (κ) is introduced defined as the ratio of tube properties to plate properties. These properties are obtained from the area of each element multiplied by the yield strength of constituent steel Equation (5.10).

$$\kappa = \frac{f_{yt}A_t}{f_{yp}A_p}$$

$$(5.10)$$
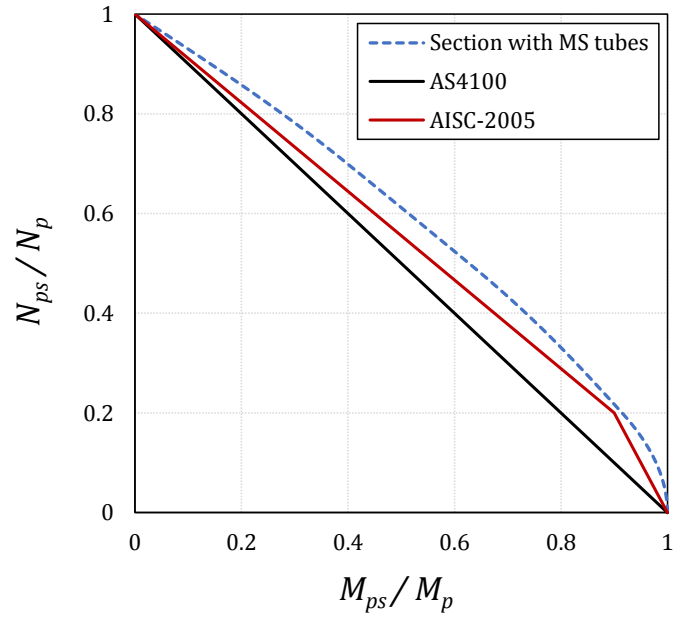
(a)
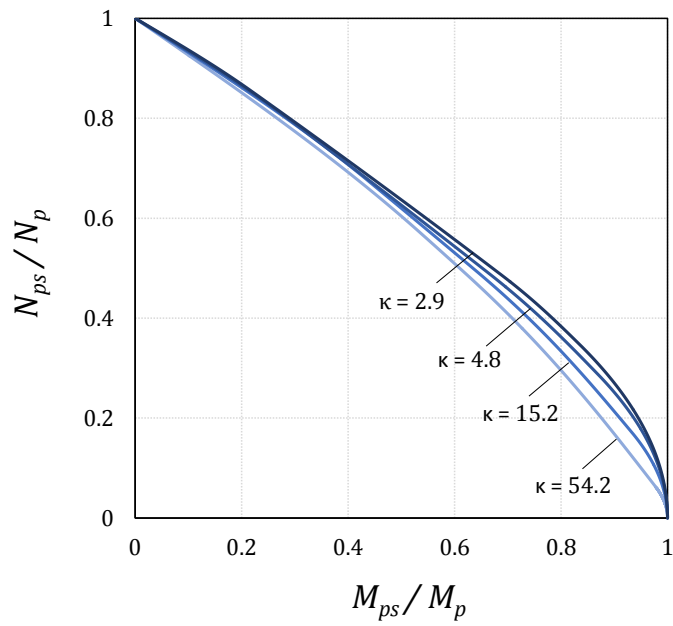
(b)

Figure 5.13. Section compression-bending moment interaction curves: (a) in comparison with design standards, (b) effect of section properties.

The obtained curves presented in Figure 5.13(b) show that with the increase in κ the interaction curve inclines towards a straight line whereas by increasing the strength and dimensions of plate elements, the interaction strength increases. Consequently, the linear

interaction formula becomes conservative for predicting sections with low values of κ while the bilinear formulation gives a more realistic estimation.

5.5.3. Compression-bending-shear interaction analysis

A thorough parametric study is conducted in this section on the combined axial-lateral performance of fabricated hybrid members. Employing the validated finite element model, 2000mm fabricated members are analysed under combined axial-lateral loadings in which shear effects are also introduced. The focus of this study is understanding how the geometry of plates and material properties of tube elements contribute to the interaction axial-lateral load bearing performance of hybrid sections as well as the failure mechanism. Practical plate thicknesses (t_p) of 6mm and 10mm were adopted in addition to the 3mm thick mild steel plate in beam column specimens consisting of HSS and UHSS tubes. Analyses were conducted under various values of applied axial forces. Axial force versus lateral load bearing capacity of these numerical cases are presented in Figure 5.14. In specimens with UHSS and HSS tubes and 3mm mild steel plates, despite the significant difference in axial load bearing capacities, the lateral strengths are almost similar under pushover lateral tests with zero axial force. Based on this observation, shear failure of plates governs the lateral performance of these specimens in the above mentioned loading states. With increasing the applied axial force, axial capacity of section with UHSS tubes increases with a higher rate compared to HSS member. In member with UHSS tubes, compared to the case with 3mm plate thickness by increasing plate thickness to 6mm, axial strength advances 15% while the rise in lateral capacity is significantly higher; approximately 150%. These percentages for section with HSS tubes are 23% and 82% respectively. In specimen with 10mm plate thickness, the percentage of increase in both lateral and axial capacities are quite similar. From these comparisons, it can be concluded that the design of these hybrid fabricated sections and selection of tube and plate properties highly depend on the axial and lateral

load bearing demands of beam-column elements. In case of structural elements with high compression loads and low lateral capacity demands, strength of tubes play an important role in increasing the axial strength. Selection of high strength steel tubes and thin walled plates in these cases can lead to an optimum design in terms of capacity and overall cross-sectional area and therefore weight of member. In cases with high demands in both axial and lateral directions, thickness of plate should be selected in a way that plate has sufficient shear strength and plate element does not fail under the applied lateral forces. It was also concluded from the results that regardless of the geometry and tube material, as the percentage of axial load increased, the lateral displacement corresponding to strength cap reduced.
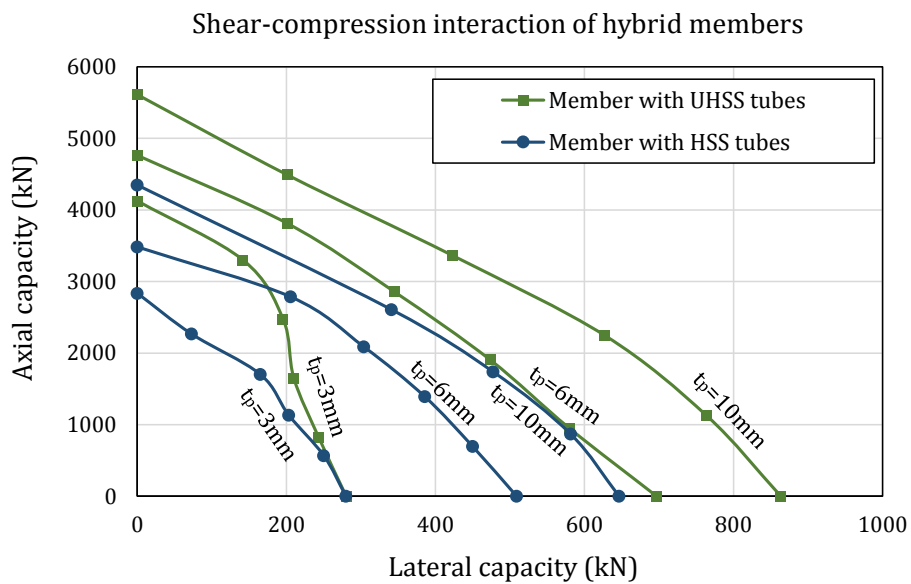
Figure 5.14. Axial-lateral interaction curves for hybrid fabricated sections

(a) Zero axial force,
t_p=3mm

(b) 40% axial force,
t_p=3mm

(c) 80% axial force,
t_p=3mm

(d) Zero axial force,
t_p=10mm

(e) 40% axial force,
t_p=10mm

(f) 80% axial force,
t_p=10mm
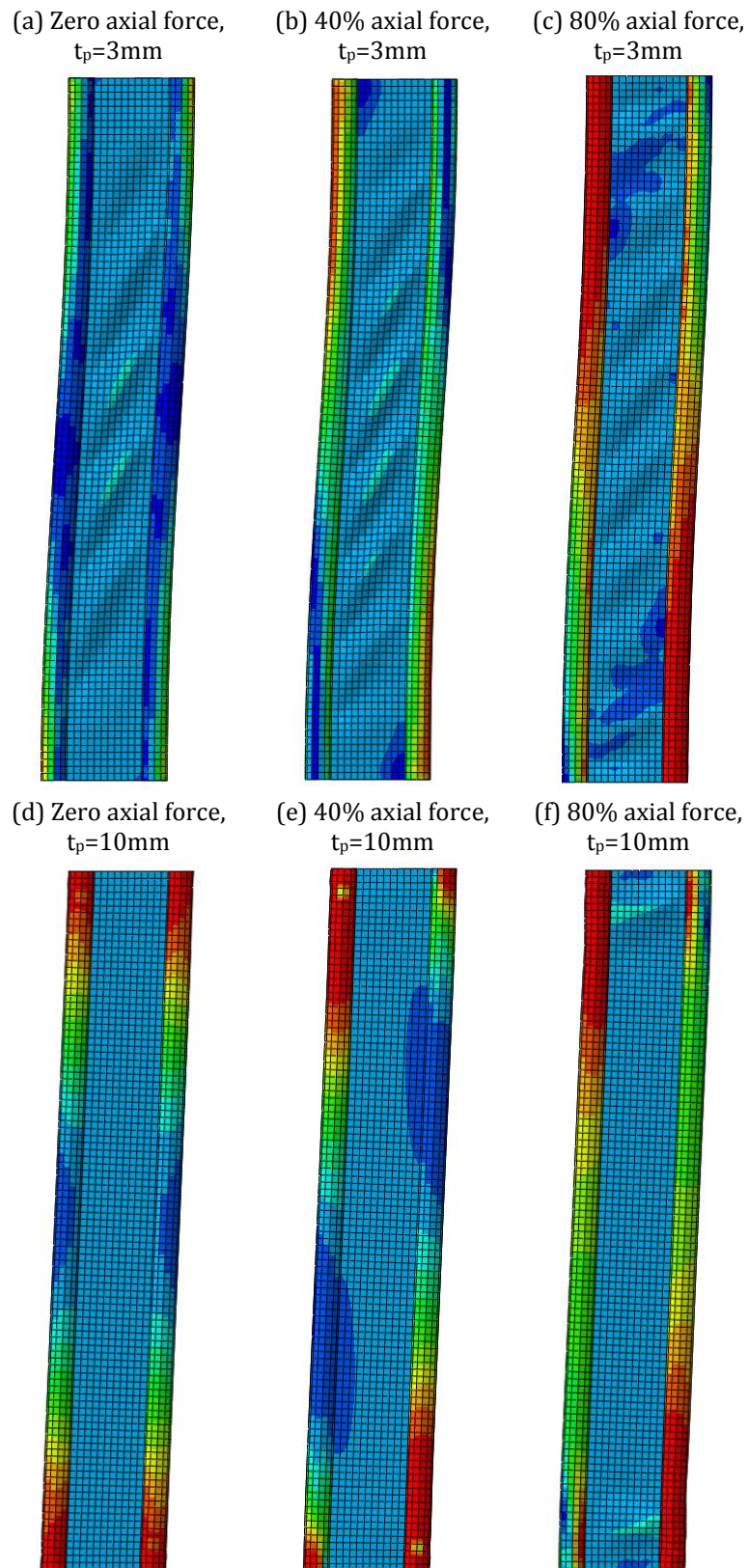
Figure 5.15. UHSS Tube-plate deformation mechanism and stress counter (MPa) at 80mm lateral displacement

Deformation mechanism defers significantly with the increase in mild steel plate thickness. Figure 5.15 shows these deformation interactions and Mises stress distribution contours for specimens with UHSS tubes analysed under different axial force-to-compression strength ratios all captured at 80mm lateral displacement. In the case of 3mm plate thickness, the factor governing failure is shear buckling of plate elements which can be understood from the local buckling occurring throughout the length of beam-column in Figure 5.15(a) to Figure 5.15(c). This local buckling is concentrated towards the centre of length in test case with pure lateral loading Figure 5.15(a). In sections with 10mm plate thickness (Figure 5.15(d) to Figure 5.15(f)) local plate buckling reduces significantly and failure initiates and progresses in tube elements. In specimen with 10mm plate thickness tested under 80% of its axial capacity, local buckling occurs in plates due to the compression stresses generated at fixed ends.

5.6.   Conclusions

This paper has investigated bending specifications of hybrid fabricated sections consisting of high strength steel tubes including pure bending and compression axial load-bending moment interaction.

Pure bending experimental tests and numerical simulations were conducted on fabricated hybrid sections in which no shear force was introduced to section. Results showed that HSS and UHSS tubes incorporated in hybrid members enhance the pure moment resisting of sections about 2 and 3.2 times, respectively, compared to the section with MS tubes. Beam-column tests, with the presence of shear effects, were also conducted on hybrid fabricated sections and compared to an equivalent fabricated box section. Lateral capacity of hybrid

sections consisting of MS tubes increased by 25% and that of hybrid section consisting of HSS increase by 42% compared to the equivalent box section.

Moment resistance of fabricated sections was predicted using a formulation based on the summation of individual tube and plate elements according to their geometric properties and was compared to the finite element results. The results showed that this expression underestimates the actual capacity by less than 10% which is a result of the plate-tube interaction of section and the restraining effect of corner tubes on plates. Ductility of fabricated hybrid beams was evaluated based on plastic rotation measurements resulting in values of 7.3, 5 and 2 for sections consisting of MS, HSS and UHSS tubes respectively. The plastic flexural strength of each section was also obtained and compared to the FE results. In the case of section geometries used in this study, plastic calculations resulted in a close prediction of the bending resistant which is consistent with the rotation capacities derived for each section.

Under combined axial force and bending moments, interaction curves were extracted for hybrid fabricated sections in the absence of shear stresses and the plastic estimation of strengths was extracted. The obtained curves for various cross-section properties showed that as the non-dimensional ratio of strength and cross section of tube elements to that of plate elements reduces, the interaction strength is enhanced. Consequently, the linear interaction formula is applicable for predicting interaction behaviour of sections with high tube to plate ratios while sections with lower ratios are closely predicted by the bilinear interaction formula.

Finally, parametric studies were conducted using a verified finite element model to obtain the axial-bending-shear interaction performance of hybrid sections. The beam-column performance of members obtained from the parametric study showed the axial-lateral curves are enhanced as the plate thickness increases in hybrid fabricated sections with high

strength tubes. Based on the axial and moment bearing demands of beam-columns, member design can be conducted for plate and tube geometries such that the most optimum section is obtained. Further analytical and numerical studies can be done continuing the current research work on the effect of member length on compression-shear-bending interactions.

5.7.   Acknowledgements

5.8.   References

[1] Shunsuke T, Koji S, Akio S. High strength steel tubes for automotive suspension parts - High strength steel tubes with excellent formability and forming technology for light weight automobiles. JFE Technical Report. 2004:32-7.

[2] Tanabe H, Anai I, Miyasaka A, Tanioka S. HAZ softening-resistant high-strength steel tubes for automobile propeller shafts. Nippon Steel Technical Report1995. p. 62-8.

[3] Vankuren RC, Scott JE. Energy absorption of high-strength steel tubes under impact crush conditions. SAE Technical Papers. 1977.

[4] Gangopadhyay KK, Guha D, Reddy PVN. Salt Lake Stadium roof, Calcutta, with high strength steel tubes. Structural engineer London. 1990;68:397-404.

[5] Jiao H, Zhao XL. Section slenderness limits of very high strength circular steel tubes in bending. Thin-Walled Structures. 2004;42:1257-71.

[6] Jiao H, Zhao X-L. Material ductility of very high strength (VHS) circular steel tubes in tension. Thin-Walled Structures. 2001;39:887-906.

[7] Zhao X-L. Section capacity of very high strength (VHS) circular tubes under compression. Thin-Walled Structures. 2000;37:223-40.

[8] Ling TW, Zhao XL, Al-Mahaidi R, Packer JA. Investigation of block shear tear-out failure in gusset-plate welded connections in structural steel hollow sections and very high strength tubes. Engineering Structures. 2007;29:469-82.

[9] Ling TW, Zhao XL, Al-Mahaidi R, Packer JA. Investigation of shear lag failure in gusset-plate welded structural steel hollow section connections. Journal of Constructional Steel Research. 2007;63:293-304.

[10] Jiao H, Mashiri F, Zhao X-L. Fatigue behavior of very high strength (VHS) circular steel tube to plate T-joints under in-plane bending. Thin-Walled Structures. 2013;68:106-12.

[11] Jiao H, Zhao XL. CFRP strengthened butt-welded very high strength (VHS) circular steel tubes. Thin-Walled Structures. 2004;42:963-78.

[12] Wiedemeier B, Sander M, Džugan J, Richard HA, Peters A. Fracure-mechanical characterization of high-strength steel tubes. 18th European Conference on Fracture: Fracture of Materials and Structures from Micro to Macro Scale2010.

[13] RAEX® R. Demand more from wear-resistant steels. RUUKKI RAEX® REFERENCES.

[14] Javidan F, Heidarpour A, Zhao X-L, Minkkinen J. Compressive Behavior of Innovative Hollow Long Fabricated Columns with High Strength and Ultra-High Strength tubes. 15th International Symposium on Tubular Structures. Rio de Janeiro, Brazil2015.

[15] Javidan F, Heidarpour A, Zhao XL, Minkkinen J. Performance of innovative fabricated long hollow columns under axial compression. Journal of Constructional Steel Research. 2015;106:99-109.

[16] Long HV, Jean-François D, Lam LDP, Barbara R. Field of application of high strength steel circular tubes for steel and composite columns from an economic point of view. Journal of Constructional Steel Research. 2011;67:1001-21.

[17] Zhao XL, Van Binh D, Al-Mahaidi R, Tao Z. Stub column tests of fabricated square and triangular sections utilizing very high strength steel tubes. Journal of Constructional Steel Research. 2004;60:1637-61.

[18] Heidarpour A, Cevro S, Song Q-Y, Zhao X-L. Behaviour of stub columns utilising mild-steel plates and VHS tubes under fire. Journal of Constructional Steel Research. 2014;95:220-9.

[19] Rhodes J, Zhao XL, Van Binh D, Al-Mahaidi R. Rational design analysis of stub columns fabricated using very high strength circular steel tubes. Thin-Walled Structures. 2005;43:445-60.

[20] Van Binh D, Al-Mahaidi R, Zhao XL. Finite element analysis (FEA) of fabricated square and triangular section stub columns utilizing very high strength steel tubes. Advances in Structural Engineering. 2004;7:447-57.

[21] Nassirnia M, Heidarpour A, Zhao X-L, Minkkinen J. Innovative Hollow Corrugated Columns: A Fundamental Study. Engineering structures 2015;94:43-53.

[22] Azhari F, Heidarpour A, Zhao X-L, Hutchinson CR. Mechanical properties of ultra-high strength (Grade 1200) steel tubes under cooling phase of a fire: An experimental investigation. Construction & Building Materials. 2015;in press.

[23] Mirmomeni M, Heidarpour A, Zhao X-L, Hutchinson CR, Packer JA, Wu C. Mechanical properties of partially damaged structural steel induced by high strain rate loading at

elevated temperatures – An experimental investigation. International Journal of Impact Engineering. 2015;76:178-88.

[24] Hosseini S, Heidarpour A, Collins F, Hutchinson CR. Effect of strain ageing on the mechanical properties of partially damaged structural mild steel. Construction and Building Materials. 2015;77:83-93.

[25] Sinaie S, Heidarpour A, Zhao XL. Stress-strain-temperature relation for cyclically-damaged structural mild steel. Engineering Structures. 2014;77:84-94.

[26] Sinaie S, Heidarpour A, Zhao XL. A multi-objective optimization approach to the parameter determination of constitutive plasticity models for the simulation of multi-phase load histories. Computers & Structures. 2014;138:112-32.

[27] Sinaie S, Heidarpour A, Zhao XL. Mechanical properties of cyclically-damaged structural mild steel at elevated temperatures. Construction and Building Materials. 2014;52:465-72.

[28] Mazzina R, Gomez G, Solano M, Perez T, Lopez E. Study on weldability of high strength steel for structural applications. ASM Proceedings of the International Conference: Trends in Welding Research2013. p. 208-16.

[29] Jiao H, Zhao X-L. Tension Capacity of Very High Strength (VHS) Circular Steel Tubes after Welding. Advances in Structural Engineering. 2004;7:285-96.

[30] Shi G, Jiang X, Zhou W, Chan T-M, Zhang Y. Experimental investigation and modeling on residual stress of welded steel circular tubes. Int J Steel Struct. 2013;13:495-508.

[31] Javidan F, Heidarpour A, Zhao X-L, Hutchinson CR, Minkkinen J. Mechanical Properties of welded High strength and Ultra-high Strength Steel Tubes in Fabricated Sections. Engineering Structures. 2015.

[32] AS/NZS1554.7 Structural steel welding-Welding of sheet steel structures. Part7. Sydney: Standards Australia; 2006.

[33] AS 4100-1998, Steel structures. Sydney: Standards Australia; 1998.

[34] E606-04 Standard Practice for Strain-Controlled Fatigue Testing. ASTM International; 2004.

[35] AS 1391-2007 Metallic Materials-Tensile testing at ambient temperature. Sydney: Standards Australia; 2007.

[36] AS/NZS 4600:2005 Cold-formed steel structures. Australian/New Zealand Standard; 2005.

[37] Park R. Evaluation of ductility of structures and structural assemblages from laboratory testing. Bulletin of the New Zealand National Society for Earthquake Engineering. 1989;22:155-66.

[38] AS 1170.4-2007 Strcutural design actions Part4: Earthquake actions in Australia. Syndey: Standards Australia; 2007.

[39] Dassault Systèmes Simulia Corp. P, RI, USA. ABAQUS/CAE 6.14-1. 2014.

[40] Hooputra H, Gese H, Dell H, Werner H. A comprehensive failure model for crashworthiness simulation of aluminium extrusions. International Journal of Crashworthiness. 2004;9:449-64.

[41] Kessler L, Beier T, Werner H, Horstkott D, Dell H, Gese H. Material selection for an ultra high strength steel component based on the failure criteria of CrachFEM. AIP Conference Proceedings2005. p. 492-9.

[42] ARAMIS User Manual - Software V6.1. In: mbH G, editor. Mittelweg 7-8 D-38106 Braunschweig Germany2009.

[43] Mahendran M. Local plastic mechanisms in thin steel plates under in-plane compression. Thin-Walled Structures. 1997;27:245-61.

Fundamental behaviour of high strength and ultra-high strength steel subjected to low cycle structural damage

Monash University

Declaration for Thesis Chapter 6

Declaration by candidate

In the case of chapter 6 my contribution to the work involved the following:

Nature of contribution	Extent of contribution (%)
Developing ideas, Establishing methodologies, Experimental work, Data analysis, Write-up and revision	70%

The following authors contributed to the work:

Name	Nature of contribution	Extent of contribution (%)
Dr. Amin Heidarpour	Developing ideas, Input into manuscript, Revision, Financial support	18%
Prof. Xiao-Ling Zhao	Revision, Financial support	7%
Mr. Hossein Fallahi	Input to manuscript	5%

The undersigned hereby certify that the above declaration correctly reflects the nature and extent of the student's and co-authors' contributions to this work.

Student signature   ▮▮▮▮▮   Date: 30/01/2017

Main Supervisor's signature   ▮▮▮▮▮   Date: 30/01/2017

6.1.   Abstract

Along with the rising application of high strength steel in civil engineering practice, it has become imperative to gain comprehensive understanding of the elastic and plastic behaviour of these materials under given strain or stress histories. For seismic analysis of structures in earthquake prone areas, this paper aims to analytically and theoretically study the cyclic behaviour of high strength steel tubes, with individual applications or incorporated in fabricated structural elements. Several low cycle tension-compression tests are conducted on high strength (grade 800) and ultra-high strength (grade 1200) steel coupons extracted from tubes. Parameters such as number of cycles, strain/stress amplitude and increment size are studied in the behaviour of cyclically strained material and its preserved mechanical properties. Numerical analysis is also conducted incorporating combined nonlinear hardening models. As opposed to conventional structural mild steel both grades of steels considered in this study exhibit cyclic softening with plastic straining having a more prominent strength reduction in higher strengths of steel. Cyclical damage applied on high tensile steel evidently influences the preserved mechanical properties of microstructure at fracture. Combined nonlinear plastic hardening and relevant parameters proposed in this study for two grades of high strength steel materials are calibrated and verified against hysteretic experimental results and proposed for further analytical and numerical modelling.

Keywords: High strength steel, ultra-high strength steel, low cycle damage, hysteretic response, cyclic softening

6.2.   Introduction

The application of high strength steel materials has recently increased in various civil constructions and is found to have convenient structural properties and cost efficiency compared to conventional mild steel material. Following this increasing trend there is a necessity to gain an extensive understanding of the mechanical properties of these materials under relevant loading conditions. Previous studies are found mostly investigating the behaviour of high strength steel structural elements with material steel grades of up to around 700MPa [1-6]. However, in more recent studies higher grades of steel (with nominal yield strength of 800MPa to 1200MPa) have also been taken into consideration to investigate the behaviour of ultra-high strength steel beams, columns, girders and other types of structural elements [7-11]. An application for high strength steel material proposed and widely investigated in literature, is utilizing these materials in "dual-steel" moment resisting frames in which high strength steel acts as non-dissipative members while mild steel is used in dissipative zones [12-15]. In these systems, high strength steel is used in order to increase the seismic performance of structural system by limiting plastic behaviour in columns and guaranteeing the weak-beam/strong-column behaviour [12, 14]. As a current development, hybrid fabricated sections are proposed in which a combination of high strength steel tubes and mild steel plates are incorporated, taking advantage of these modern materials in load bearing structural elements [16-19]. In these sections, taking benefit of the interaction between different grades of constituting steel elements, both strength and ductility of the structural element are enhanced.

Following the numerous amount of work on conventional mild steel under extreme loadings such as cyclic, impact and fire conditions [20-24] high strength and ultra-high strength steel in form of tubular elements have recently been investigated under potential extreme conditions [25-29] due to their light weight and convenient geometry. Understanding the

hysteretic response of high strength steel material is of significant importance for seismic analysis of members especially in case of energy dissipating members constituting of these high tensile materials. The mechanical properties and plastic behaviour of high strength material is of importance both during seismic loading and beyond that which is where the structure continues to undergo post-earthquake service loads. The aim of material scale examinations on high strength steel specifically under cyclic loadings include material characterisation and modelling, obtaining preliminary constitutive equations and failure or fracture mode prediction. High tensile structural steel with yield strengths within the range of 300 to 500MPa have previously been experimentally tested to obtain the hysteretic response and relevant parameters such as hardening and ductility [30-33] and steel grades up to 600MPa under low cycle damage have been considered. Nip et al. [32] tested carbon and stainless steel under low cycle fatigue and obtained a combined hardening model to be incorporated in numerical models. Two different test arrangements of axial and bending were considered and cyclic parameters of either type was compared [32]. In other research work constitutive material models were established based on various experimental loading patterns which were implemented in nonlinear time history analysis of steel frames [30] and quasi-static simulation of steel beam-columns [33]. Effect of cyclic loading on the occurrence of brittle failure and ductility was studied by Iwashita et al. [31] and a method was proposed to evaluate the brittle failure under various loading conditions. In steel grades higher than 500MPa, Silvestre et al. [34] tested a range of (ferritic) steel material including high and ultra-high strength steel with approximate yield stress within the range of 200 to 1200 MPa and developed a mixed hardening model. However the test coupons were extracted from 1.5mm sheets and limited to constant strain amplitudes of 2%. In terms of standard recommendations for design purposes, previous studies [18, 35] have focused on the ductility of HSS and UHSS steel materials and comparison have been made with regards to recommended standard criteria against a variety of design standards showing that these steel grades fail to meet some of the proposed requirements which consequently affects the

design and prediction of section performance against local buckling. This highlights the demand for further investigations focused on high tensile steel grades to derive practical design recommendations which are not included in current available standard classifications. Experimental and numerical model proposed in this study provide primary knowledge for these investigations.

The present study, examines the hysteretic response of high strength (grade 800) and ultra-high strength (grade 1200) steel material to contribute to the limited data currently available on these grades of steels in structural applications. All test specimens are extracted from high and ultra-high strength circular steel tubes and tested under strain and stress controlled amplitudes. Strain controlled tests are conducted in two types of constant and incremental amplitudes. Number of cycles and strain amplitude percentage are the two parameters considered in the constant strain controlled tests. Incremental strain amplitude tests are also conducted with varying strain steps. The obtained results show the occurrence of cyclic softening in both high and ultra-high strength steel materials. Hysteretic curves for both high strength steel materials are analysed in terms of strength softening, preserved strength and ductility and its correlation to final fracture, energy absorption etc. From hysteretic responses, a simplified stress-strain formulation based on the Ramberg-Osgood model is suggested. Besides, relevant kinematic/isotropic plasticity parameters are proposed for high strength and ultra-high strength steel tubes which are applicable for modelling various scales of structures and structural components.

6.3. Cyclic testing of High Strength Steel (HSS) and Ultra-High Strength Steel (UHSS) specimens

6.3.1. Test setup

A series of experimental tests were designed and conducted to obtain the necessary parameters for modelling the cyclic behaviour of HSS and UHSS steels. Various test paths were considered with different combinations of tension and compression straining. All monotonic and cyclic test specimens were extracted directly from grade 800 (HSS) and grade 1200 (UHSS) circular steel tubes, having a 90-degree angle from the tube weld. Manufacturing process and detailed mechanical properties of these steel tubes are the same as tube material reported in authors' previous research work [36]. Due to the thin-walled geometry of tube (nominal thickness of 3.2mm and external diameter of 76.1mm) and also limitations in the minimum gauge length for strain measurement, the dimensions of test specimens were chosen in a way to reduce the chance of buckling during the compression phase of cyclic test. These dimensions follow the ASTM E606-04 standard practice guidelines [37] for strain controlled fatigue testing and are presented in Figure 6.1. Similar to previous literature on thin-walled specimens [38], strain corresponding to buckling initiation was found by conducting trial tests, to assure buckling does not occur within the strain levels considered in the present study.

(a)
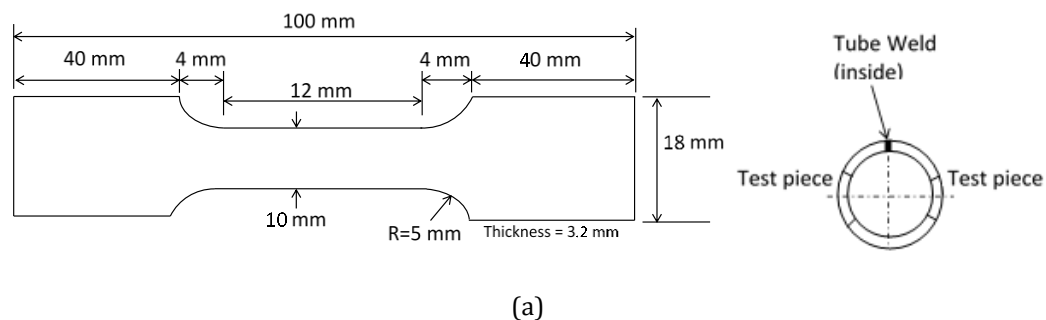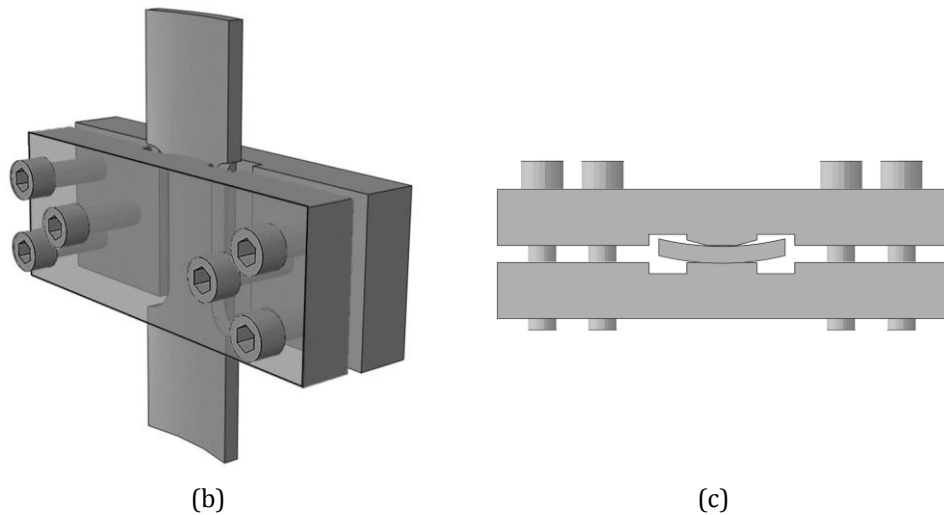
Figure 6.1. (a) Cyclic specimen dimensions and extraction location from tube; (b) An overall view of anti-buckling fixture for tube specimens; (c) top view of anti-buckling fixture for tube specimens.

In all cyclic specimens the length of reduced section to nominal thickness is around 3.8 and the measured gauge length to nominal thickness ratio is approximately equal to 3. However, to assure that buckling is fully prevented, an anti-buckling fixture was also designed and utilised during each test. Based on previous literature, in-plane compression testing can be done using either side loading, or using constraint, to suppress buckling in the thickness direction [39]. The anti-buckling fixture used in this study consists of two steel segments covering each side of the specimen, fastened with high strength bolts. A layer of high performance grease was applied between the specimen surface and fixture to prevent friction. The anti-buckling fixture is specifically designed for testing the tube specimens with grooves designed to run along the specimen reducing the contact in curved areas. Figure 6.1(b) and (c) show the shape and and cross-section of the fixture covering the cyclic specimen.

Test specimens were loaded in the Instron 8802 servo-hydraulic testing machine and the data acquisition was done through the machine readings in addition to precise strain measurement of gauge length obtained from a non-contact MTS LX500 laser extensometer with a strain resolution of 0.001 mm and scan rate of 100 scans/second. Standard tensile

tests were also conducted on both HSS and UHSS tube materials to gain understanding of the typical mechanical properties of these materials under quasi-static monotonic loading. The cyclic test setup is shown in Figure 6.2. Quasi-static displacement rate of 0.3mm/min was applied to all specimens under monotonic and cyclic loadings.

Figure 6.2. Cyclic test setup
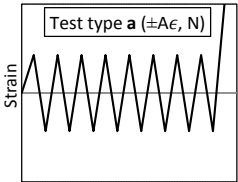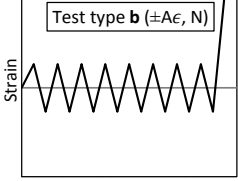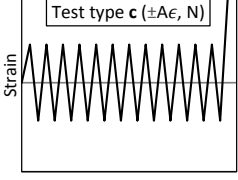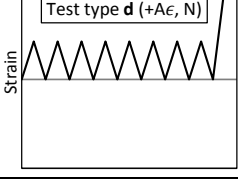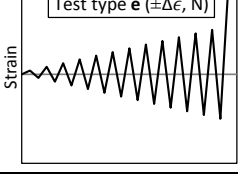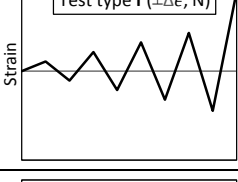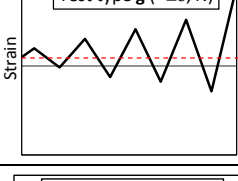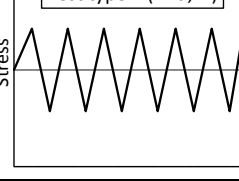
6.3.2. Test paths and outcomes

Various types of monotonic, strain controlled and stress controlled cyclic tests were conducted on both HSS and UHSS steel materials. The variables considered in the tests were amplitude, strain step, number of cycles and residual strain applied to the specimen before cyclic loading. Two values of maximum plastic strain were chosen for each material one of which is close to the strain corresponding to ultimate tensile strength (ϵ_{UTS}) and the second a lower percentage of that strain. Tests were conducted applying different number of cycles (N) for each of the materials. Strain was applied to specimens either with constant amplitude (A_ϵ) or increasing steps of strain amplitudes ($\Delta\epsilon$) and in some cases a residual strain (Rϵ) was applied by an initial displacement controlled monotonic loading followed

by the strain cycles. In addition to the above mentioned cases, stress-controlled cyclic tests with constant stress amplitudes (A_σ) were conducted at two different stress values. All strain/stress paths applied to HSS and UHSS are shown in Table 6.1. Test types (a) and (b) vary in terms of the amplitude of applied strain while in test type (c), number of cycles (N) is the factor which was increased from 8 to 12. Keeping both amplitude and number of cycles the same as previous types, in case (d) only tensile strains are applied to the material. With a slightly different strain pattern, in test types (e) and (f) an increasing amplitude of strain is applied having different cycle numbers (N) and strain steps ($\Delta\epsilon$) with a similar final strain amplitude in both cases. The effect of pre-strain ($R\epsilon$) is taken into consideration in part (g) which repeats the strain pattern of (f) with an initial strain of 0.5% primarily applied to the specimen. Case (h) considers a constant stress amplitude up to a certain percentage of the ultimate tensile strength (UTS). Cyclic strain or stress paths of the conducted tests on HSS and UHSS are illustrated in Table 6.1.

The stress-strain curves resulted from each cyclic test based on the strain or stress patterns described in Table 6.1 are presented in Figure 6.3 for HSS and in Figure 6.4 for UHSS. It is observed in all test cases that with the rise in number of cycles, strength in material decreases which is referred to as cyclic softening. This is dissimilar to the cyclic performance of structural mild steel and high strength steel material with grades up to approximately 500 MPa reported in literature [23, 30, 32] in which material strength increases under very low cycle damage. This finding confirms the results reported from cyclic tests conducted on higher grades of steel [34]. After 12 strain-controlled cycles in both HSS and UHSS materials at amplitudes of around 95% and 60% of the strain corresponding to ultimate strength, this strength reduction percentage reaches around 1% with respect to the previous cycle and the stress-strain curves from that cycle are considered stable in this study.

Table 6.1. Cyclic test parameters of test types on HSS and UHSS

Test type	Specimen Label	Test parameter	No. of cycles	Cycle pattern
a	HSS-a <hr> UHSS-a	$A_\epsilon 1 \approx \pm 95\%\ \epsilon_{UTS}$	N1: 8	
b	HSS-b <hr> UHSS-b	$A_\epsilon 2 \approx \pm 60\%\ \epsilon_{UTS}$	N1: 8	
c	HSS-c <hr> UHSS-c	$A_\epsilon 1 \approx \pm 60\%\ \epsilon_{UTS}$	N2: 12	
d	HSS-d <hr> UHSS-d	$A_\epsilon 1 \approx +60\%\ \epsilon_{UTS}$	N1: 8	
e	HSS-e <hr> UHSS-e	$\Delta\epsilon 1 \approx 7\%\ \epsilon_{UTS}$	N2: 12	
f	HSS-f <hr> UHSS-f	$\Delta\epsilon 2 \approx 20\%\ \epsilon_{UTS}$	N3: 4	
g	HSS-g <hr> UHSS-g	$\Delta\epsilon 2 \approx 20\%\ \epsilon_{UTS}\ \ R\epsilon: 0.5\%$	N3: 4	
h	HSS-h <hr> UHSS-h	$A_\sigma 1 \approx \pm 90\%\ UTS$	N4: 6	

Energy dissipation calculated from the load versus displacement curves of each complete cycle in both steel materials under test type (a) shows that this value is higher in UHSS compared to HSS. The energy dissipation reduces along with the increase in number of cycles applied in both HSS and UHSS materials in the above mentioned test case. In order to have a comparison among the levels of energy dissipation in high strength materials with conventional mild steel, cyclically damaged mild steel has also been taken into consideration [23]. The area under cyclic stress-strain curve reported for a stabilized response of cyclically damaged mild steel grade 300 at ambient temperature tested under 2% strain [23], is obtained and compared to that of test case (a) for UHSS which has been tested under a similar strain amplitude. Energy dissipation of a stabilized cycle with around 2% strain amplitude in UHSS (grade 1200) material shows to be around 2.5 times of that in mild steel (grade 300). This is obviously the effect of the difference in strength of these materials. This conclusion, however, is dependent on the strain amplitude and number of cycles applied. At higher strain amplitudes, with the reduction in strength of UHSS, the ratio of energy absorption may change when comparing these materials. Energy dissipation coefficient which is the ratio of energy dissipation capacity to energy absorption capacity proposed by Cai et. al [28] is a realistic parameter to analyse the energy efficiency of structural elements. Energy dissipation coefficient in HSS is higher than that of UHSS which is consistent with the observations reported in [28] for two different grades of steel tubes tested under cyclic loading.
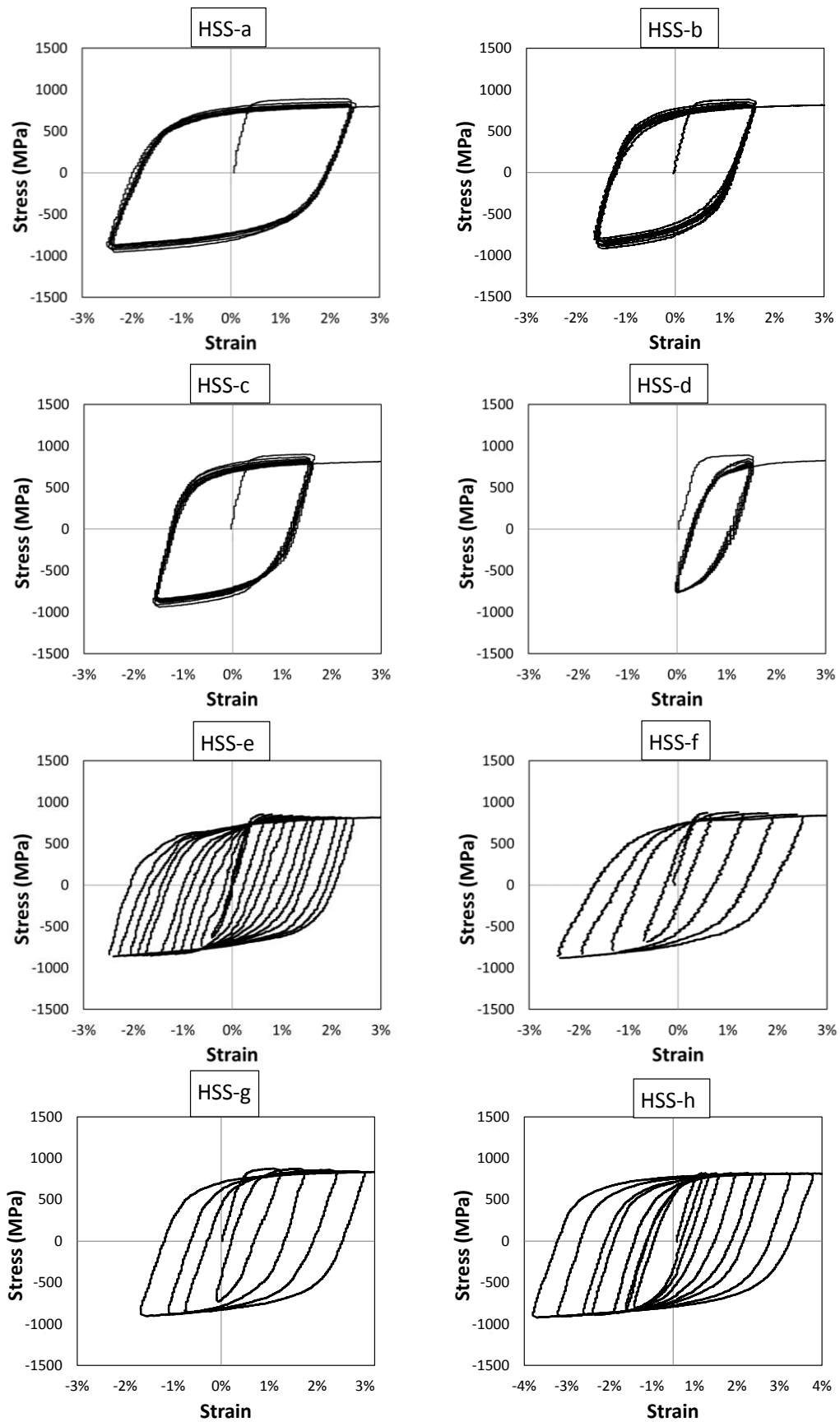
Figure 6.3. Cyclic stress-strain curves for HSS material based on test types defined in Table 6.1
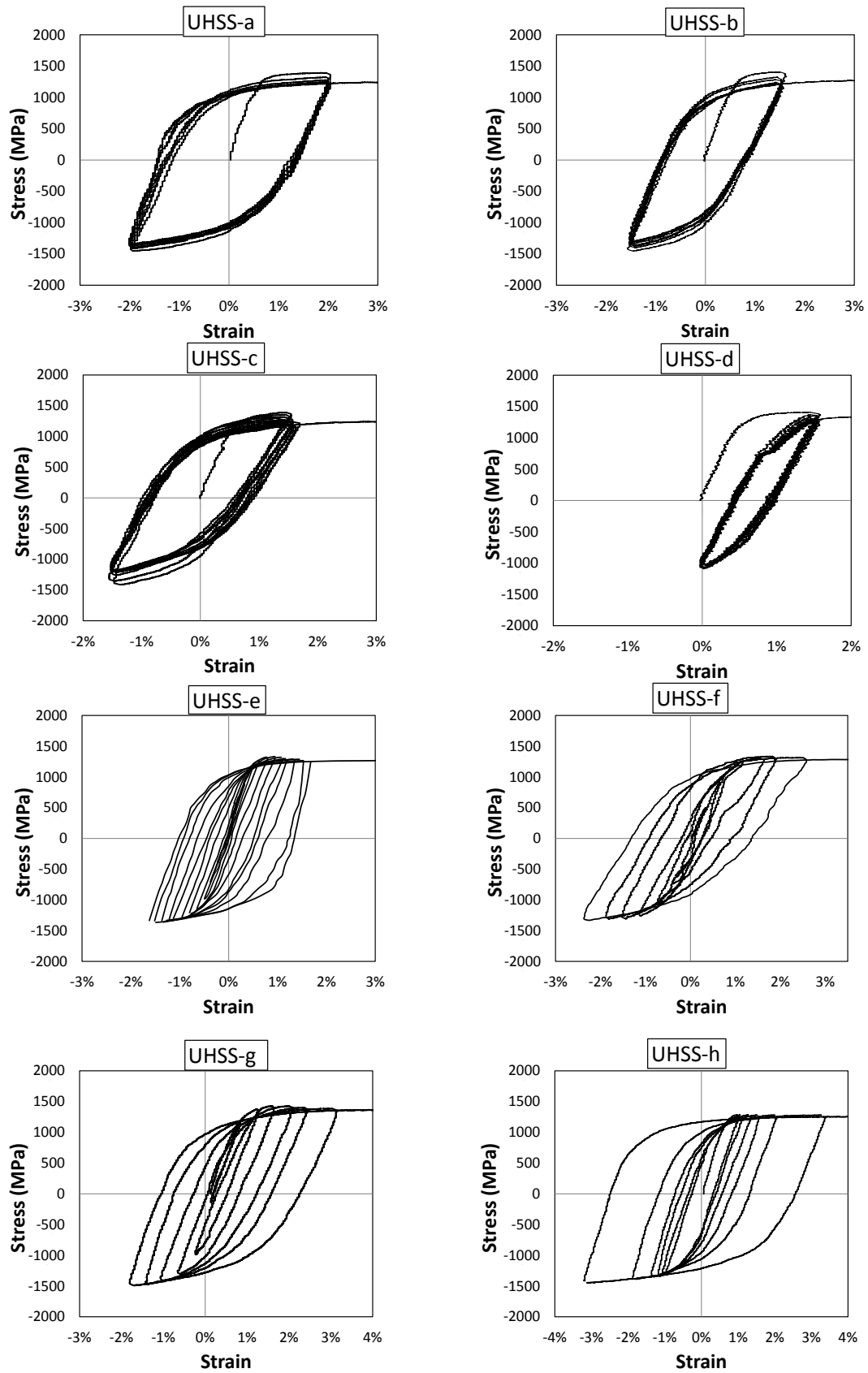
Figure 6.4. Cyclic stress-strain curves for UHSS material based on test types defined in Table 6.1

6.4. Analysis of Experimental results

6.4.1. Tests with constant strain amplitude

Figure 6.5(a) and (b) illustrates the normalised strength versus number of cycles of test types (a) and (b) on HSS and UHSS materials, respectively. From Figure 6.5 and the values of CS% the overall softening percentage of UHSS is higher than that in HSS which means that this phenomenon is more prominent when material strength is increased. In these test types, amplitudes are in a range between the strain corresponding to 0.2% proof strength and the ultimate strain (ϵ_{UTS}) of both material types. The normalized stress versus number of cycles for test type (c) is also shown against and compared to that of type (b) in Figure 6.5 for HSS and UHSS. From these curves, HSS and UHSS materials exhibit higher cyclic softening as the cyclic straining progresses. *Cyclic softening percentage (CS%)* introduced in the present study is defined as the percentage of material's strength reduction at a specific cycle number calculated relative to the material's strength at the first cycle. This gives a quantitative overview of how the material strength deteriorates under various cyclic patterns and how each cyclic parameter will affect the ultimate strength at different stages of testing. The amount of *CS%* of test cases (a) to (c) are extracted and plotted in Figure 6.6. As can be expected, with increasing strain amplitude (test case a compared to b) and increasing the number of cycles (test type c compared to b), damage is introduced and both test factors result in a higher softening percentage. From the values of *CS%* in Figure 6.6 the overall softening percentage of UHSS is higher than that in HSS which means that this phenomenon is more prominent when material strength is increased. In order to drive a comparison among all the above mentioned test cases, the total accumulated plastic strain (s^p) is obtained and analysed against *CS%*. Accumulated plastic strain (s^p) [40], can provide a more general quantitative evaluation of plastic history of the applied strain patterns in various test cases which is defined as follows:

$$s^p = \int_0^t |d\varepsilon^{pl}/dt| dt \tag{6.1}$$

in which ε^{pl} is the plastic strain applied over time (t). Figure 6.6 shows the similar trend of CS% and the accumulative plastic strain applied on each specimens. In test case (b) both materials experience lowest accumulated plastic strain which accordingly show a lower percentage of cyclic softening. In test cases (a) and (c) a relatively higher level of accumulative plastic strain is applied which similarly results in a more significant cyclic softening percentage.
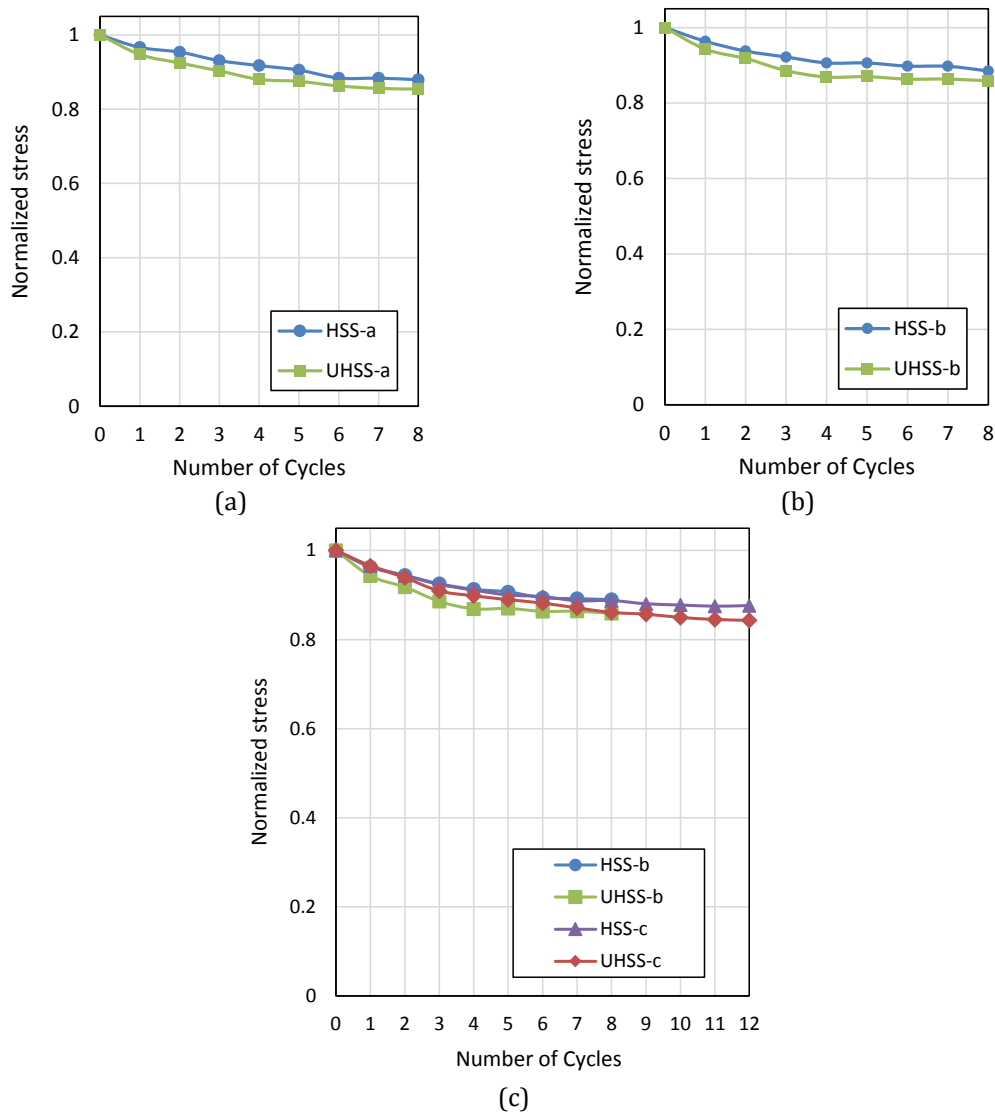
Figure 6.5. (a) Normalized stress of: a) cases HSS-a and UHSS-a, b) cases HSS-b and UHSS-b, c) HSS and UHSS cases (b) and (c).
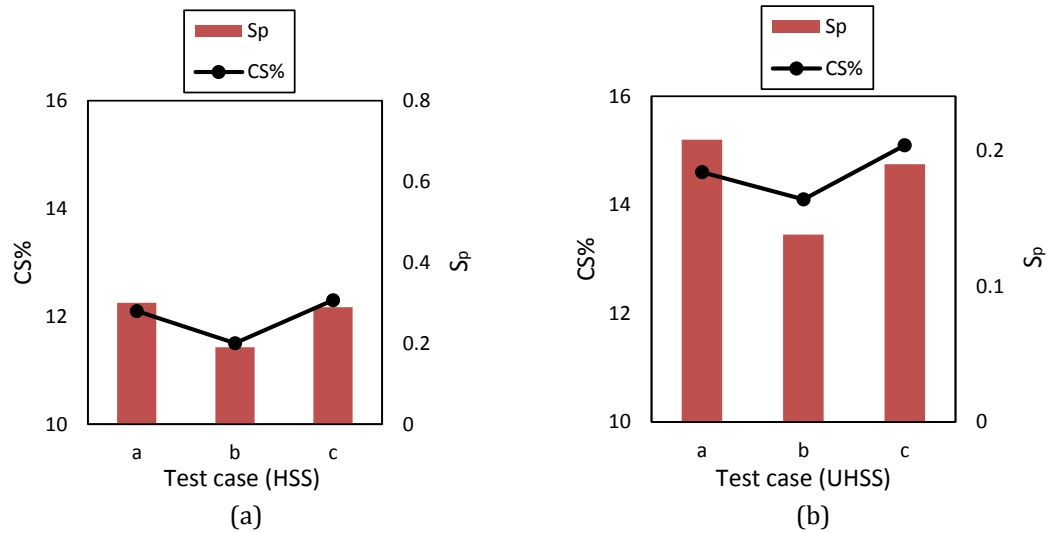
Figure 6.6. Cyclic softening (CS%) versus accumulated plastic strain (Sp) for: a) HSS and b) UHSS

6.4.2. Tests with incremental strain amplitude

Test cases (e) to (g) refer to strain patterns in which the amplitude gradually increases at each cycle. The strain increments at each cycle are chosen as a percentage of the strain corresponding to ultimate strength. Two different strain increments are considered for HSS and UHSS materials in test cases (e) and (f) and the maximum strain for the last cycle of both tests is similar. In test type (g) a residual strain amplitude of 0.5% is applied to the material which is followed by strain increments similar to case (f). Figure 6.7 presents the stress at the end of each cycle in three test cases shown against the monotonic tensile tests for comparison. It can be seen that in both HSS and UHSS materials, having higher number of cycles -and therefore less incremental strain step- results in a more obvious strength degradation compared to less number of cycles -and therefore higher incremental strain step- for which almost no strength degradation is observed in UHSS material in test type (f) and (g). This observation is consistent with the calculated accumulative plastic strain for these test cases which test case (e) in both materials have a higher s^p value.
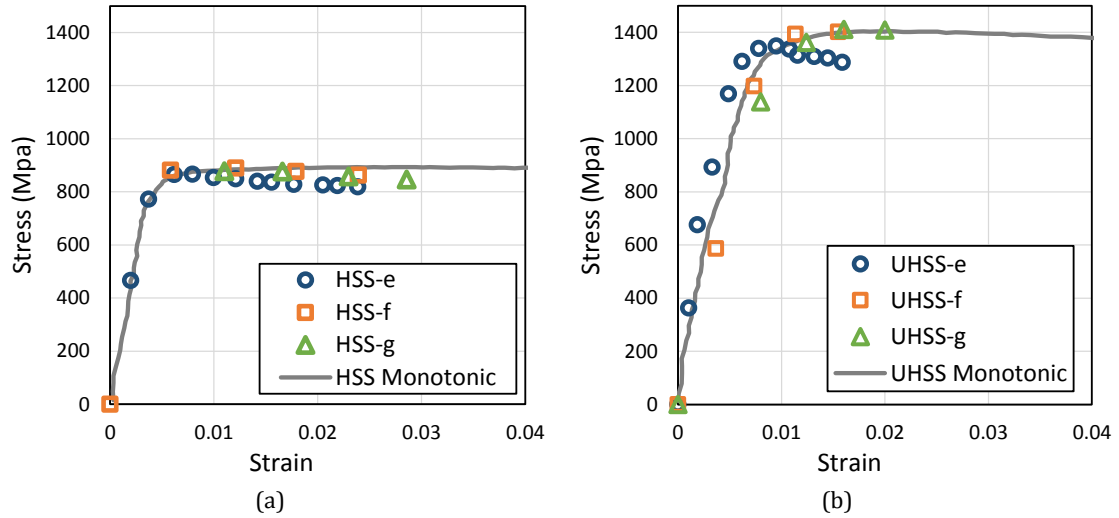
Figure 6.7. Cyclic softening of cases "e", "f" and "g" against monotonic tensile test for: (a) HSS and (b) UHSS materials

6.4.3. Tests with incremental stress amplitude

As opposed to all previous tests, in case (h), the maximum stress in all cycles was kept constant and the changes observed in the corresponding strain was recorded. The stress versus strain points at end of each cycles in test case (h) are shown against the monotonic tensile curves in HSS and UHSS material (see Figure 6.8). It is observed that at the end of each cycle, the strain corresponding to stress amplitude experiences a higher increase compared to the previous cycle. The strain increment which is defined as the difference of strain at each cycle relative to that of the previous cycle increases as the number of cycles progresses. It is known that the strain increment variation depends on the stress controlled cyclic tests i.e. values of mean stress and amplitude. In case (h) the mean stress is equal to zero with an amplitude of 90% of UTS.
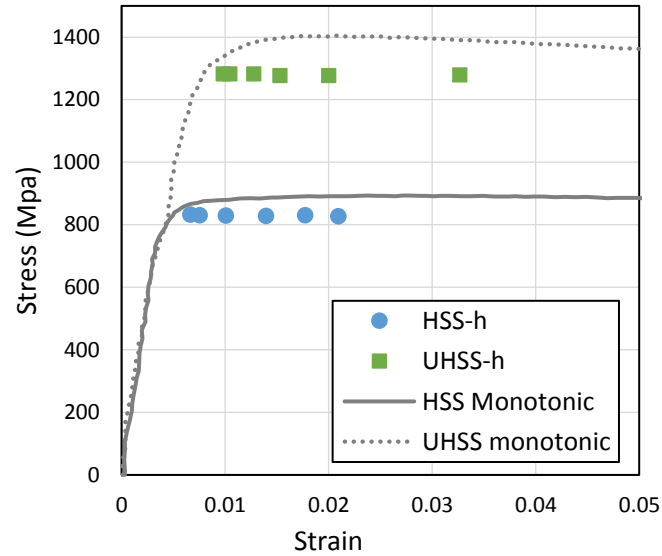
Figure 6.8. Constant stress amplitude test results of HSS and UHSS

6.4.4. Preserved mechanical properties of cyclically strained HSS and UHSS

To obtain the material properties of steel strained by cyclic loading, a monotonic displacement was applied at the end of each cyclic test case up to fracture. . The importance of these tests is obtaining the preserved material properties under very low cycle damage and assessing the potential structural performance of these steel material after the event of cyclic damage such as earthquake which is not found to be investigated for HSS and UHSS steel materials in literature. The cyclically strained tensile strengths of two types of steel with constant (i.e. test types a, b, c and d) and incremental strain amplitudes (i.e. test types e, f and g) are presented in Figure 6.9. In general it is observed that the ultimate tensile strength of cyclically strained HSS and UHSS reduces compared to that of virgin material under monotonic tensile strain. Based on results presented in test types with constant strain amplitude, it can be concluded that the reduction in the preserved tensile strength of HSS and UHSS is more prominent with higher strain amplitude compared to the effect of increasing number of cycles. Also, in tests with incremental strain amplitudes, with higher

applied number of cycles and therefore smaller strain steps (test case e), larger tensile strength reduction is observed in both HSS and UHSS materials. Accumulated plastic strains are also derived for test cases a, b and c of section 6.4.1 and test cases e and f of section 6.4.2 and compared for these cases. Results of test cases a, b and c showed that having the highest value of accumulated plastic strain exhibits less preserved tensile strength (test case a). Moreover, in test cases with incremental strain amplitude, test case e has higher value of accumulated plastic strain (s^p) which justifies the observation in preserved tensile strength and effect of cycle number on softening behaviour.
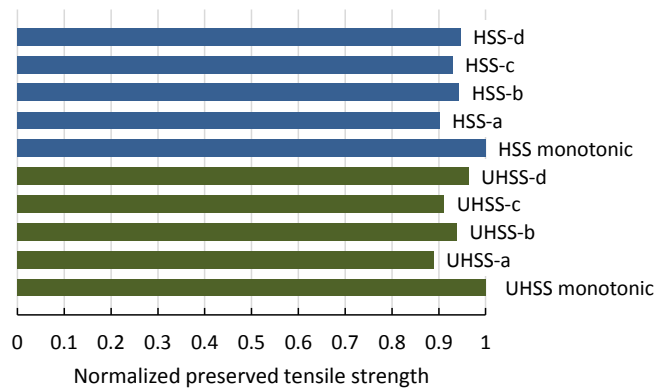
(a)
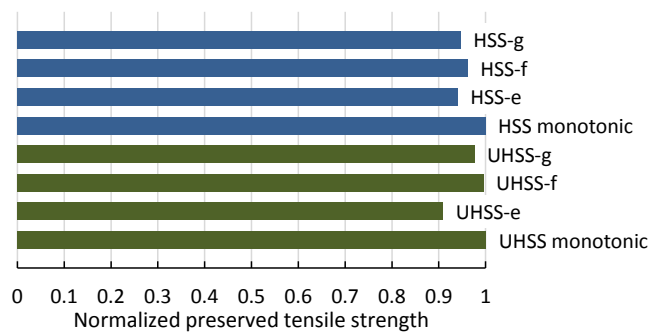
(b)

Figure 6.9. Normalised tensile strength for cyclic tests HSS and UHSS: (a) tests with constant strain amplitude, (b) tests with incremental strain amplitude

Ductility of steel material also undergoes considerable changes after cyclic damage is applied to specimen. As opposed to the reduction in stress, the ultimate tensile strength of cyclically strained UHSS and HSS material happens in a higher strain compared to that of

the virgin material. This observation is valid in both constant and incremental strain amplitude test types. The exact value of strain corresponding to ultimate strength varies depending on the cyclic test type, however for cases (a)-(g) this value falls in the strain range presented in Figure 6.10. The average value of strain corresponding to ultimate strength increases around 2.5 times in HSS and around 2 times in UHSS material. The values of ultimate strength and the corresponding strain of material strained under a cyclic loading history which are obtained in this study can be compared to the findings on mild steel reported in previous studies [23]. As opposed to HSS and UHSS materials, the cyclic history of 3 and 9 cycles at room temperature, does not have any obvious effect on the ultimate strength of 300PLUS mild steel. Ultimate strain, however, decreases in the presence of a cyclic loading history in mild steel which is dissimilar to the increasing trend observed in test results on HSS and UHSS. To further investigate these observations, Considère's criterion is considred which indicates the onset of plastic instability being the point where hardening rate falls below the true stress- true strain curve ($d\sigma_t/d\varepsilon_t = \sigma_t$) [36]. For UHSS and HSS materials the true stress versus true strain data was obtained from test results and the strain hardening rate was derived. In both these materials it was observed that strain hardening rate affects the changes in ultimate strain (uniform elongation). In HSS and UHSS material undergoing cyclic damage, the slope of strain hardening rate is higher compared to monotonic tensile tests. This results in the onset of damage taking place at higher strain values compared to the undamaged material which leads to a higher ultimate strain in cyclically damaged high strength steel materials. In case of mild steel material, however, the slope of strain hardening rate in the absence of cyclic damage is higher compared to that of the cyclically damaged steel.
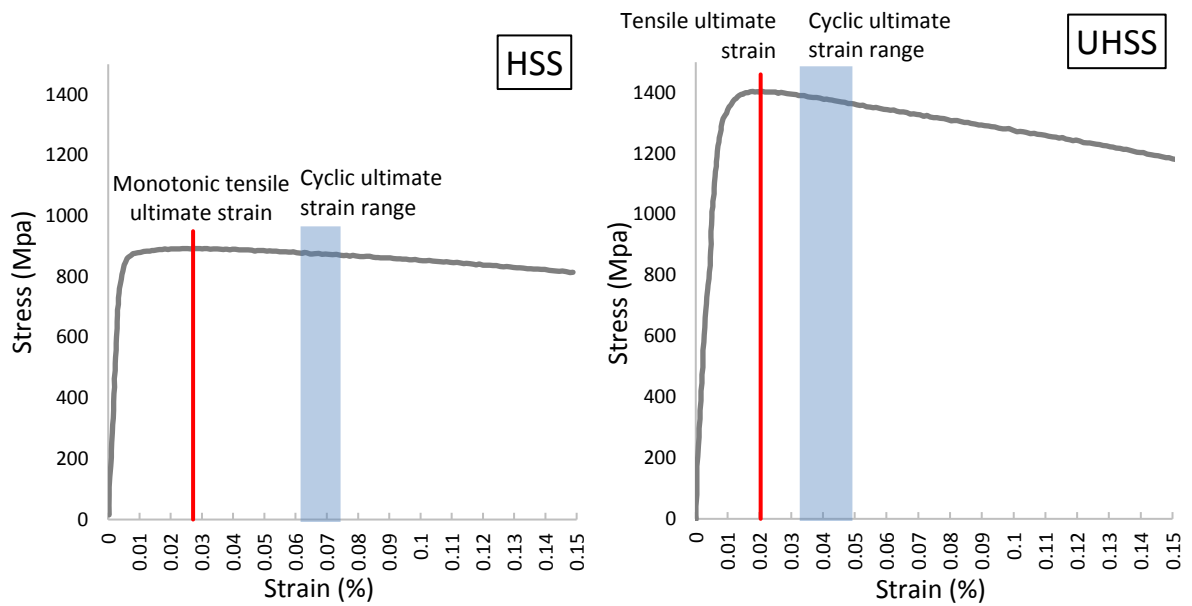
Figure 6.10. Strain corresponding to UTS of cyclically strained HSS and UHSS

As mentioned previously, after cyclically straining HSS and UHSS, all samples were monotonically tensioned until failure. The fracture surface of HSS samples tested under strain path type (a) (see Table 6.1) and also virgin HSS sample tested under monotonic tensile test are investigated and compared against that of UHSS. Figure 6.11(a) shows SEM micrograph of virgin HSS under monotonic loading and Figure 6.11(b) shows HSS-a specimen, both in 21X and 500X magnifications. The fracture surfaces of these materials are similar and fracture mode is ductile consisting of voids and ductile dimples. However, these voids are not deep, and their distribution is uniform throughout the samples. Therefore, the voids have not lead to catastrophic fracture. At higher magnifications (500X), dimples are detected. Dimples and the way they are deformed can prove the ductile fracture behaviour in most parts of the fracture surface. Figure 6.11(c) shows SEM micrograph of virgin UHSS subject to monotonic tensile loading and Figure 6.11(d) shows that of UHSS-a cyclically damaged specimen, both in 21X and 500X magnifications. The fracture surface of these materials are quite similar and fracture mechanism is mixed mode consisting of some voids

and dimples. A mixed mode of fracture can be seen consisting of voids, ductile dimples and cleavage facets, which are shown in higher magnification 500X of Figure 6.11(d). These cleavage facets and rupture interfaces are a major feature of the fracture surface and show the crack growth path under the applied load. Grains and grain boundaries are very clear in the SEM micrograph in high magnification which are evident of intergranular fracture. Such fracture is not considered fully ductile due to the crack path being through grain boundaries. The modes of fracture observed from fractographs is closely related to the strain values at fracture obtained from flow curves of each test. These fracture strain values can also be a good indicator of the fracture type [41, 42]. Fracture of UHSS specimen under monotonic tensile loading occurs at a lower strain amount compared to that of HSS specimens which is similar to the observation in cyclically strained specimens.
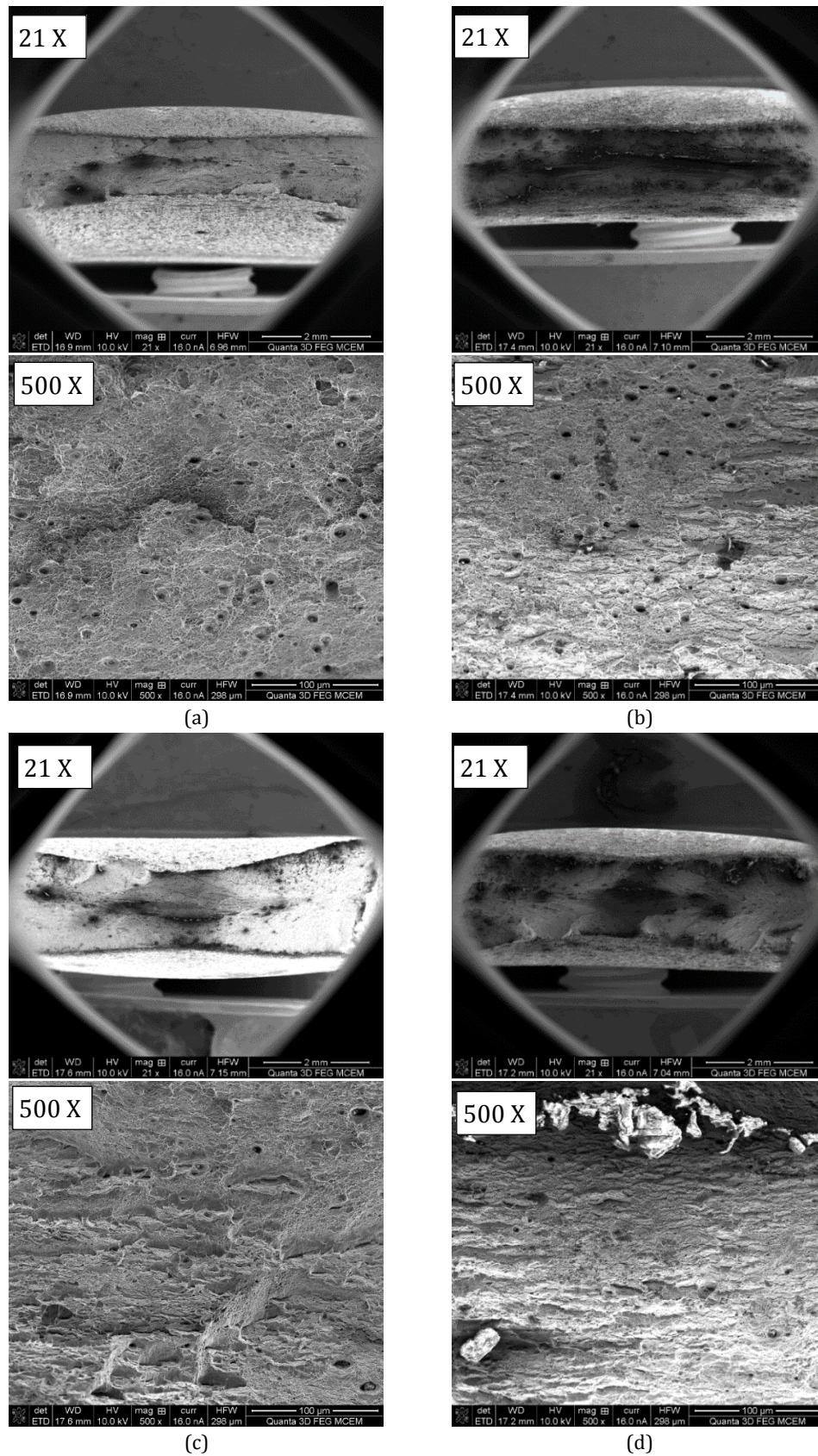
Figure 6.11. Fractographs at 21X and 500X magnifications: a) virgin HSS subject to monotonic tensile loading, b) cyclically strained HSS-a specimen c) virgin UHSS subject to monotonic tensile loading, d) cyclically strained UHSS-a specimen

6.5.   Numerical cyclic modelling of HSS and UHSS material

6.5.1.   Stress versus strain relationship for varying amplitude tests

As mentioned earlier, the strength of HSS and UHSS materials degrades as the loading cycles increase. A basic model is required to simulate this phenomenon. The hysteresis skeleton envelope of high strength steel stress-strain curves with yield strength around 500MPa shows a cyclic hardening trend and is reported to follow the Ramberg-Osgood model [43] such that

$$\frac{\Delta\varepsilon}{2} = \frac{\Delta\sigma}{2E} + \left(\frac{\Delta\sigma}{2K}\right)^n \tag{6.2}$$

Due to the fact that in Ramberg-Osgood model Equation (6.2) strain is a dependent variable and a function of stress, this formula is not convenient to predict the cyclic behaviour of HSS and UHSS steel in which stress experiences a reduction. Therefore, a strain dependent model is presented to predict the hysteresis softening skeleton of HSS and UHSS under incremental strain controlled symmetric cyclic loading (6.3) so that

$$\begin{cases} \dfrac{\Delta\sigma}{2} = \dfrac{\Delta\varepsilon}{2E} & \varepsilon < \varepsilon_0 \\ \dfrac{\Delta\sigma}{2} = K'\left(\dfrac{\Delta\varepsilon}{2}\right)^{n'} & \varepsilon \geq \varepsilon_0 \end{cases} \tag{6.3}$$

where ε_0 is the strain at which the end of elastic region ends and initiation of plastic behaviour, $\Delta\sigma$ and $\Delta\varepsilon$ are the total tension to compression stress and strain amplitudes, respectively. Coefficients of the proposed softening equation can be calibrated for incrementally increasing strain controlled cyclic test conducted on HSS and UHSS material (test type e). These parameters are obtained and presented in Figure 6.12. As mentioned earlier, for the remaining incrementally increasing strain controlled cyclic tests (e.g. test

type f) no significant stress reduction was observed. The formulation presented in (6.3) can be applicable for other types of high strength steel materials with cyclic softening behaviour in which the parameters can be calibrated in accordance to the cyclic mechanical properties.
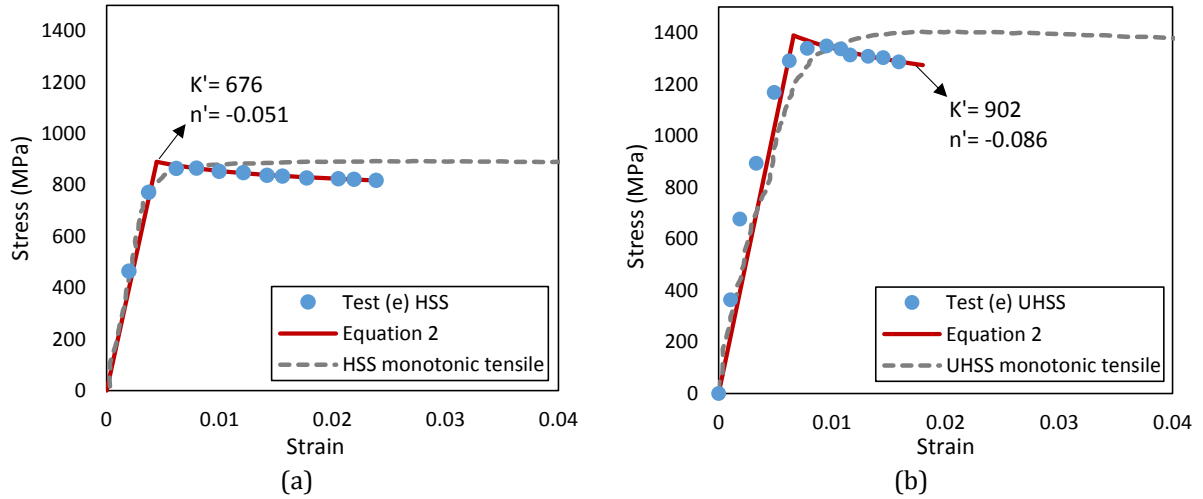
Figure 6.12. Parameters of strain dependent cyclic softening equation (Eq. 6.2) for incremental strain controlled test: (a) HSS, (b) UHSS

6.5.2. Nonlinear combined kinematic/isotropic hardening model for constant amplitude tests

Experimental results obtained in this study can be used to develop a combined isotropic/kinematic model to simulate the low cycle behaviour of HSS and UHSS steel material. These models have previously been proposed for steel materials mostly with strengths up to 700 MPa therefore a preliminary plastic model for 800 and 1200 steel grades under very low cyclically damaged steels is considered in this study. Lemaitre's nonlinear plasticity model [44] is considered here which can be incorporated in plasticity models or commercial modelling software such as ABAQUS [45]. Kinematic hardening data is obtained from the stress and corresponding plastic strain of a single stabilized cycle. Based on results obtained from a stabilised cycle the hardening law for backstress α_k can be formulated as a function of the plastic strain value:

$$\alpha_k = \frac{C_k}{\gamma_k}\left(1 - \exp(-\gamma_k \varepsilon^{pl})\right) + \alpha_1 \exp(-\gamma_k \varepsilon^{pl}) \qquad (6.4)$$

Where C_k and γ_k are the kinematic hardening parameters which can be calibrated from experimental cyclic outputs. To model the isotropic flow, yield surface σ^0 which is a function of equivalent plastic strain ($\bar{\varepsilon}^{pl}$) can be defined either as direct tubular data or as a simple exponential model for which material parameters (Q_∞ and b) can be calibrated from the following equation.

$$\sigma^0 = \sigma|_0 + Q_\infty(1 - \exp(-b\bar{\varepsilon}^{pl})) \qquad (6.5)$$

For the isotropic softening from tabular data, the equivalent stress is defined as a tabular function of the equivalent strain $\bar{\varepsilon}^{pl}$ such that

$$\bar{\varepsilon}_i^{pl} = \frac{1}{2}(4i - 3)\Delta\varepsilon^{pl} \qquad (6.6)$$

The equivalent stress defining the size of yield surface at zero equivalent plastic strain, for the peak tensile stress at ith cycle is obtained form

$$\sigma_i^0 = \sigma_i^t - \alpha_i \qquad (6.7)$$

where here, the backstress is calculated from

$$\alpha_i = (\sigma_i^t + \sigma_i^c)/2 \qquad (6.8)$$

Stresses and corresponding plastic strains are obtained from symmetric strain-controlled cyclic experimental tests. Figure 6.13 illustrates the stress versus plastic strain of high

strength steel material showing how the strength softens after each tension-compression cycle.
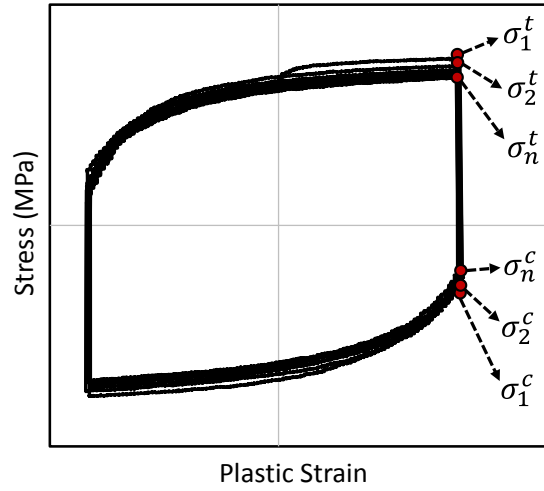
Figure 6.13. Cyclic isotropic softening of HSS and UHSS

Using the obtained cyclic isotropic/kinematic hardening data, a predictive model is developed in ABAQUS and the cyclic behaviour of HSS and UHSS material specimens are verified against experimental curves. In the model, the boundary conditions were applied to realistically model the effect of anti-buckling fixture on the specimen. The verified hysteresis curves are illustrated in Figure 6.14 with special attention given to the cyclic softening. Additionally, in order to incorporate behaviour of HSS and UHSS in similar plasticity models, relevant kinematic hardening parameters (C_k and γ_k) from Equation (6.4) and Isotropic softening parameters (Q_∞ and b) from Equation (6.5) are calibrated against experimental data. The results are presented in Table 6.2. It is worth noting that Q_∞ is a negative value which demonstrates cyclic isotropic softening of HSS and UHSS materials. It is also worth noting that higher absolute value of Q_∞ is an indication of a more significant softening occurring in the material which in this case is UHSS. Furthermore, a step-wise increasing strain test case (test case e) has also been verified using the proposed plastic model which is considered to be a useful pattern for quantifying the deterioration

properties of structures and structural component analysis and modelling under seismic ground motions. The numerical model provides a reasonable prediction of the softening performance of specimen at each cycle in addition to predicting the peak stress prior to the commencement of softening in the 8th cyclic strain amplitude (Figure 6.14(e)).

Table 6.2. Cyclic kinematic hardening and isotropic softening parameters

Specimen	Isotropic Softening		Kinematic Hardening	
	Q_∞	b	C_k	γ_k
HSS-a	-198.1	15.8	24940	117.7
HSS-b	-194.9	13.3	37040	164.6
UHSS-a	-305.7	15	112700	192.1
UHSS-b	-287.5	18.1	167700	286.8
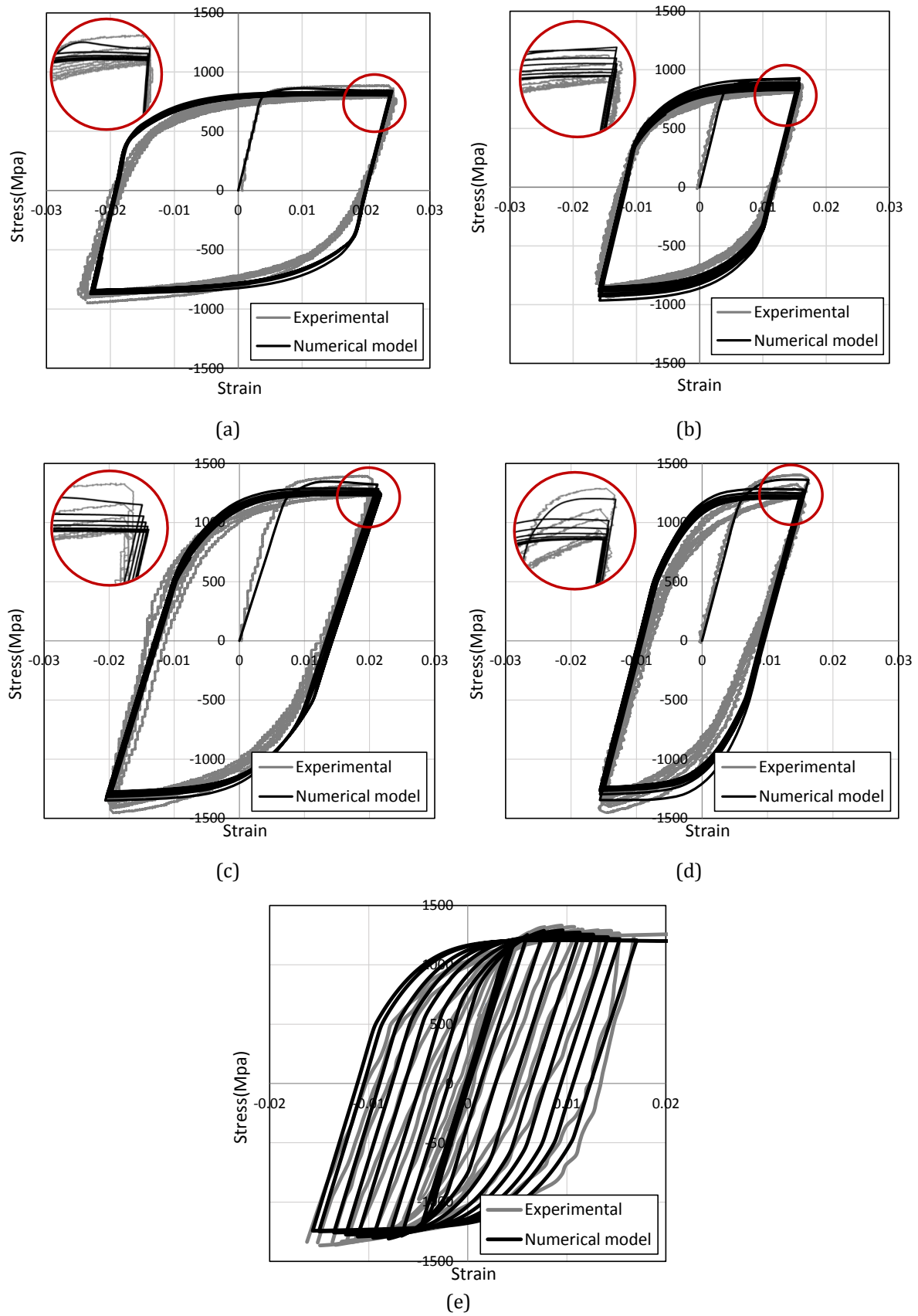
Figure 6.14. Numerical combined hardening model versus experimental results for samples: a) HSS-a, b) HSS-b, c) UHSS-a, d) UHSS-b, e) UHSS-e

6.6.   Conclusions

The concluding remarks are listed below:

- High strength steel (HSS) and ultra-high strength steel (UHSS) materials exhibit cyclic softening with increasing the number of cycles applied. This phenomenon was examined in various cyclic test cases applied on the two above mentioned materials.

- Under cyclic loading with constant amplitude, the overall softening percentage of UHSS was higher than that in HSS which means that this phenomenon is more prominent when material strength increases.

- It was observed that in both HSS and UHSS materials under incremental cyclic loading, having higher number of cycles with less strain increments results in a more obvious strength degradation compared to less number of cycles and higher strain increments.

- In cyclic loading with constant stress amplitude, it was observed that at the end of each cycle, the strain corresponding to stress amplitude experiences a higher increase compared to the previous cycle which depends on the stress controlled cyclic status i.e. values of mean stress and amplitude.

- UHSS material shows a higher energy dissipation value and lower energy dissipation coefficient compared to HSS considering complete load-displacement cycles in a similar test type (case a). Energy dissipation obtained from a stabilized cycle of UHSS (grade 1200) is also compared with that of mild steel (grade 300) with similar cyclic test conditions, showing a 2.5 higher energy dissipation in the UHSS steel material.

- Preserved mechanical properties of very low cyclically strained HSS and UHSS were measured for the aim of assessing the potential structural performance of elements consisting of these steel materials after the event of cyclic damage. As opposed to the reduction in stress, the ultimate strength of UHSS and HSS material corresponds to a higher strain compared to that of virgin material under monotonic tension. Preserved mechanical properties of cyclically damaged HSS and UHSS were also compared to similar results available on Mild steel.

- Examining the fracture surface of HSS and UHSS cyclically strained material showed that HSS fracture is ductile while UHSS material exhibits a mixed fracture mode.

- Using the obtained cyclic isotropic/kinematic hardening data from experiments, a predictive model was developed in ABAQUS and the cyclic behaviour of HSS and UHSS material specimens were verified against experimental curves. Cyclic kinematic hardening and isotropic softening parameters were also calibrated and presented. Proposed numerical model proves to accurately predict the cyclic softening of high strength material under the limited number of constant and incremental strain amplitudes considered in this study. Future steps of this research are developing comprehensive constitutive equations for high strength steel materials to conduct large-scale modelling of sections comprising of these materials under cyclic loads.

6.7. Acknowledgements

6.8.   References

[1] Fukumoto Y. New constructional steels and structural stability. Engineering Structures. 1996;18:786-91.

[2] Ricles JM, Sause R, Green PS. High-strength steel: implications of material and geometric characteristics on inelastic flexural behavior. Engineering Structures. 1998;20:323-35.

[3] Young B. Experimental and numerical investigation of high strength stainless steel structures. Journal of Constructional Steel Research. 2008;64:1225-30.

[4] Pham CH, Hancock GJ. Numerical simulation of high strength cold-formed purlins in combined bending and shear. Journal of Constructional Steel Research. 2010;66:1205-17.

[5] Wang W, Yan S, Liu J. Studies on temperature induced creep in high strength Q460 steel. Materials and Structures. 2016;50:68.

[6] Wang Y-B, Li G-Q, Chen S-W, Sun F-F. Experimental and numerical study on the behavior of axially compressed high strength steel box-columns. Engineering Structures. 2014;58:79-91.

[7] Ban H, Shi G, Shi Y, Bradford MA. Experimental investigation of the overall buckling behaviour of 960 MPa high strength steel columns. Journal of Constructional Steel Research. 2013;88:256-66.

[8] Shi G, Ban H, Bijlaard FSK. Tests and numerical study of ultra-high strength steel columns with end restraints. Journal of Constructional Steel Research. 2012;70:236-47.

[9] Ma J-L, Chan T-M, Young B. Experimental investigation of cold-formed high strength steel tubular beams. Engineering Structures. 2016;126:200-9.

[10] Choi YS, Kim D, Lee SC. Ultimate shear behavior of web panels of HSB800 plate girders. Construction and Building Materials. 2015;101, Part 1:828-37.

[11] Ling TW, Zhao XL, Al-Mahaidi R, Packer JA. Investigation of block shear tear-out failure in gusset-plate welded connections in structural steel hollow sections and very high strength tubes. Engineering Structures. 2007;29:469-82.

[12] Dubina D, Stratan A, Dinu F. Dual high-strength steel eccentrically braced frames with removable links. Earthquake Engineering & Structural Dynamics. 2008;37:1703-20.

[13] Longo A, Montuori R, Nastri E, Piluso V. On the use of HSS in seismic-resistant structures. Journal of Constructional Steel Research. 2014;103:1-12.

[14] Tenchini A, D'Aniello M, Rebelo C, Landolfo R, da Silva LS, Lima L. Seismic performance of dual-steel moment resisting frames. Journal of Constructional Steel Research. 2014;101:437-54.

[15] Tenchini A, D'Aniello M, Rebelo C, Landolfo R, da Silva LS, Lima L. High strength steel in chevron concentrically braced frames designed according to Eurocode 8. Engineering Structures. 2016;124:167-85.

[16] Heidarpour A, Cevro S, Song QY, Zhao XL. Behaviour of stub columns utilising mild-steel plates and VHS tubes under fire. Journal of Constructional Steel Research. 2014;95:220-9.

[17] Javidan F, Heidarpour A, Zhao XL, Minkkinen J. Compressive behavior of innovative hollow long fabricated columns utilizing high strength and ultra-high strength tubes. Tubular Structures - Proceedings of the 15th International Symposium on Tubular Structures, ISTS 20152015. p. 319-25.

[18] Javidan F, Heidarpour A, Zhao XL, Minkkinen J. Application of high strength and ultra-high strength steel tubes in long hybrid compressive members: Experimental and numerical investigation. Thin-Walled Structures. 2016;102:273-85.

[19] Nassirnia M, Heidarpour A, Zhao X-L, Minkkinen J. Innovative hollow columns comprising corrugated plates and ultra high-strength steel tubes. Thin-Walled Structures. 2016;101:14-25.

[20] Farahi M, Heidarpour A, Zhao XL, Al-Mahaidi R. Compressive behaviour of concrete-filled double-skin sections consisting of corrugated plates. Engineering Structures. 2016;111:467-77.

[21] Hosseini S, Heidarpour A, Collins F, Hutchinson CR. Strain ageing effect on the temperature dependent mechanical properties of partially damaged structural mild-steel induced by high strain rate loading. Construction and Building Materials. 2016;123:454-63.

[22] Mirmomeni M, Heidarpour A, Zhao X-L, Hutchinson CR, Packer JA, Wu C. Mechanical properties of partially damaged structural steel induced by high strain rate loading at elevated temperatures – An experimental investigation. International Journal of Impact Engineering. 2015;76:178-88.

[23] Sinaie S, Heidarpour A, Zhao XL. Mechanical properties of cyclically-damaged structural mild steel at elevated temperatures. Construction and Building Materials. 2014;52:465-72.

[24] Sinaie S, Heidarpour A, Zhao XL. Stress-strain-temperature relation for cyclically-damaged structural mild steel. Engineering Structures. 2014;77:84-94.

[25] Chen J, Young B. Design of high strength steel columns at elevated temperatures. Journal of Constructional Steel Research. 2008;64:689-703.

[26] Abedrabbo N, Mayer R, Thompson A, Salisbury C, Worswick M, van Riemsdijk I. Crash response of advanced high-strength steel tubes: Experiment and model. International Journal of Impact Engineering. 2009;36:1044-57.

[27] Sadeghi N, Heidarpour A, Zhao XL, AM R. Numerical investigation of innovative modular beam-to-fabricated column connections under monotonic loading. In: Zingoni A, editor. Insights and Innovations in Structural Engineering, Mechanics and Computations. Cape Town, South Africa: Taylor and Francis Group2016. p. p. 1247–52.

[28] Cai J, He S, Jiang Z, Chen Q, Zuo Z. Experimental investigation on hysteretic behavior of thin-walled circular steel tubes under constant compression and biaxial bending. Materials and Structures. 2016;49:5285-302.

[29] Azhari F, Heidarpour A, Zhao X-L, Hutchinson CR. Effect of creep strain on mechanical behaviour of ultra-high strength (Grade 1200) steel subject to cooling phase of a fire. Construction and Building Materials. 2017;136:18-30.

[30] Shi G, Wang M, Bai Y, Wang F, Shi Y, Wang Y. Experimental and modeling study of high-strength structural steel under cyclic loading. Engineering Structures. 2012;37:1-13.

[31] Iwashita T, Azuma K. Effects of cyclic loading on occurrence of brittle fracture in notched specimens. Tubular Structures - Proceedings of the 15th International Symposium on Tubular Structures, ISTS 20152015. p. 599-604.

[32] Nip KH, Gardner L, Davies CM, Elghazouli AY. Extremely low cycle fatigue tests on structural carbon steel and stainless steel. Journal of Constructional Steel Research. 2010;66:96-110.

[33] Wang YB, Li GQ, Cui W, Chen SW, Sun FF. Experimental investigation and modeling of cyclic behavior of high strength steel. Journal of Constructional Steel Research. 2015;104:37-48.

[34] Silvestre E, Mendiguren J, Galdos L, Sáenz de Argandoña E. Comparison of the hardening behaviour of different steel families: From mild and stainless steel to advanced high strength steels. International Journal of Mechanical Sciences. 2015;101–102:10-20.

[35] Heidarpour A, Tofts NS, Korayem AH, Zhao XL, Hutchinson CR. Mechanical properties of very high strength steel at elevated temperatures. Fire Safety Journal. 2014;64:27-35.

[36] Javidan F, Heidarpour A, Zhao X-L, Hutchinson CR, Minkkinen J. Effect of weld on the mechanical properties of high strength and ultra-high strength steel tubes in fabricated hybrid sections. Engineering Structures. 2016;118:16-27.

[37] E606-04 Standard Practice for Strain-Controlled Fatigue Testing. ASTM International; 2004.

[38] Dusicka P, Itani AM, Buckle IG. Cyclic response of plate steels under large inelastic strains. Journal of Constructional Steel Research. 2007;63:156-64.

[39] Boger RK, Wagoner RH, Barlat F, Lee MG, Chung K. Continuous, large strain, tension/compression testing of sheet material. International Journal of Plasticity. 2005;21:2319-43.

[40] Tanaka E, Murakami S, Ōoka M. Effects of plastic strain amplitudes on non-proportional cyclic plasticity. Acta Mechanica. 1985;57:167-82.

[41] Callister WD. Materials science and engineering : an introduction. New York: Wiley; 2000.

[42] Fallahi H, Nurulakmal MS, Fallahi A, Abdullah J. Modifying the mechanical properties of lead-free solder by adding iron and indium and using a lap joint test. Journal of Materials Science: Materials in Electronics. 2012;23:1739-49.

[43] Ramberg W, Osgood WR, United S, National Advisory Committee for A. Description of stress-strain curves by three parameters. Washington D.C.: National Advisory Committee for Aeronautics; 1943.

[44] Lemaitre J, Chaboche J-L, Germain P, Leckie F, Shrivastava B. Mechanics of solid materials. Cambridge: Cambridge University Press; 1994.

[45] Dassault Systèmes Simulia Corp. P, RI, USA. ABAQUS/CAE 6.14-1. 2014.

Multiaxial seismic performance of high capacity hybrid fabricated beam-columns

Monash University

Declaration for Thesis Chapter 7

Declaration by candidate

In the case of chapter 7 my contribution to the work involved the following:

Nature of contribution	Extent of contribution (%)
Developing ideas, Establishing methodologies, Experimental work, Data analysis, Write-up and revision	70%

The following authors contributed to the work:

Name	Nature of contribution	Extent of contribution (%)
Dr. Amin Heidarpour	Developing ideas, Input into manuscript, Revision, Financial support	15%
Prof. Xiao-Ling Zhao	Revision, Financial support	7%
Prof. Riadh Al-Mahaidi	Financial support through access to Swinburne testing facilities, revision,	8%

The undersigned hereby certify that the above declaration correctly reflects the nature and extent of the student's and co-authors' contributions to this work.

Student signature ████████ Date: 30/01/2017

Main Supervisor's signature ████████ Date: 30/01/2017

7.1. Abstract

High strength and ultra-high strength materials are widely used in industrial applications to improve load-bearing capacity and reduce the overall weight and cost. To take advantage of the benefits of these types of steels in construction, an innovative member consisting of high strength and ultra-high strength steel tubes welded to mild steel plates has recently been developed. Following previous series of investigations under various compression and bending loads, this study aims to evaluate the seismic performance of these hybrid members by conducting various cyclic experiments. Component scale uniaxial and multiaxial cyclic tests were conducted with simultaneous constant or varying axial compression loads using a multi-axial substructure testing facility. The effect of utilising high strength and ultra-high strength steel tubes was investigated in terms of member capacity, strength and stiffness deterioration, deformation and the development of plastic hinges. Failure modes and axial shortening observations are justified considering the effect of loading direction and variation of axial forces. A coupling mechanism of plate and tube elements was observed during the cyclic performance of high strength hybrid members, in which tubes serve as load-bearing components and mild steel plates mostly as lateral ductile elements.

Keywords: Ultra-high strength steel tubes; hybrid fabricated members; unilateral cyclic loading; bilateral cyclic loading; varying axial force

7.2.   Introduction

One of the main benefits of incorporating high strength steel materials apart from the increase in load-bearing capacity is the significant reduction in the overall weight of structure. For structures designed for seismic-prone areas, less overall system mass plays an important role in the reduction of shear force distributed at different levels which is stimulated by utilising high strength materials. In addition to the structural and mechanical advantages, high strength steel components lead to a significant reduction in transportation and construction costs. To improve the performance of high strength structural elements such as ductility, an innovative hybrid section is proposed fabricated from tubes of high grade steel welded to corners of mild steel plates, forming a high performance hollow steel section. The performance of these sections has been comprehensively studied under various loading cases such as monotonic compression and fire [1-5]. Monotonic compression tests conducted on the component scale proposed fabricated steel members showed up to three times increase in strength compared to conventional welded box sections [6] and cold-formed hollow steel sections [7] with equivalent cross-sectional areas and weights. It was found from these studies that the structural plate-tube interaction in these sections results in a reasonable increase in the ductility of structural components compared to what is expected from the high strength steel material alone.

Although the monotonic performance of the proposed fabricated hybrid structural elements under quasi-static loading has been investigated, the seismic behaviour of these elements still remains unknown. The closed hollow geometry of these proposed hybrid sections makes them less vulnerable to lateral torsional instabilities [8] compared to deep steel sections, especially in tall moment-resisting frames subjected to combined axial and cyclic lateral loading [9]. As opposed to the wide range of studies available on the cyclic performance of hollow steel sections [10-12] consisting of mild steel material, limited

research is available on the cyclic performance of high strength steel structural elements, most of which involves steel grades around or below 700. Experimental and numerical investigations were conducted on H-shaped and box sections with steel yield strengths of 460 and 700MPa under cyclic loading [13, 14]. Hollow structural steel sections with a yield strength around 400MPa were considered under cyclic bending to study the influence of geometry on yielding and plastic hinging behaviour [15]. Building frames consisting of column elements with high strength steel material (up to grade 700) were proposed and studied to improve seismic resistance of building frames [16].

To understand the lateral bending and cyclic load-bearing performance of fabricated hybrid sections, basic deformation-controlled unidirectional cyclic tests are performed considering the effect of axial gravity forces. Many experimental and numerical studies on hollow thin-walled steel beam-columns under cyclic bidirectional loading confirm the considerable effect of additional cyclic loading direction on the seismic mechanical performance of steel members, such as strength and ductility [12, 17-20]. In these studies, various bidirectional loading patterns with circular and square load paths were applied along with simultaneous axial loads at a specific ratio of the axial cross-sectional capacity. Furthermore, the vertical component of earthquake leads to varying applied axial loads on column elements degradation [21]. This can be practically modelled by applying varying axial loads proportional to lateral seismic excitation. Considering the strong effect of varying axial forces as lateral amplitudes are applied in one or two directions results in an increase of hysteretic energy dissipation [22]. Previous investigations, mostly on reinforced concrete specimens, have shown that axial load variations as well as bi-lateral displacements have significant effects on capacity degradation and the nonlinear performance of structural elements. These effects include reductions in the amount of lateral drift corresponding to damage initiation and stiffness degradation [21, 23]. Multi-

directional loading has shown to be more sensitive to loading rates than uniaxial loading, which generally depends on several parameters including the applied axial load [24].
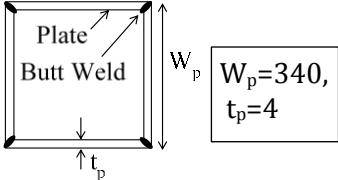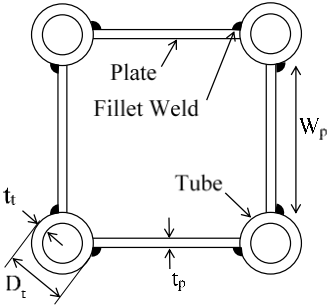
Research on steel sections with yield strength values above 700MPa is very limited, let alone under lateral and axial cyclic loadings. Following the previous series of experimental tests conducted on the proposed fabricated hybrid sections, this paper focuses on the behaviour of these sections under multiaxial cyclic loads. In order to quantify the hysteretic performance of fabricated hybrid sections, uniaxial cyclic tests were conducted under unilateral displacement-controlled conditions with constant axial forces. Furthermore, multiaxial cyclic tests were performed investigating the coupled influence of varying axial forces and bilateral cyclic deformations. Strength and stiffness degradations are compared considering the effect of steel tube material. Plastic hinge development along hybrid members is also studied in the case of unilateral and bilateral reversed amplitudes. Influence of tube material, loading directions and varying compression force on failure modes and axial shortening of sections are also described. Results of the complete set of experimental cyclic tests led to an overview of the seismic performance of thin-walled high strength fabricated hybrid sections and can be incorporated in nonlinear structural models to accurately assess structures consisting of these types of high capacity components from the onset of damage through to collapse. This study has been conducted as part of a group research study on steel and fabricated hybrid elements under extreme loading scenarios [25-32].

7.3. Design of Experiments

7.3.1. Test plan

The hybrid fabricated specimens considered in this paper are square-shaped hollow sections consisting of mild steel plates with circular tubes welded to the corners. The cross section and dimensions of these hollow steel members are shown in the first column of Table 7.1. Tube elements used in the hybrid sections were chosen from three different steel materials, the mechanical properties of which were obtained from standard material testing. Mild steel (MS) tube with yield and ultimate strengths of 305 and 340 MPa, high strength steel (HSS) with yield and ultimate strengths of 770 and 850 MPa and ultra-high strength steel (UHSS) with yield and ultimate strengths of 1250 and 1385 MPa were used. Mild-steel plate elements in all sections were of a similar grade of steel with a yield strength of 265 MPa. Tube specimens were externally welded to the corners of plates using gas tungsten arc welding (GTAW). More information regarding the mechanical properties of steel materials, welding and fabrication procedures can be found in a previous paper [33]. To compare the performance of these fabricated sections with conventional structural sections, a control test was conducted on an equivalent fabricated MS box section with a similar section width and cross-sectional area and therefore similar weight. A monotonic lateral displacement-controlled pushover test was conducted to obtain the lateral backbone curve of this box section for comparison purposes. Table 7.1 summarises a description of the characteristics of each section and each test.

Table 7.1. Description of specimen specifications and testing conditions

Specimen geometry (Dimensions units: mm)	Test label	Material	Nominal Length	Loading conditions	
				Lateral	Axial
$W_p=340$, $t_p=4$	Box-M	Mild steel plate	2m	Lateral Monotonic	Constant
	MS-C-1D	Mild steel plate, Mild steel tube	2m	Unilateral Cyclic	Constant
	HSS-C-1D	Mild steel plate, Mild steel tube	2m	Unilateral Cyclic	Constant
	UHSS-C-1D	Mild steel plate, HSS tube	2m	Unilateral Cyclic	Constant
$D_t=76.1$, $t_t=3.2$, $W_p=210$, $t_p=3$	UHSS-C-2D	Mild steel plate, UHSS tube	2m	Bilateral Cyclic	Varying

The test labels are presented in the second column of Table 7.1. Description of specimen specifications and testing conditions. Except for the fabricated box section, the first term of each test label represents the material of the corner tube used in that section (e.g. MS refers to the section with mild steel tubes). The second term indicates the type of test conducted on the specimen, where M and C stand for monotonic and cyclic, respectively. If there is a third term included in the label, it shows the direction(s) in which lateral cyclic loading is applied. Three types of fabricated steel specimens (MS-C-1D, HSS-C-1D, UHSS-C-1D) were tested under lateral displacement-controlled cyclic loading in one direction. An additional cyclic test was conducted on a specimen consisting of UHSS tubes (UHSS-C-2D), where lateral displacement was applied cyclically in two directions and the axial load varied as a

function of lateral displacement. Displacement-controlled amplitudes were applied based on the testing protocol proposed in FEMA461 [34]. The smallest targeted deformation was chosen such that the predicted lowest damage state would occur after at least six cycles. The amplitude of each step (a_{i+1}) was increased as a function of the previous step's amplitude (a_i) and each cyclic amplitude was repeated twice during testing such that

$$a_{i+1} = 1.4a_i \qquad\qquad (7.1)$$

All lateral cyclic displacements were continued until the physical limits of testing machine were reached and major damage to specimens occurred. These displacements in all test cases satisfied the minimum total number of cycles (20 cycles) and the recommended magnitude of targeted maximum deformation amplitude (storey drift: 0.03) recommended by FEMA461 . The applied displacement rate was kept within the quasi-static range, with a gradual increase after each set of cycles to avoid excessive test duration. All unilateral and bilateral cyclic tests followed a similar displacement history in the lateral X direction, while in the latter test type, displacement in Y direction was half that in the perpendicular path. The applied axial force on each test specimen in MS-C-1D, HSS-C-1D, UHSS-C-1D tests was 25% of the axial capacity of member. In the multiaxial cyclic test (UHSS-C-2D), axial force reached its minimum magnitude when the positive X direction amplitude was applied and reached its maximum magnitude when the negative X direction amplitude was applied. At zero X direction displacement, specimen was subjected to the mean axial force value, i.e. 25% of the compressive strength of member, in Z direction. Illustrations of displacement histories are presented in Figure 7.1.
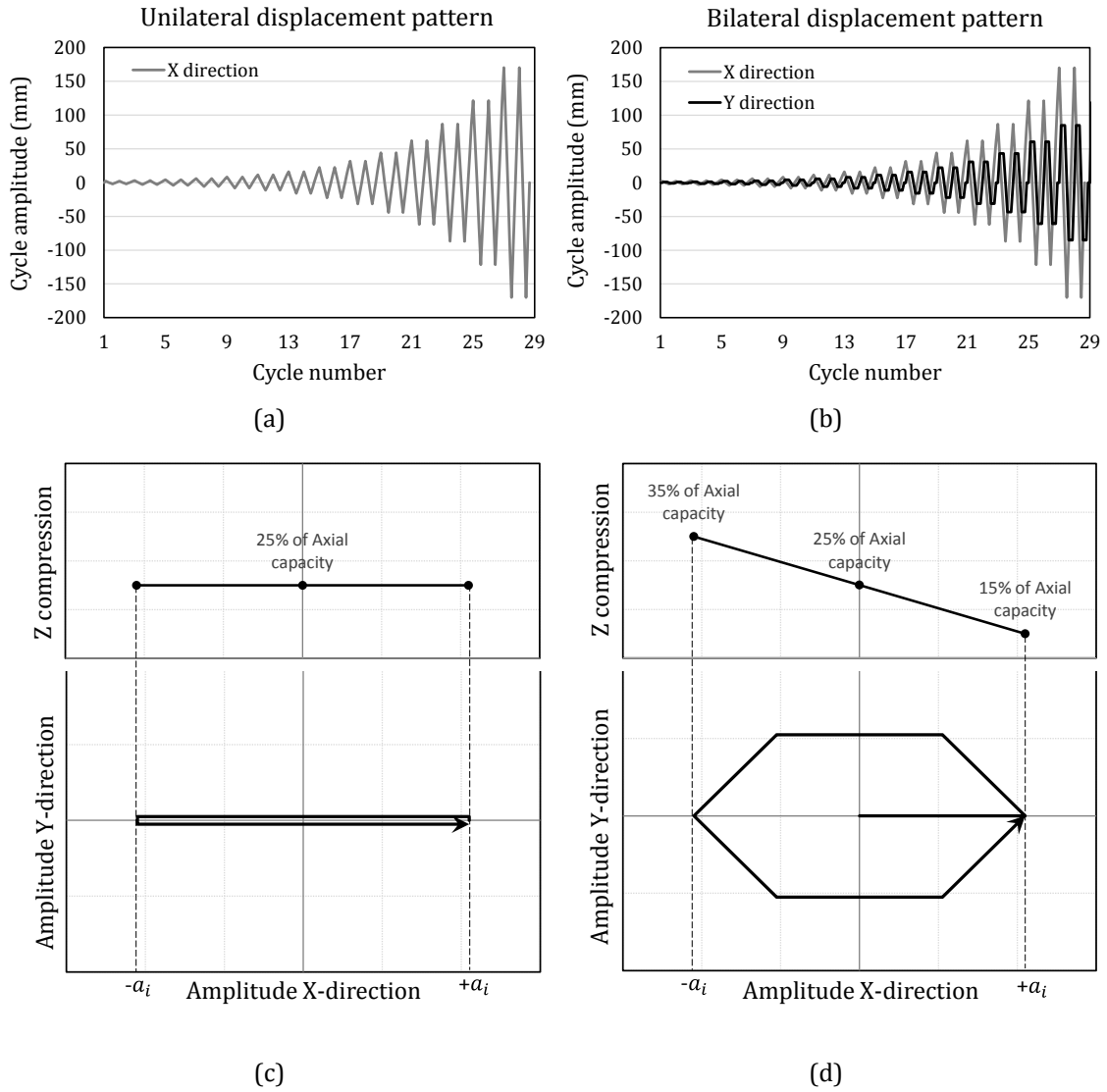
Figure 7.1. Deformation-controlled loading history: (a) Unilateral test displacement pattern, (b) Bilateral test displacement pattern, (c) Axial force variation in unilateral test for each cycle, (d) Axial force variation in bilateral test for each cycle.

7.3.2. Testing equipment

Displacement-controlled cyclic tests were performed using the Multi-Axis Substructure Testing (MAST) system [35] which can accommodate the loading capacity and stroke requirements of the intended test plan shown in Figure 7.2. Using the servo-hydraulic control system of MAST, rotation degrees of freedom at both ends were controlled and kept zero throughout all tests and end force and moment reactions were measured and recorded.

To ensure adequate clamp conditions at both ends, the outer specimen perimeters were welded to anchor plates and triangular stiffeners were also used on four sides. In order to meet the testing machine's dimension requirements, two concrete pedestals were used at the top and bottom ends of test specimens, connecting the top end of column to the MAST crosshead and the bottom end of column to the strong floor. For ease of member instalment in each test, the end anchor plates were bolted to the concrete base plates connecting the specimen to concrete pedestals and the MAST system. To ensure that no rotation or slip has occurred in the setup during each test, linear variable differential transformers (LVDTs) were set at contact locations to measure and control relative displacements. These controls include relative horizontal displacement measurements for the occurrence of any slip between concrete and crosshead and vertical displacement measurements for any uplifting of anchor plate on the baseplate. Figure 7.3(a) shows various parts of the experimental test setup. It is worth noting that the effective length of the column is obtained from the net span of member, excluding stiffener dimensions at both ends.
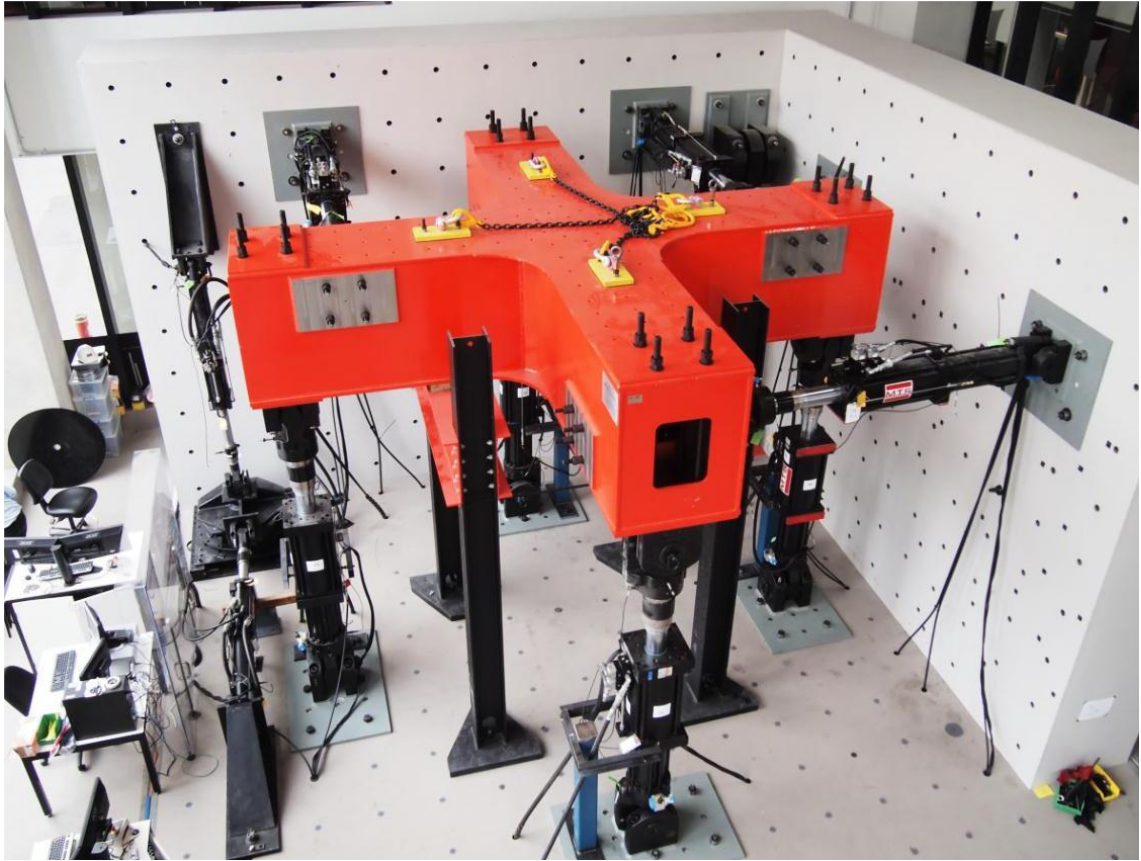
Figure 7.2. Multi-Axis Substructure Testing (MAST) system [35]

7.3.3. Data acquisition

The main force and displacement measurements of all cyclic tests reported in this paper were obtained from the MAST system actuators. The acquisition setting of MAST was arranged such that the system motions were controlled and calculated for a coordinate at the centre of column's top surface (see Figure 7.3(a)). Apart from the data readings directly obtained from the MAST system, additional displacement and strain measurements were also performed. Strain gauges were attached to specific points at the bottom end of specimen. For displacement and curvature measurements, string pots were attached at three points along the height of each member on one side for unilateral tests and on two sides for the bilateral test. In addition to the above mentioned devices, a three-dimensional digital image correlation system [36] was utilised for non-contact deformation

measurements of two perpendicular faces of the bottom half of each specimen. The initial general displacement matrix was transformed to obtain deformations at local column coordinates. Figure 7.3(b) shows an example of digital image correlation surface measurement with initial (α, β, γ) and transformed (α', β', γ') coordinate systems. In addition to displacements, strain values were derived from measured displacements at any given 2-D plane. Depending on the column surface from which strain data were intended to be obtained, the deformation matrix was transformed such that the considered surface ended up parallel to the strain plane. Due to the geometry of members considered in this study, for each side of the column, the derived strain system is applicable to the entire plate surface parallel to the strain plane, in addition to a sufficiently small area of the front of each tube which can be approximated to a planar surface parallel to the strain plane (Figure 7.3(b)). For accurate strain calculations on the curved area, the density of speckled surface should be sufficiently small in order to reduce plane approximation errors. After coordinate transformations, the data extracted from image correlation system were checked against string pots measurements, and the results showed a satisfactory correlation. An example of the lateral displacement measurement of a point on one of the tested specimens compared to the digital image correlation outputs is shown in Figure 7.3 (c).
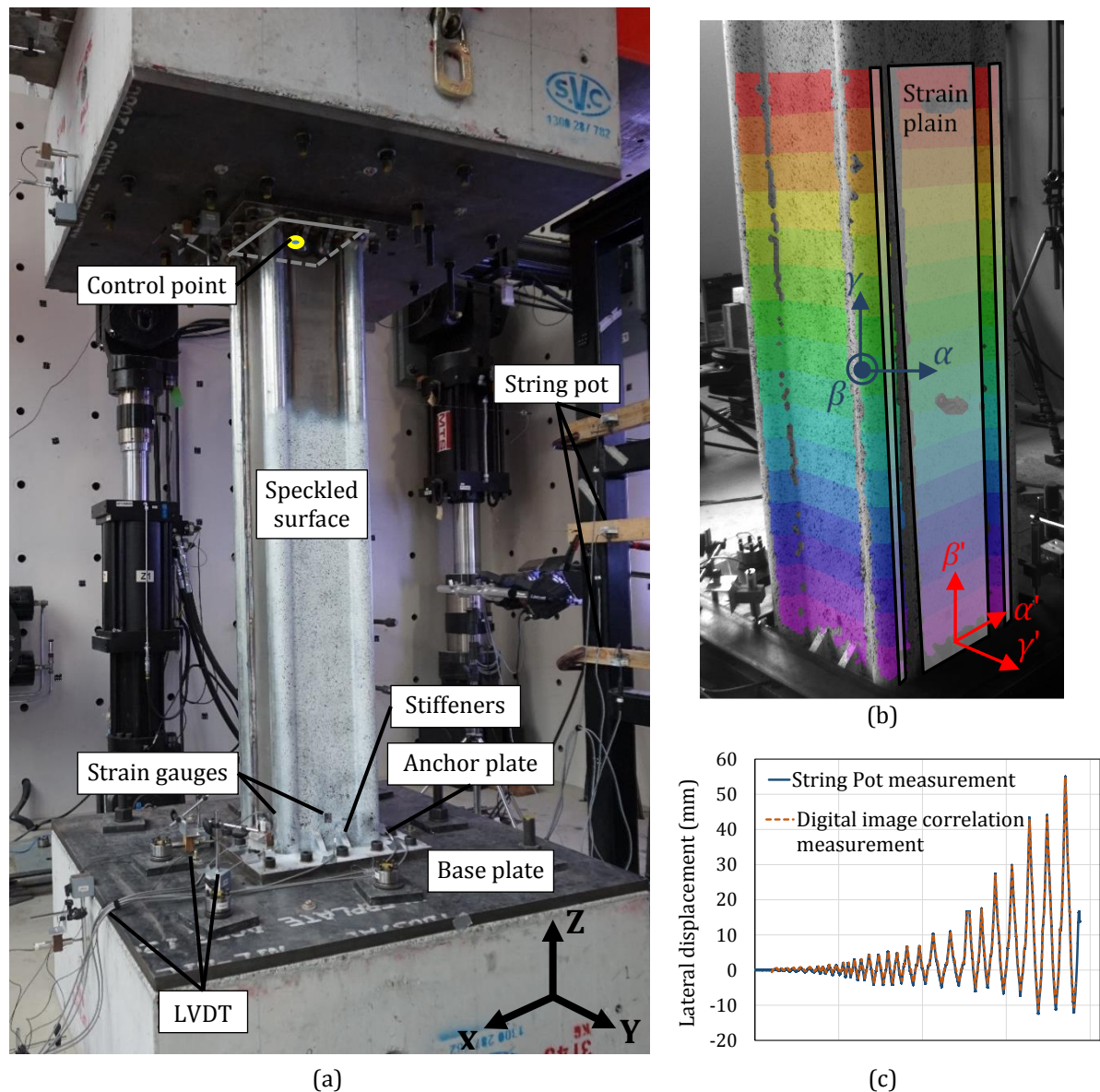
Figure 7.3 (a): Multiaxial cyclic experimental set-up and global loading coordinates; (b) Digital image correlation system together with local displacement and strain coordinates; (c) Digital image correlation measurement versus string pot reading for an example point

7.4.   Unilateral Experimental Results

Hysteresis curves for MS-C-1D, HSS-C-1D and UHSS-C-1D specimens tested under unilateral cyclic loading along with the backbone curve of the lateral pushover test conducted on equivalent fabricated box section are shown in Figure 7.4. As mentioned above, each

specimen was subjected to an axial force equal to 25% of the member's compressive strength. The magnitude of the axial force applied on each specimen is compared in Table 7.2. By increasing the strength of tubes in fabricated sections, the overall strength and proportionally the applied axial force are increased [5]. This increase is three times greater in UHSS-C-1D specimen compared to the MS-C-1D specimen. The lateral strength cap increases with the rise in tube material strength and reaches its maximum in UHSS-C-1D. Compared to the backbone curve of the equivalent box, lateral strength and ductility improve as a result of the section geometry and the material of tube elements. Although the ductility of HSS and UHSS tube materials is individually lower than that of MS, the section geometry results in the interaction of plate and tube elements, which improves the overall ductility and lateral deformation capacity of sections by around 1.5 times. A slight pinching mechanism is observed in the lateral load-displacement curves of all three specimens initiating at displacement ratios higher than the cap strength. This phenomenon is due to the local buckling which occurs in MS plates under compression stresses generated by the applied lateral shear forces. Hysteresis properties obtained from unilateral tests show that the incorporation of HS and UHSS tubes enhances the lateral strength cap, while the sections with stronger tube elements undergo a higher gravity load proportional to their axial capacity. However, the increase in lateral load-bearing capacity and the rise in tube strength properties do not show a linear relationship in the tested specimens. This nonlinearity is understood to be due to the relation between the strength and geometry of plate and tube elements. According to the observed deformations of tested specimens, plate elements fail under shear buckling due to compression stresses generated from the applied lateral load. This means that in hybrid fabricated sections with high strength steel tubes tested here failure is governed by the plate behaviour compared to the effect of tube material, which mostly governs the axial compression performance. Consequently, the design of tube and plate materials and geometries in the proposed hybrid fabricated sections should be done

such that an optimum coupled performance of both components is achieved, in accordance with the combined compressive and lateral load-bearing demands of the beam-column.

(a)

(b)

(c)
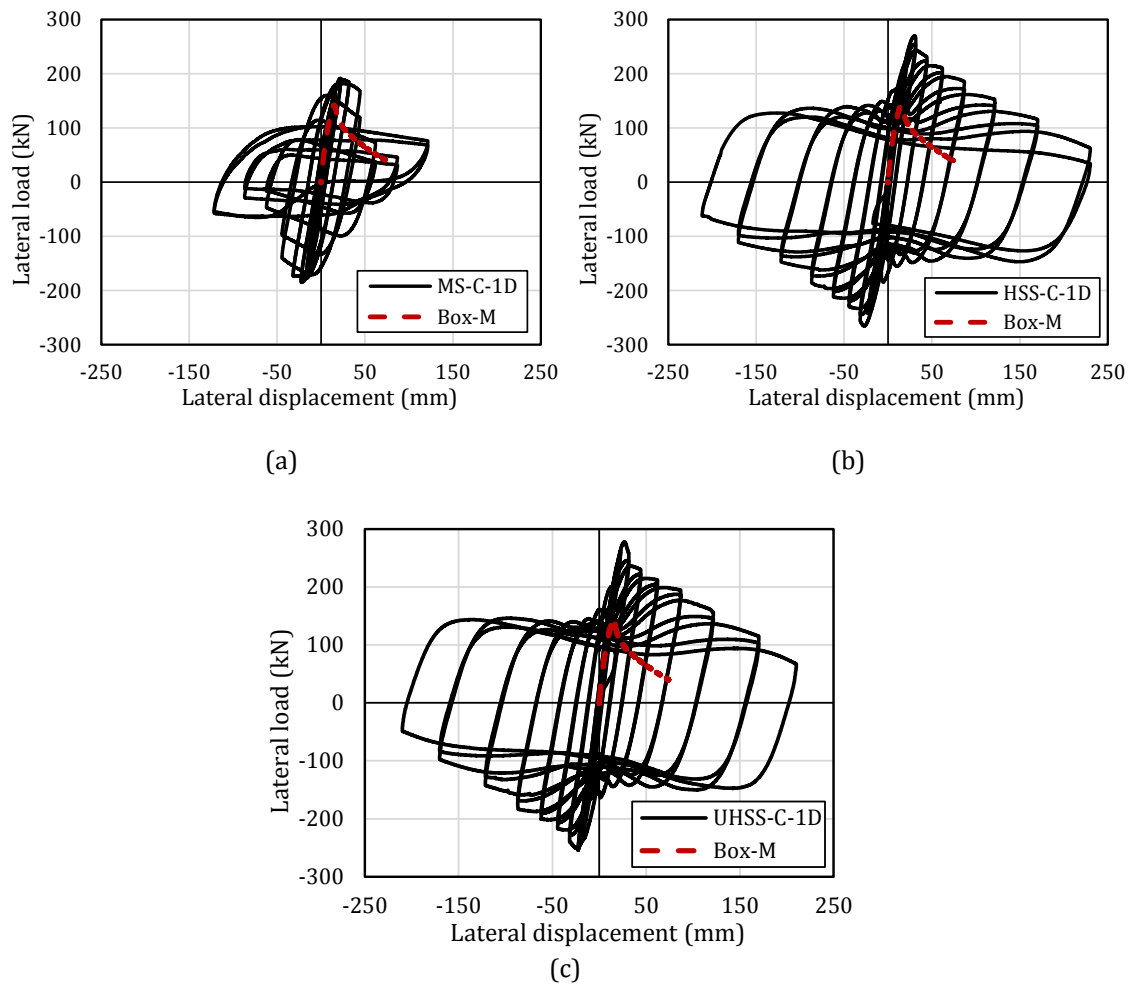
Figure 7.4. Unilateral hysteresis curves (a) MS-C-1D; (b) HSS-C-1D and (c) UHSS-C-1D.

Table 7.2. Main hysteresis properties of unilateral cyclic tests

	Box-M	MS-C-1D	HSS-C-1D	UHSS-C-1D
Axial compression capacity (kN)	660	1411	2836	4126
Applied axial force (kN)	165	353	709	1031
Lateral strength cap F_c (kN)	142	191	270	278

7.4.1.   Strength and stiffness degradation

Application of cyclic displacement amplitudes on fabricated sections results in both stiffness and strength degradation after a certain number of cycles. Normalised strength reductions of three specimens were compared in two positive and negative loading directions, and the results are presented in Figure 7.5(a). The lateral strength of each individual member is normalised relative to the hysteresis strength cap of that member presented in Table 7.2. Strength reduction was first observed after the 16th cycle in MS (corresponding to around 1.2% drift) and after the 18th cycle for HSS and UHSS sections (corresponding to around 1.6% and 1.5% drifts, respectively). From this observation it is clear that increasing the tube strength can postpone the displacement corresponding to strength degradation in the system. Post peak strength reduction is similar in both HSS and UHSS specimens; however, a significantly sharper strength reduction is observed in MS member compared to the other two members. For instance, at a specific drift of 3.3%, the lateral strength of column consisting of MS tubes is less than half of the full capacity, whereas for the two high strength sections around 80% of full lateral strength is preserved. A slight difference can be observed in the strength reduction of negative and positive directions, which is understood to be due to the very small asymmetry present in the fabricated section. However, since the specimen undergoes lateral displacements in the positive direction of any given cycle, stresses are generated in the material, which explains the slight reduction observed in the negative direction of the similar amplitude.

Lateral stiffness also deteriorates as the number of cycles applied on the hybrid specimens increases. The trend of normalised deterioration is shown in Figure 7.5(b). Stiffness values for each specimen are normalised to the initial stiffness of UHSS specimen. Since the stiffness of each cycle amplitude repeat is almost similar, the second repetition of each amplitude is presented. From the measurements it is evident that initial stiffness reduces with the decrease in tube strength, which is due to the higher lateral capacity of UHSS

member compared to HSS and that compared to MS member. All member types show quite

a similar stiffness degradation rate as cyclic loading progresses.

(a)

(b)
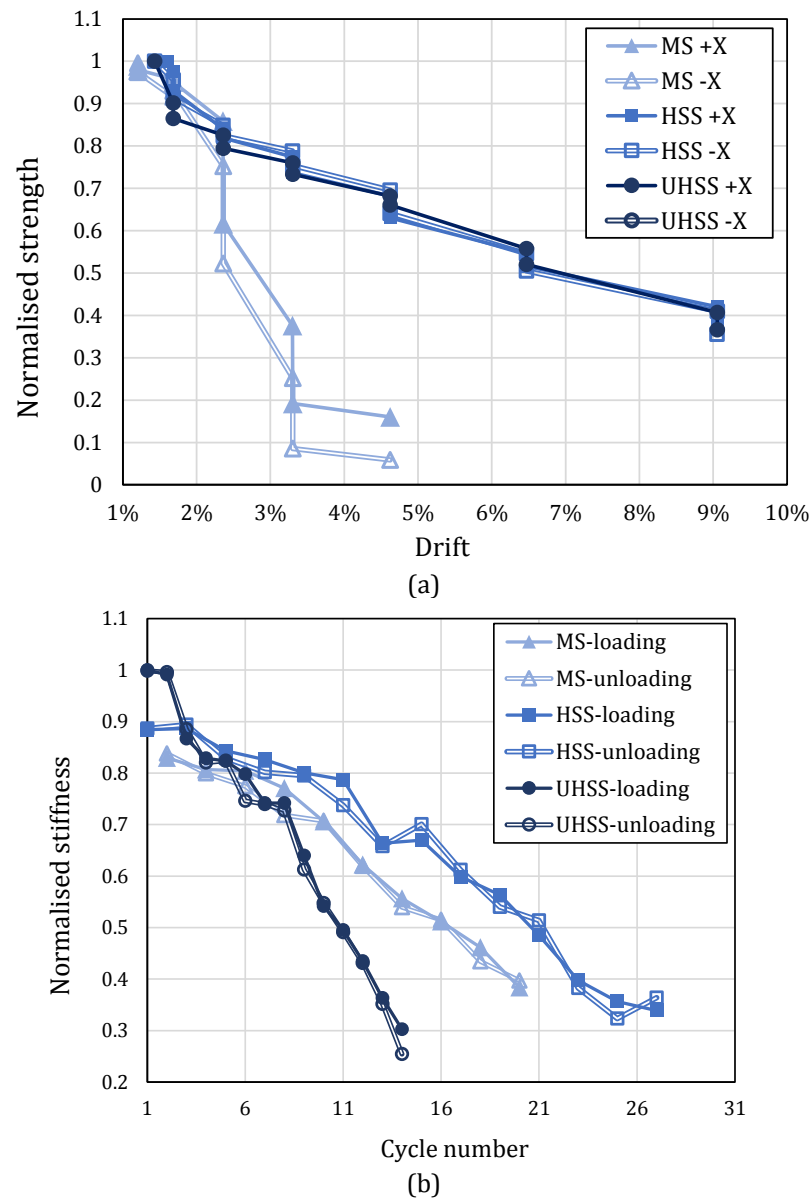
Figure 7.5(a) Strength deterioration and (b) Stiffness deterioration in MS-C-1D, HSS-C-1D and UHSS-C-1D specimens

7.4.2. Deformations and plastic hinge formation

A major effect of the tube material on the behaviour of fabricated sections is in the plastic

deformations along each member which contribute to different failure mechanisms. Using

digital image correlation, comprehensive records of displacement and strain measurements were obtained for two perpendicular surfaces in the bottom half of the tested members. Based on displacement measurements, strain values were obtained at a number of consecutive points in the longitudinal direction on the centreline of plates and tubes at the surface perpendicular to the unilateral amplitude direction. These longitudinal strains are presented in Figure 7.6 for plate centrelines and in Figure 7.7 for tubes centrelines of MS-C-1D, HSS-C-1D and UHSS-C-1D specimens. It is worth noting that the vertical axis represents the initial longitudinal location of each point and does not include any changes in coordinates of these points. Strain measurements are plotted for 5 points throughout the loading procedure, which sufficiently represent the general progress of cyclic test until failure. These measurement intervals are from the end of second repeat of cycles with drift percentages of 0.1%, 0.4%, 1.7%, 4.6% and 9%. For MS-C-1D specimen, the ultimate applied drift was 6.5% due to reaching axial displacement limits being reached. Therefore, the graphs are plotted up to this drift percentage. With the aim of interpreting the magnitude of strain at different stages, values of yield and/or ultimate strain in each graph are also potted with dashed lines. The maximum value of longitudinal strain in MS-C-1D reaches a significantly higher value compared to that of the two other sections where the peak strain hardly reaches 2%. The excessive strain values generated in the plates incorporated in MS-C-1D are due to the different failure mechanism and extreme axial shortening occurred in this member compared to other specimens, which is understood to be a result of the distinct material properties of MS tube. Longitudinal strains at the end points of member are predicted to have reached peak values close to the ultimate strain of material (23%), some of which have failed to be precisely captured due to extensive rates of displacement.
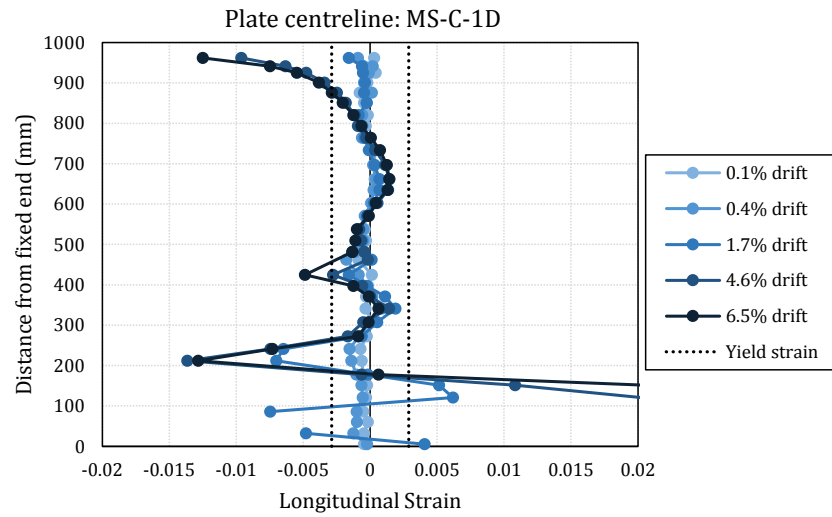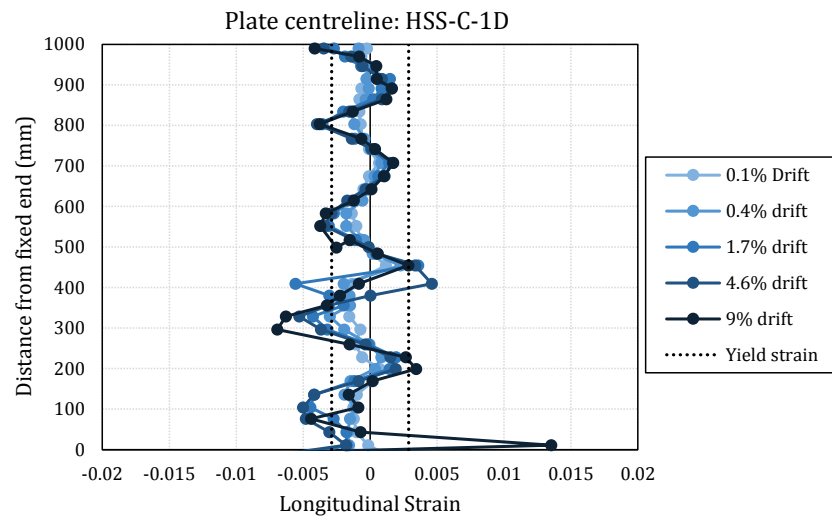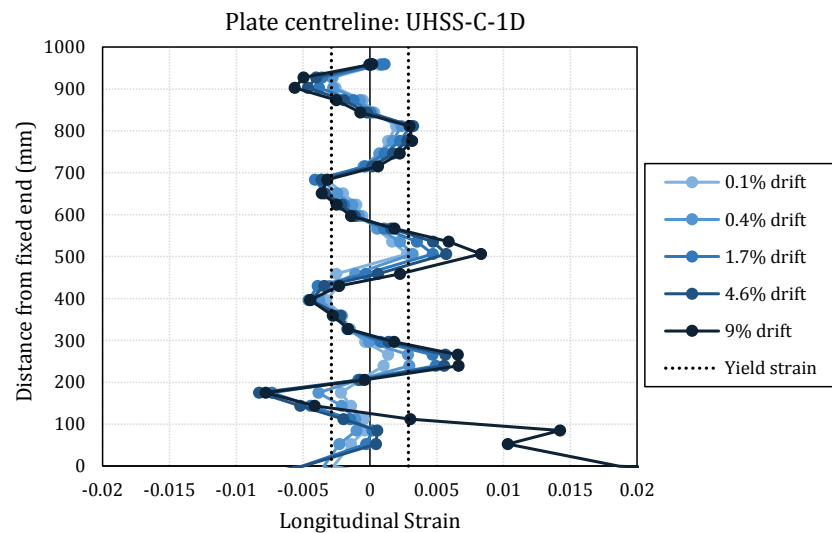
Figure 7.6. Longitudinal strain distribution along plate centreline: (a) MS-C-1D; (b) HSS-C-1D; (c) UHSS-C-1D

The distinct behaviour of MS-C-1D member is also noticeable from the strain measurements of tube centrelines (Figure 7.7). MS tube reaches strain values up to 12% (i.e. higher than the strain corresponding to ultimate strength of MS tube material) when the column is subjected to a final drift of 6.5%, while the ultimate strain values achieved by the other two specimens remain less than the ultimate strain of HSS and UHSS tube materials. The strain values exceeding ultimate strain may explain the higher rate of degradation in MS-C-1D specimen compared to other high strength sections. This indicates that high grades of steel material in the members postpones material failure along beam-column elements preventing high rates of strength degradation and delaying overall failure. The distribution of plastic strain along the column is also worth comparison. In all tested specimens the strain distribution is distributed along the entire length of the plate elements which is different from the behaviour observed in tube elements. In tube elements, plastic deformation is localised at the lower end of MS-C-1D plus a small part of the mid-length. In the tube elements of HSS-C-1D and UHSS-C-1D, plastic deformation is less localised in tubes at the bottom end of member compared to MS-C-1D and is distributed more towards the mid-length.
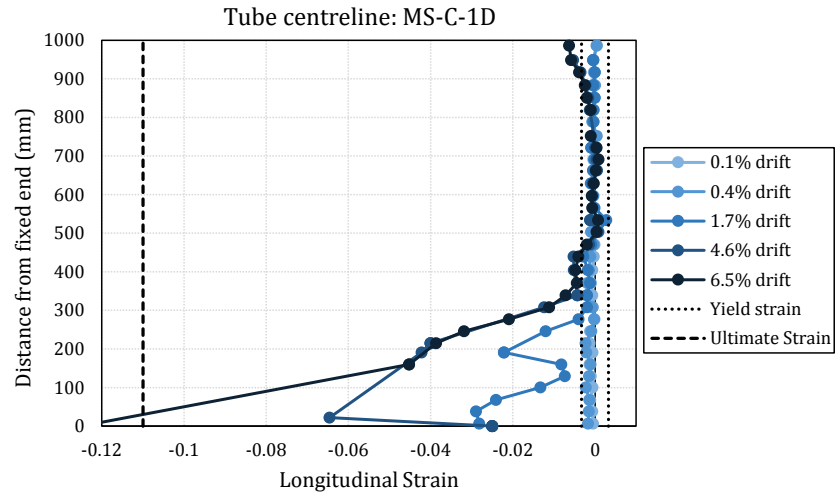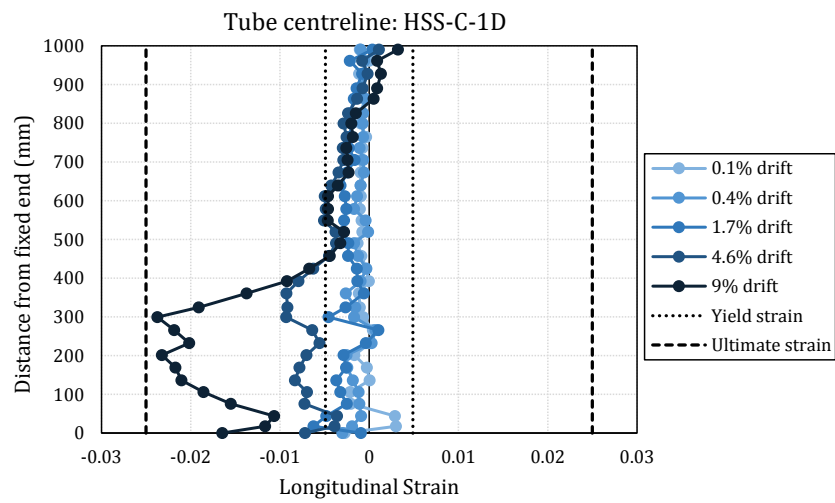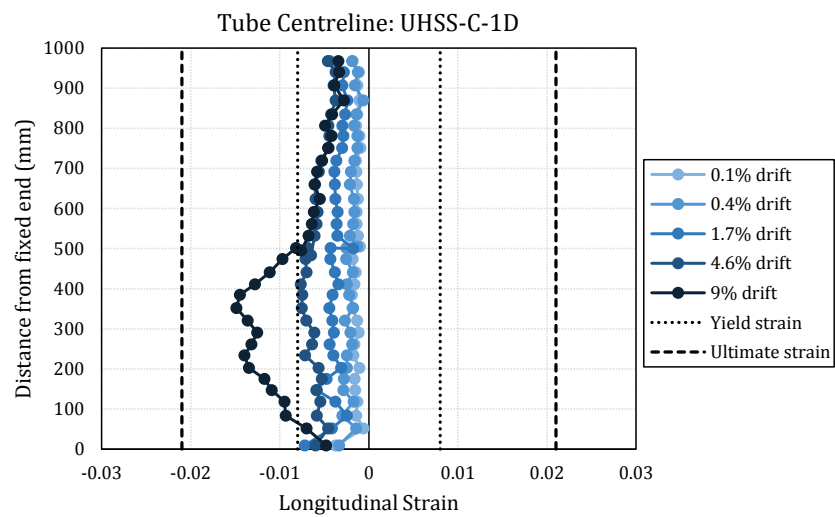
Figure 7.7. Longitudinal strain distribution along a tube centreline: (a) MS-C-1D; (b) HSS-C-1D; (c) UHSS-C-1D

The width of the region on tube centreline with strain values higher than yield strain can be considered as the plastic hinge length. This length varies for different drift levels, depending on the value of cyclic amplitude and the steel tube material. The *plastic hinge ratio* is proposed for evaluating the plastic behaviour and is defined as the ratio of the overall length of beam-column where strain values exceed the material's yield strain to the total effective length of the element. In this study, since the plastic hinge length is measured at the bottom half of specimens, the plastic lengths are divided by 940mm, which is half of the effective length of each member. Plastic hinge ratios of tubes presented in Figure 7.8 for three fabricated specimens are obtained for four different drift levels, starting from the drift corresponding to strength cap up until ultimate failure. The plastic hinge length of UHSS-C-1D is equal to zero at the drift corresponding to strength cap meaning that the tube behaviour is elastic. Plastic hinge ratio of HSS-C-1D is only approximately equal to 10% in strength cap values. By progressing the applied lateral displacement to 4.5% drift, the hinge length tends to increase in all members. At a drift level of 6.5%, which is the final loading stage applied to MS-C-1D, the plastic hinge length slightly reduces meaning that failure is localised at the lower end of the column where excessive plastic axial deformations take place. For HSS-C-1D tube plastic hinge length stabilises with increasing cycle number, whereas that of UHSS-C-1D continues to increase up to the final cycle. The localisation of longitudinal strain distribution of MS-C-1D at the lower end of the specimen can be seen in Figure 7.9(a) extracted from the digital image correlation system at the final stage of testing. In this figure, the obvious difference in axial deformation and plastic hinge length of three fabricated members at the final loading stage can be compared. Figure 7.9 also shows that the plastic hinge region of HSS-C-1D and UHSS-C-1D is more distributed towards the top of the specimen than that of MS-C-1D.
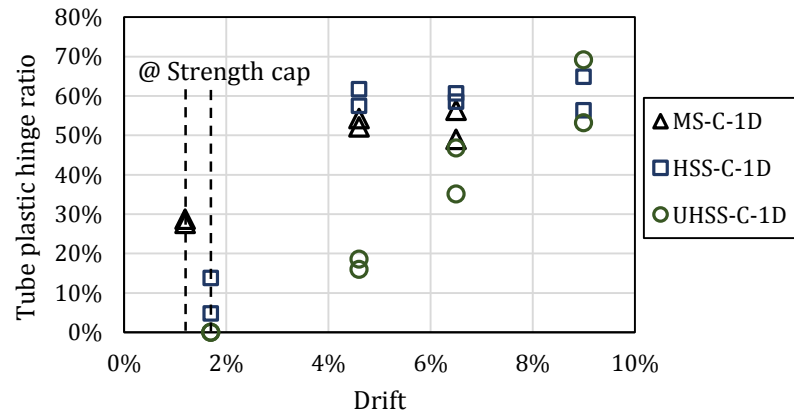
Figure 7.8. Plastic hinge ratio of tube centrelines in unilateral cyclic tests

(a)   (b)   (c)
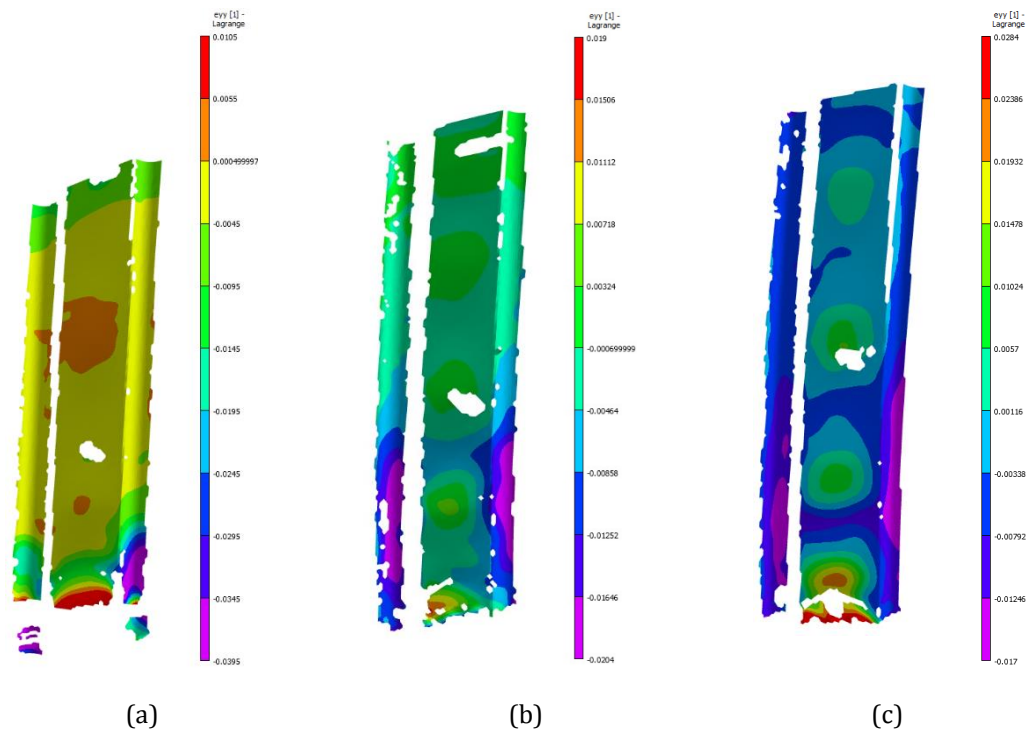
Figure 7.9. Comparison of longitudinal total strain (eyy) distribution along bottom half of:
(a) MS-C-1D, (b) HSS-C-1D, (c) UHSS-C-1D specimens.

7.5. Bilateral Experimental Results

Multiaxial cyclic tests were conducted to account for the effect of the vertical component of earthquake forces and the overturning effects that are generated in external columns of structures subjected to earthquake. In order to understand the effect of cyclic axial and lateral loading on the mechanical performance and failure of high strength fabricated steel beam-columns, comparisons are drawn among experimental results of uniaxial and multiaxial tests (i.e. UHSS-C-1D and UHSS-C-2D). The multiaxial cyclic pattern of applied displacement and load amplitudes are shown in Figure 7.1. The strength in +X direction which undergoes less axial loading reaches higher values of lateral strength force compared to that of the –X direction and the strength degradation initiates at higher lateral displacement amplitudes compared to that in –X direction (see Table 7.3).

Table 7.3. Main hysteresis properties of uniaxial and multiaxial cyclic tests

	UHSS-C-2D (+X)	UHSS-C-2D (-X)	UHSS-C-1D
Axial compression capacity (kN)	4126	4126	4126
Axial force (kN)	618	1444	1031
Lateral strength cap F_c (kN)	277	255	278

7.5.1. Strength and stiffness degradation

In this section, the results of multiaxial cyclic loading on UHSS-C-2D specimen are discussed and compared to those of UHSS-C-1D. Figure 7.10(a) shows the strength degradation trend of the four lateral displacement directions (+X, -X, +Y and –Y) of the UHSS specimen against that of similar member under unilateral cyclic loading versus the drift values of each direction. In the Y direction, displacement amplitudes at each cycle are half of those applied

in the X direction and the strength reduction in Y direction initiates at a greater number of cycles.

(a)

(b)
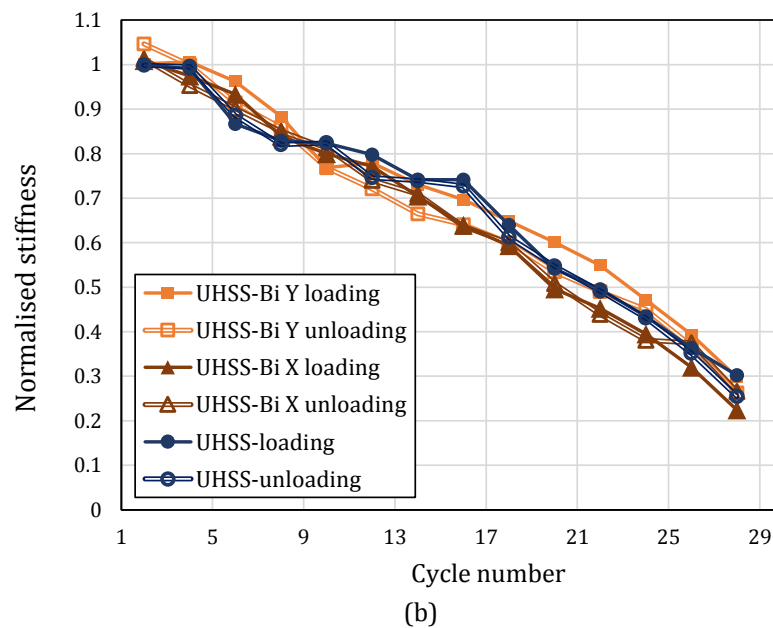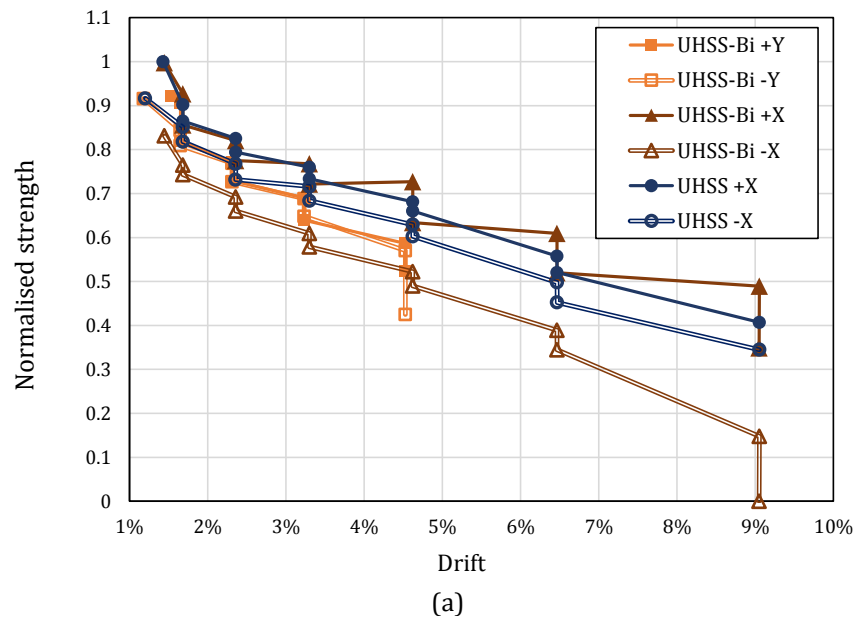
Figure 7.10(a) Strength degradation; (b) stiffness degradation of multiaxial cyclic tests compared to uniaxial cyclic tests.

When the column is laterally moved in +Y and –Y directions it undergoes similar axial loads which show a similar strength degradation trend. The column cyclically loaded in the +X direction is subjected to 618kN axial load which is 20% less than that of the -X direction,

and this difference is evident in the normalised strength degradation curves that showing the lowest lateral strength. At the end of cycle number 28 with the equivalent drift of 9% in –X direction, the member fails to withstand the combination of applied lateral and axial loads. Stiffness degradation follows quite a similar trend despite the differences in axial load and amplitude.

7.5.2. Deformations and plastic hinge formation

Similar to the investigations reported in Section 7.4.2, variations in longitudinal strain values were captured at various stages of cyclic loading and the plastic deformations were analysed. The longitudinal plastic strain along the beam-column under multiaxial cyclic loading in both -X and -Y directions are illustrated in comparison with steel material yield and ultimate strains (Figure 7.11). Note that in the -X direction 35% of axial compressive force is applied on the column while in the –Y direction 25% is applied. In the cycle with 1.7% drift, UHSS tube exceeds yield strain level in the X direction and from that point onward strain levels increase with the increasing number of cycles applied. By the end of the final cycle (9% drift) some parts of the UHSS tube exceed the material ultimate strain, which is the point of complete failure of the column. During each bilateral cycle applied on the column the Y direction amplitude is half that of X direction which results in lower strain values being observed. The material's yield strain level are exceeded after applying drift levels of 0.8% in Y direction and remain below ultimate strain by the end of cyclic testing (28th cycle).
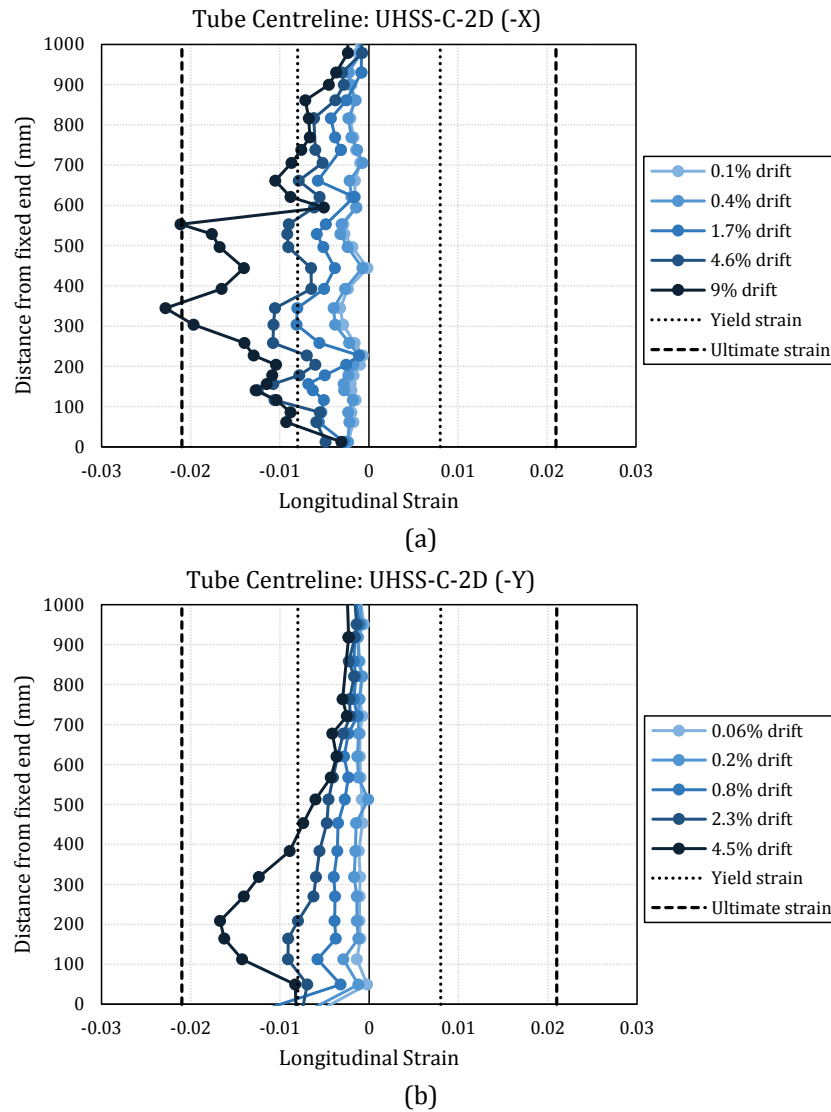
Figure 7.11. Longitudinal strain distribution along tube UHSS-C-2D centreline: (a) X direction, (b) Y direction.

The plastic hinge ratio was also obtained for both X and Y directions in the bilateral tests and compared with those for the unilateral UHSS-C-1D test (Figure 7.12). In both test cases, all tube elements remain elastic until the strength cap. In the –X direction with higher axial loads applied, the length of the plastic hinge ratio is higher than that in the unilateral test. The plastic hinge ratios of the two tube elements differ, due to the asymmetric application of axial forces in different directions. The specimen in –Y direction undergoes less drift compared to the –X direction, however, as a consequence of the replicated displacement cyclic history applied to the specimen, plastic hinge ratio increases with a higher slope and

reaches amounts more than two times that in the unilateral specimen when subjected to similar drift values.
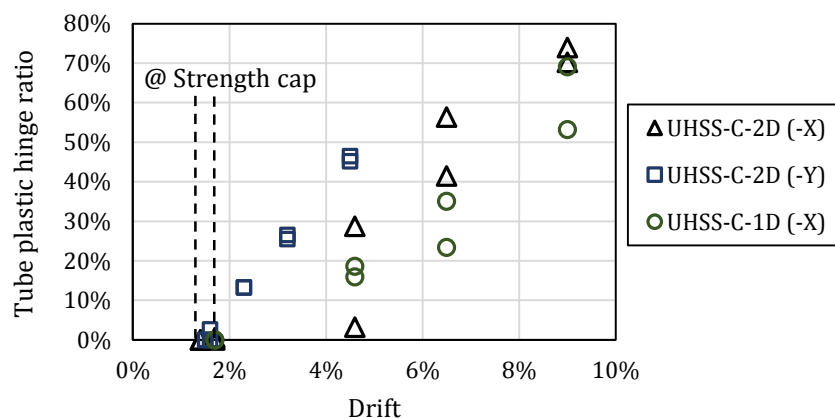
Figure 7.12. Plastic hinge ratio of tube centrelines in bilateral test

7.6.   Effect of Axial Force on Lateral Performance of Hybrid Members

The variety of axial forces applied on hybrid high capacity members throughout the multiaxial cyclic protocols affect trend of strength deteriorations. The results of experimental tests showed a direct effect of axial load magnitude on the performance of hybrid fabricated beam-columns under unilateral and bilateral cyclic loading. To quantify these effects, strength deterioration was measured from the value of the slope of the normalised strength versus drift curve for each specimen and the results are presented in Figure 7.5(a) and Figure 7.10(a). The *strength deterioration slope* is defined as the slope of absolute or normalised strength deterioration versus applied lateral drift at the peak amplitude in that direction. These negative slope values are extracted from both bilateral and unilateral tests conducted on specimens consisting of UHSS tubes which were subjected to a variety of axial load ratios in different directions. Strength deterioration slopes plotted

as a function of the axial compression load ratio are illustrated in Figure 7.13. The horizontal axis represents the ratio of axial force to the axial capacity of the member. The strength deterioration slope is shown to follow a linear decreasing trend for lateral X direction subjected to similar drift magnitudes. The strength deterioration slope in Y direction is more significant than that in the X direction, although the applied displacement amplitudes are half those in the X direction. At strength deterioration initiation in Y direction, the number of cycles undergone by the specimen is 22 compared to 18 cycles experienced with strength deterioration initiation in X direction. The greater number of cycles in addition to the effect of cycle damage from the X direction displacement history, results in a more significant strength deterioration slope in this direction. Due to the fact that only one direction of lateral cyclic load was applied to UHSS-C-1D specimen, the strength deterioration slope for this specimen is slightly less than that of the multiaxial test. It can be concluded that in a situation with similar number of cycles applied, axial force is the factor which has a more significant effect on the strength deterioration slope compared to the effect of a second direction cyclic deformation with displacement amplitudes half those of the main cyclic direction.
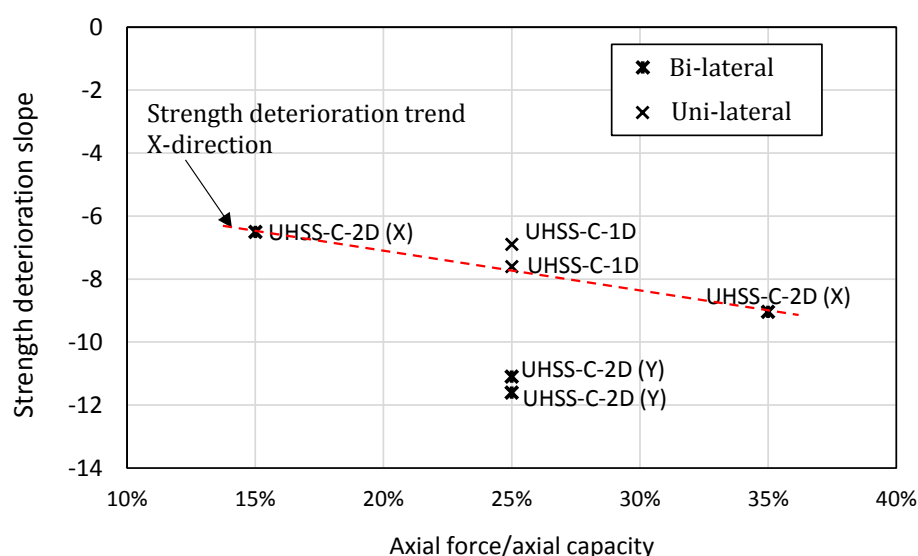
Figure 7.13. Strength deterioration slope of UHSS-C-1D and UHSS-C-2D specimens versus applied axial force ratio

7.7.   Failure Mechanism and Axial Shortening

In addition to investigating the effect of tube materials with various strengths incorporated in fabricated hybrid sections on the overall strength, displacements and plastic behaviour of these elements, different mechanisms of failure were observed in each member. The deformed shape of each member under uniaxial and multiaxial cyclic loading is shown in Figure 7.14. These images show the failed specimen at the final cyclic displacement amplitude. In the first three images effect of the steel tube material on the failure of hybrid fabricated components is clearly evident. After applying the initial compression, local buckling deformation occurs along MS plates. In MS-C-1D specimen with the application of cyclic lateral displacement the majority of local deformation occurs in areas close to the end of specimen in both MS plates and MS tubes. The type of deformation observed is the folding mechanism known to be an indication of ductile behaviour [37]. This folding occurs at both ends of the hollow section which is similar to the results reported for hollow circular steel sections [38]. However, due to the simultaneous effect of axial and lateral forces, inward folding is observed in the surface vertical to lateral cyclic direction (X) and outward folding in the direction parallel to lateral cycles at the top and bottom of specimen. In HSS-C-1D and UHSS-C-1D, however, local lateral shear deformation occurs along the total length of MS plates which is due to the compression forces generated throughout the width of plates on the side parallel to the lateral displacement direction. Because of the higher ductility of MS tubes compared to that of high strength steel tubes, MS-C-1D undergoes severe local deformations at both ends under the applied axial and lateral displacements. In contrast, HSS and UHSS tubes show global deformation curvature along the members without any severe local deformations. In UHSS-C-2D specimen plate deformations occur in two directions and the most severe deflections are formed in the X direction compared to that of Y direction and also compared to the unilateral specimens. In addition to the differences

in plate and tube mechanisms, the bilateral displacement applied to the UHSS-C-2D specimen with asymmetric axial loads affects the overall squareness of the section geometry at failure.
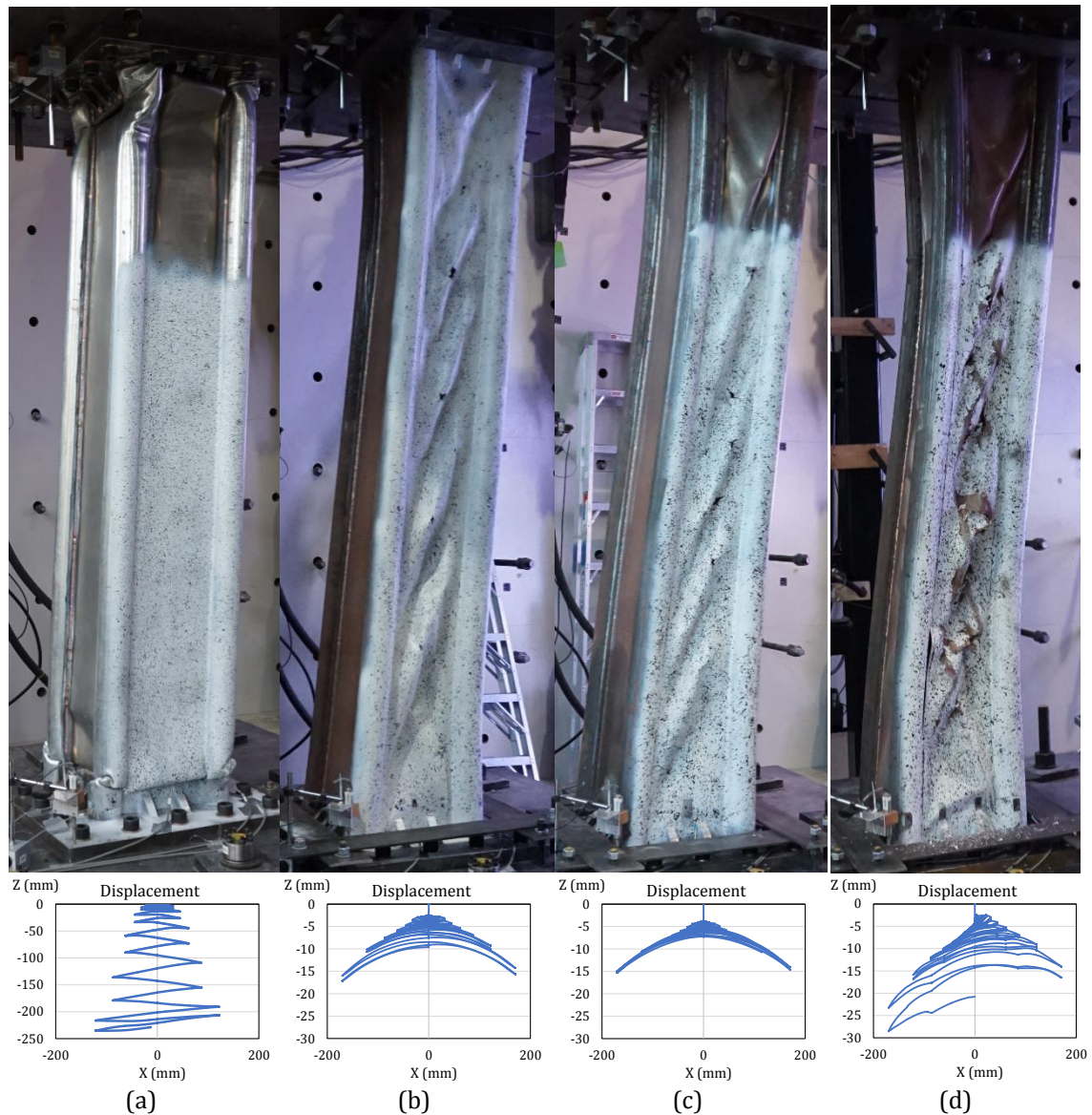
Figure 7.14. Failure mechanisms of fabricated members and axial displacement throughout the cyclic test in X direction for: (a) MS-C-1D, (b) HSS-C-1D, (c) UHSS-C-1D and (d) UHSS-C-2D specimens.

When a steel frame is subjected to earthquake excitation, column elements undergo axial deformations. This shortening is a result of the longitudinal strains generated from the combined action of axial loads, coming from the constant effect of gravity load and the

vertical component of earthquake load, as well as the cumulative longitudinal strains of bending moments developed from reversed lateral displacements. Depending on the direction of lateral loads bending moments cause compressive strains at either side of the neutral axis which result in a gradual axial shortening [39]. The axial deformation in Z direction is obtained from the testing machine crosshead reading and because the LVDT measurements showed no deformation in the concrete pedestal and the top steel plates relative to the crosshead, this value actually demonstrates the axial displacement at the top of each specimen. Axial displacements are plotted for four specimens tested under unilateral and bilateral cyclic loads shown below the failure mechanisms in Figure 7.14. These displacement measurements indicate the significant effect of tube material properties on the axial shortening of beam-column members subjected to lateral cyclic displacements. MS-C-1D (Figure 7.14(a)) shows an axial shortening of around 10 times more than members consisting of high strength tubes (Figure 7.14(b), (c) and (d)). The asymmetric axial loading pattern applied on UHSS-C-2D specimen resulted in asymmetric axial displacements in two opposite directions. Detailed comparisons of the axial shortenings among MS-C-1D and HSS-C-1D are illustrated in Figure 7.15 normalised by the effective length of specimen. Axial deformation values of MS-C-1D increase significantly after the specimen reaches its lateral strength cap, shown with dashed lines in Figure 7.15(a), which is due to the distinct plastic behaviour of MS tubes resulting in local buckling and excessive local deformations during cyclic testing. This observation is similar in all other specimens which shows that significant axial shortening initiates after exceeding the displacement corresponding to lateral strength cap. The effect of multiaxial loading can be observed by comparing UHSS-C-1D and UHSS-C-2D curves in Figure 7.15(b). Based on the multiaxial test, it can be concluded that lower axial force results in less shortening in specimens. This conclusion is confirmed by comparing the bilateral axial shortening measurements with the unilateral test case, in which the magnitude of axial force is the mean value of that in the bilateral test. However, this trend is observed before reaching the

strength cap. After exceeding the drift corresponding to strength cap, axial shortening of UHSS-C-2D in the direction with less axial compression force starts to increase relative to the unilateral test. This is because in bilateral tests, moments in the X direction result in axial compressive strains in half of the section, which accumulate with the compressive strains generated from the moments occurring during lateral displacements in Y direction. The change in length of a column Δ_a was also obtained for HSS-C-1D and UHSS-C-1D specimens as a function of the cumulative inelastic rotation $\sum \theta_H = \sum \mu_H \, \delta_p / L_c$, where $\sum \mu_H$ is the cumulative inelastic ductility, δ_p is the displacement at the top of the beam-column and L_c is the total length [40]. The results show that shortening versus accumulative inelastic rotation follows a trend which approximates a bilinear curve with different slopes before and after the cycle corresponding to the cap lateral strength. The accumulative inelastic rotation at strength cap was 0.17 for HSS-C-1D and 0.19 for UHSS-C-1D at the end of the 18th cycle when 1.7% drift was applied.
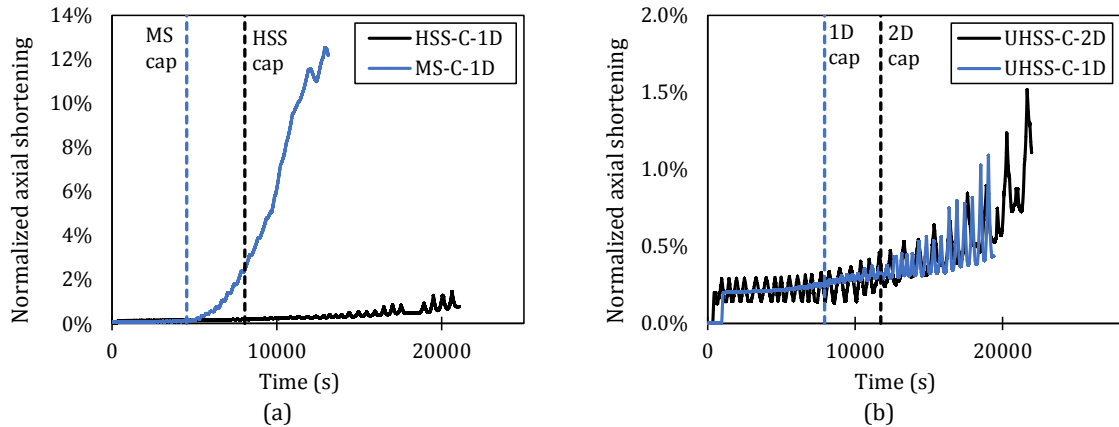
Figure 7.15. Normalised axial shortening comparison of (a) MS-C-1D and HSS-C-1D and (b) UHSS-C-1D and UHSS-C-2D specimens.

7.8.   Conclusions

Hysteresis characteristics obtained from unilateral tests on fabricated hybrid sections showed that the incorporation of high and ultra-high strength tubes enhances the lateral strength cap compared to section with mild tubes by more than 2 times, while the difference between displacement corresponding to lateral yield and ultimate strength does not alter significantly. The rise in lateral load-bearing capacity does not increase linearly with the rise in tube strength properties, and the amount of lateral strength increase depends on the combination of plate and tube properties. Consequently, it is suggested that the design of tube and plate materials and geometries in the proposed hybrid fabricated sections is be done such that an optimum coupled performance of both components is achieved in accordance with the combined compressive and lateral load-bearing demands on the beam-column.

From plastic strain measurements along members tested under unilateral and bilateral cyclic amplitudes, it was observed that utilisation of high grades of steel material in hybrid fabricated members postpones material failure along beam-column elements, preventing high rates of strength degradation and delaying the overall failure. Plastic strain measurements also showed that mild steel plates undergo greater amounts of plastic deformation distributed along the specimen length compared to that of high strength tubes which is more localised towards the fixed ends. Longitudinal strains exceed yield values just after drift corresponding to strength cap (10% plastic hinge ratio) in specimen with HSS tubes and remains fully elastic (0% plastic hinge ratio) in section with UHSS tubes which shows how a greater strength of tube delays the initiation and progression of plastic deformation. Based on the observed dual action of two different steel materials during seismic actions, it is understood that mild steel plates act as lateral ductile elements while

high strength steel tubes are the load-bearing elements performing mostly in the elastic region.

In section with MS tubes at 3.3% drift, a sharp strength reduction of more than 50% was observed, whereas in the two high strength sections under same drift, 80% of strength was preserved. The strength deterioration slopes extracted from UHSS unilateral and bilateral tests showed that the rate of reduction of strength follows a linear decreasing trend in the lateral direction where specimens are subjected to similar drift magnitudes. This linear trend can be used to predict the strength-softening rate for these specimens under various axial compression load ratios.

The results obtained from the complete set of experimental cyclic tests based on available recommendations [41] led to an overview of seismic performance of thin-walled high strength hybrid fabricated sections and can be incorporated in nonlinear structural models to accurately assess and predict the seismic response of structures consisting of these types of high capacity components from the onset of damage through to collapse.

7.9.   Acknowledgements

7.10. References

[1] Kwon YB, Seo GH. Prediction of the flexural strengths of welded H-sections with local buckling. Thin-Walled Structures. 2012;54:126-39.

[2] Shin D-K, Cho E-Y, Kim K. Ultimate flexural strengths of plate girders subjected to web local buckling. Int J Steel Struct. 2013;13:291-303.

[3] Sudha K, Sukumar S. Behaviour of cold-formed steel built-up i section under bending. International Journal of Engineering and Technology. 2013;5:4622-31.

[4] Kim SS, Kim JW, Lee ET, Ha TH, Yang JG, Kim SB. Flexural and shear behaviors of welded H-beam fabricated with hot-rolled steel coils. Int J Steel Struct. 2014;14:73-82.

[5] Ziemian RD. Box girders. Guide to Stability Design Criteria for Metal Structures: John Wiley & Sons, Inc.; 2010. p. 205-56.

[6] Sause R. Innovative steel bridge girders with tubular flanges. Bridge Maintenance, Safety, Management, Resilience and Sustainability: CRC Press; 2012. p. 98-113.

[7] Sause R, Abbas H, Kim B, Driver R. Innovative High Performance Steel Bridge Girders. Structures 2001. p. 1-8.

[8] Keerthan P, Mahendran M. Experimental studies on the shear behaviour and strength of LiteSteel beams. Engineering Structures. 2010;32:3235-47.

[9] Keerthan P, Hughes D, Mahendran M. Experimental studies of hollow flange channel beams subject to combined bending and shear actions. Thin-Walled Structures. 2014;77:129-40.

[10] Rhodes J, Zhao X-L, Van Binh D, Al-Mahaidi R. Rational design analysis of stub columns fabricated using very high strength circular steel tubes. Thin-Walled Structures. 2005;43:445-60.

[11] Heidarpour A, Cevro S, Song QY, Zhao XL. Behaviour of stub columns utilising mild-steel plates and VHS tubes under fire. Journal of Constructional Steel Research. 2014;95:220-9.

[12] Zhao XL, Van Binh D, Al-Mahaidi R, Tao Z. Stub column tests of fabricated square and triangular sections utilizing very high strength steel tubes. Journal of Constructional Steel Research. 2004;60:1637-61.

[13] Trahair NS. The behaviour and design of steel structures to AS 4100 / N.S. Trahair and M.A. Bradford. London: E & FN Spon; 1998.

[14] Kamtekar AG. The fully plastic behaviour of monosymmetric steel sections. Engineering Structures. 2015;105:289-98.

[15] Nowzartash F, Mohareb M. Upper bound plastic interaction relations for elliptical hollow sections. Journal of Engineering Mechanics. 2010;136:1015-27.

[16] AS 4100-1998, Steel structures. Sydney: Standards Australia; 1998.

[17] ANSI/AISC:360-05. Specification for structural steel buidlings. Chicago, Illinois.

[18] Javidan F, Heidarpour A, Zhao XL, Minkkinen J. Performance of innovative fabricated long hollow columns under axial compression. Journal of Constructional Steel Research. 2015;106:99-109.

[19] Javidan F, Heidarpour A, Zhao X-L, Hutchinson CR, Minkkinen J. Effect of weld on the mechanical properties of high strength and ultra-high strength steel tubes in fabricated hybrid sections. Engineering Structures. 2016;118:16-27.

[20] Javidan F, Heidarpour A, Zhao X-L, Minkkinen J. Application of high strength and ultra-high strength steel tubes in long hybrid compressive members: Experimental and numerical investigation. Thin-Walled Structures. 2016;102:273-85.

[21] Sinaie S, Heidarpour A, Zhao XL. A multi-objective optimization approach to the parameter determination of constitutive plasticity models for the simulation of multi-phase load histories. Computers & Structures. 2014;138:112-32.

[22] Mirmomeni M, Heidarpour A, Zhao X-L, Hutchinson CR, Packer JA, Wu C. Mechanical properties of partially damaged structural steel induced by high strain rate loading at elevated temperatures – An experimental investigation. International Journal of Impact Engineering. 2015;76:178-88.

[23] Nassirnia M, Heidarpour A, Zhao X-L, Minkkinen J. Innovative Hollow Corrugated Columns: A Fundamental Study. Engineering structures 2015;94:43-53.

[24] Farahi M, Heidarpour A, Zhao XL, Al-Mahaidi R. Compressive behaviour of concrete-filled double-skin sections consisting of corrugated plates. Engineering Structures. 2016;111:467-77.

[25] Sadeghi N, Heidarpour A, Zhao XL, AM R. Numerical investigation of innovative modular beam-to-fabricated column connections under monotonic loading. In: Zingoni A, editor. Insights and Innovations in Structural Engineering, Mechanics and Computations. Cape Town, South Africa: Taylor and Francis Group2016. p. p. 1247–52.

[26] Hosseini S, Heidarpour A, Collins F, Hutchinson CR. Effect of strain ageing on the mechanical properties of partially damaged structural mild steel. Construction and Building Materials. 2015;77:83-93.

[27] Song QY, Heidarpour A, Zhao XL, Han LH. Performance of Unstiffened Welded Steel I-Beam to Hollow Tubular Column Connections Under Seismic Loading. International Journal of Structural Stability and Dynamics. 2014;15:Article number: 1450033.

[28] Azhari F, Heidarpour A, Zhao XL, Hutchinson CR. Effect of creep strain on mechanical behaviour of ultra-high strength (Grade 1200) steel subject to cooling phase of a fire. Construction and Building Materials. 2017;136:18-30.

[29] Ziemian RD. Appendix B: Technical Memoranda of Structural Stability Research Council. Guide to Stability Design Criteria for Metal Structures: John Wiley & Sons, Inc.; 2010. p. 963-1029.

[30] Hashemi MJ, Al-Mahaidi R, Kalfat R, Burnett G. State-of-the-Art System for Hybrid Simulation at Swinburne. Australian Earthquake Engineering Society Conference 2014, Lorne, Australia2014.

[31] Dassault Systèmes Simulia Corp. P, RI, USA. ABAQUS/CAE 6.14-1. 2014.

[32] Galambos TV. Deformation and energy absorption capacity of steel structures in the inelastic range. In: Steel Research and Construction A, editor.1968.

[33] Ziemian RD. Beams. Guide to Stability Design Criteria for Metal Structures: John Wiley & Sons, Inc.; 2010. p. 205-56.

Conclusions and Future Work

8.1.   Research outcomes

Experimental tests conducted on hybrid fabricated sections and the subsequent analytical and numerical investigations undertaken in this thesis give rise to a novel and comprehensive perspective into the application of high and ultra-high strength tubular sections for analysis and design. Results and outcomes of each part of the thesis are summarised individually based on the loading and scale of studies. Aside from describing a summary of chapter conclusions, this part also aims to look at the results in a big picture, comparing and relating the outcomes of each chapter.

Monotonic: material scale phase

Taking the effects of material characterisation and weld affected areas into consideration, a finite element model was validated against experimental results in terms of load-displacement curves, failure modes and strain distribution. Detailed finite element modelling conducted in this thesis showed an acceptable match with the experimental behaviour of the proposed sections in different lengths which was used for analysing columns with various slenderness. Including HAZ (heat affected zone) properties in the numerical analysis of innovative hybrid sections reduced the load bearing capacity of sections consisting of ultra-high strength tubes around 20%. A detailed microscale investigation was performed on welded high strength steel tubes which resulted in practical outcomes of how welding processes in fabricated sections can affect the initial properties of these materials. Effect of weld induced heat on the mechanical properties of steel tubes in the vicinity of weld (up to ~4mm from weld) resulted in an overall reduction around 8% in HSS and 30% in UHSS tubes. In contrast, welding enhanced the tensile strength of mild steel to around 13% above its original value. Welding heat also increased the ultimate strain of MS, HSS and UHSS tube material to 2.5, 2.1 and 3.5 times of the original ultimate strain, respectively. The individual effect of strain hardening rate and yield strength on the

mechanical properties was studied for each steel type in both the heat affected position and furthest areas from weld. Optical micrographs were obtained from different locations from weld in each of the steel materials and analyses helped rationalise the HAZ properties. The manufacturing process, heat input due to welding and the cooling after welding were taken into consideration by means of observing the microscopic images and microhardness profiles taken along the welded connection of MS plate and UHSS tubes. It was concluded that at the immediate vicinity of UHSS to weld, due to the presence of mild steel plate which acts as a heat sink, in addition to the cooling argon gas, rapid cooling resulted in the re-forming of the martensite microstructure. It was observed that moving further from the vicinity of weld, the material softening occurs within the transition zone which starts at 4mm from weld substance having a width around ~3mm which are values close to the element thickness.

Monotonic: Compression, bending and compression-bending interaction

In general the advances in compressive strength of hybrid fabricated sections consisting of three types of tube materials is concluded. Compressive strength of section increases with incorporation of high tensile steel material compared to similar columns with lower tube strength (up to three times) and compared to a conventional section with similar effective slenderness (around three time more). This advantage is more obvious when comparing the overall compression behaviour in terms of strength and ductility with the superposition of similar sections tested individually. The increase is shown to be around 20% for one meter columns and reaches 50% in two-meter ones. It can be concluded from these results that more advantage is taken from the material of tubes with the increase in length of members. In terms of utilising high strength steel tubes it was found that sections fabricated from high strength steel tubes and ultra-high strength tubes advance the energy absorption to 10% and 30% more compared to that of a similar section consisting of mild steel tubes.

Further analytical and numerical comparison among innovative and conventional columns with similar cross-section and slenderness ratios indicated that the proposed section shows an increase in compressive load bearing capacity and the displacement corresponding to peak load especially in high strength tube material with respect to conventional welded box section.

From a loading point of view (compression and bending), the experimental results showed a somewhat similar observation in terms of the influence of steel tubes in 2000mm members. It was found that incorporating high strength steel tubes increases the peak strength 1.5 times and 2 times in pure compression and pure bending respectively compared to a section with mild steel tubes. These values increase to 2.7 and 3.2 in the case where ultra-high strength tubes are used. Comparing the ductility of 2000mm hybrid fabricated members under compression and bending shows that the members showed an approximately similar reduction trend of ductility in sections as the strength of tubes increased. It is worth mentioning that the ductility in compression is derived using the ductility factor while in bending is obtained from the rotation capacity. In both cases ductility is quantified by obtaining the ratio of displacement (in compression) or rotation (in bending) at yield to that at ultimate load.

A general conclusion derived from comparing failure mechanisms and strain behaviour of fabricated hybrid sections with the conventional specimens under compression or bending or the interaction of both, is the coupling interaction effect of tubes and plates. This effective interaction between tubes and plates of fabricated hybrid members was to enhance the strength and ductility performance. The improved performance of hybrid fabricated sections was obvious in the case of axial loading by comparing the member's compressive strength with that of superposition of individual elements. In case of flexural behaviour, the moment capacity of sections was compared to that obtained from AS4100 design standard. Under both loading cases a higher strength was achieved. The tested geometry of sections

was such that the plate elements of hybrid sections possessed a high width to thickness ratio. Utilizing tube elements at two sides of this slender element proved to reduce the catastrophic local buckling and while this element can undergo high levels of deformation, the section takes advantage of tube strength until global failure. This restraining effect of tubes for plates was also evident from the failure mechanism of sections under compression, bending and compression-bending interaction compared to conventional box sections. Mild steel plates in box sections failed under a single local mechanism along the member while in hybrid sections this failure was distributed along the length of member.

In an economical point of view, a cost estimation analysis was conducted which justified the benefit of innovative fabricated sections in terms of overall weight and production compared to that of a conventional column with similar width, length and compressive strength. These sections are found to have beneficial applications in structures in demand of very high strength compressive members such as bridges and high rise buildings with reasonable ductility and desirably low weight and also acceptable architectural appearance.

Under combined axial force and bending moments, interaction curves were extracted for various cross-section properties which showed that as the non-dimensional ratio of strength and cross-sectional area of tube elements to that of plate elements reduces, the interaction strength enhances. Consequently, a linear interaction formula is applicable for predicting interaction behaviour of sections with high tube to plate ratios while sections with lower ratios are closely predicted by the bilinear interaction formula.

The parametric finite element studies conducted on hybrid members under compression-bending interaction showed the significant effect of shear on the lateral performance of these section. This effect reduced as the ratio of axial compression increased. The beam-column performance of members obtained from the parametric study also showed the

axial-lateral curves are enhanced as the plate thickness increases in hybrid fabricated sections consisting of high strength and ultra-high strength tubes.

Cyclic: material scale phase

In the material scale experiments, the main point of distinction in the cyclic behaviour of high strength and ultra-high strength steel materials was cyclic softening phenomenon exhibited with increasing the number of cycles applied. More specifically, under cyclic loading with constant amplitude, the overall softening percentage of ultra-high strength steel tube was higher than that in high strength steel tube meaning that this phenomenon is more prominent when material strength increases. It was also observed that in both tube materials under incremental cyclic loading, having higher number of cycles with less strain increments results in a more obvious strength degradation compared to less number of cycles and higher strain increments. In cyclic loading with constant stress amplitude, it was shown that at the end of each cycle, the strain corresponding to stress amplitude experiences a higher increase compared to the previous cycle which depends on the stress controlled cyclic status i.e. values of mean stress and amplitude. In a similar cyclic test case, ultra-high strength tube material showed a higher energy dissipation value but lower energy dissipation coefficient compared to high strength steel considering complete load-displacement cycles in a similar test type. Preserved mechanical properties of cyclically strained high strength and ultra-high strength steel tubes were also a critical part of investigations. As opposed to the reduction in stress, the ultimate strength of ultra-high strength and high strength steel tube material corresponds to a higher strain compared to that of virgin material under monotonic tension resulting in a higher ductility of these materials. Examining the cyclically strained fracture surface of both steel tube materials showed that high strength steel fracture is ductile while ultra-high strength material exhibits somewhat a mixed fracture mode.

Using the obtained cyclic isotropic/kinematic hardening data from experiments, a predictive model was developed in ABAQUS and the cyclic behaviour of high and ultra-high strength steel tube materials were verified against experimental curves. Cyclic kinematic hardening and isotropic softening parameters were also calibrated and proposed.

Cyclic: component scale

Multiaxial cyclic tests conducted on three types of fabricated steel sections resulted in a comprehensive overview of the effect of loading direction and axial load on the seismic performance of these sections.

Cyclic tests under constant axial load and unilateral cyclic load showed that incorporating high and ultra-high strength tubes enhances the lateral strength cap compared to the section with mild tubes more than 2 times, while the difference between displacement corresponding to lateral yield and ultimate strength does not alter significantly. The rise in lateral load-bearing capacity does not increase linearly with the rise in tube strength properties and the amount of lateral strength increase depends on the combination of plate and tube properties. In section with MS tubes at 3.3% drift, a sharp strength reduction of more than 50% was observed, whereas in the two high strength sections under same drift, 80% of strength was preserved. The strength deterioration slopes extracted from UHSS unilateral and bilateral tests showed that the reduction rate of strength follows a linear decreasing trend in lateral direction where specimens are subjected to similar drift magnitudes. This linear trend can be used to predict a strength softening rate for these specimens under various axial compression load ratios.

From plastic strain measurements along the members tested under unilateral and bilateral cyclic amplitudes, it was observed that utilising high grades of steel material in hybrid fabricated members postpones the material failure along beam-column elements preventing high rates of strength degradation and delaying the overall failure. Plastic strain

measurements also showed that mild steel plates undergo higher amounts of plastic deformation distributed along the specimen length compared to that of high strength tubes which is more localised towards the fixed ends. Longitudinal strains exceed yield values just after drift corresponding to strength cap (10% plastic hinge ratio) in specimen with HSS tubes and remains fully elastic (0% plastic hinge ratio) in section with UHSS tubes under constant and varying axial loads which shows how higher strength of tube delays initiation and progression of plastic deformation. Based on the observed dual action of two different steel materials during seismic actions, it was understood that with plate and tube specifications used in this study, mild steel plates act as lateral ductile elements while high strength steel tubes are the load bearing elements performing mostly in the elastic region.

Documentation of results obtained from complete set of experimental cyclic tests based on available seismic assessment recommendations leads to an overview of seismic performance of thin-walled high strength hybrid fabricated sections and can be incorporated in nonlinear structural models to accurately assess and predict the seismic response of structures consisting of these types of high capacity components from the onset of damage through to collapse.

8.2. Future work

Recommendations outlined below can be incorporated in future works to follow the research fields covered in this thesis which are proposed based on the current knowledge gaps.

- Studies conducted on the effects of weld induced heat on mechanical properties of all involved steel materials specifically high strength and ultra-high strength steel justified the direct influence of welding procedures on the local and global section performance. Taking advantage of the preliminary cost-effectiveness analysis conducted in the early stages of the present thesis as well as the investigations conducted on the heat affects can give rise to future study pathways focusing on the development of an optimised fabrication procedure for hybrid sections. This can include optimising the welding and post-welding factors such as welding methods, heat inputs, welding and cooling rates so that the least softening occurs in the steel materials considering cost-effective techniques for mass fabrications and productions.

- Bending, compression-bending and compression-bending-shear interaction performance of hybrid fabricated sections can be further investigated through studying and quantifying effect of length on the local failure and global performance.

- Material scale cyclic experimental and numerical works conducted on high strength and ultra-high strength steel materials resulted in the introduction of constitutive equations for material modelling of these types of steels under various strain histories. These studies can be extended to alternative steel grades and constitutive equations can be proposed for the nonlinear hardening and softening behaviour

relating the parameters of constitutive equations to the microstructural properties of high grades of steel. The isotropic softening parameters of grade 800 and 1200 steels recommended in this thesis are proposed for specific magnitudes of strain amplitude. These parameters can be further investigated for finding a specific strain range to which the formulations are applicable. Furthermore, constitutive formulations can be developed as a function of or independent from strain amplitudes.

- Large scale analysis of structural components or frames can be conducted incorporating the constitutive equations derived from the material scale cyclic performance of high strength and ultra-high strength steel tubes under cyclic loadings in finite element software packages or other tools. Attention can be placed on the effect of cyclic softening on large scale performance of high strength steel components and comparisons can be driven with that of conventional mild steel components.

- For the aim of evaluating the behaviour of a structural system at various hazard levels, performance-based earthquake design can be conducted on structures consisting of hybrid fabricated members. The experimental and analytical results obtained from large scale cyclic tests can be processed and calibrated to obtain relevant hysteretic models for damage and collapse prediction. From the deteriorating backbone curves obtained from experimental studies conducted on various hybrid sections, strength and stiffness degradations can be evaluated. Furthermore, additional hysteretic parameters can be obtained from the load-displacement experimental results which lead to the calibration of models. These models can be incorporated as component input specifications of full-scale frame simulations. Several seismic evaluations can be made on the application of high capacity hybrid members in structures such as extracting fragility functions and

probabilities, damage and collapse assessment. Discussions can be developed comparing results to those obtained for similar structures designed with conventional structural components. Furthermore, effect of steel material in similarly designed sections can be investigated.